STUDY OF FRACTURE BEHAVIOUR OF EXTRA DEEP DRAWN STEEL SHEETS

THESIS

Submitted in partial fulfilment
of the requirements for the degree of

DOCTOR OF PHILOSOPHY

By

Kulkarni Dhananjay Madhukar

Under the Supervision of

Prof. Ravi Prakash

BIRLA INSTITUTE OF TECHNOLOGY AND SCIENCE
PILANI (RAJASTHAN) INDIA

2004

ACKNOWLEDGEMENTS

I wish to express deep sense of gratitude and sincere thanks to my thesis supervisor Prof. Ravi Prakash, Dean, Research and Consultancy Division for his able guidance, encouragement and suggestions throughout the period of this research work. It has been a privilege for me to work under his guidance.

I am grateful to Dr S. Ray and Dr. N. Gope (Scientific Services Division, TISCO, Jamshedpur) for the supply of EDD steel samples as well as some technical information on formability behaviour of EDD steel sheets.

Much appreciation is expressed to Prof. A.N. Kumar (I.I.T., Delhi) and Prof. Jim Newman, Mississippi State University for their valuable suggestions, moral support and assistance.

I sincerely thank to Sri Tarachandji (Workshop, BITS), Sri B.L. Soniji (Centre of Material Science and Technology, BITS), Mr. Goyal and Mr. Omkar (Metallography lab, I.I.T. Delhi) who gave unending support right from the work-plan was conceived.

Gratitude is also accorded to BITS, Pilani and BITS-Pilani, Goa Campus for providing all the necessary facilities to complete the research work. My special thanks go to Prof. S. Venkateswaran, Vice Chancellor, B.I.T.S. for giving me an opportunity to do research at the Institute. I also thank Prof. T.C. Goel, Director, BITS-Pilani, Goa Campus and Prof. L. K. Maheshwari, Director, BITS, Pilani for their encouragement and guidance. I take this opportunity to thank Prof. K. E. Raman Deputy Director (Administration), Prof. V. S. Rao, Deputy Director (Off-Campus) and Prof. A. K. Sarkar, Dean, Instruction Division, for providing the necessary infrastructure and other facilities.

Special thanks are due to Prof. Rajiv Gupta, Dean Educational Hardware Division for his guidance and invaluable assistance throughout my research work. Special thanks are also due to Mr. Pravin Talan who worked with me to learn more about fracture mechanics.

I also express my gratitude for the kind encouragement and appreciation of my work by my colleagues Dr. M.S. Dasgupta and Dr. S. Kanagraj and Dr. I.V. Singh. Thanks are also due to and Mr. Sanjay D. Pohekar from Research and Consultancy Division.

Finally a very special expression of appreciation is extended to my family members. Without their encouragement, patience, and understanding, this endeavor would not have been possible. I would like to record my special affection and thanks to my parents and my wife Reshma, whose constant persuasion and moral support has been a source of inspiration to me.

ABSTRACT

The present attempt aims to generate more information and understanding on fracture behaviour of EDD steel sheets based on fracture parameters. In the present work, information on conventional indicators of formability parameters is obtained to study good deep drawing qualities. The fracture behaviour of EDD steel sheets is studied in two phases namely, generation (i.e. crack initiation) and application (i.e. crack propagation) phase. Experimental techniques and finite element (FE) analysis using commercial software ANSYS 7.0 are used as tools for the analysis in generation phase. *J*-integral and crack tip opening displacement (*CTOD*) are used as fracture parameters.

In generation phase, after successive experimental attempts, 'load drop technique' is used as a fracture criterion. A few specimens are checked before load drop to verify the fracture criterion using thermal shock treatment as well as with metallographical observations. The *J*-integral is measured using area under load – load-line displacement curve obtained from fracture test. As the plastic load-line displacement is high in case of EDD steel sheets, crack flank opening angle (CFOA) model is suggested to find out plastic *CTOD*, in addition to existing plastic hinge model (PHM), *J-CTOD* relation and FE analysis. CFOA model accounts for nonlinearities in the relationship between plastic *CTOD* and plastic load-line displacements. An attempt has been made to verify the *J-CTOD* relation in general yielding fracture mechanics. The Shih factor d_n in *J-CTOD* relation is found to be in the range 0.9-1.1 based on CFOA, PHM and FE models.

The 3-D FE analysis is used to predict the fracture parameters. In non-linear material model, breaking point strain is used as a fracture criterion. The true stress-strain curve is used up to a breaking point strain with a constant value of ultimate stress after the ultimate limit. This has allowed sufficient necking before crack initiation. Virtual crack tip opening method is used to find critical load, *J*-integral and *CTOD* values. The FE analysis results on critical load, *J*-integral and *CTOD* are overestimated and within 5-12% of experimental results. This discrepancy is attributed towards assumed idealised conditions in FE analysis.

The *J*-integral and *CTOD* are found to increase with increase in thickness of EDD steel sheets. Formability study shows that the EDD steel is insensitive to strain rate at room temperature. However, from the fracture study, it is found that the EDD steel sheet is sensitive to high strain rate even at room temperature and fracture toughness decreases with increase in strain rate beyond a limiting strain rate value. Thus, it is concluded that the forming of the EDD steel sheet should be done at lower strain rates for high formability. The study on influence of notch radius on fracture parameters has confirmed that fatigue pre-

cracking, which is a costly and time-consuming job, is not essential. An attempt has been made to study 'crack tip contraction' as a fracture criterion. From this study, it is found that crack tip opening displacement is equal to crack tip contraction for lower thickness, however, for higher thickness, the difference between them increases; the amount of crack tip contraction being on lower side. Moreover, this study has shown that, strain rate and notch radius has no effect on crack tip contraction. Therefore, crack tip contraction as a fracture criterion becomes questionable.

In application phase, crack growth behaviour is characterised using *J-R*, critical crack tip opening angle *CTOA-R* and *CTOD-R* curves. The *J*-integral is calculated using the area under load – load-line displacement plot and following ASTM E 1820-01. The critical *CTOA* model is suggested to infer the crack growth *CTOD*. It is found that after crack initiation the resistance increases with increase in crack extension. The rising nature of *R* curves implies continued increase in toughness during stable tearing, and the increase in tearing resistance is the governing parameter for stability rather than the critical initiation toughness value. From the critical *CTOA* model, it is found that the unit propagation energy includes the crack initiation energy, which is supported by ASTM standard E 1820-01. Fracture surface study has shown high degree of shear lips with crack tunneling. High degree of shear lips support the existence of predominantly plane stress condition and crack tunneling support the stable tearing of EDD steel sheet.

It is concluded that only conventional indicators of formability are not sufficient to haracterise the fracture behaviour of EDD steel sheets, however, the fracture mechanics ays an important role to cover all aspects of fracture behaviour. This study is equally portant to manufacturers as well as users in order to understand and analyse the crack iation and crack propagation in products as well as EDD steel sheet structures. A few esign aspects are summarised in conclusions.

TABALE OF CONTENTS

LIST OF TABLES

LIST OF FIGURES

LIST OF SYMBOLS

a_0	initial crack length
b	unbroken ligament length
A_{pl}	plastic area under load – load-line displacement curve
B	thickness of specimen
B_n	net section thickness of ductile fracture surface
J	J-integral (a fracture parameter in the honor of J. Rice)
d_n	Shih factor
E	elastic modulus
J_{el}	elastic J integral
J_{pl}	plastic J integral
J_c	critical J integral
K	stress intensity factor
K_I	mode I, stress intensity factor
K_{Ic}	critical stress intensity factor
P_c	critical load
P_{unl}	load at unloading point
S_Y	yield strength
T_x, T_y	traction forces along x- and y-direction
U	strain energy density
V_{el}	elastic load line displacement
V_{ll}	load line displacement
V_{pl}	plastic load line displacement
V_{unl}	load-line displacement at unloading point
W	width of specimen
m	strain rate sensitivity index

n	strain hardening exponent.
n_x and n_y	normal vector to the path of J-integral
r	distance of node from crack tip
r_0	strain ratio along 0° to rolling direction
r_{45}	strain ratio along 45° to rolling direction
r_{90}	strain ratio along 90° to rolling direction
$\bar{r}$	normal anisotropy factor
r_{pl}	plastic rotational factor
r_{pz}	plastic zone size
$(\Delta a)_s$	crack extension measured on surface
$(\Delta a)_{b1}$	crack extension measured on broken ligament 1
$(\Delta a)_{b2}$	crack extension measured on broken ligament 2
$(\Delta a)_{avg}$	average crack extension
	$(\Delta a)_{avg} = [(\Delta a)_{b1} + (\Delta a)_{b2}]/2$
α	a_0/W ratio
β	factor to calculate plastic rotational factor (r_{pl})
γ	geometry factor
Γ	path for J-integral calculation
η	geometry factor
δ_{el}	elastic CTOD
δ_{CG}	crack growth *CTOD*
δ_{CI}	crack initiation *CTOD*
δ_n	thickness contraction or crack tip necking
δ_{pl}	plastic *CTOD*
δ_c	critical *CTOD*
ε_u	ultimate strain

ε_z	strain in thickness direction
ρ	notch radius
υ	Poisson's ratio
σ_{ij}	nodal stress value
σ_x	stress in x-direction
σ_y	stress in y-direction
σ_z	stress in z-direction
θ	nodal angle with reference to crack plane
θ_{CT}	crack tip opening angle measured at current crack tip

LIST OF ABBREVIATIONS

ASTM	American Society of Testing and Materials
BLD	before load drop
CG	crack growth
CI	crack initiation
CT	compact tension
CFOA	crack flank opening angle
CMOD	crack mouth opening displacement
CTOA	crack tip opening angle
CTOA-R	crack tip opening angle controlled resistance curves
CTOD-R	crack tip opening displacement controlled resistance curves
CTOD	crack tip opening displacement
DD	deep drawn
EDD	extra deep drawn
EPFM	elastic plastic fracture mechanics
FC	fatigue pre-cracked
FE	finite element
FEA	finite element analysis
FLC	forming limit curve
GYFM	general yielding fracture mechanics
HV	Vickers hardness
J-R	*J* controlled resistance curves
LEFM	liner elastic fracture mechanics
LLD	load-line displacement
ppm	parts per million
R	resistance
RD	rolling direction

YS	yield strength
UTS	ultimate tensile strength
WEDM	wire electric discharge machine

LIST OF SUBSCRIPTS

FEM	Finite Element Method
CFOA	Crack Flank Opening Angle
PHM	Plastic Hinge Model

Chapter –1

INTRODUCTION

1.1 Introduction to EDD Steel Sheets

Extra deep drawn (EDD) steel is the most widely used material for automotive applications involving simple to complex products, which require very high formability. Exterior components such as starter, end-covers, petrol tanks, etc. are made of EDD grade steel sheets. Apart from Automobile industry, the EDD steel sheets are extensively used in enameling applications such as baths, sink units, kitchenware, cooker, washing machine and refrigerator bodies, etc. These EDD steel sheets account for a sizable proportion of the manufactured goods produced and used by industries.

1.2 Present Practice of Quality Control of EDD Steel Sheets

The goal of every industry is to reduce the cost by reducing the wastage and increase the performance of the manufactured products. Quality control of EDD steels at present is dependent on intrinsic and simulative tests, which are dealt in the discipline of formability characterisation. Sheet metals used for such applications are subjected to various types of forming operations depending on the desirable shape. The performance of such operations is recently assessed by Ravi Kumar (2002), Raulea *et al.* (2001) and Takuda *et al.* (1999) in terms of formability indices. The formability characterisation tests can be broadly classified into two groups namely, simulative tests and intrinsic tests. The former ones are empirical in nature whereas the latter

ones are fundamental or semi empirical in nature. As mentioned by Rao and Mohan (2000), in the simulative tests, the formability characterisation can be accomplished by the employment of Erichsen cup test, hole-expansion test and Olsen cup test. In the intrinsic tests, the formability characterisation can be accomplished by the determination of either one or the combination of strain hardening exponent, strain rate sensitivity index, normal anisotropy factor ($\bar{r}$) and formability limit curve (FLC).

1.3 Need for Alternative Method

This is discussed with reference to drawbacks of formability approach and the present status of fracture mechanics approach for EDD steel sheets.

1.3.1 Formability approach

While forming a sheet into a specific shape, material variables and process variables have greatest influence on the overall formability and are usually assessed during die tryout. However, due to the complex interaction of large number of variables, which affect formability of sheet metals, there is no single parameter, which can comprehensively describe the forming characteristics of a material.

The principle of the intrinsic and simulative tests, attempt to search for an engineering parameter, which indicates the mechanical environment for crack initiation and/or crack propagation under corresponding experimental conditions. The assessment of different parameters by these tests primarily seeks to ascertain the safe limits up to which a sheet metal can be deformed without crack initiation or its subsequent propagation. However, the phenomena of crack initiation and crack propagation are dealt within the discipline of fracture mechanics.

1.3.2 Fracture mechanics approach

In fracture mechanics, the criterion for crack initiation is ascertained either for plane strain or for plane stress-plane strain conditions. The demarcation between these two states of stress is generally made using the thickness dependence of fracture criterion, i.e. $B \geq 2.5\left(K_{Ic} / S_{y}\right)^{2}$. At the initial stage, during the application of fracture mechanics, many investigators like Griffith (1920) and Irwin (1948) have laid emphasis primarily on determining plane strain fracture toughness using linear elastic fracture mechanics (LEFM). Thereafter, in the development of fracture mechanics, several fracture criteria for elastic-plastic fracture mechanics (EPFM) are formulated using crack tip opening displacement (*CTOD*) by Wells (1961) and *J*-integral technique by Rice (1968). However, these investigations could be utilised on structural load bearing components having sufficient thickness, which can not be categorised under the domain of sheet metals. Henceforth, very little attention has been paid for assessing EDD steel sheet characteristics in the discipline of fracture mechanics.

The formability study by Ravi Kumar (2002) and technical reports by Ray (2000-2004) have showed that the problem of crack initiation in EDD steel sheet metals is intimately connected with significant deformation ahead of crack tip. Significant deformation ahead of crack tip plays an important role in crack initiation and crack propagation process. According to Cotterell (2002), extensive deformation ahead of a crack tip has emerged a new discipline in fracture mechanics called general yielding fracture mechanics (GYFM).

The objective of the present investigation is to study the application feasibility of fracture mechanics in characterising the quality of EDD steel sheets through experimental and finite element analysis.

1.4 Overview of Research Work

In the present work, an attempt has been made to study the deep drawing qualities and the complete fracture behaviour using formability and fracture mechanics approach. Information about the conventional indicators of formability is obtained first to characterise the formability of EDD steel sheets. Two important phases of fracture behaviour namely, generation (i.e. crack initiation) phase and application (i.e. crack propagation) phase of EDD steel sheets are studied in the present work. In the crack initiation phase, after several experimental attempts, a 'load-drop technique' is suggested as a fracture criterion in EDD steel sheets using CT type specimens. Crack tip opening displacement (*CTOD*) and *J*–integral are used as fracture parameters for quantitative fracture analysis.

The results on crack initiation are verified with the help of 3-D FE analysis. In 3-D FE analysis, breaking strain is used as a fracture criterion and virtual crack tip opening method is used to determine the fracture parameters. The results of 3-D FE analysis on critical load, *J*-integral and *CTOD* are overestimated and within 5-12% of experimental results. This discrepancy is attributed towards assumed idealised conditions in FE analysis.

Crack flank opening angle (CFOA) model is suggested to infer the plastic *CTOD*. This model accounts for the non-linearity between *CTOD* and load-line

displacement. In addition to CFOA model, the plastic CTOD is inferred with the help of plastic hinge model (PHM), *J-CTOD* relation and finite element method (FEM). The *J–CTOD* relation is verified in the predominantly plane stress condition and the value of Shih factor (d_n) is found to be in the range 0.9-1.1 using PHM, CFOA model and FE analysis. The fracture parameters, like *J* integral and *CTOD* are shown to increase with increase in thickness unlike that of thin plates as reported by Srawley and Brown (1975) and Pandey *et al.* (1997). The results on physical significance of such inverse fracture behaviour are explained with the help of a 3-D finite element stress analysis. The EDD steel sheet is tested at various strain rates. From the study of effect of strain rate, it is found that the EDD steel sheet is sensitive to high strain rate even at room temperature. The EDD steel sheet is also tested for the study of influence of notch radius on fracture parameters. The study of influence of notch radius on fracture parameters has shown that the fatigue pre-cracking is not essential as it is time consuming and costly process.

In this study an attempts has been made to study the thickness contraction ahead of crack tip as a fracture criterion. It is found with experimental and FE analysis that, thickness contraction can not be an appropriate measure of fracture criterion as there is no effect of strain rate and notch radius on thickness contraction. The other observation from this study is, for lower value of sheet thickness, the thickness contraction is equal to crack tip opening displacement. However, as thickness increases, the difference between them increases, with thickness contraction on lower side. The reason behind this is slow increase of stress in thickness direction, restricts the material flow in thickness direction. With the help of 3-D FE stress

analysis and observations of fracture surface, it is concluded that the fracture behaviour falls in the regime of predominantly plane stress condition.

In application phase of fracture behaviour, *J-R*, crack tip opening angle resistance (*CTOA-R*) and crack tip opening displacement resistance (*CTOD-R*) curves are used to characterise the crack growth behaviour. Slow and stable crack extension is observed with high degree of shear lips and crack tunneling over entire fracture surface. This is unlike other engineering materials, wherein either there is a stationary crack extension after crack initiation or a continuous exponential decay right from crack initiation or a stationary crack extension followed by a continuous exponential decay. These three interpretable parameters (*J*, *CTOA* and *CTOD*) characterise ductile fracture resistance both quantitatively and physically. From the metallographic study, it is found that the predominantly plane stress condition exists ahead of crack tip.

1.5 Scope and Objectives of the Present Study

The insufficient attention on studies related to fracture behavior of EDD steel sheet metals originates from the fact that engineering materials with thinner sections are not considered as load bearing structural parts. The problem of crack initiation and its subsequent propagation in thin sheet of EDD steel materials is not well defined. Engineers are more concerned with the formation of cracks in thin sheets during the fabrication work i.e. in generation phase and when the product is in use i.e. in application phase.

Complex products from EDD steel sheets are required for todays automotive and various other industries. Such EDD steel sheets are now developed with the aid

of data obtained from laboratory experiments that enable the fracture characterisation of sheet metals to be reliably predicted. Therefore, an understanding of formability and fracture behaviour of EDD steel sheet is essential to manufacturer as well as to user for the successful production of quality products.

The objectives of the present study are as follows.

Study of formability behaviour of EDD steel sheets

(a) To study the deep drawing qualities of EDD steel sheets.

Study of fracture behaviour of EDD steel sheets in generation phase

(b) To present a simple experimental technique for obtaining fracture criterion of EDD steel sheets and produce results on fracture parameters like *CTOD* and *J*-integral.

(c) To examine the effect of thickness of EDD steel sheets on fracture parameters.

(d) To study the physical significance of fracture behaviour of EDD steel sheets.

(e) To examine the effect of strain rate on fracture parameters.

(f) To verify the crack tip contraction as a fracture criterion.

(g) To verify the results on fracture parameters by 3-D FE analysis.

Study of fracture behaviour of EDD steel sheets in application phase

(i) To study the crack growth behaviour with the help of *J*, *CTOA*, and *CTOD* parameters.

(j) To study the fracture surface for the characterisation of fracture behaviour.

1.6 Organisation of Thesis

In order to present the subject matter in a logical order, the thesis work is discussed in six chapters.

The text matter in Chapter–1, serves as an introductory part to the past and present status of the formability and fracture characterisation of EDD steel sheets. It also serves for the understanding of the present investigation and consequently defines the scope and objectives of research work. The overview of research work is briefly presented with major contributions and critical findings. This Chapter also discusses the logical order of presentation of the thesis work in six chapters.

Chapter–2 is a literature review for the present study. The literature review is presented in four major sections. First section presents literature review on various studies on formability characterisation of EDD steel sheets and consequently emphasises on the need for other alternative. Second section starts with the overview of fracture mechanics and subsequently presents literature on the past and present status of fracture behaviour of EDD steel as well as other sheet metals. The manner in which the present perspective of this thesis is reached is discussed in third section. Fourth section discusses various experimental methods and standards available on various issues related to fracture behaviour and their application feasibility to the present problem.

Chapter–3 discusses the methodology followed to study the formability and fracture behaviour. In Chapter–3, the experimental techniques required to fulfill the objectives of the present investigation are given at various stages. Various available experimental methods as well as mathematical relations are discussed for quantitative

fracture analysis. The suggested fracture criterion i.e. 'load drop technique' is explained. The suggested models namely, CFOA for crack initiation *CTOD* and critical crack tip opening angle (*CTOA*) for crack growth *CTOD* are explained in detail. This Chapter also gives a list of number of specimens and the specimen code followed for different objectives.

In Chapter–4, 3-D finite element analysis (FEA) of compact tension (CT) type specimen is discussed in order to verify the experimental results in generation phase. The commercial software ANSYS–7.0 (2002) is used for 3-D FE analysis. The idealisation of the problem and generation of crack tip element is discussed in detail. Non-linear (elastic-plastic) material model, virtual crack tip opening method and breaking strain as a fracture criterion are discussed. The procedure for the determination of fracture parameters like *J*, *CTOD* and the plastic zone size and shape is explained.

Chapter–5 presents the results and discussions on formability behaviour, fracture behaviour in generation phase, fracture behaviour in application phase and metallographic studies of EDD steel sheets. The comparative studies on the experimental and computational work are presented in tabular as well as graphical form. The results are discussed with reference to recently published articles and technical reports related to every specific objective. Summary, conclusions, advantages of the present work and suggestions in design are discussed in Chapter–6. A few suggestions for future scope of work are also mentioned at the end of Chapter-6.

The List of Tables, List of Figures, List of Abbreviations and List of Subscripts are presented after Contents. The References are cited in the text by author(s) name(s) with year of publication in parenthesis. In Reference section, the references are listed alphabetically by author's names, followed by initials, year of publication, title of the article, name of the journal (abbreviated according to standard practice), volume number, and numbers of first and last pages. The list of publications is shown after the Reference section. Appendices are labeled as A, B, C, ... etc., in the order of appearance. Various results on tensile tests, fracture tests, micrographs, additional observations and specifications of equipment and machines are included in Appendices. The brief biography of the supervisor and the student is given in the last two pages.

Chapter-2

LITERATURE SURVEY

2.1 Introduction

This chapter reports the major aspects of the background pertaining to the present problem from recently published literatures. The content of this chapter is grouped under four major sections. In the first section, basics on formability parameters, formability tests and their drawbacks are documented. In the second section, overview of fracture mechanics, background of fracture behaviour in thin steel sheets, and the present status are covered. In the third section, gap areas are defined and critical appraisal of the problem is presented. Fourth section selection deals with the selection of fracture parameters, test methods and their applicability for the present problem. This section also covers a literature on FE analysis. The referred journals are specified at the end of this Chapter.

2.2 Formability of Thin Sheets

One of the important characteristics of sheet metals is, high ratio of surface area to thickness. According to Ray (2000-2004), metal plate, flat or curved, having thickness between 0.5 mm and 6 mm is called sheet metal. The products made by sheet-forming processes include a large variety of shapes and sizes, ranging from simple bends to double curvatures with shallow or deep recesses. Compared to other manufacturing processes (e.g., casting, forging and machining), forming has several

technical and economical advantages. Steel, copper, aluminium and their alloys are most frequently used materials for formed parts. Low carbon steel (up to 1.5 % Carbon) is generally used for forming operations. However, for precision parts, according to ASTM standard 8 M (1999) and E 517-92 (1992), EDD steel sheets up to about 0.06 % Carbon is widely used.

Information about the formability of thin metal sheet is important to both, sheet manufacturers as well as users. From the manufacturer's point of view, the most significant is the knowledge of the characteristics of the sheet metal correlated to its formability and fracture behaviour. From the user's point of view, it is important to be able to select the semi-product that allows him to obtain finished products of definite size and shape without difficulties.

According to Hosford and Caddell (1993), sheet metal forming is the process of converting a flat metal sheet into a component of any desired shape without fracture or excessive localised thinning. The basic modes of forming a sheet metal are: stretching, drawing and bending. The primary difference between these forming modes originates from the nature of the strains imparted in the different directions in a sheet due to the forming operation. Stretching implies a forming process in which the strains along the principal directions in the sheet plane are tensile; while in drawing, a sheet is subjected to compressive strain in the circumferential direction together with tensile strain in the radial direction. Bending, the most common amongst the three is associated with tensile stresses on the outer surface along with compressive stresses on the inner surface of the deformed sheet.

The term formability of sheet metal can be defined as the relative ease with which a sheet can be shaped through plastic deformation. The term workability (instead of formability) is also used; but it is more popular with bulk deformation processes like forging, extrusion or rolling. Sheet metal formability is influenced by several process variables and material variables. The process variables determine the constraints of the forming process, while the material variables reflect the tendency of the material to deform easily. The process variables depend on the mode of forming whereas the material variables are of generalised nature for all the different modes. Different variables affecting the formability of EDD steels are discussed in the sub-section 2.2.1.

2.2.1 Variables affecting formability

Process Variables

According to Haung and Leu (1998), the prominent process variables are punch and die geometry, punch and die configuration, degree of lubrication, type of lubricants and clearances.

Material variables

The yield strength (S_y), modulus of elasticity (E), strain hardening exponent (n), strain rate sensitivity index (m), and normal anisotropy factor ($\bar{r}$) are the principal material variables that affect the formability of a sheet metal. The good deep drawing qualities are specified in ASTM standard 8 M (1999) and E 517-92 (1992). Based on these standards, following are the discussions on individual variables.

(a) Yield strength (S*y*)

It should be low enough so that it can be exceeded by the applied stresses in all localised regions during the forming process.

(b) Modulus of elasticity (*E*)

It should be high enough to keep the elastic spring-back at a minimum. Elastic spring back is the elastic recovery, which decides the final shape.

(c) Strain hardening exponent (*n*)

It signifies the intrinsic ability of the material to harden with plastic deformation, which is of tremendous importance in sheet metal forming. A higher value of *n* ensures a region undergoing thinning can resist further deformation, and can spread the deformation to its neighboring region. This process promotes uniform thinning. The important requirement for good formability is not only a high value of *n* but also maintaining it up to a large strain.

(d) Strain rate sensitivity (SRS) index (*m*)

It is defined as an increase in flow stress with increase in strain rate. The values of *m* for most of the cold forming materials are small (≈0.05). However, the presence of even a small value of *m* (e.g. 0.015 in low carbon steel) can be responsible for about 50% of the total elongation to failure.

(e) Normal anisotropy factor ($\bar{r}$)

Anisotropy is difference in behaviour of material in different loading directions. Anisotropy is present not only in the plane of sheet, but also in its thickness direction. The former is called planer anisotropy and the latter is called as normal or plastic anisotropy. Both should be high enough for good formability.

Apart from these variables, the necking or localised thinning of sheet material depends on material as well as process variables.

2.2.2 Formability tests

Different tests have been developed with time for evaluating sheet metal formability. Formability characterisation of materials is done either by using intrinsic tests or by carrying out simulative tests. The intrinsic tests attempt to measure some basic mechanical properties, which can be related to the formability of the material. On the other hand, by using simulative tests, attempts are made to achieve some engineering information about a particular forming process mostly on an empirical basis. Following are the brief discussions on intrinsic and simulative tests.

(a) Intrinsic Tests

The most widely used test is, plotting forming limit curve (FLC), which represents the acceptable limits of strains (in a plot of the principal major (ϵ_1) and minor (ϵ_2) strains in a sheet metal). The combination of principal major and minor strains leads to failure during forming. Keeler (1963, 1965) and Goodwin (1968) pioneered the construction of plotting FLC. The FLC is evaluated following Hecker's (1972) simplified technique. In this method, the experimental procedure mainly involves three stages: marking of grids in the sheet specimens, punch-stretching the grid-marked samples to failure or onset of localised necking and measurement of strains. In this test, the goal is to measure fracture strain in thin sheets.

Several investigations have been made to encompass large strain ranges in sheet metal forming using different geometries of punch and die and varying the

degrees of lubrication. Keeler (1965), Nakazima *et al.* (1968), and Hecker (1972) are some of the investigators on FLC, whose contributions are widely cited.

(b) Simulative Tests

According to Wu *et al.* (2000), the Erichsen and Olsen cup tests are the most popular simulative tests for formability characterisation. In these tests, a specimen is stretched using a hardened steel ball and the height of the cup thus produced is measured. In these tests, the engineering criterion of interest is to determine the maximum load at which a crack initiates.

According to Haung and Leu (1998), the test results are significantly influenced by the size of the penetrator, degree of lubrication and rate of drawing, and hence, careful control of these parameters is a pre-requisite. Another simulative test is the hole-expansion test. In this test, a flat sheet specimen with a circular hole in the centre is clamped between two annular die plates and deformed by a punch, which expands and ultimately cracks the edge of the hole. Flat bottomed, hemispherical and conical punches have been used. The test is terminated when a visible crack is observed and the hole-expansion is expressed as the percentage increase in the hole diameter.

2.2.3 Major drawbacks of formability characterisation

Following are the drawbacks of formability characterisation mentioned in various literatures.

(a) According to Ravi Kumar (2002), due to the complex interaction of large number of variables, which affects formability of sheet metals, there is no single parameter,

which can comprehensively describe the forming characteristics of a material under various conditions in actual press working.

(b) According to Wu *et al.* (2000), in formability limit curves, the construction becomes time consuming and tedious and consequently is limited in engineering applications. Since the measurements involve some amount of subjective judgment in defining necking, a band of ± 2% in engineering strain values is drawn instead of a single line.

(c) According to Rao and Mohan (2000), measure of cup depth and hole-expansion in simulative tests is an empirical basis because cup depth or hole-expansion brings out a relative engineering index for formability. However, these tests lack any fundamental scientific basis in such quantitative measurement.

The use of Olsen or Erichsen cup tests in association with FLC constructions is an appropriate solution for characterising the quality of sheet metals. However, from the engineering applications point of view, it leads one for the search of alternative criterion for obtaining fracture limits of sheet metals.

2.3 Fracture Behaviour in Thin Sheets

2.3.1 Overview of fracture mechanics

The science of fracture mechanics was born and came to maturity in the 20th century. Its literature is now vast. For a long time men had some idea about the role of a crack or a notch. While cutting a tree, he would make a notch with an axe at its trunk and then pull it down in a particular direction with a rope. As mentioned by Cotterell (2002), Leonardo da Vinci (1452-1519) was the first person to make a setup to

measure the strength of a wire. Griffith (1920) developed the right ideas for growth of a crack in 1920s. The energy release, when a crack advances is measured with a parameter called, energy release rate, denoted by the symbol G in honor of Griffith. For all practical purposes, the modern fracture mechanics was born in 1948 when Irwin (1948) formulated the fracture mechanics and devised a workable parameter like stress intensity factor K. Since K completely defines the state of stress at the crack-tip, crack initiation can be assumed to occur when a critical value of stress intensity factor (K_{Ic}) of the material is exceeded. However, K presumes totally linear elastic conditions as mentioned by Anderson (1994).

According to Anderson (1994), Irwin's analysis is mainly for brittle or low ductile materials. The analysis is conservative for most engineering materials which are generally ductile. Other parameters like *CTOD* by Wells (1961) and J-integral by Rice (1968) are developed to account for elastic-plastic analysis ahead of the crack tip. In last three decades, more realistic computational methods like finite element method, finite difference method are extensively used for understanding of fracture behaviour for elastic-plastic analysis.

As mentioned by Kulkarni *et al.* (2004b), in recent years, the field of fracture mechanics is widely used for failure analysis and prevention. More recent work has gone a step further, incorporating time-dependent non-linear material behaviour. Fracture mechanics has also been used in the characterisation of composite materials e.g. Castrodeza *et al.* (2004). The crack propagation problems, which are difficult with simple finite element method, are solved with the help of meshless methods as described by Rao and Rahman (2003).

2.3.2 Fracture behaviour in steel sheets and the present status

In recent years, there have been considerable emphasis in the production of Deep Drawn and Extra Deep Drawn (EDD) steel sheets in industries. The wide applications of EDD steel sheets are well known not only for domestic appliances like storage containers, bodies of electric motor, refrigerator and washing machine and household utensils, but also for automotive applications. As communicated by Ray (2000-2004), with increasing global competition for quality materials, there is a need to understand the fundamentals of crack initiation in these bulk products. The event of crack initiation and crack propagation could be precisely determined using fracture mechanics principles; but so far, little attention has been paid in this direction in case of thin sheets.

According to Liu and his co-workers (1976, 1978 and 1981), the basic principle for obtaining fracture criteria of thin and tough sheets / plates is related to examinations of a strip necking zone which remains embedded inside the plastic zone ahead of a crack tip in a deformed specimen. These investigators have contended that such strip necking phenomenon is governed by the ratio of the plastic zone size and the plate thickness (B), and they concluded that a physical parameter $(K/S_Y)^2/B$ controls the occurrence of crack tip necking. The parameter henceforth will be referred to as the strip necking parameter. In addition, Liu and Kuo (1978) and Liu (1981), have observed that the crack tip opening displacement in the strip necking zone is equal to the thickness contraction at the crack tip as given by Eq. (2.1) for HY-80 steel.

$$CTOD = \delta_n = \varepsilon_z . B \tag{2.1}$$

where, δ_n is thickness contraction at the crack tip and ε_z is strain in thickness direction. The *CTOD* in turn is related to the stress intensity factor. The estimation of the stress intensity factor for tough and thin plates by Liu (1981) has been carried out following the Dugdale model (1960), using the relationship (Eq 2.2):

$$\frac{K^2}{E} = S_y.CTOD = S_y.\delta_n \tag{2.2}$$

The salient conclusions of Liu's reports (1981) indicate that the near tip strain or crack tip contraction can be used as a fracture criterion. The replica technique is used for the detection of crack tip necking and Moire fringe technique is used for the detection of crack tip opening displacement. However, these techniques could not become popular, as they are too elaborate in nature to employ them for quality control of sheet metals in terms of fracture mechanics based criteria. In addition, these investigations have not indicated any rationale for detecting the physical event of crack initiation.

Atkins and Mai (1987) have proposed a relationship between the specific work on fracture obtained from test pieces incorporating starter cracks and the work required locally to nucleate a crack in flawless thin sheet metals. According to him, the failure of thin sheets during forming occurs first by localised necking, which is then followed by fracture inside the neck. Problems of the effect of necking preceding fracture are also studied by Atkins (1993, 1995 and 1997). However, these investigations address how damage should be added in a 'plane strain neck'. Also these investigations do not consider effect of thickness, effect of strain rate and effect

of notch radius on necking, which in turn leads to fracture. Majerus and Santhanam (1997) have studied an anisotropy effect in thin plates of aluminium alloy 7075-T651. They have shown a significant effect of anisotropy in plane stress condition characterised by stress intensity factor. However, as mentioned by Kumar (1996), the hot rolled and cold rolled sheets are subjected to annealing treatment to relieve the internal stresses and eliminate any anisotropy in the alloy. The anisotropic effects in strips or sheets are reported to be highly detrimental to sheet forming and deep drawing operations. Recently, Cotterell *et al.* (2002) have studied the dependence of micro-hardness on deformation of deep-drawing steel sheets with a formability approach. More recently, Seshadri and his team (1998) have presented a report on stable tearing and residual strength behaviour of a flat 7475-T7351 aluminium alloy panel using finite element analysis.

2.4 Critical Appraisal of the Present Problem

After going through this literature, three important issues are pointed out. Firstly, various literatures are available on formability characterisation of EDD steel sheets. However, investigation on fracture behaviour of EDD steel sheets is not reported. Secondly, investigations on other sheet materials are to search for an appropriate fracture criterion. Thirdly, every investigation shows a study on specific issue (e.g. anisotropy effect, necking effect, micro-hardness effect, etc.) related to fracture behaviour in thin sheets. However, for complete characterisation of sheet material, study of forming qualities, fracture behaviour in generation phase and fracture behaviour in application phase is perceived to be essential.

The motivation for this work stems directly from the needs of a sheet (i.e. semi-product) manufacturers and users who finishes a semi-product into a finished product. A study of complete fracture behaviour is important to both of them. Complete Fracture behaviour of thin sheets requires a promising line of attack for the prediction of the onset of fracture. Further, to establish a criterion for crack initiation in ductile fracture needs huge experimental trials before coming to specific conclusion. The complete characterisation of fracture behaviour of EDD steel sheet requires an extensive work on various influencing parameters. These are like deep drawing qualities, thickness effect, strain rate effect, influence of notch radius, and effect of necking on crack initiation. The crack growth study is also essential in order to tolerate some amount of crack extension during application phase.

2.5 Review on Test Methods

For a complete fracture study, fracture criterion, selection of proper test methods and suitable fracture parameters are essential in generation as well as in application phase. According to Anderson (1994), the *J*-integral and *CTOD* are the suitable parameters to describe crack tip conditions in elastic-plastic materials. However, the existing fracture criterion, test methods need to be reviewed and modified in order to understand the significant deformation ahead of crack tip. Following sub-sections 2.5.1 - 2.5.6 discuss on available fracture criteria, ASTM standards, test methods and their applicability or limitations to the present problem.

2.5.1 Fracture criterion

According to Pardoen and Delannay (2000), in very tough metals, the main issue is not crack initiation but rather crack propagation. However, in case of EDD steel sheet applications, it is very essential to predict accurate value of crack initiation toughness. Thus, these data could be used to design any critical components. The analyses of the load – load-line displacement curve are generally used to determine the load at crack initiation.

As mentioned in annual book of ASTM standards (1987), the general practice to find out point of crack initiation is by drawing a 5% secant line having its slope 5% less than the initial slope of load – load-line displacement curve. This method is similar to 0.2% offset used in determining yield stress of a material, mentioned by Callister (2003). As mentioned by McClintock (1971), Bray *et al.* (1992) and Sun *et al.* (1994), the 'blunting line' method is questionable when blunting is very large as in thin ductile plates. Several indirect methods like acoustic emissions, resonance frequency, given by Eng and Gang (2001), can be used in order to detect cracking initiation. The success of these methods varies from material to material and from geometry to geometry. In addition, these methods rely on a preliminary assessment of their sensibility by comparison to an independent and accurate detection of cracking initiation. Theoretically, measurement of a stretch zone width can be correlated to the value of the *CTOD* at cracking initiation. Measurement of stretch zone width requires only one broken specimen and does not necessitate the detection of crack initiation. However, according to Pluvinage and Lanvin (1993), this method gives large experimental scatter, which depends on the way the measurement is performed. It

outlines a test method for estimating the critical J near initiation of ductile crack growth in elastic-plastic materials. This standard is described in detail in Chapter-3 and used for the present analyses.

2.5.3 *CTOD* estimation methods

High toughness is obviously desirable to designers and fabricators. The degree of crack blunting increases in proportion to the toughness of the material. There are a number of alternative definitions of *CTOD*. The displacement at the original crack tip is given by Wells (1961) and 90° intercept is given by Rice (1968). These two methods are shown in Fig. 2.1 (a) and (b).

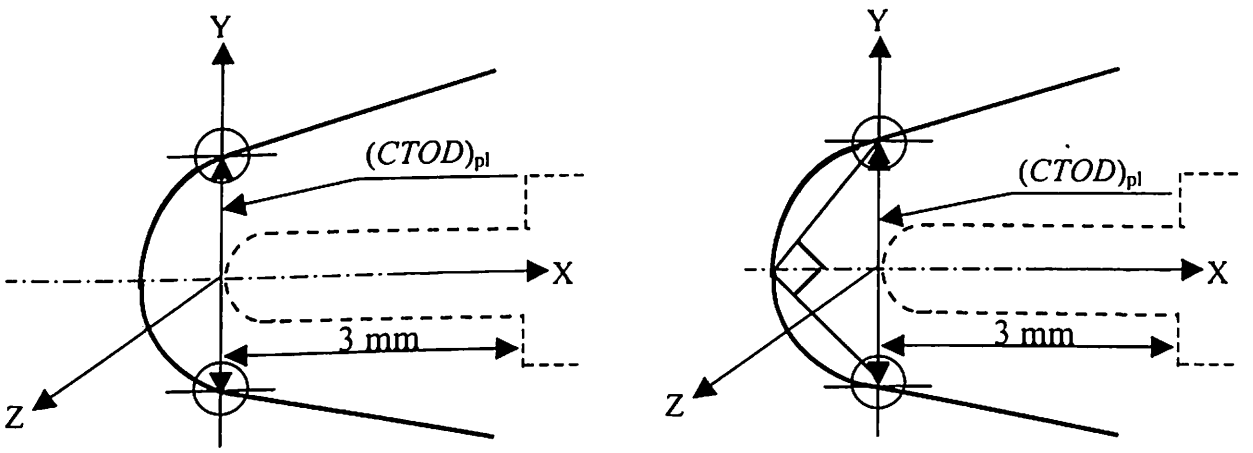

Fig.2.1 Measurement of *CTOD* **(a)** using the displacement at the original crack tip. **(b)** 90° intercept method.

Using these methods, Kulkarni *et al.* (2002, 2003a) have published the results on fracture behaviour of EDD steel sheets. The former method requires a profile projector to superimpose the crack geometry before and after fracture test and find out the *CTOD* at original crack-tip. This could also be measured with the help of an optical microscope with reference to non-deformed dimension. In 90° intercept

method, two mutually perpendicular lines are drawn at blunt notch tip using an image of notch profile after the test. These lines intersect the crack flanks. The distance between two intersecting points at crack flanks is inferred as a plastic *CTOD*.

Standard methods for *CTOD* testing described in BS 5762: 1979 and ASTM E 1290-89 adopt a plastic hinge model (PHM) in which displacements are separated into elastic and plastic components. The PHM is based on determination of plastic rotational factor (PRF) r_{pl}, which allows the *CTOD* value to be extrapolated from load-line displacement data. According to ASTM E 1290-89, the PRF value for compact tension (CT) specimen is given by Eq. (2.3).

$$r_{pl} = 0.4\left\{1 + 2\left[\left(\frac{a_0}{b}\right)^2 + \frac{a_0}{b} + 0.5\right]^{1/2} - 2\left[\frac{a_0}{b} + 0.5\right]\right\} \tag{2.3}$$

The PRF value depends on initial crack length and unbroken ligament length as seen from Eq. (2.3).

A large bank of PRF data is already published by Kumar and Bhattacharya (1995) and Bhattacharya and Kumar (1995a, 1995b). Various standards like BS 5762 (1979), GB 2358-80 (1980) accept different values of PRF for the estimation of *CTOD* values. Results on plastic *CTOD*, based on PHM with PRF given by Merkle and Corten (1990) are published by Kulkarni *et al.* (2002, 2003a and 2004a). This is explained in sub-section 3.5.2 (a). However, these reports lead to measure a PRF value, which does not account the thickness of specimen.

2.5.4 *J-CTOD* relation

The Shih analysis (1981) showed that there is a unique relationship (Eq. 2.4) between *J* and *CTOD* for a given material.

$$J = \frac{\delta . S_y}{d_n} \tag{2.4}$$

where, δ is *CTOD*, S_y is yield strength and d_n is a Shih factor. *J* and *CTOD* are two equally valid crack-tip characterising parameters for elastic-plastic materials. As mentioned above, the *J*-integral and *CTOD* are connected. Thus, if *J* is a feasible measure of the crack tip conditions, so are *CTOD*.

2.5.5 Finite element analysis

Finite element analysis (FEA) is one of the numerical methods widely used in fracture mechanics applications. The important aspects of FE analysis are selection of element to model the crack region and modeling of the material behaviour. As mentioned in the report of Degiorgi and Matic (1990), the singular element, derived by Blackburn (1976) is capable of sustaining the anticipated large strain. According to Newman (1984), the nonlinear material behaviour can be modeled using incremental theory of plasticity.

Newman *et al.* (1984, 1991 and 2003) has used a small strain code, wherein true stress-strain curve up to ultimate strain value is used for plane strain analysis. However, a large strain code with multi-linear isotropic hardening is used by Kulkarni *et al.* (2004a) to account for the necking (i.e. crack tip contraction). In large strain code, true stress-strain curve is used up to a breaking-strain point with constant value of ultimate stress beyond the ultimate point on the curve. Virtual crack tip

opening method described by Kulkarni *et al.* (2004a) can be used to find *J*-integral and *CTOD*. In virtual crack tip opening method, the coincident nodes in the wedge shaped elements along the crack front are left unconstrained to allow appropriate development of crack tip blunting.

2.5.6 *R* curve characterisation

According to Kumar (1989), the prediction of failure by crack extension is one of the main issues in the assessment of safety and reliability of components for industrial applications. Crack growth resistance in high toughness ductile materials is characterised using *J-R, CTOA-R and CTOD-R* curve.

The ASTM standards E 813-87 (1987) and E 1152-87 (1987) produce *R* curve, a plot of *J* versus crack extension. The ASTM standard E 1152-87 applies to the entire *R* curve, while E 813-87 is concerned only with *J* value at crack initiation, a single point on the *R* curve. As per ASTM standard E 1152-87, only single specimen test with unloading compliance is allowed. According to this standard, test specimens should be side grooved in order to avoid tunneling and maintain a straight crack front. In addition, the standard has limits on size of the specimen and crack growth. Many users would like to extend the crack growth limits, because ductile stability analysis of structures typically requires an *R* curve data with large amounts of crack growth. The recent standard, ASTM E 1820-01 (2001) poses no limitations on type of specimen, crack tunneling, size of the specimen and amount of crack growth. The standard is explained in Chapter-3 for the crack growth behaviour study.

In several investigations of Heerens and Schodel (2002), Dawicke and Sutton (1994) and Dawicke *et al.* (1999) light microscopy and optical methods have been used to determine critical crack tip opening angle (*CTOA*) on laboratory specimens. In general these techniques are not easy to apply. In the present work, as mentioned by Kulkarni and Ravi Prakash (2004c), a simple geometric model on critical crack tip opening angle (*CTOA*) is suggested.

2.6 Referred Journals

The important referred journals on formability characterisation are: Journal of Material Processing Technology (1986–2003), Material Science and Engineering (1999 – 2000), Material Science and Technology (1985), *Material Transaction*, JIM (1998). For the fracture behaviour study, the important referred journals are: *Engineering Fracture Mechanics* (1976–2004), *International Journal of Fracture* (1987 – 2003), *Fatigue and Fracture of Engineering Materials* (1992–2003), *Theoretical and Applied Fracture Mechanics* (1995–2003), *International Journal of Mechanical Sciences* (1995-2003) and *International Journal of Pressure Vessel and Piping* (1990-1998).

Chapter -3

EXPERIMENTAL PROCEDURE

3.1 Introduction

Various tests are conducted to investigate the complete characterisation and fracture behaviour of EDD steel sheets. For the determination of fracture parameters, available and suggested experimental methods are discussed in detail. The number of specimens along with their specimen codes and geometry are tabulated for various objectives. The preparation for the metallographic study is also discussed to understand the phenomenon of ductile tearing process.

3.2 Methodology

The methods of accomplishing the experimental programme involve testing EDD steel sheets using compact tension (CT) type specimen. Three EDD materials are selected for the present study. They are designated as EDD335, EDD277 and EDD258, wherein the three-digit number stands for the yield strength value in MPa. The complete characterisation of fracture behaviour is done in three parts, namely: 'formability behaviour', 'fracture behaviour in generation phase' and 'fracture behaviour in application phase'. In formability part, some data is obtained from the manufacturer, Ray (2000-2004). For complete fracture behaviour study, mechanical

tests, chemical analysis, grain size measurement, fracture test for crack initiation and fracture test for crack propagation are conducted. The post fracture tests and metallographic study is done to verify critical observations. Various experimental techniques and ASTM standards are used to achieve the results. For comparative study, numerical analysis is done by finite element method using standard commercial software ANSYS 7.0 (2002). The details of experimental procedure, various tests, referred ASTM standards, experimental programme, preparation for metallographic study is studied in subsequent sections.

3.3 Experimental Procedure

Various tests and ASTM standards, followed in the present investigations are discussed in this section.

3.3.1 Specimen preparation

The geometry of CT specimen used in the current work is as per the recommended design in ASTM standard E 399-91 (1991). Specimens are fabricated by using wire electric discharge machine (WEDM) to maintain the exact relationship in between all the dimensions. During wire cutting operation, a bunch of ten to twelve specimens, placed on a stack is cut, which reduces the cost as well as time. Instead of fatigue pre-cracking, a notch is cut with a 0.2 mm wire diameter. This operation creates a notch of 0.1 mm radius. Because of unavoidable heating during the notch cutting process,

notch radii are not exactly 0.1 mm. The radii have gone up to about 0.13 mm. The configuration of the test specimen is shown in Fig. 3.1 (a). Fig. 3.1 (b) shows the photograph of prepared CT specimen using WEDM process. The photograph of notch-profile is taken using a digital camera attached to optical microscope at a magnification of 100X. The notch radius is measured on the photograph, as shown in Appendix D. All specimens in the current study are fabricated with crack/notch perpendicular to rolling direction.

The specimens are ground with emery papers following 1/0 (coarse), 2/0, 3/0 and 4/0 (fine). In order to have surface finish sufficient to distinguish between the elastic and plastic zone, these specimens are then polished first using alundum and finally using 0.25 μm diamond paste in polishing machine. A set of anti-buckling guide plates are designed and fabricated to avoid out-of-plane buckling during testing. The critical dimensions along with their codes are given in Table 3.1 to Table 3.4 for various studies.

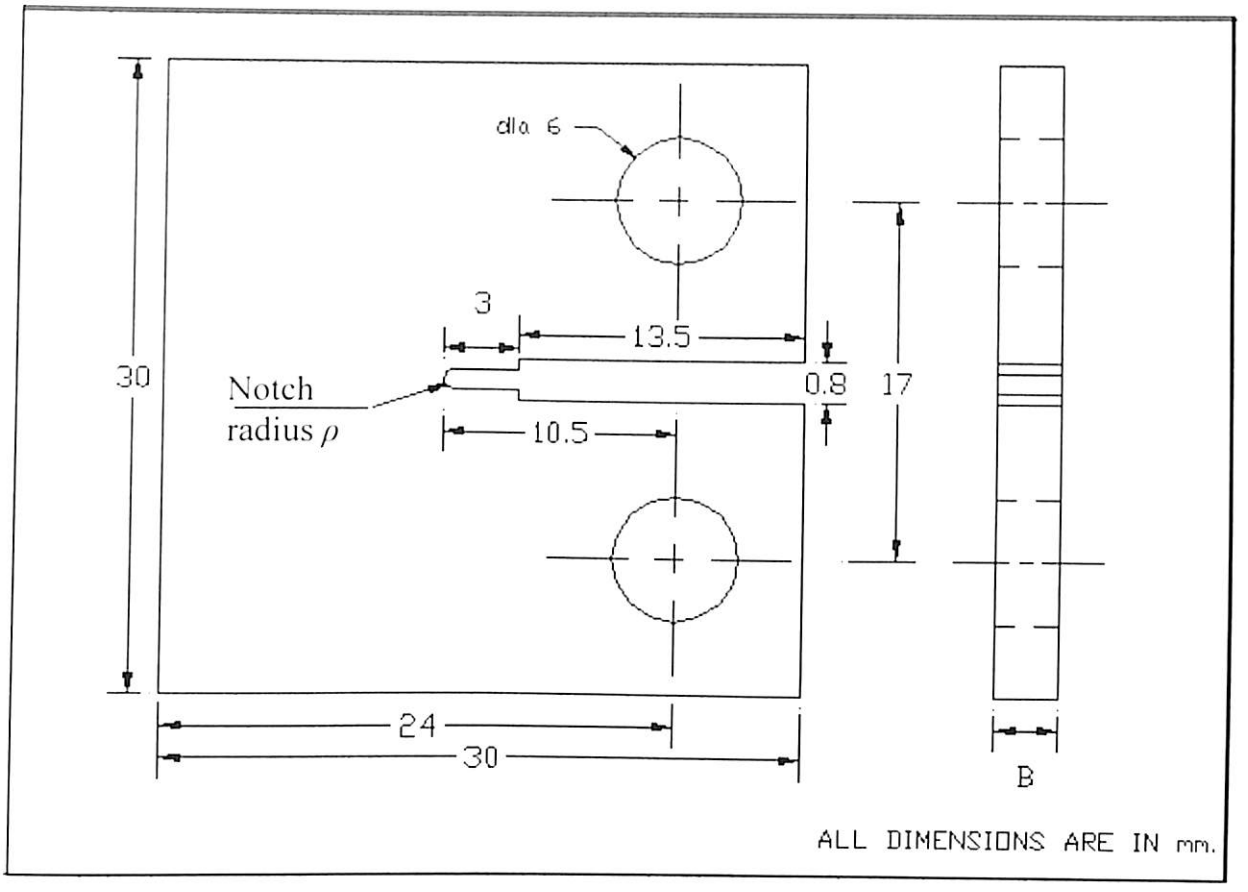

Fig. 3.1. (a) Geometry of the test specimens used in fracture test as per ASTM E 399-91.

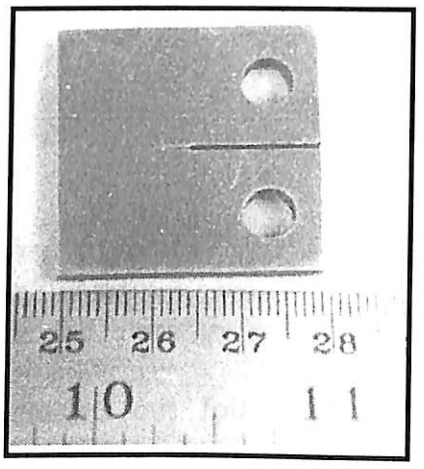

Fig. 3.1 (b) Prepared CT specimen using WEDM process.

3.3.2 Chemical analysis

The chemical composition of the materials (in wt. %) is analysed by using a chemical analyser, made by Worldwide Analytical System (WAS), model Foundry Master. The nitrogen content (in ppm) is estimated in the EDD steel samples using a LECO gas analyser. The information of model for these two equipments is given in Appendix F.

3.3.3 Grain size measurement

The two-dimensional grain size is measured using the average linear intercept method as described by Callister (2003). The average grain size is determined from individual grain intercept by viewing the two-phase microstructure at a magnification of 1000X. In this method, a graduated line grid is superimposed on the microstructure and the number of the smallest divisions of the grid intercepted by individual ferrite grain is counted. A total number of 300 random intercepts are considered for obtaining the average value of the grain size.

3.3.4 Mechanical tests

Tensile test data is obtained from Ray (2000-2004), Scientific Services Division, TISCO Jamshedpur. As per the literature and technical reports sent by Ray (2000–2004), tensile tests are carried out following ASTM standard E 8 M (1999) specification. The specimens are tested along the three directions, with the tensile axis being parallel (0^{o}), diagonal (45^{o}), and perpendicular (90^{o}) to the rolling direction of the sheet. The standard tensile properties namely, yield strength (YS), ultimate tensile

strength (UTS), uniform elongation (e_u), total elongation (e_f) and strain hardening exponent (n) are determined from the load–elongation data obtained from these tests. A constant cross head speed of 0.5 mm/min is employed in all cases. Three samples are tested in each of the three directions and average values are taken to account for the scatter.

Strain rate sensitivity index, m, is calculated from the results of strain rate jump tests carried out on tensile specimens. The strain rate is suddenly increased during the uniform plastic deformation and in such a strain rate change test, m is defined according to Dieter (1988) as Eq. (3.1).

$$m = \frac{\ln(\sigma_2 / \sigma_1)}{\ln(\varepsilon_2 / \varepsilon_1)} = \frac{\ln(P_2 / P_1)}{\ln(V_2 / V_1)} \tag{3.1}$$

where, σ_1 and σ_2 are flow stress values at strain rates ε_1 and ε_2, respectively. P_1 and P_2 are loads corresponding to cross head speeds of V_1 and V_2, respectively. The Vicker's hardness (HV) of the three EDD steels is measured using SHIMADZU-HMV hardness testing machine. The specifications are given in Appendix F.

3.3.5 Formability parameters

The strain hardening exponent (n), normal anisotropy ($\bar{r}$), strain rate sensitivity index, yield strength and modulus of elasticity are the conventional indicators of formability of sheet metals. According to Caddell (1980), the stain hardening exponent is taken as value of ultimate true strain (ε_u) from the true stress – true strain

data. The normal anisotropy is calculated using the standard formula (Eq. 3.2) obtained from Hosford and Caddell (1993).

$$\bar{r} = \frac{1}{4}(r_{0} + 2r_{45} + r_{90}) \tag{3.2}$$

where, the r_0, r_{45}, and r_{90} are the strain ratios along 0, 45 and 90 degree to rolling direction, respectively given by Eq. (3.3).

$$strainratio = \frac{true - widthstrain}{true - thicknessstrain} \tag{3.3}$$

The values of strain ratio are obtained from the supplier of EDD steel material. ASTM E 8 M (1999) and E 517-92 (1992) standards are used to access the deep drawing qualities.

3.3.6 Fracture test

The fracture tests are carried out using a 100 kN Universal Testing Machine (FIE make). The specifications of this machine are given in Appendix F. The experimental set up is shown in Fig. 3.2 (a). The lower load cell (0 – 5 kN) is used for more accuracy.

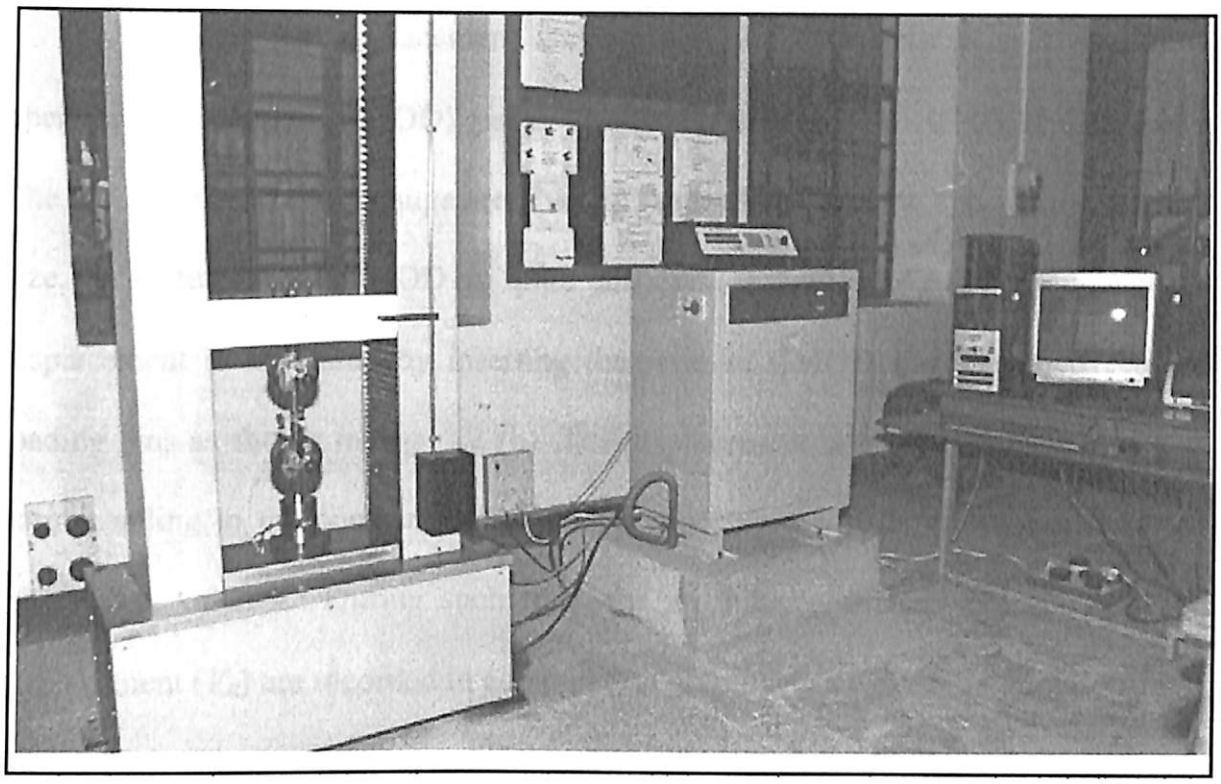

Fig. 3.2 (a) Schematic of Experimental set-up for the fracture test.

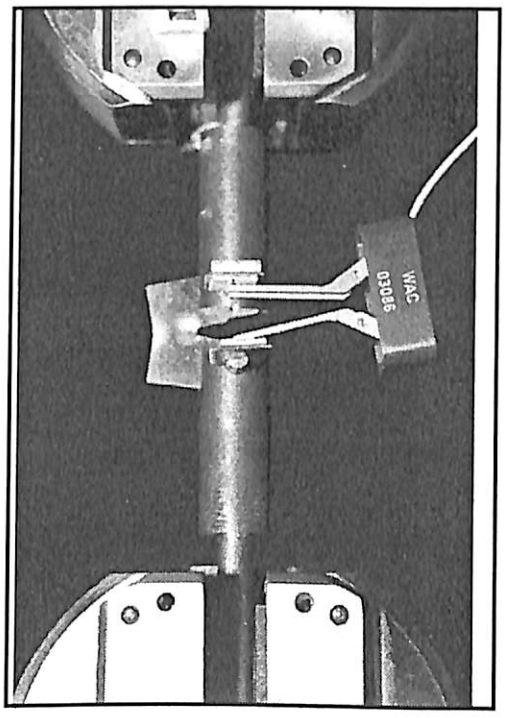

Fig. 3.2 (b) Test set-up for CT type specimen along with the CMOD gauge.

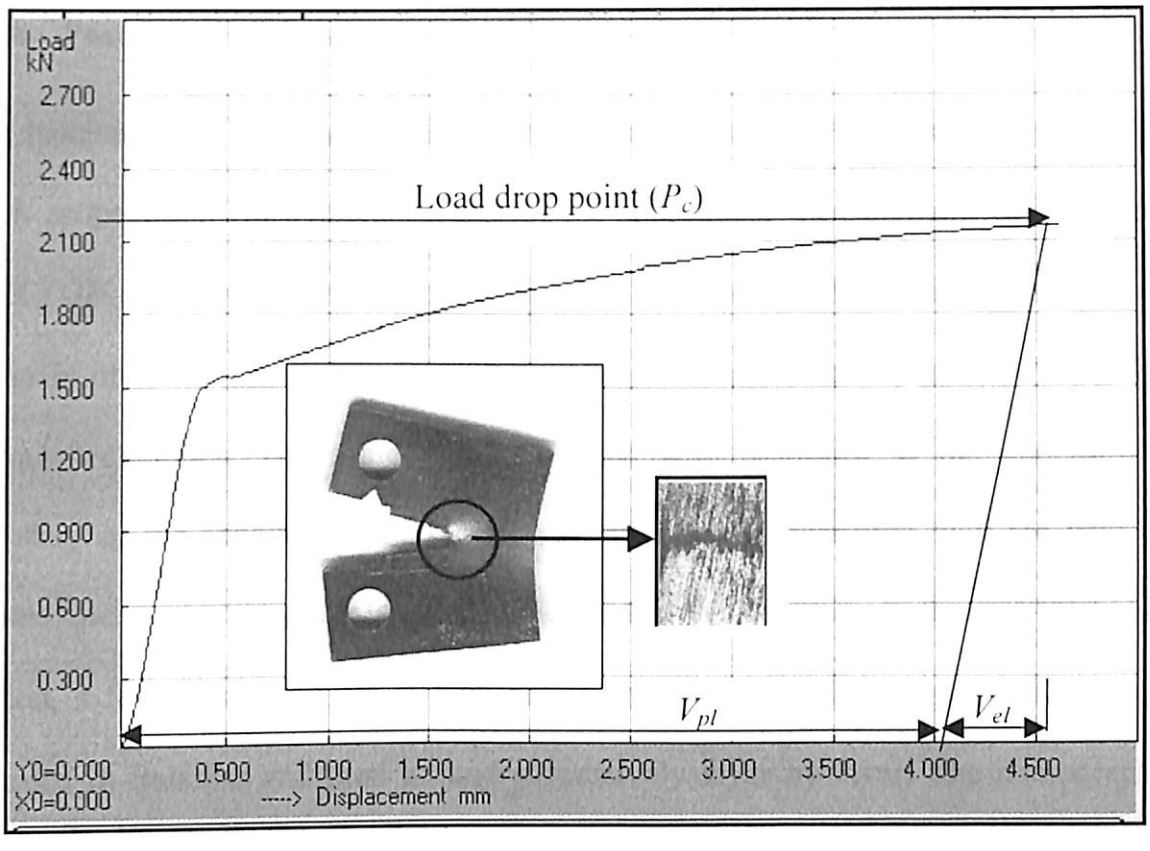

Fig. 3.3 Load drop in load – load-line displacement plot as a fracture criterion along with a micrograph (200X) showing the event of crack initiation in CT specimen.

It is observed from Fig. 3.3 that, load is continuously increasing till a P_c value, however, the rate of increment of load just before the critical load is very low as compared with prior portion of the plot. The rate of increment of load continues to decrease and as soon as surface crack initiates, load drops. This observation is unlike other engineering materials, in which, crack initiates before the maximum load reaches. This is due to excessive plasticity possessed by the material before it fractures. Therefore in case of EDD materials, the critical event of cracking initiation is defined as the load drop point, at which the process of plastic deformation at the original crack tip (i.e. the blunting process) is stopped.

3.3.8 Post fracture tests

The specimens are taken out at the event of crack initiation (in generation phase) or crack propagation (in application phase) for subsequent measurement of *J*-integral and *CTOD*. Specimens are scanned using a flat bed scanner (HP make) and a skeleton figure is obtained using AutoCAD2000 software to measure the plastic *CTOD* by various techniques. The scale factor is taken with reference to the undeformed boundary of the specimen. The crack tip contraction is measured with the help of pointer micrometer. In order to check, whether the crack initiates at the mid-thickness section, a few specimens are chosen before and at the load drop point. These are mounted in Bakelite and then ground successively layer by layer. The photographs are taken with a digital camera attached to optical microscope to study the damage and microstructure ahead of a crack tip. This is to check the validity of fracture criterion with the help of a damage study ahead of crack tip. The thermal shock treatment is done using liquid nitrogen to break the specimens along the crack. The fracture surfaces of broken open up specimens are studied to check the validity of fracture criterion.

3.4 Estimation of *J*-Integral

Rice *et al.* (1973) proposed to determine *J*-integral directly from the load – load-line displacement curve. The ASTM standard E 813-87 (1987) outlines a test method for estimating the value of *J* near crack initiation of ductile materials. For estimation

purpose by ASTM E 813-87, J_c is divided into elastic and plastic components as given by Eq. (3.4).

$$J_c = J_{el} + J_{pl} \tag{3.4}$$

The elastic J is computed from the elastic stress intensity for plane stress condition using Eq. (3.5).

$$J_{el} = \frac{K^2}{E} \tag{3.5}$$

Referring to Murakami (1987), K, the linear stress intensity factor for CT specimens can be obtained by using Eq. (3.6).

$$K = \frac{P}{BW^{1/2}} f(\alpha) \tag{3.6}$$

The value of P is equal to P_c, load at crack initiation, B is the thickness of specimen, W is the width of the specimen and

$$f(\alpha) = \frac{(2+\alpha)(0.886 + 4.64\alpha - 13.32\alpha^2 + 14.72\alpha^3 - 5.6\alpha^4)}{(1-\alpha)^{3/2}}$$

where, $\alpha = \frac{a_0}{W}$.

The ASTM standard enables the plastic J to be estimated from the plastic area (A_{pl}) under the load – load-line displacement curve (Fig. 3.3). J is defined in terms of the energy absorbed divided by the net cross sectional area (Thickness (B) x unbroken ligament length (b)) as shown in Eq. (3.7).

$$J_{pl} = \frac{\eta A_{pl}}{Bb} \tag{3.7}$$

where, A_{pl} is the area under load – load-line displacement curve, the geometry factor $\eta = 2.0 + 0.522(1 - a_0 / W)$ and b is unbroken ligament length.

3.5 Estimation of Critical *CTOD*

According to the ASTM standard E 1290-89, the critical crack tip opening displacement during the loading consists of elastic and plastic part, given by Eq. (3.8)

Critical *CTOD* = Elastic *CTOD* + Plastic *CTOD*

$$\delta_c = \delta_{el} + \delta_{pl} \tag{3.8}$$

3.5.1 Calculation for the elastic part (δ_{el})

The elastic part is calculated by using a standard Eq. (3.9) for plane stress condition,

$$\delta_{el} = \frac{K^2}{ES_y} \tag{3.9}$$

where, the elastic modulus (E), and yield strength (S_y) are the mechanical properties. The linear stress intensity factor K is calculated from Eq. (3.6).

3.5.2 Calculation for the plastic part (δ_{pl})

It seems reasonable to assume that the crack initiation of a ductile material is based solely on the plastic deformation behaviour near the crack tip. In the present investigation, the plastic *CTOD* is estimated by using four methods. The plastic *CTOD* is measured with the help of existing plastic hinge model (PHM) specified in ASTM E 1290-89 (1989), crack flank opening angle (CFOA) model and from *J*-

CTOD relation specified by Shih (1981). These methods are discussed in next sub-sections. The fourth method based on FE analysis is discussed in Chapter-4.

(a) Plastic hinge model (PHM)

The plastic *CTOD* (δ_{pl}) is determined by assuming that the unbroken ligament works like a plastic hinge with its center (i.e. apparent axis of rotation) at a distance $r_{pl}b$ from the crack tip (G) as shown in Fig. 3.4 (a). Referring to the Fig. 3.4 (a) and (b): O is the apparent axis of rotation, G is crack tip, AB is plastic part of the *CTOD*, CD is plastic load-line displacement (V_{pl}), and GH is initial crack length (a_0). The OG is taken equal to $r_{pl}b$, where r_{pl} is a plastic rotational factor and b is the unbroken ligament length.

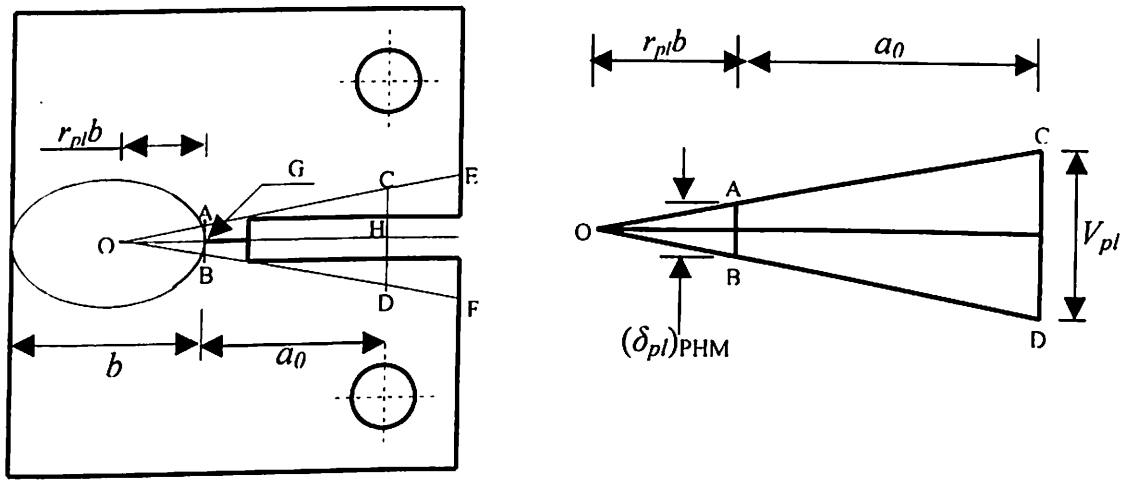

(a) **(b)**

Fig. 3.4 Plastic hinge model to determine plastic *CTOD*.

From properties of the similarity of triangles given in Fig. 3.4 (b),

$$\frac{AB}{CD} = \frac{OG}{OG + GH} \quad \text{or} \quad \frac{(\delta_{pl})_{PHM}}{V_{pl}} = \frac{r_{pl} b}{r_{pl} b + a_0}$$

$$(\delta_{pl})_{PHM} = \frac{r_{pl} b}{r_{pl} b + a_0} V_{pl} \tag{3.10}$$

Eq. (3.10) gives a plastic *CTOD* based on a plastic hinge model. According to Merkle and Corten (1990), the value of PRF is given by Eq. (3.11).

$$\text{PRF} = r_{pl} = (1+\beta)/2 \tag{3.11}$$

where, $\beta = \left[\left(\frac{2a_0}{b}\right)^2 + \frac{4a_0}{b} + 2\right]^{1/2} - \left[\frac{2a_0}{b} + 1\right]$. The value for V_{pl} is taken from Fig. 3.3. With the help of equations (3.8), (3.9) and (3.10), the value of critical *CTOD* (δ_c) is calculated. This model assumes a linear relation between plastic load-line displacement (V_{pl}) and plastic *CTOD* (δ_{pl}). According to Wilson and Landes (1994), this model can be used for smaller plastic load line displacement. In case of EDD steel sheet, it is observed that there is a significant deformation ahead of crack tip resulting in higher value of plastic load line displacement. Moreover, in PHM, the determination of PRF is independent of thickness of the specimen.

(b) Crack flank opening angle (CFOA) model

This is a modified plastic hinge model to account for the non-linearity between plastic *CTOD* and plastic load-line displacement. The photograph of a specimen is taken using flat bed scanner. The scanned image of specimen is imported in drafting

software AutoCAD-2000 and a skeleton figure is obtained as shown in Fig. 3.5. Similar to PHM, the plastic portion (δ_{pl}) is determined by assuming that the unbroken ligament works like a plastic hinge with its center at a distance O'G from the crack tip G as shown in Fig. 3.5.

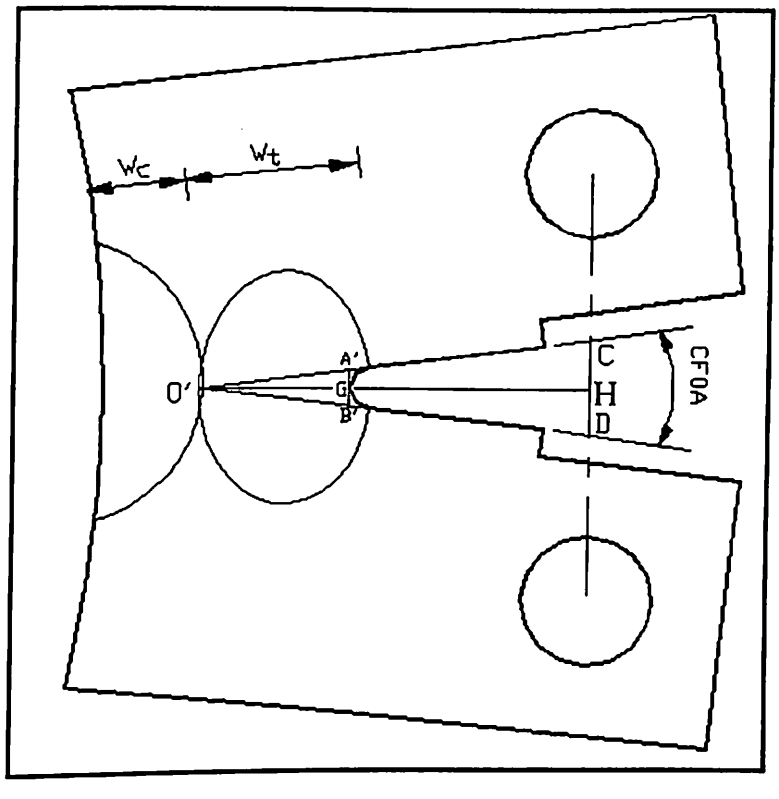

Fig. 3.5 CFOA model to determine plastic *CTOD*.

Referring to the Fig. 3.5, A'B' is the plastic part of *CTOD* i.e. $(\delta_{pl})_{CFOA}$, CD is plastic load line displacement, and GH is initial crack length. In this model, the common point of tensile plastic and compressive plastic zone along the unbroken ligament length is taken as an apparent axis of rotation, as shown in Fig. 3.5. This is due to the reason that the apparent axis of rotation acts as a neutral axis similar to neutral axis in theory of bending. This is also supported by hardness measurement

along the unbroken ligament length as discussed in section 5.14. It is observed that the location of point O′ depends on crack flank opening angle (CFOA) which in turn depends on thickness of specimen. This location can be obtained as an intersection of lines coinciding with the crack flanks. The angle made by two crack flanks is measured at point O′ as CFOA. The width of compressive zone and tensile zone is shown as W_c and W_t, respectively in Fig. 3.5.

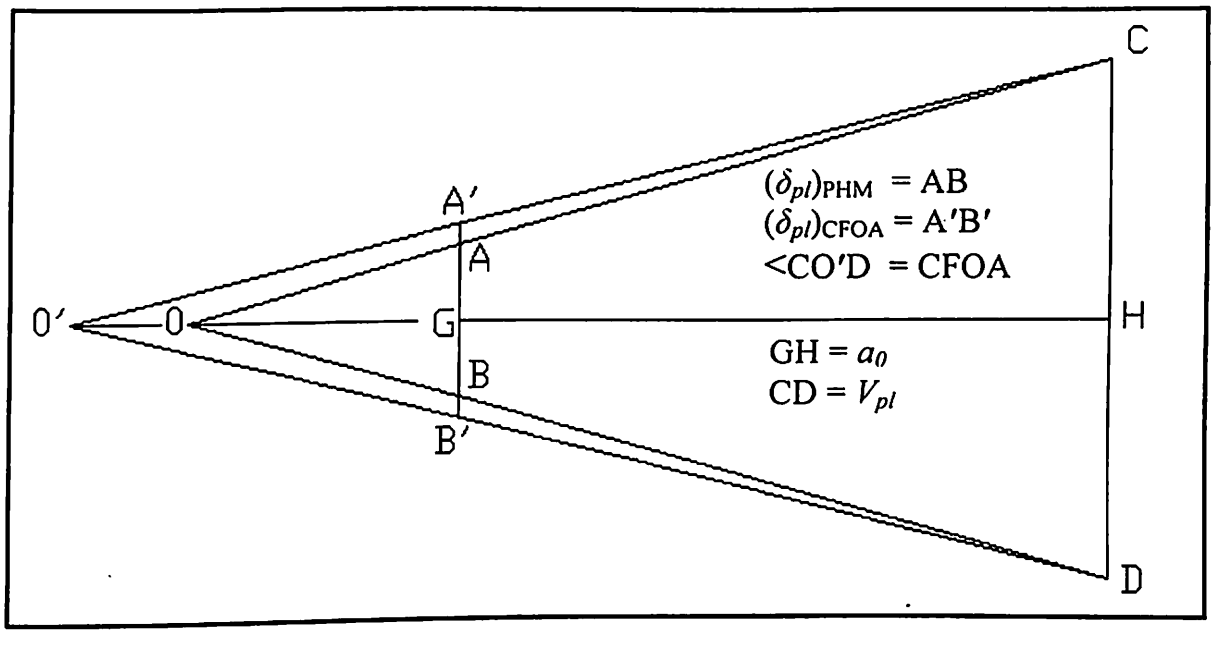

Fig. 3.6 Comparison of PHM and CFOA model.

Fig. 3.6 shows a comparison of geometry of triangles used in PHM and CFOA. From properties of the similarity of triangle with reference to Fig. 3.5 and Fig. 3.6,

$$\frac{A'B'}{CD} = \frac{O'G}{O'G + GH}$$

$$\frac{(\delta_{pl})_{CFOA}}{V_{pl}} = \frac{O'G}{O'G + a_0}$$

$$(\delta_{pl})_{CFOA} = \frac{O'G}{O'G + a_0} V_{pl}$$

Now $O'G$ can be simply expressed as

$$O'G = O'H - a_0$$

However, the location of point O' depends on crack flank opening angle $CFOA$. This dependency is expressed with the help of Eq. (3.12).

$$O'G = O'C\cos\left(\frac{CFOA}{2}\right) - a_0 \tag{3.12}$$

The $(\delta_{pl})_{CFOA}$ depends on O'G and V_{pl}, whereas $(\delta_{pl})_{PHM}$ depends only on OG, and is independent of thickness of specimen. In this model, the value of PRF depends upon the crack flank opening angle, which in turn depends upon the thickness of specimen.

(c) $J - CTOD$ relation

The plastic $CTOD$, (δ_{pl}), is derived from the value of J_{pl}, using the well known relationship given by Shih (1981). In plastic zone, Eq. (2.4) is rewritten as Eq. (3.13).

$$(CTOD)_{pl} = d_n \frac{J_{pl}}{S_y} \tag{3.13}$$

where, d_n is a factor tabulated by Shih (1981). With the help of results on plastic $CTOD$, using CFOA, PHM and FE analysis and using Eq. (3.13) the value of d_n is obtained. The value of Shih factor, obtained with the help of CFOA, PHM and FE analysis is found within the range 0.9-1.1. Thus, plastic $CTOD$ can be found with the average value of Shih factor as 1 in Eq. (3.13).

3.6 Crack Tip Necking Measurement

It is observed that the failure of EDD steel sheets during forming process occurs initially by localised necking, which is then followed by fracture inside the neck. In the present work, the crack tip necking is measured with the help of a pointer micrometer as shown in Fig. 3.7. The points of the pointer micrometer are placed in the deep region ahead of the crack tip to measure crack tip contraction. Average of three readings is taken to find out amount of crack tip contraction (δ_n).

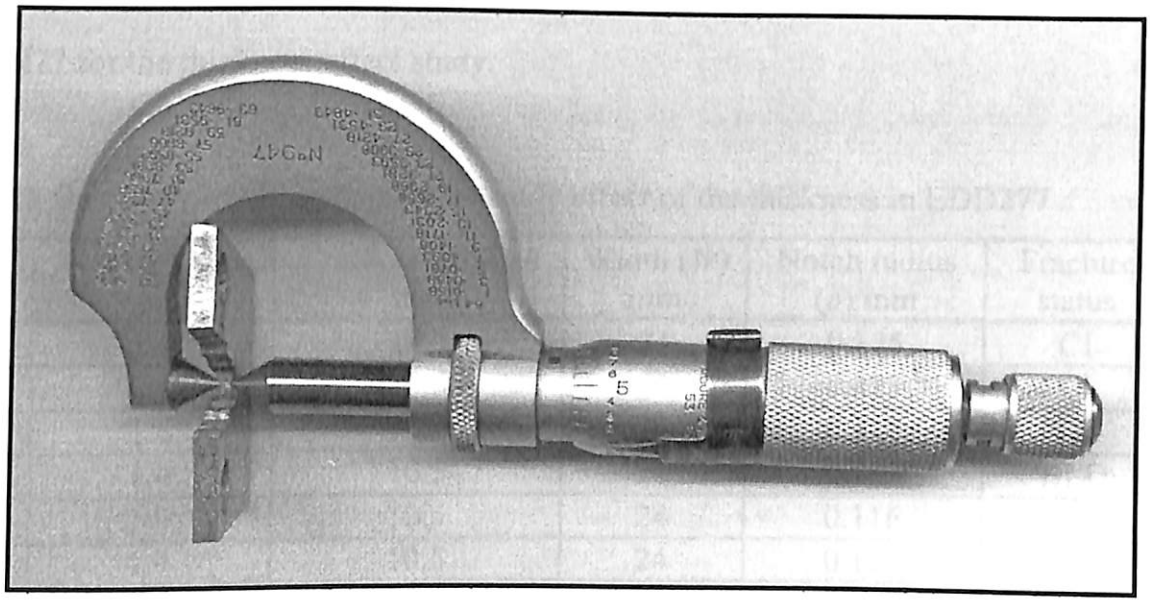

Fig. 3.7 Measurement of thickness contraction in the deep region ahead of the crack tip using pointer micrometer.

3.7 Thickness Effect Study

This study is carried out on EDD335 and EDD277 material to understand the effect of thickness on fracture parameters. In EDD335, specimens of seven categories of thickness are studied. Six specimens are tested till crack initiation (CI) point and seventh one is studied before crack initiation or before load drop (BLD) point. The critical dimensions along with the specimen codes are given as given in Table 3.1.

Table 3.1 Geometry of CT specimens to study the effect of thickness in EDD335

Sp-code	Thickness (B) mm	Crack length (a_0) mm	Width (W) mm	Notch radius (ρ) mm	Fracture status
S1	1.18	10.5	24	0.124	CI
S2	1.28	10.5	24	0.117	CI
S3	1.38	10.5	24	0.122	CI
S4	1.48	10.5	24	0.115	CI
S5	1.58	10.5	24	0.117	CI
S6	1.64	10.5	24	0.121	CI
S7	1.75	10.5	24	0.116	BLD

Table 3.2 shows the critical dimensions along with the specimen codes in case of EDD277 for the thickness effect study.

Table 3.2 Geometry of CT specimens to study effect of the thickness in EDD277

Sp-code	Thickness (B) mm	Crack length (a_0) mm	Width (W) mm	Notch radius (ρ) mm	Fracture status
1.4a	1.4	10.5	24	0.125	CI
1.4b	1.4	10.5	24	0.123	CI
1.4c	1.4	10.5	24	0.117	CI
1.4d	1.4	10.5	24	0.118	BLD
1.9a	1.9	10.5	24	0.116	CI
1.9b	1.9	10.5	24	0.122	CI
1.9c	1.9	10.5	24	0.125	BLD
1.9d	1.9	10.5	24	0.126	CI
2.4a	2.4	10.5	24	0.119	CI
2.4b	2.4	10.5	24	0.114	CI
2.4c	2.4	10.5	24	0.121	CI
2.4d	2.4	10.5	24	0.115	BLD
2.9a	2.9	10.5	24	0.119	BLD
2.9b	2.9	10.5	24	0.123	CI
2.9c	2.9	10.5	24	0.118	CI
2.9d	2.9	10.5	24	0.120	CI
3.2a	3.2	10.5	24	0.118	CI
3.2b	3.2	10.5	24	0.112	CI
3.2c	3.2	10.5	24	0.115	CI
3.2d	3.2	10.5	24	0.121	BLD

In case of EDD277, five categories of thickness are chosen with specific thickness interval. In each category, four specimens are prepared. Three specimens are tested till crack initiation point to get an average value of fracture toughness and fourth is tested before crack initiation point or before load drop point to verify the fracture criterion. Specimens are coded with a, b, c and d followed by thickness value in mm (e.g. 1.4a).

3.8 Strain Rate Effect Study

This study is carried out on EDD277. For the strain rate study, six specimens of same configuration and same thickness (1.4 mm) are prepared. All are tested at crack initiation point and tested at various strain rates. Following various literatures mentioned in Reference Section, the word 'strain rate' is used in place of displacement rate with a unit mm/min. The specimens are coded with A, B, ..., F followed by thickness value in mm. The critical dimensions along with their codes are given in Table 3.3.

Table 3.3 Geometry of CT specimens to study the effect of strain rate in EDD277

Sp-code	Thickness (B) mm	Crack length (a_0) mm	Width (W) mm	Notch radius (ρ) mm	Fracture status
1.4A	1.4	10.5	24	0.125	CI
1.4B	1.4	10.5	24	0.116	CI
1.4C	1.4	10.5	24	0.119	CI
1.4D	1.4	10.5	24	0.124	CI
1.4E	1.4	10.5	24	0.118	CI
1.4F	1.4	10.5	24	0.122	CI

3.9 Study of the Influence of Notch Radius

The study of the influence of notch radius is carried out on EDD258. For this study, sixteen specimens of same configuration and same thickness (3.2 mm) are prepared with various notch radii. The specimens are coded as SP1, SP2, ..., SP16. The critical dimensions along with their codes are given in Table 3.4. The notch operation is mentioned as FC for fatigue pre-cracked specimens, WEDM for notched specimens using wire electric discharge machining process and saw blade for notched specimens using saw cut operation.

Table 3.4 Geometry of CT specimens to study the effect of notch radius in EDD258

Sp-code	Thickness (B) mm	Crack length (a_0) mm	Width (W) mm	Notch radius (ρ) mm	Fracture status	Notch operation
SP1	3.2	10.5	24	0.07	CI	FC
SP2	3.2	10.5	24	0.085	CI	FC
SP3	3.2	10.5	24	0.10	CI	FC
SP4	3.2	10.5	24	0.11	CI	WEDM
SP5	3.2	10.5	24	0.12	CI	WEDM
SP6	3.2	10.5	24	0.13	CI	WEDM
SP7	3.2	10.5	24	0.14	CI	WEDM
SP8	3.2	10.5	24	0.15	CI	WEDM
SP9	3.2	10.5	24	0.16	CI	WEDM
SP10	3.2	10.5	24	0.17	CI	WEDM
SP11	3.2	10.5	24	0.18	CI	WEDM
SP12	3.2	10.5	24	0.25	CI	Saw-blade
SP13	3.2	10.5	24	0.40	CI	Saw-blade
SP14	3.2	10.5	24	0.60	CI	Saw-blade
SP15	3.2	10.5	24	0.75	CI	Saw-blade
SP16	3.2	10.5	24	0.077	BLD	FC

It is observed that fatigue pre-cracking operation takes about six to eight hours with low cycle fatigue. A few specimens are damaged when pre-cracking is done

using high cycle fatigue. Fifteen specimens are tested at crack initiation point and one before load drop point. The specimen SP2, which is a fatigue pre-cracked specimen, is reported as a faulty specimen.

3.10 *R* - Curve Test

Resistance (*R*) curve test is performed on eight specimens to study the crack growth behaviour while the sheet metal product is in application phase. *J*, *CTOA* and *CTOD* are used as crack growth toughness parameters to describe the resistance behaviour during crack growth. The configuration and thickness of all eight specimens is same. In this study, the specimens are coded as R1, R2, ..., R8.

3.10.1 Experimental procedure

Fig. 3.8 shows a complete rupture test on R1 specimen. The unloading points for individual specimens (e.g. R2, R3, ..., R8) are shown in the same figure.

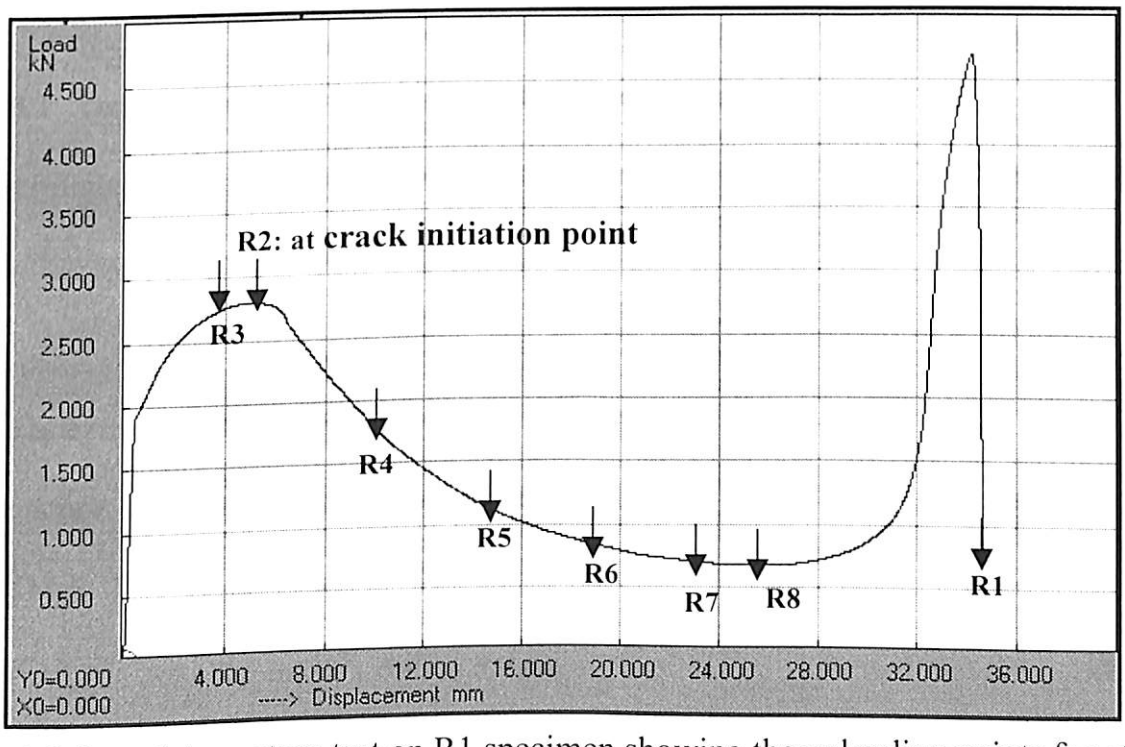

Fig. 3.8 Complete rupture test on R1 specimen showing the unloading points for other identical specimens.

Point R8 onwards, the load is increased as the crack is passing through the compressive plastic zone. In the present work, the crack growth study is carried out only in tensile plastic zone. Table 3.5 shows the geometry and status of each specimen used in this test.

Table 3.5 Geometry of CT specimens to study the crack growth behaviour in EDD258

Sp-code	Thickness (B) mm	Crack length (a_0) mm	Width (W) mm	Notch radius (ρ) mm	Fracture status
R1	3.2	10.5	24	0.115	Complete Rupture
R3	3.2	10.5	24	0.121	BLD
R2	3.2	10.5	24	0.117	CI
R4	3.2	10.5	24	0.116	CG
R5	3.2	10.5	24	0.122	CG
R6	3.2	10.5	24	0.118	CG
R7	3.2	10.5	24	0.116	CG
R8	3.2	10.5	24	0.113	CG
					CG: Crack growth

3.10.2 Determination of crack growth parameters

Determination of the crack growth fracture parameters like J and $CTOD$ are described in following paragraphs (a) and (b), respectively.

(a) Determination of crack growth J-integral

The crack growth toughness (J) is determined by using Eq. (3.14) mentioned in ASTM E 1820-01 (2001).

$$J_i = J_{el(i)} + J_{pl(i)} \tag{3.14}$$

The value of J_i, at a point corresponding to a_i on the specimen is split into elastic and a plastic contribution. The elastic part of J_i results from $J_{el(i)} = K^2_{(i)} / E$. The plastic part of J_i is determined from the area under the load versus plastic load-line displacement curve and using Eq. (3.15). Since the crack length changes continuously during R curve test, the J-integral must be calculated incrementally.

$$J_{pl(i)} = \left[J_{pl(i-1)} + \left(\frac{\eta_{(i-1)}}{W - a_{(i-1)}} \right) \frac{A_{pl(i)} - A_{pl(i-1)}}{B_n} \right] \left[1 - \gamma_{(i-1)} \frac{a_{(i)} - a_{(i-1)}}{W - a_{(i-1)}} \right] \tag{3.15}$$

where, the geometry factors $\eta = 2.0 + 0.522(1 - a_i / W)$ and $\gamma = 1.0 + 0.76(1 - a_i / W)$ for CT specimens. The B_n is the net section thickness of ductile fracture surface.

(b) Determination of crack growth *CTOD*

Critical *CTOA* model is suggested to determine *CTOA* and *CTOD* as crack growth fracture parameters. This model is explained by Kulkarni *et al.* (2004c) and demonstrated in Fig. 3.9.

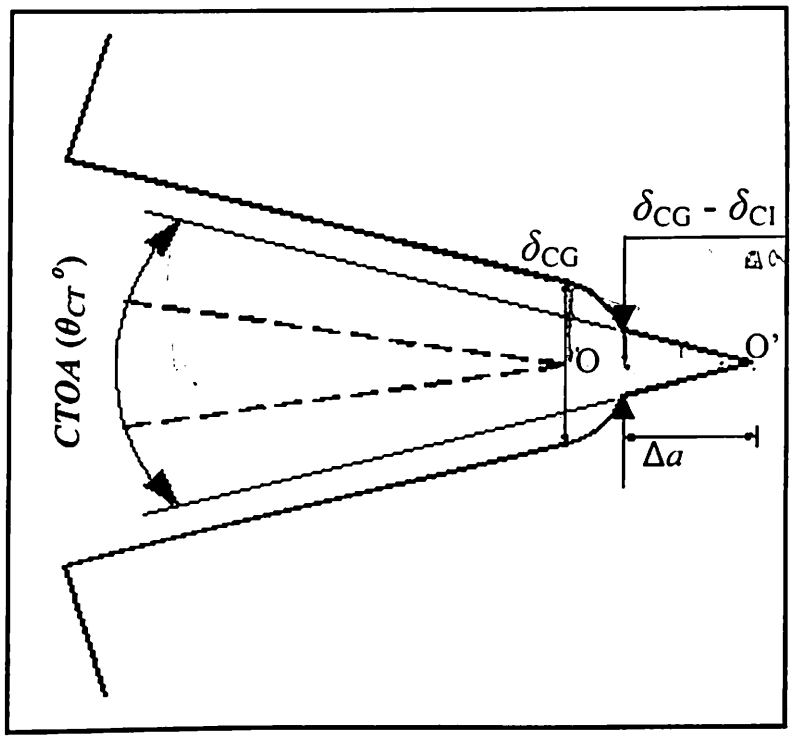

Fig. 3.9 Critical *CTOA* model.

As shown in Fig. 3.9, the dashed line represents a crack profile before crack initiation with point O as original crack tip. The continuous dark line represents a crack profile after some crack extension Δa. The current crack tip is shown at point O′, which is a meeting point of current crack flanks. The crack growth *CTOD* (δ_{CG}) is measured at original crack tip position (point O). The height of broken profile of blunt crack equals $\delta_{CG} - \delta_{CI}$ for Δa. This is because when Δa is zero and at the moment of crack initiation, δ_{CG} is equal to δ_{CI}. The δ_{CI} is fixed for a given configuration. The angle made by the current crack flanks at point O′ is called crack tip opening angle (*CTOA*). This is shown in the Fig. 3.9 as an angle θ_{CT}. From the geometry of Fig. 3.9, equation can be written as

$$\tan\left(\frac{\theta_{CT}}{2}\right) = \frac{(\delta_{CG} - \delta_{CJ})}{2\Delta a} \tag{3.16}$$

The crack growth *CTOD* is evaluated using a *CTOA* model and using Eq. (3.16) as described by Eq. (3.17).

$$\delta_{CG} = \delta_{CJ} + 2(\Delta a)\ \tan\left(\frac{\theta_{CT}}{2}\right) \tag{3.17}$$

3.11 Measurement of Plastic Zone Size and Shape

According to Anderson (1994), plastic zone plays a vital role in fracture behaviour. If the yield criterion is continuously applied along a radial line from a far field region (elastic stress field) towards the crack tip and when the material is found to yield, the point can be marked as the boundary point between elastic and plastic fields.

3.11.1 Von Mises criterion

To ensure yielding of material, Von Mises criterion states that

$$(\sigma_1 - \sigma_2)^2 + (\sigma_2 - \sigma_3)^2 + (\sigma_3 - \sigma_1)^2 \geq 2S_y^{\ 2} \tag{3.18}$$

where, σ_1, σ_2 and σ_3 are the principal stresses in Eq. (3.16). Referring to Anderson (1994), the radius of the plastic zone (r_{pz}) is derived as Eq. (3.19).

$$r_{pz} = \frac{1}{4\pi}\frac{K_I^{\ 2}}{S_y^{\ 2}}\left(1 + \frac{3}{2}\sin^2\theta + \cos\theta\right) \tag{3.19}$$

where, θ is angle measured in anticlockwise direction with reference to crack plane. The plastic zone size is estimated using Eq. (3.19).

3.11.2 Experimental determination

In this method, after fracture test, specimen photograph is taken using a flat bed scanner. The elastic plastic zone, which is clearly visible to naked eyes, also reflects clearly in the scanned image. This scanned image is imported in drawing software AutoCAD2000. The unchanged dimension during fracture test (i.e. top or bottom side of specimen) is taken as reference scale in AutoCAD unit. A poly-line is drawn with number of key points following the elastic-plastic boundary. This poly-line is then fitted as a curve. The x and y dimension of key points on this curve are measured with reference to a crack tip and plotted as a conventional graph.

3.11.3 Measurement of hardness across plastic zone

The plastic zone size and shape can also be predicted by measuring hardness across plastic zone. The hardness is measured by using a micro-hardness tester (SHIMADZU HMV).

3.12 Metallographic Study

3.12.1 Microstructure study

The objectives of micro-structural investigation are to obtain a representative microstructure and determine the grain size of the material. The specimen surface is ground with successively finer abrasive papers and powders. It is then polished first using alundum and finally using 0.25 μm diamond paste in polishing machine. The

polished specimens are etched with 2% nital solution for approximately 4-5 seconds to reveal the microstructure.

The micrographs are taken before and after the fracture test, for all three EDD steel sheets using a digital image camera attached to scanning electron microscope at a magnification of 400X. The specific region chosen is ahead of crack tip as it is highly deformed after the fracture test. In order to understand the successive damage, the macrographs of crack profile are taken at the surface level, one fourth of sample thickness and half of sample thickness.

3.12.2 Fracture surface study

Fracture surface study is carried out to understand the phenomenon of ductile tearing process and type of fracture. A few specimens from all three materials are selected to study the fracture surface. They are kept in an oven at 300° C for 30 minutes. By annealing process, the temperature of sample is brought to room temperature keeping them in furnace only. The heating process makes the specimen to be oxidised. The oxidisation process helps to distinguish between the ductile tearing and brittle fracture. The specimens are put one by one into the thermo flask wherein liquid Nitrogen (at -190°C) is kept. After 10 minutes, they are taken out. Liquid nitrogen makes the specimens brittle. A chisel is positioned at the tip of crack and with a proper support the hammer is blown to break the specimen. The broken ligaments are studied for the damage ahead of crack tip and the fracture process.

Chapter 4

3-D FINITE ELEMENT ANALYSIS

4.1 Introduction

The computational approach involves detailed finite element analysis to verify the experimental results. In addition to this, it is possible to determine the stress and strain fields in the vicinity of the crack front and obtain the type of fracture behaviour using 3-D FE analysis. The important topics like element selection, creation of crack tip element, material modeling, boundary conditions and non-linear solution are discussed in detail. This analysis determines the critical load, *J*-integral and *CTOD*, independently.

4.2 3-D Finite Element Analysis of CT Specimen

The 3-D geometry (solid model) of a CT specimen is modeled similar to ASTM standard E 399-91, as shown in Fig. 3.1 (a). Standard primitives such as block, cylinder with Boolean operations are used to create a solid model.

4.2.1 Element selection

In the present analysis, 3-D, twenty-nodded structural solid i.e. SOLID95 element is used. This element is a higher order version of 3-D, eight-nodded structural solid. It has capability to tolerate irregular shapes without much loss in accuracy. The regions undergoing plastic deformation require a high integration point density. Higher-order elements have been preferred for plasticity analysis. This element has compatible shapes and also suitable to model the curved boundaries.

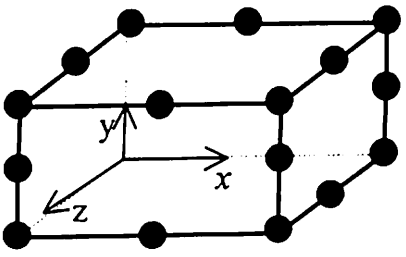

Fig. 4.1 3D, twenty-nodded brick element.

This element is having three degrees of freedom per node, i.e. translations in *x*-, *y*- and *z*-direction as shown in Fig. 4.1. Fig. 4.1 also shows the geometry, node location and the coordinate system. This element possesses plasticity, stress stiffening, large deflection and large strain capabilities.

4.2.2 Creation of crack tip element

A triangular wedge shaped element is formed by collapsing the top plane of a brick element along the surface diagonal, as shown in Fig. 4.2. The mid side nodes of the element are placed at the quarter positions towards crack front to produce the appropriate $1/r$ singularity as the limit of the plasticity is approached. The use of this element, in conjunction with surrounding isoparametric elements, gives a powerful method for analysing fracture parameters.

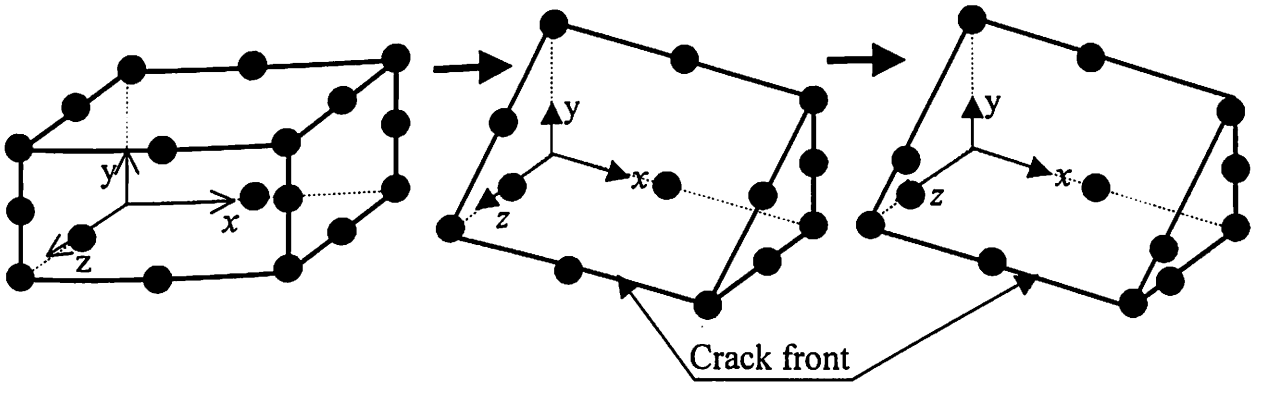

Fig. 4.2 Creation of crack tip element.

The most important region in a fracture model is the region around the crack front. Meshing has to be graded from fine at the crack tip to coarse at the solid boundary. The element size, which varies from 0.0035% to 0.06% of the absolute crack length (i.e. a_0), is considered around the crack front. Fig. 4.3 shows the arrangement of elements with multiple nodes along different radial rows around the crack front. Approximately 12,648 elements and 8,184 nodes are generated. However, these numbers depend upon the thickness of the specimen model.

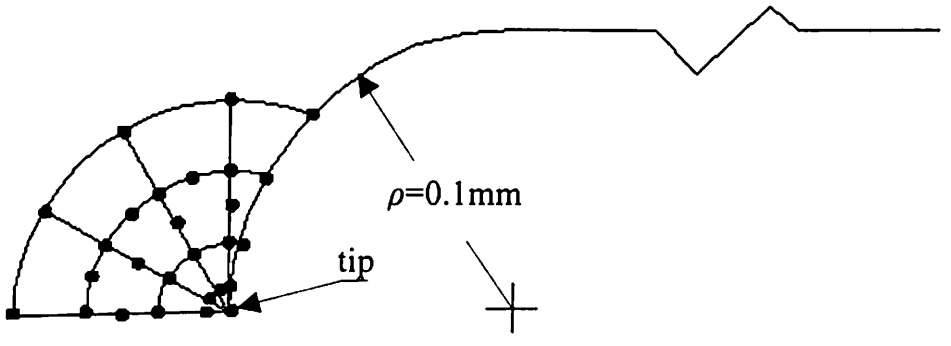

Fig. 4.3 Arrangement of crack tip elements in radial rows.

4.2.3 Non-linear material model

Elastic-plastic finite element analysis can be considered as an extension of elastic analysis by incorporating extra conditions pertaining to nonlinear plasticity conditions as suggested by Newman (1984). According to Newman (1984), nonlinear material behaviour is modeled by using the incremental theory of plasticity. Von Mises yield criterion is considered to be valid for these materials. A true stress-strain curve up to breaking-strain point is used with multi-linear isotropic hardening to incorporate non-linear material properties. This is referred as a large strain code by Kulkarni *et al.* (2004a). In a large strain code, true stress-strain curve is used up to breaking-strain point with constant value of ultimate stress beyond the ultimate point. The true stress-

strain curves for three EDD materials are shown in Fig. 4.4, 4.5 and 4.6 for EDD335, EDD277 and EDD258, respectively. The values of true stress-strain curve for these materials are tabulated in Appendix Table A1.3, A2.3 and A3.3, respectively for EDD335, EDD277 and EDD258.

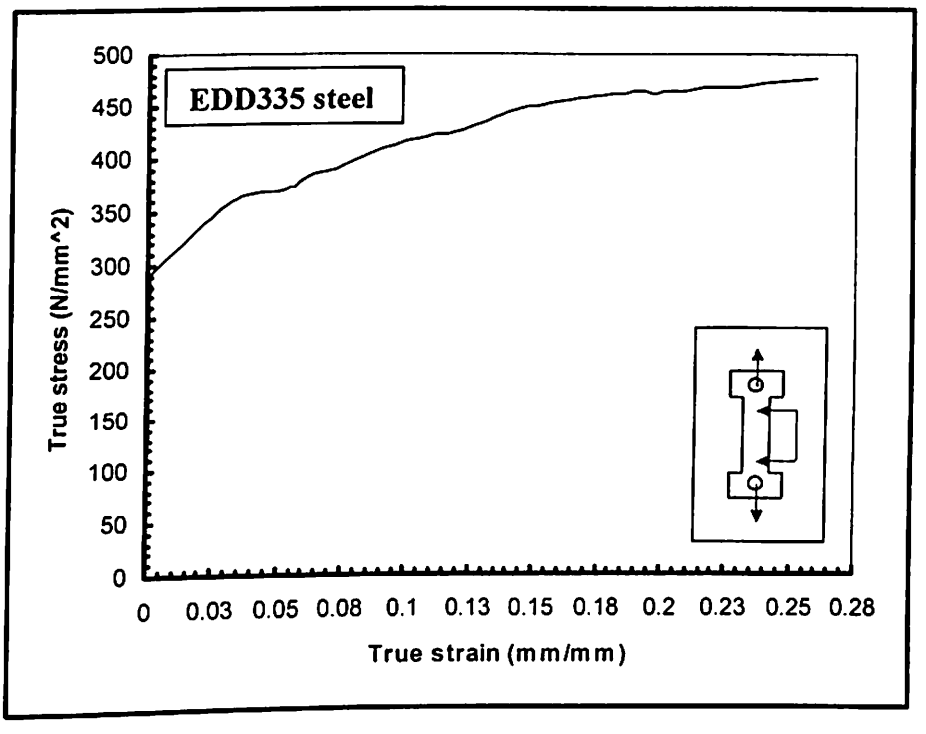

Fig. 4.4 True stress-strain curve for EDD335 steel sheet.

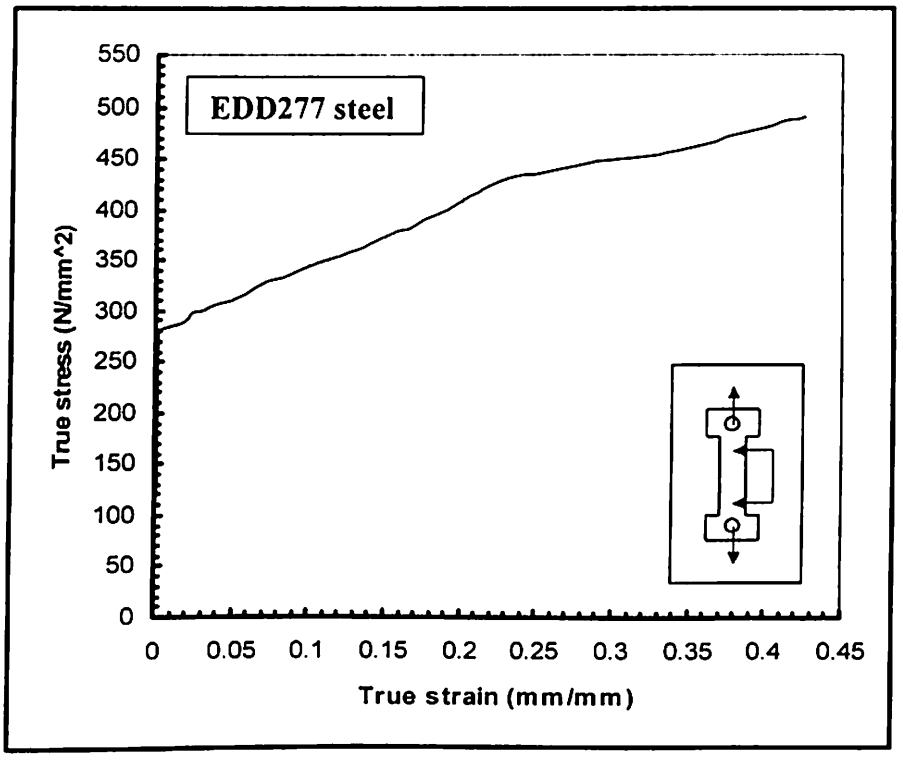

Fig. 4.5 True stress-strain curve for EDD277 steel sheet.

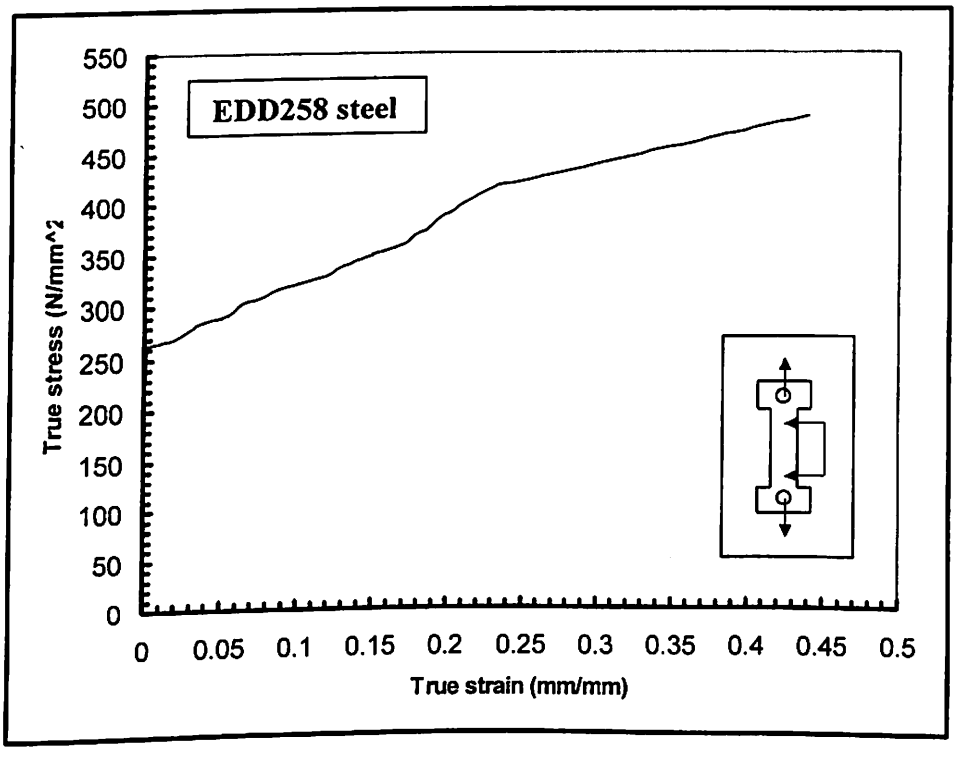

Fig. 4.6 True stress-strain curve for EDD258 steel sheet.

4.2.4 Loading and boundary conditions

Fig. 4.7 shows the loading and boundary conditions for the FE analysis. The nodal displacement is applied at pinhole, as a crack driving force. For mode-I type modeling, by using the geometry, loading, material and support symmetry conditions, two planes of symmetry are considered: one at mid-height (30/2 = 15 mm) and other at mid-thickness (*B*/2) of the specimen model as shown in Fig. 4.7. The tip of the notch is released (i.e. opened) from constraint as shown in Fig. 4.7. This is referred as virtual crack tip opening method, described by Kulkarni *et al.* (2004a). Fig. 4.8 (a) shows a FE model of a full CT specimen with mid-thickness symmetry, whereas Fig. 4.8 (b) shows a FE model of a half CT specimen with mid-height symmetry.

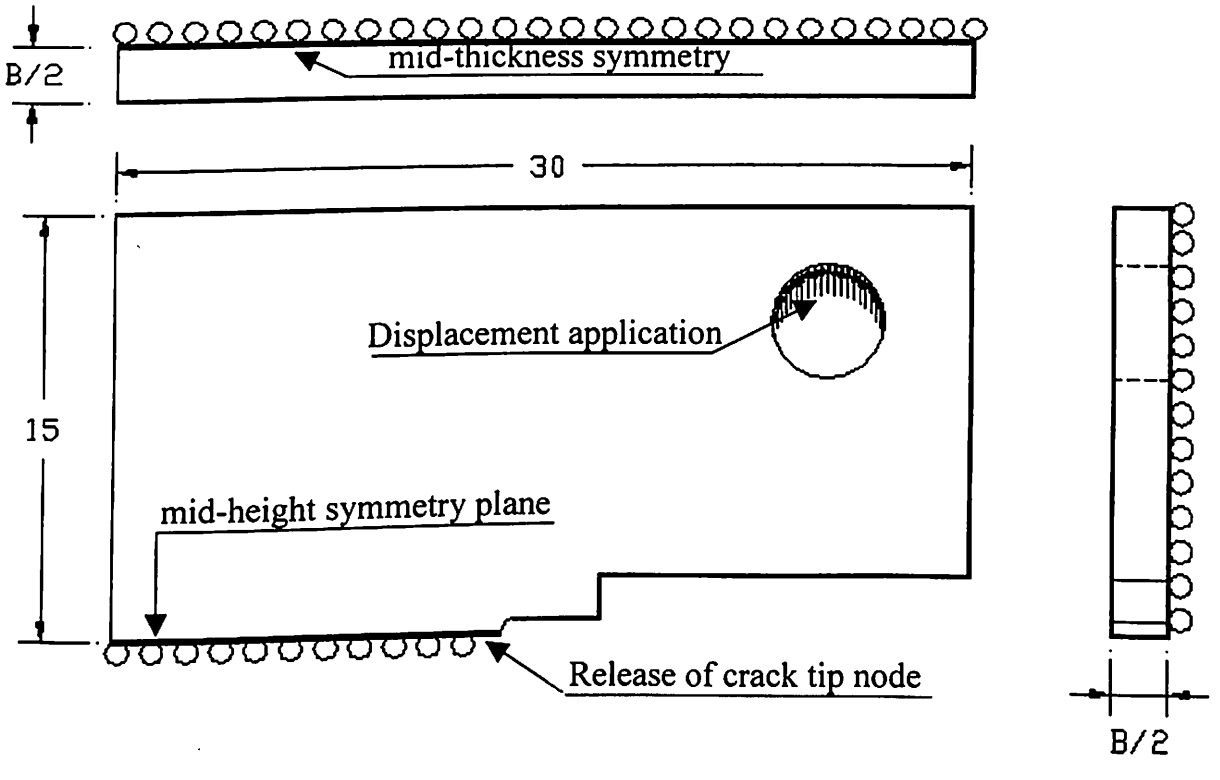

Fig. 4.7 Boundary conditions for CT specimen.

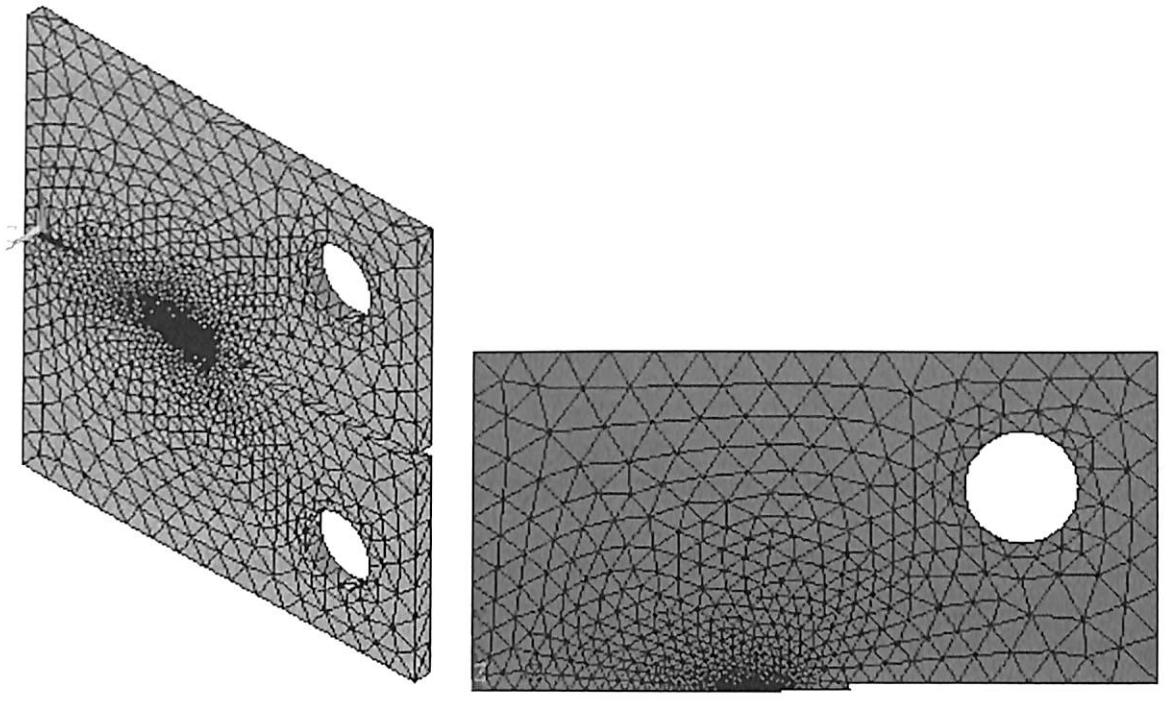

(a) (b)

Fig. 4.8 (a) FE model of a CT specimen with a mid-thickness symmetry.
(b) FE model of a CT specimen with a mid-height symmetry.

4.3 Non-Linear Solution and Analysis

The non-linear material model predicts elastic as well as plastic fracture parameters. Following ANSYS 7.0 (2002), the load (i.e. displacement) is applied with load steps, sub-steps and equilibrium iterations. Sub-steps are time points within a load step at which intermediate solutions can be obtained. A single load (i.e. displacement) step is used for the analysis. The time at the end of load step is assigned as 1.0. Appropriate numbers of sub-steps are assigned for one load step to establish the experimental displacement (i.e. strain) rate. The difference in time between two successive sub-steps is called 'time step size' or 'time increment'. Equilibrium iterations are additional solutions, calculated at a given sub-step for converging process. Newton-Raphson equilibrium iterations drive

tolerance limit) at the end of each load increment. Before each solution, this method evaluates the out of balance load vector, which is the difference between restoring forces and the applied loads and checks for the convergence. If the convergence criterion is not satisfied, the out of balance load is reevaluated, the stiffness matrix is updated and a new solution is obtained. This iterative procedure continues till the result is converged.

Load-line displacement is applied gradually to ensure that analysis closely follows the structure's load-response curve. The elastic-plastic process requires a continuous assessment of stress and plastic strain at all points of the structure, as the load-line displacement increases. Within each time step, check on stress and equilibrium is made. As load-line displacement starts, the program starts to iterate the stress above the yield stress to consider the plastic effects. The whole nonlinear curve is considered to consist of number of straight lines with a multi-linear isotropic hardening.

4.4 Calculation of Fracture Parameters

As given by Eq. (3.5) and (3.9), the calculation of elastic part of *J*-integral and *CTOD* involves the determination of stress intensity factor (*K*). In FE analysis, following Anderson (1994), the value of stress intensity factor is found using Eq. (4.1),

$$K_I = \sigma_{ij} \frac{\sqrt{2\pi r}}{g^I{}_{ij}(\theta)} \tag{4.1}$$

where, σ_{ij} is the elastic stress value of the node with maximum displacement at radius r, and an angle θ with the crack plane. The subscripts i and j stand for the directions x and y. g^I_{ij} is a function of θ. The radius (r) and angle (θ) are taken for the

node in first radial row simulating the crack tip at mid-thickness section. Now using Eq. (3.5) and Eq. (3.9), the elastic *J*-integral and *CTOD* are calculated.

4.4.1 Evaluation of plastic *CTOD* and crack tip contraction

Similar to elastic *CTOD*, the total *CTOD* is found at the node in first radial row with maximum displacement in *y*-direction using the last set of results. The plastic part of *CTOD* is found by deducting the elastic *CTOD* from total *CTOD*. The crack tip contraction has been found at the same node where, these elastic and total *CTOD*s have been found. This is to verify the 'crack tip contraction' as a fracture criterion.

4.4.2 Evaluation of plastic *J*-integral

Anderson (1994) explains the evaluation of plastic *J*-integral. Fig. 4.9 shows the path Γ around the crack tip, which starts from any point of a crack face and ends on any point on the other crack face. The path can be chosen arbitrarily within the material, however, closer to crack tip.

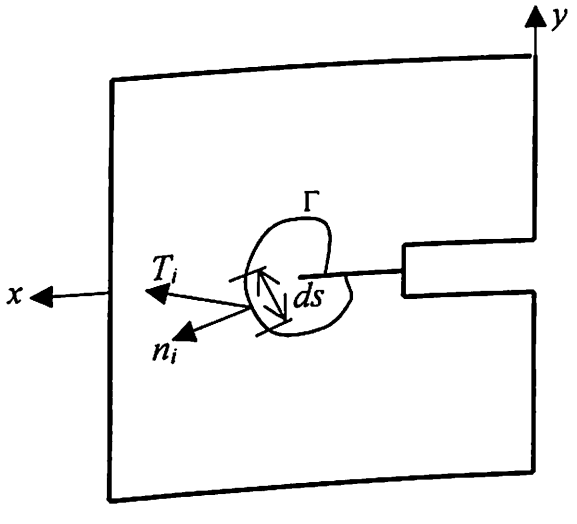

Fig. 4.9 Evaluation of plastic *J*-integral using path Γ.

Numerical definition of J-integral is given by Rice (1968) as Eq. (4.2)

$$J_{pl} = \int_{\Gamma} U dy - \int_{\Gamma} \left(T_x \frac{\partial u_x}{\partial x} + T_y \frac{\partial u_y}{\partial x} \right) ds \tag{4.2}$$

where, U is strain energy density, T_x and T_y are traction forces, respectively along x- and y-direction, over a defined path, u_x and u_y are the displacement vector at a point on the path along x- and y-direction. For evaluation of J-integral values, large strain code is run and the last set of results is used. Following ANSYS 7.0 (2002), the J-integral is separated into two parts, which can be written as Eq. (4.3):

$$J_{pl} = J_a - J_b \tag{4.3}$$

where $J_a = \int_{\Gamma} U dy$ and $J_b = \int_{\Gamma} \left(T_x \frac{\partial u_x}{\partial x} + T_y \frac{\partial u_y}{\partial x} \right) ds$.

To evaluate J_a, element table is defined, which contains strain energy and volume for the elements under consideration. The strain energy density is mapped onto a path from element table. Using path integration, J_a value is estimated and stored as scalar data.

Using similar procedure, J_b is also estimated. Stress components (σ_x, σ_y and τ_{xy}) are mapped onto the same path to evaluate a traction force over a path. For a unit area, traction forces are estimated by defining unit normal vector i.e. Eq. (4.4) and Eq. (4.5).

$$T_{1x} = \sigma_x n_x, \; T_{2x} = \tau_{xy} n_y \tag{4.4}$$

$$T_{1y} = \sigma_y n_y, \; T_{2y} = \tau_{xy} n_x \tag{4.5}$$

Path operation (addition) is used to evaluate T_x and T_y (i.e. $T_x = T_{1x} + T_{2x}$ and $T_y = T_{1y} + T_{2y}$). Virtual crack tip opening method is used to find $\frac{\partial u_x}{\partial x}$ and $\frac{\partial u_y}{\partial x}$. All values are stored in element table. Finally path integration is used to evaluate J_b value and stored as scalar data. Further, J value is estimated as $J_{pl} = J_a - J_b$.

The *J-CTOD* relation is also verified by FE analysis using Eq. (3.13), which is reproduced here.

$$(CTOD)_{pl} = (\delta_{pl})_{FEM} = d_n \frac{J_{pl}}{S_y} \tag{3.13}$$

Stress analysis has been performed across the thickness i.e. from surface to mid-thickness section (i.e. zero to $B/2$) to study the crack tip loading condition. The stress analysis is also performed along the unbroken ligament length (b) to study the stress variation ahead of crack tip.

4.4.3 Measurement of plastic zone size and shape

Using FE analysis, the nodes on elastic-plastic boundary showing the yield or above yield stress value are noted. The x and y dimensions of these nodes are found with origin at current crack tip and a conventional graph is plotted. This is shown in section 5.14.

Chapter 5

RESULTS & DISCUSSION

5.1 Introduction

This Chapter discusses results obtained from the experiment and 3-D FE analysis. The results are given in tabular and graphical form. The discussion follows the results for various objectives. The results are discussed on formability indices, fracture behaviour in generation phase, fracture behaviour in application phase, and metallographic studies. These results are discussed with reference to previously published journal papers, technical reports and conference proceedings.

5.2 Formability Parameters

Information about formability of thin sheets is important to sheet manufacturers as well as users. In the present investigation, the conventional indicators of formability of EDD steel sheets are discussed in the light of good deep drawing qualities mentioned by ASTM E 8 M (1999) and E 517-92 (1992) standards.

5.2.1 Chemical composition

The chemical compositions of three EDD steel sheets are given in weight % in Table 5.1. The amount of carbon in EDD335 is 0.06%. According to ASTM E 517-92, this is an upper limit for EDD steel sheets, below which, the desired carbon level is good for formability. Higher carbon content leads to a decrease in the normal anisotropy

($\bar{r}$). This is attributed to an increase in the amount of cementite. High $\bar{r}$ values (>1.6) have been observed by Mizui and Okamoto (1990) in case of EDD steel sheets containing carbon less than 0.06%. According to Ravi Kumar (2002), a sheet with a high $\bar{r}$ value generally possesses a high planar anisotropy value also. In the present study, since the difference in the carbon content among the three EDD steel sheets is significant, any variation in their formability can arise from carbon levels. Mizui and Okamoto (1991) studied the effect of Mn content (in the range 0.02–0.44%) on deep drawability of continuous annealed Al-killed steel sheets. They concluded that the $\bar{r}$ value in the rolling direction exhibited a maximum value at a medium Mn content. They attributed this to the changes in the distribution of MnS inclusions and the precipitations of Al/N. Dasarathy and Hudd (1974) indicated that the presence of aluminum up to 0.08% have no adverse effect on the mechanical properties.

Table 5.1 Composition of the investigated EDD steel sheet in wt. %

No.	Material	C	Mn	S	P	Si	Al	N, ppm	Fe
1	EDD335	0.06	0.38	0.03	0.017	0.05	0.040	47	Balance
2	EDD277	0.025	0.18	0.010	0.013	0.005	0.040	40	Balance
3	EDD258	0.015	0.16	0.010	0.010	0.005	0.041	33	Balance

G.S.
7.2 M
13 M
15 M

5.2.2 Grain size

The microstructure of the three EDD steel sheets in the as-received condition is studied using scanning electron microscopy. The values of average grain size determined by the linear intercept method are 7.2, 13, and 15 μm, respectively for

EDD335, EDD277 and EDD258 steel. These values are accurate to within 2 μm. The investigations of Wilson and Acselrad (1984) on the effect of grain size showed that the favourable grain size for good formability is in the range of 7–18 μm. It has been concluded that, strain hardening exponent, n and normal anisotropy, $\bar{r}$ increase with increase in grain size.

5.2.3 Strain hardening exponent

The formability of sheet metals is strongly influenced by the strain hardening exponent (n). The n values of three EDD steel sheets, determined by two methods are listed in Table 5.2.

Table 5.2 Strain hardening exponent (n) of EDD steel sheets

EDD-STEEL	Method-I $n = \varepsilon_u$	Method-II Eq. (5.1)
EDD335	0.145	0.148
EDD277	0.24	0.224
EDD258	0.26	0.231

By method-I, the value of n is taken equal to value of ultimate strain ε_u in true stress-strain curve, following Caddell (1980). In the method-II, the value of n is calculated by using an empirical relationship given by Schedin and Melander (1987). This empirical relation i.e. Eq. (5.1) is given below.

$$\varepsilon_u = 0.28 - 0.2[C] - 0.25[Mn] - 0.44[Si] - 0.39[S] - 1.2\,[N] \qquad (5.1)$$

However, factors like grain size, heat treatment, on which n greatly depends, are not taken into account in this relation. Clearly this empirical equation (i.e. Eq. 5.1) has very limited applicability. In the present work, only the value obtained from the true

stress-strain curve is used. The material EDD335 possesses a lower n value (0.145) indicating its inferior formability. Other two materials have n values in the range of 0.224 – 0.231 and hence greater formability.

5.2.4 Mechanical properties

The mechanical properties of the EDD steel sheets for three different rolling directions (RD), obtained from Ray (2000-2004) are summarised below, in Table 5.3.

Table 5.3 Mechanical properties of EDD steel obtained from TISCO, Jamshedpur

EDD steel	Orientation w.r.t RD (°)	YS (MPa)	UTS (MPa)	Uniform elongation (%)	Total elongation (%)	SRS index, m
EDD335	0	335.08	387.12	15.60	29.69	
	45	332.87	391.88	15.31	25.23	
	90	331.74	386.65	14.46	23.87	
Average		333.14	389.38	15.12	26.26	0.017
EDD277	0	276.97	342.04	26.40	49.60	
	45	279.22	348.45	24.89	41.53	
	90	274.32	339.04	22.29	37.15	
Average		277.43	344.49	24.52	42.76	0.012
EDD258	0	258.88	327.14	30.00	55.19	
	45	260.02	331.24	28.14	45.72	
	90	255.17	326.49	24.67	39.52	
Average		258.52	329.02	27.60	46.81	0.01
Average, $X = (X_0 + 2X_{45} + X_{90})/4$						

From Table 5.3, it is observed that, except EDD335, in all cases the YS and UTS values are higher at 45° to the rolling direction than in the direction parallel or perpendicular to the rolling direction. The elongation to fracture is greater along the rolling direction than along directions perpendicular or diagonal to the same. EDD335 possesses higher YS and UTS values and lower ductility when compared with the other two. The results obtained from the tension tests in all three directions are

qualitatively same. The average values of strength are closest to the values of strength in rolling direction. Therefore, the results are described by means of values obtained from the tests in the rolling direction only. The tensile test data along rolling direction is tabulated in Appendix Table A1, A2 and A3 for EDD335, EDD277 and EDD258, respectively.

The strain rate sensitivity index (m), determined by strain rate jump tests, is found to be very similar for all the three directions, i.e. 0°, 45°, and 90° to the rolling direction (RD). The m values are also reported in Table 5.3, which are seen to be moderate. This is consistent with the fact that most of the common metals like low carbon steel have low sensitivity to the strain rate at room temperature. This is also observed by Swaminathan and Padmanabhan (1991).

5.2.5 Normal anisotropy ($\bar{r}$)

As given in Table 5.4, the product $n\bar{r}$, which is indicative of overall press performance factor, is high for EDD277 and EDD258. As expected, EDD335 has relatively low value. However, according to Mellor (1981), this factor has little physical significance, as it is only a numerical index used for a rough assessment of formability.

Table 5.4 Press performance factor of three EDD steel materials

EDD-STEEL	n	r_0	r_{45}	r_{90}	$\bar{r}$	$n\bar{r}$
EDD335	0.14	0.97	0.82	1.21	0.95	0.14
EDD277	0.24	1.37	1.04	1.58	1.26	0.30
EDD258	0.26	1.47	1.21	1.83	1.43	0.37
$\bar{r} = (r_0 + 2r_{45} + r_{90})/4$						

Following ASTM E 8 M (1999) and E 517-92 (1992) standards, EDD277 and EDD258 steel sheet has relatively high formability than EDD335 steel sheet. However, from the above study, it is very clear that the formability test is influenced by number of material variables. Apart from these material variables, the process variables also affect the forming test. These include punch and die configuration/assembly, clearances, and lubrications. According to Ravi Kumar (2002), any minor discrepancy in the relative overall formability could be due to the complex interaction of large number of (process and/or material) variables. Hence it is difficult to single out any parameter to completely explain the formability limits.

Fracture mechanics may not be able to remove all variables of the conventional forming tests. However, the fracture test data could be utilised to find out critical load at which crack initiates, amount of necking and fracture stress/strain with least number of variables. The test facilities also need not to be changed as it is done in case of forming tests discussed by Ravi Kumar (2002).

5.3 Fracture Criterion

As discussed by Pardoen and Delannay (2000), the detection of cracking initiation is a remnant problem in fracture tests performed on ductile materials. From the application point of view, the present study investigates precise load and fracture parameter calculations at crack initiation. The criterion should ascertain that either the crack has already moved by a small amount or it is definite to move if load is increased by a small amount.

The 'load drop technique', mentioned by Kulkarni *et al.* (2002, 2003a) is used as a fracture criterion to measure the fracture parameters. As soon as the load drops the crack is initiated on the surface in the necking zone. However, to check the possibility of crack initiation inside the neck, a few specimens are chosen before and at the load drop point. Fig. 5.1 shows a crack profile at mid-thickness section for a specimen unloaded just before load drop point. The blunt profile does not show any crack. From this observation, it is concluded that the crack is not initiated at mid-thickness section before it reach the load drop point.

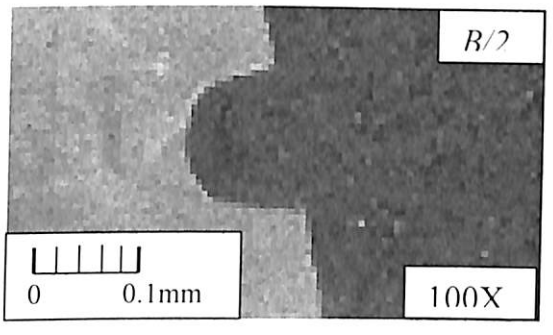

Fig. 5.1 Crack profile at mid-thickness section of a specimen unloaded before load drop point.

Fig. 5.2 (a) and (b) shows a small crack initiated, respectively on the surface and at mid-thickness section of a specimen unloaded at the load drop point. Both the cracks show same length, only the damage in front of crack tip at surface level is not clearly visible. This observation supports that the crack is initiated only at load drop point. Therefore, it is concluded that, the crack initiates at the center of necking zone and reaches the surface without any significant travel.

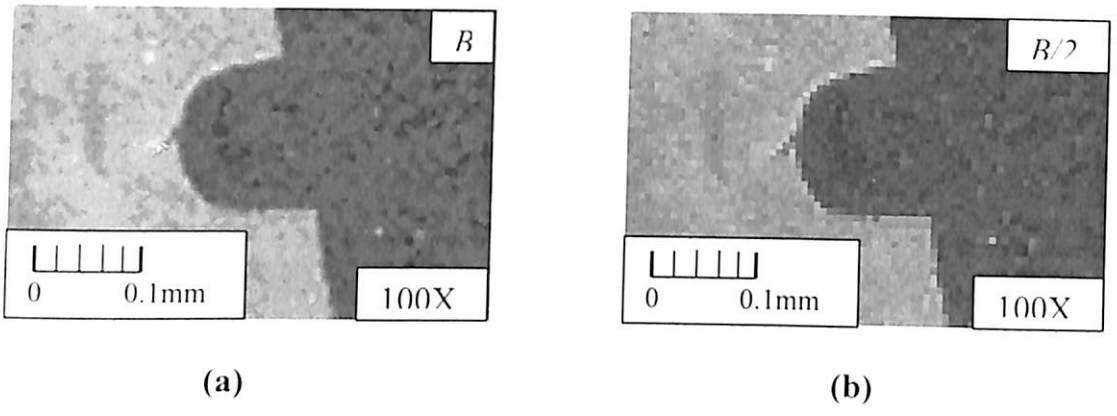

(a) **(b)**

Fig. 5.2 (a) Crack on surface of a specimen unloaded at the load drop point.
(b) Crack at the mid-thickness section of specimen at the load drop point.

From this observation, it is found that cracking initiation corresponds to the nucleation of a micro-crack in front of a blunt notch. This is the result of linking of the blunted crack tip with the closet damage site (a void or a micro-crack). Therefore, more accurate definition of cracking initiation is proposed that 'the critical event of cracking initiation is the point at which the process of plastic deformation at the original crack tip (i.e. the blunting process) is stopped'. Thereafter, the load is carried mainly by the new crack tip.

Fig. 5.3 (a) and (b) shows fracture surface of broken open up specimen at load drop point and before load drop point, respectively. The fracture surface before load drop point in Fig. 5.3 (b) is complete shiny, right from the notch tip with an indication of complete brittle fracture and no crack initiation or ductile tearing. Whereas, the fracture surface at the load drop point in Fig. 5.3 (a) consists of two parts. The smaller part is with minute ductile tearing in the necking zone with an indication of crack initiation and a large shiny zone with an indication of brittle fracture. The brittle fracture is due to the thermal shock treatment.

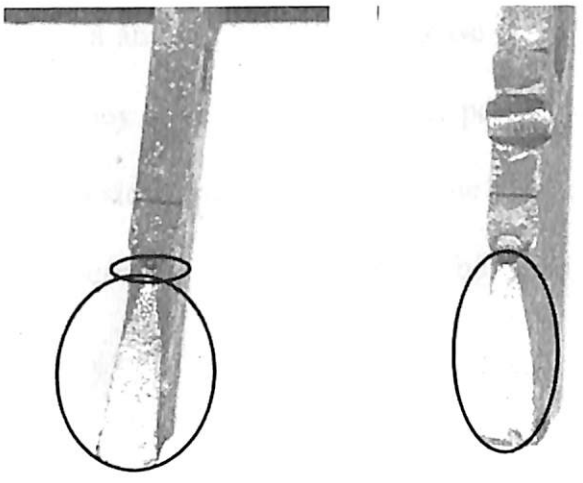

(a) (b)

Fig. 5.3 Fracture surface of broken open up specimens.
(a) at the load drop point **(b)** before the load drop point

From these observations i.e. Fig. 5.1, 5.2 and 5.3, it is clear that in case of EDD steel sheets, the crack initiation occurs when load drops. Another important thing, which is observed in this study, is that, like other ductile materials, EDD steel samples are not becoming brittle, immediately when they are put in liquid Nitrogen. This is unlike other ductile materials mentioned by According to Kumar (1988a). The reason may be excessive ductility possessed by EDD material. The fracture surface observations present the advantage of giving insight into the macro-mechanisms of damage ahead of crack tip.

The fracture tests are also conducted on Copper, Aluminium, Brass and Mild Steel materials to observe the event of crack initiation using the CT specimen. The load – load-line displacement plots for these tests are shown in Appendix B6. While conducting the tests, it is clearly observed that the surface crack is initiated well before the peak load is reached and before the maximum blunting occurs. This is also

reported by Bhattacharya and Kumar (1991) in case of 7004 grade Aluminium alloy and free cutting steel. They have separated plastic part of load-line displacement into the displacements due to slow crack growth and true plastic yielding. They found that the crack growth displacement in Aluminium to be three times that of free cutting steel.

5.4 3-D FE Analysis

The 3-D finite element analysis is performed to predict the fracture parameters independently. Important aspects of this analysis are: creation of crack tip element, non-linear material model and prediction of fracture parameters. The 2-D FE analysis does not account for the out of plane (z-direction) displacement field. Though the fracture behaviour in the present work is found to be a predominantly plane stress, a 3-D FE analysis is preferred because the necking (crack tip contraction) and blunting (crack tip opening displacement) proceeds simultaneously preceding the event of crack initiation. The $1/4^{th}$ symmetry (about mid-thickness and mid-height) allowed a study of critical sections to predict fracture behaviour accurately. Load-line displacement is controlled using a time step analysis. Fig. 5.4 (a) and (b) shows the crack tip opening displacement and the crack tip necking, respectively at a node in first radial row around the crack tip. The fine meshes at and around the crack tip along with the virtual crack tip opening method discussed by Kulkarni *et al.* (2004a), allowed proper blunting of crack. In non-linear material model, the breaking strain is used as a fracture criterion. This criterion as discussed by Kulkarni *et al.* (2004a) allowed the necking to continue till a breaking strain value.

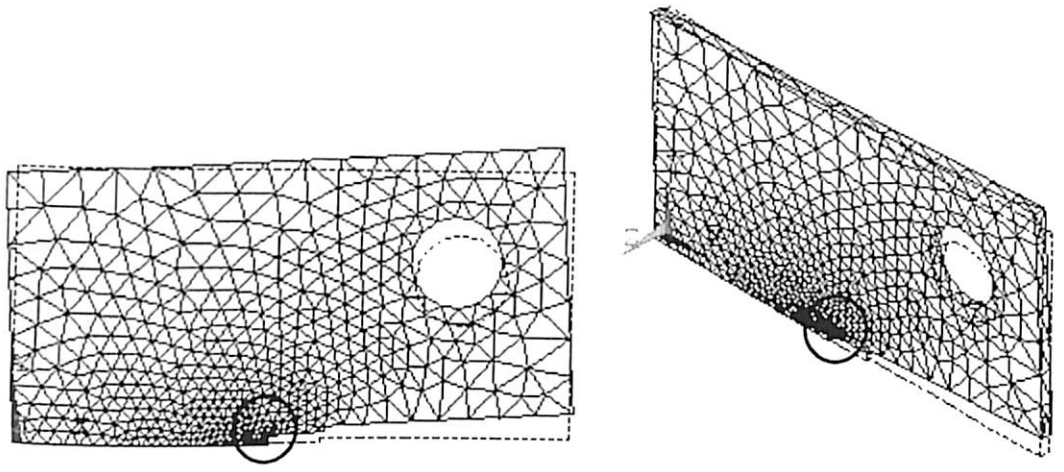

(a) (b)

Fig. 5.4. FE analysis results on **(a)** crack tip opening displacement.
(b) crack tip necking.

The total plastic zone across the unbroken ligament length b, consists of tensile plastic zone around crack tip and compressive plastic zone towards the ligament boundary as shown in Fig. 5.5 (a) and (b).

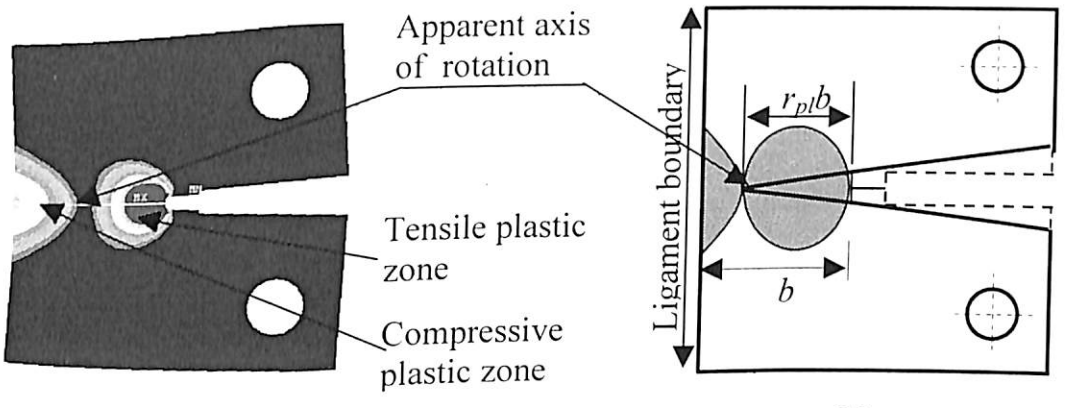

(a) (b)

Fig. 5.5 (a) Plastic zone by FE analysis.
(b) Apparent axis of rotation in Plastic Hinge Model (PHM).

Similar to the observation made in experiments, FE analysis also shows a specific nodal point on unbroken ligament (b), which is having a far field stress value.

This point is a neutral point or an apparent axis of rotation. Hardness measurement also supports this observation as discussed in section 5.14. However, this location depends on thickness of specimen.

5.4.1 FE stress analysis

In order to understand the fracture behaviour and to determine fracture parameters, a stress analysis is performed at and around crack front as well as along the unbroken ligament length. Figures 5.6, 5.8 and 5.10 show the plots of the normalised stresses along unbroken ligament length. The normal stresses (σ_x, σ_y, σ_z) are normalised with respect to the yield stress for EDD335, EDD277 and EDD258. The coordinate system is shown at blunt crack tip in every plot. The normalised stress σ_z is also plotted across the thickness direction, starting from the mid-thickness section (z/B = 0) to a surface (z/B = 0.5). This is shown in Fig. 5.7, 5.9 and 5.11, respectively for EDD335, EDD277 and EDD258.

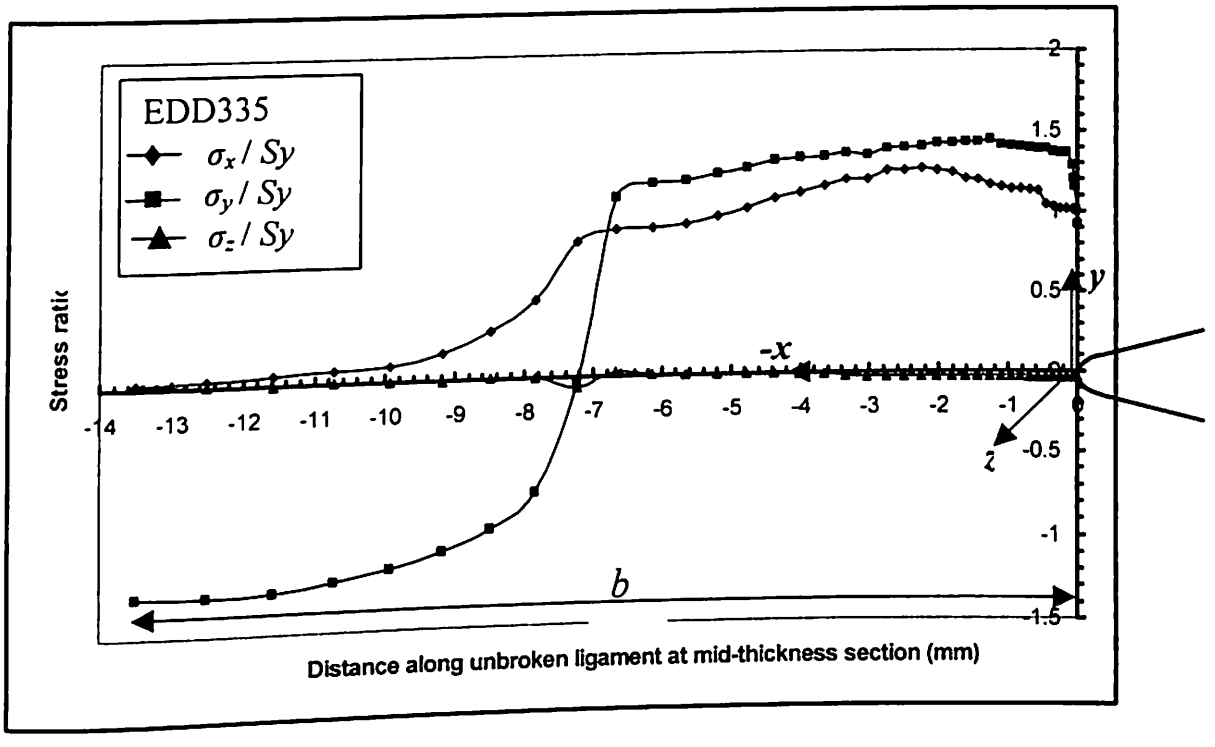

Fig. 5.6 Normalised stresses σ_x, σ_y, σ_z along the unbroken ligament of specimen at mid-section thickness in EDD335 (B = 3.2 mm).

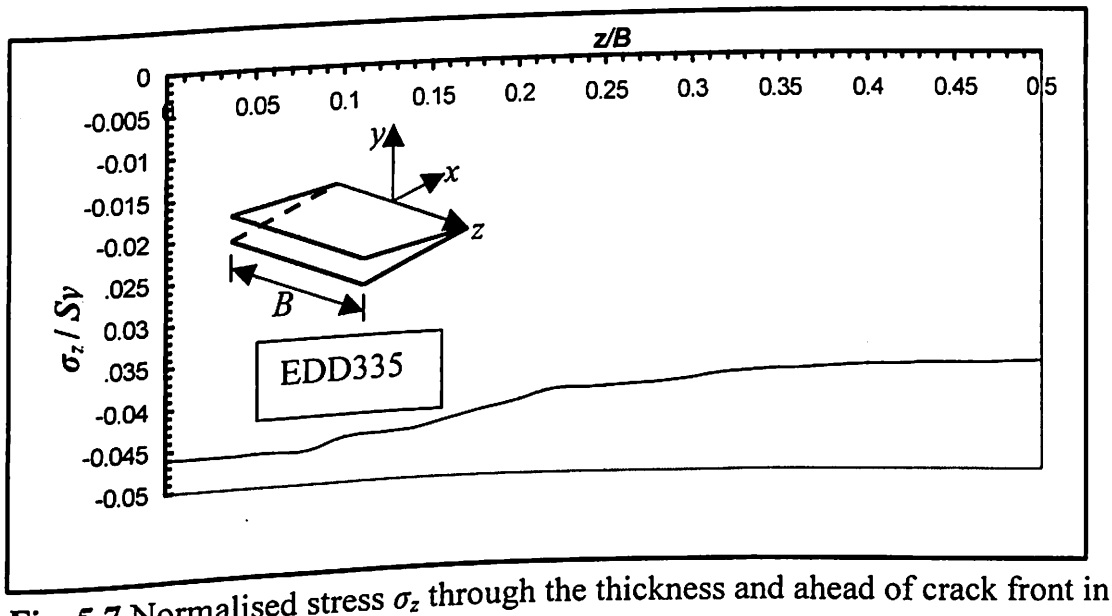

Fig. 5.7 Normalised stress σ_z through the thickness and ahead of crack front in EDD335 (B = 3.2 mm).

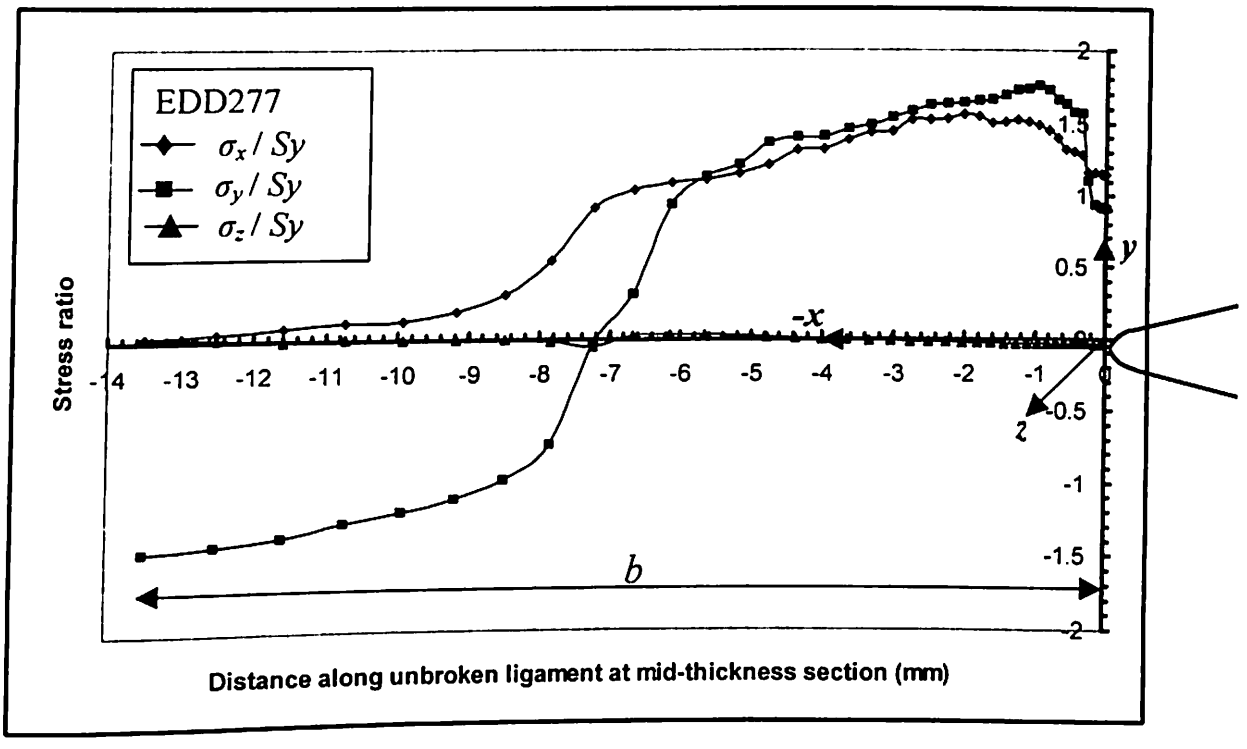

Fig. 5.8 Normalised stresses σ_x, σ_y, σ_z along the unbroken ligament of specimen at mid-section thickness in EDD277 (B = 3.2 mm).

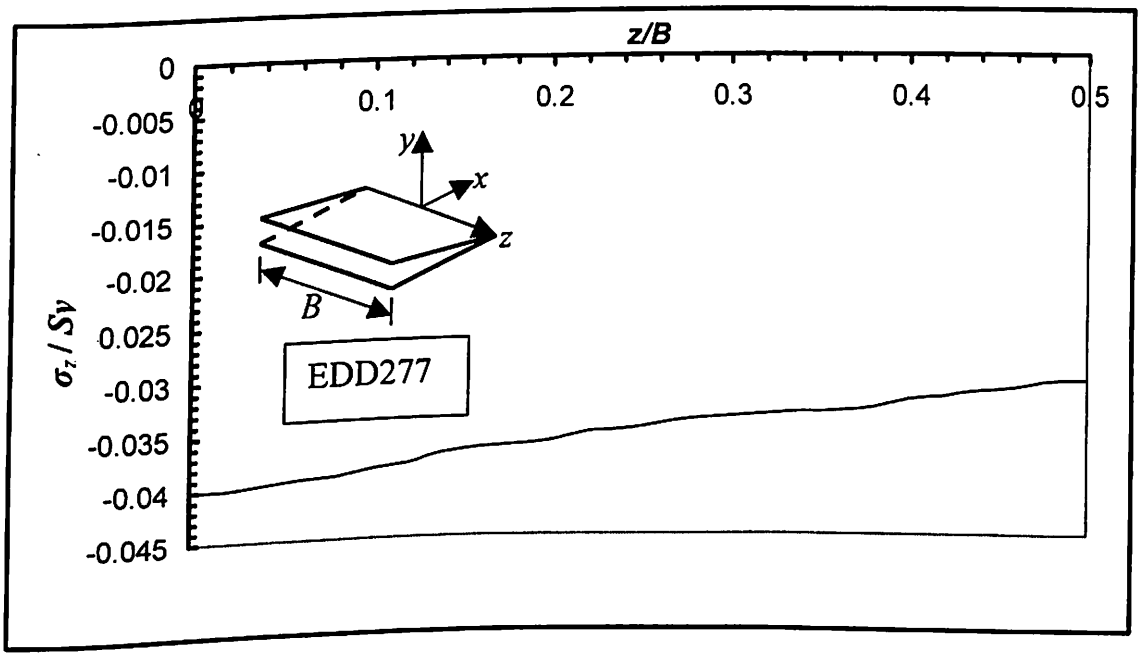

Fig. 5.9 Normalised stress σ_z through the thickness and ahead of crack front in EDD277 (B = 3.2 mm).

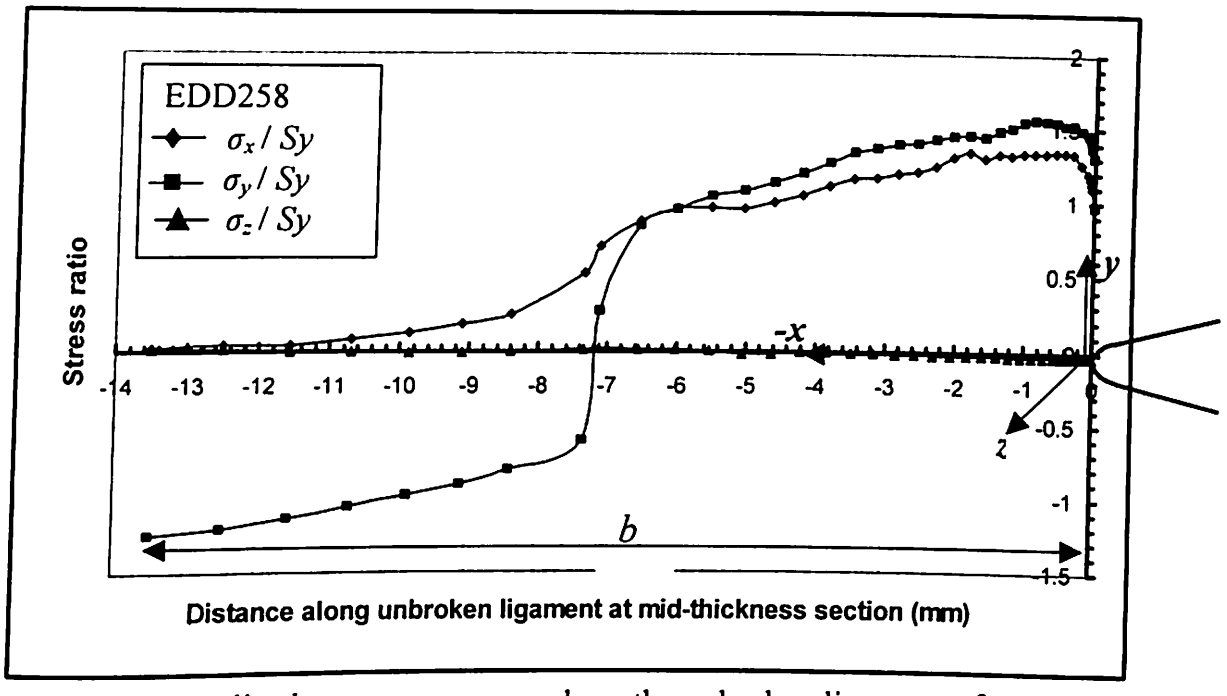

Fig. 5.10 Normalised stresses σ_x, σ_y, σ_z along the unbroken ligament of specimen at mid-section thickness in EDD258 (B = 3.2 mm).

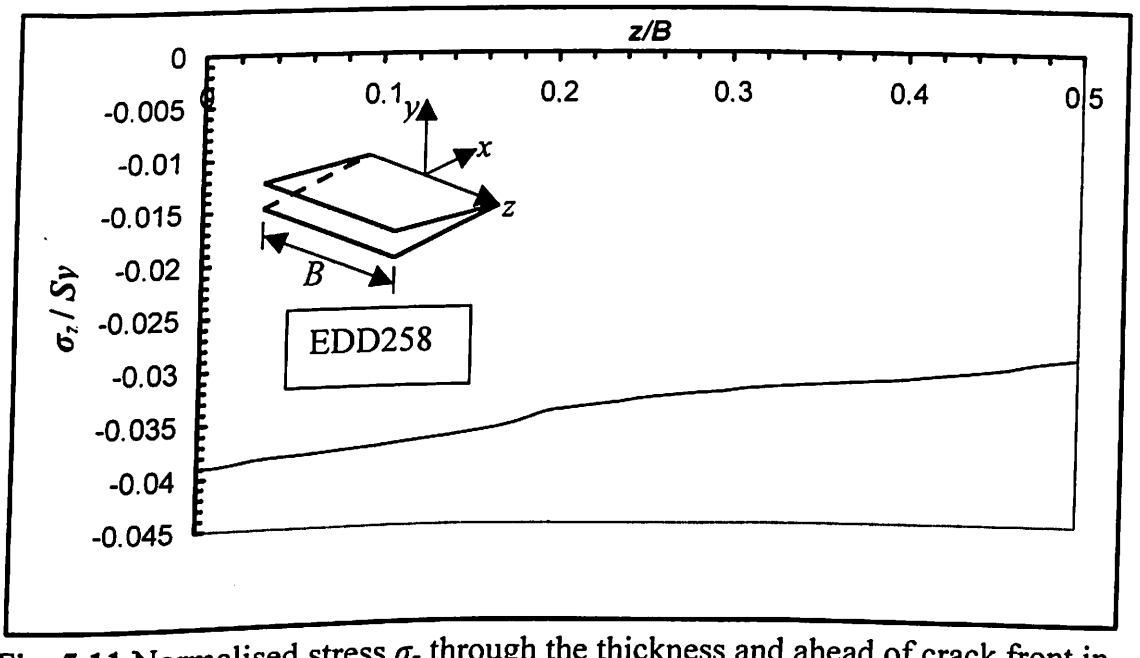

Fig. 5.11 Normalised stress σ_z through the thickness and ahead of crack front in EDD258 (B = 3.2 mm).

Fig. 5.6, 5.8 and 5.10 show that the normalised stress σ_x is high in the vicinity of crack tip and decreases to an almost zero value at the ligament boundary of specimen. The most dominant normalised stress σ_y is also high in the vicinity of crack tip. The σ_y decreases as we move away from the crack tip towards the ligament boundary of specimen. On the way towards ligament boundary, σ_y passes through a zero value and enters in a compressive zone with high negative value on the ligament boundary. In the vicinity of crack tip, stresses σ_x and σ_y drop down because of blunting of crack tip and release of crack tip node. The normalised stress σ_z is negligibly small compared with σ_x and σ_y, which shows the predominantly plane stress fracture behaviour.

As observed from Figures 5.7, 5.9 and 5.11, the stress magnitude as well as the difference in stress magnitude across the thickness is very small. In the present analysis, it is concluded that the crack front is almost uniformly loaded in plane stress condition. This is unlike various reported observations for plane stress – plane strain case by Kumar (1988b, 1991), Zhang (1996), Heerens and Schodel (2002) and for plane strain case by Panontin *et al.* (2000). These reports show a zero value on the surface (z/B = 0.5) indicating a plane stress condition on the surface and a relative high value at mid-thickness section indicating plane strain condition at mid-thickness. The FE analysis results on critical load, *J*-integral and *CTOD* are overestimated and are within 5-12% of experimental results. This discrepancy is attributed towards assumed idealised conditions in FE analysis. In FE analysis, the defect free material, exact size of the specimen (i.e. without any machining allowance) and error free loading are the idealised conditions.

5.5 Discussion on CFOA Model

In the present work, CFOA model is proposed to account for nonlinearities in the relationship between *CTOD* and plastic load-line displacement. The plastic *CTOD* is measured using PHM, *J-CTOD* relation, CFOA model and the results are verified with FEM. The results reveal small difference between the $(\delta_c)_{FEM}$ and $(\delta_c)_{CFOA}$.

In comparison, the PHM results on plastic *CTOD* are on lower side due to the assumption of linear relation between *CTOD* and plastic load-line displacement (V_{pl}) given by Eq. (3.10). This is also discussed by Wilson and Landes (1994). In PHM, the PRF is shown to have a constant value by ASTM E 1290-89 (1989) and BS: 5762 (1979). This factor is shown to depend on initial crack length and unbroken ligament length by Merkle and Corten (1990) as given by Eq. (3.11). For present specimen dimensions using Eq. (3.11), the value of PRF is found to be 0.59. The results on plastic *CTOD* based on PHM and using PRF as 0.59, are reported by Kulkarni *et al.* (2002, 2003a and 2004a).

However, by using CFOA model it is found that the PRF is not constant, however, it depends on crack flank opening angle, which in turn depends on thickness of specimen. The percentage difference in between CFOA and PHM is found to be 9 - 12%. Whereas, the percent difference in between CFOA and FEM is found to be within 5 %. The reason behind this is the nonlinear relation between the plastic *CTOD* and plastic load-line displacement, which is taken into account by CFOA model. Thus, the CFOA is suitable for large load-line displacement.

5.6 Verification of $J - CTOD$ Relation

The unique relationship between J and $CTOD$ i.e. Eq. (3.13) is given by Shih (1981) and is verified with the help of PHM, CFOA and FE methods. The Shih factor d_n is obtained using equations (5.4), (5.5) and (5.6), respectively from PHM, CFOA and FE methods.

$$(d_n)_{PHM} = \frac{S_y(\delta_{pl})_{PHM}}{J_{pl}} \tag{5.4}$$

$$(d_n)_{CFOA} = \frac{S_y(\delta_{pl})_{CFOA}}{J_{pl}} \tag{5.5}$$

$$(d_n)_{FEM} = \frac{S_y(\delta_{pl})_{FEM}}{(J_{pl})_{FEM}} \tag{5.6}$$

The values of $(d_n)_{PHM}$, $(d_n)_{CFOA}$ and $(d_n)_{FEM}$ are tabulated in Table 5.5, 5.6, 5.7 and 5.8, respectively for thickness effect in EDD335, thickness effect in EDD277, strain rate effect in EDD277 and influence of notch radius in EDD258. The corresponding graphical representations are shown in Fig. 5.12 – 5.15.

Table 5.5 Shih factor, d_n for various thickness in EDD335 steel sheet

Sp-code	(B) mm	$(d_n)_{PHM}$	$(d_n)_{CFOA}$	$(d_n)_{FEM}$
S1	1.18	0.9258	0.9930	1.0559
S2	1.28	0.9701	1.0411	1.0032
S3	1.38	0.8867	0.9868	0.9735
S4	1.48	0.9588	1.0927	1.0592
S5	1.58	0.9451	1.0755	1.0220
S6	1.64	0.9476	1.0965	1.0803

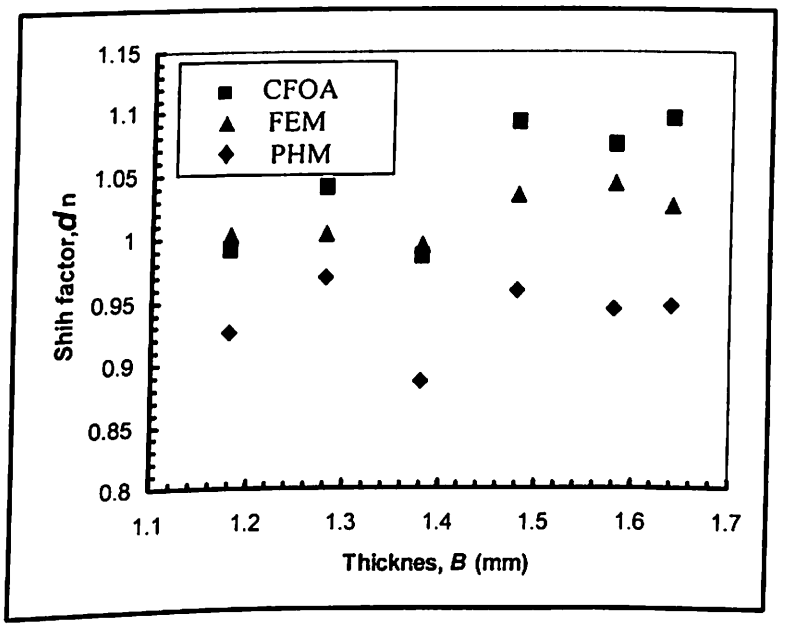

Fig. 5.12 Shih factor for various thicknesses in EDD335.

Table 5.6 Shih factor, d_n for various thickness in EDD277 steel sheet

Sp-code	(B) mm	$(d_n)_{PHM}$	$(d_n)_{CFOA}$	FEM thickness (mm)	$(d_n)_{FEM}$
1.4a	1.4	1.0888	1.1351	1.4	1.042785
1.4b	1.4	1.0817	1.1358		
1.4c	1.4	1.0789	1.1195		
1.9a	1.9	1.0681	1.1185	1.9	1.026728
1.9b	1.9	1.0888	1.1437		
1.9d	1.9	1.0445	1.1472		
2.4a	2.4	1.0205	1.1285	2.4	1.002404
2.4b	2.4	0.9544	1.0366		
2.4c	2.4	0.9485	1.0533		
2.9b	2.9	1.0147	1.0899	2.9	0.979556
2.9c	2.9	1.0268	1.0887		
2.9d	2.9	1.0175	1.0724		
3.2a	3.2	1.0105	1.0661	3.2	0.993058
3.2b	3.2	1.0168	1.0616		
3.2c	3.2	1.0245	1.0671		

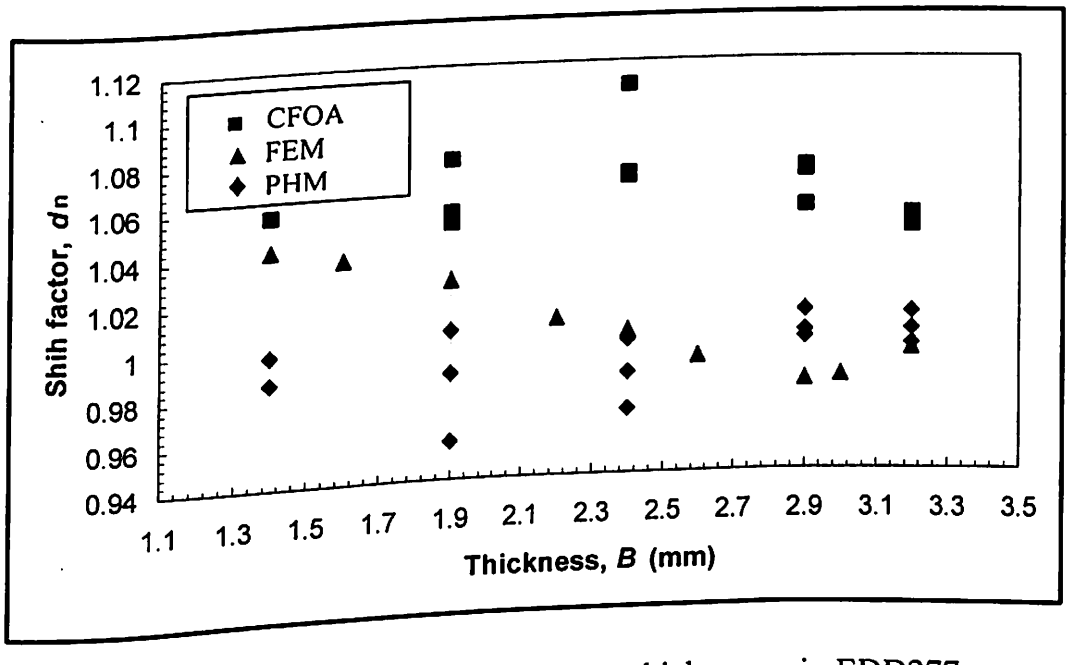

Fig. 5.13 Shih factor for various thicknesses in EDD277.

Table 5.7 Shih factor, d_n for various strain rates in EDD277 steel sheet

Strain rate (mm/min)	$(d_n)_{PHM}$	$(d_n)_{CFOA}$	$(d_n)_{FEM}$
0.2	1.1312	1.1650	1.0995
0.4	1.1357	1.1618	1.0965
0.6	1.1268	1.1545	1.1046
1.0	1.1121	1.1817	1.1081
1.5	1.1830	1.2493	1.1467
2.5	1.2476	1.3473	1.2366

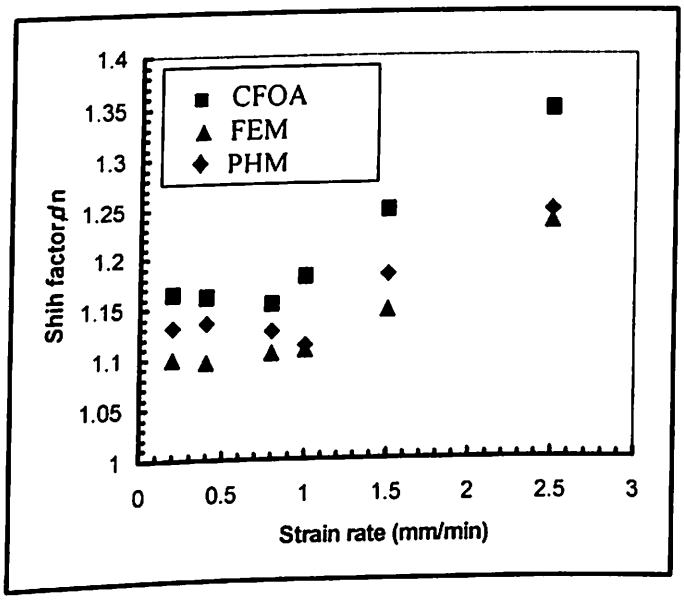

Fig. 5.14 Shih factor for various strain rates in EDD277.

Table 5.8 Shih factor, d_n for various notch radii in EDD258 steel sheet

Notch radius (ρ) mm	$(d_n)_{PHM}$	$(d_n)_{CFOA}$	$(d_n)_{FEM}$
0.07	0.91369	0.985813	1.00102
0.085	0.96521	1.007327	1.000965
0.10	0.9356	1.02897	1.001319
0.11	0.8845	0.975001	1.00108
0.12	0.96631	1.074677	1.001132
0.13	0.99588	1.084972	1.000479
0.14	0.92775	1.028032	1.000633
0.15	1.01226	1.098809	1.001041
0.16	0.84407	0.960977	1.001111
0.17	0.8785	0.967472	1.016727
0.18	0.86967	0.95452	1.000769
0.25	0.93115	0.998764	1.001081
0.40	0.92318	1.001429	1.010686
0.60	0.92681	1.004465	0.99489
0.75	0.95649	1.012362	1.005366

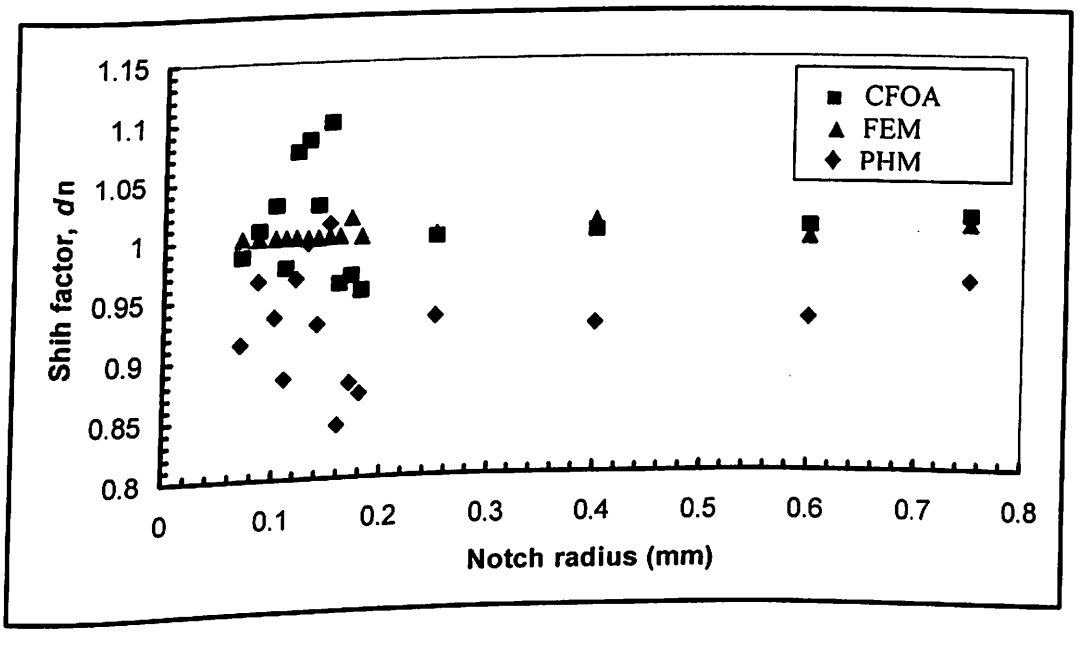

Fig. 5.15 Shih factor for various notch radii in EDD258.

The *J-CTOD* relation is verified in general yielding fracture mechanics and a Shih factor (d_n) is obtained for various objectives, in all three EDD steel. Figures 5.12 – 5.15 show the variation of Shih factor d_n with respect to the influencing parameters under study. It is observed that the d_n is in the range 0.9-1.1 and is independent of effect of thickness and notch radius. In case of strain rate effect, the d_n is increasing beyond the strain rate level of 0.6 mm/min. This implies that there is no consistency in *J-CTOD* relation at higher strain rate value. The $(d_n)_{PHM}$ value is found to be conservative because of lower values of $(\delta_{pl})_{PHM}$ in all cases. The Shih factor, according to Shih (1981), is taken as 0.5 for plane strain analysis. This factor is reported by Paulino *et al.* (2001), in the range of 0.4-0.8 in structural materials for plane stress – plane strain analysis. However, in the present work, for predominantly plane stress condition the average Shih factor is found to be 1 based on various *CTOD* estimations. This is reported by Kulkarni *et al.* (2003b).

The results on plastic *CTOD* are also obtained using *J-CTOD* relation and average value of d_n equal to one. The plastic CTOD based on this relation is referred as $(\delta_{pl})_J$. These results are compared with PHM, CFOA and FEM. The critical *CTOD* values based on *J-CTOD* relation (i.e. $(\delta_c)_J$) are calculated by adding elastic *CTOD* (δ_{el}) and plastic *CTOD*, $(\delta_{pl})_J$. These results are presented in various sections 5.7, 5.8 and 5.9 for the objectives under study.

5.7 Effect of Thickness on Fracture Behaviour

The results on fracture parameters are generated to study thickness effect in EDD335 and EDD277. These results are summarised and discussed in the following two sub-sections for EDD335 and EDD277.

5.7.1 Thickness effect on EDD335

Table 5.9 shows the fracture test results and Table 5.10 shows the results of 3-D FE analysis on critical load and load-line displacement in case of EDD335, for six specimens. The load – load-line displacement plots are shown in Appendix B1.

Table 5.9 Fracture test results to study the effect of thickness in EDD335 steel sheet

Sp-code	(B) mm	Critical load (P_c) kN	LLD (V_{pl}) mm	Fracture Status
S1	1.18	1.194	1.235	CI
S2	1.28	1.311	1.322	CI
S3	1.38	1.431	1.334	CI
S4	1.48	1.572	1.401	CI
S5	1.58	1.704	1.466	CI
S6	1.64	1.773	1.499	CI

Table 5.10 3-D FEA results on EDD335 steel sheet

(B) mm	Critical load (P_C) kN	LLD (V_{pl}) mm
1.18	1.2997	1.22
1.28	1.3941	1.29
1.38	1.5416	1.35
1.48	1.6997	1.42
1.58	1.8332	1.48
1.64	1.9136	1.52

Results on critical load and load-line displacements are plotted in Fig. 5.16 and 5.17 with respect to thickness. Both of these figures show increase in critical load as well as load-line displacement with increase in thickness.

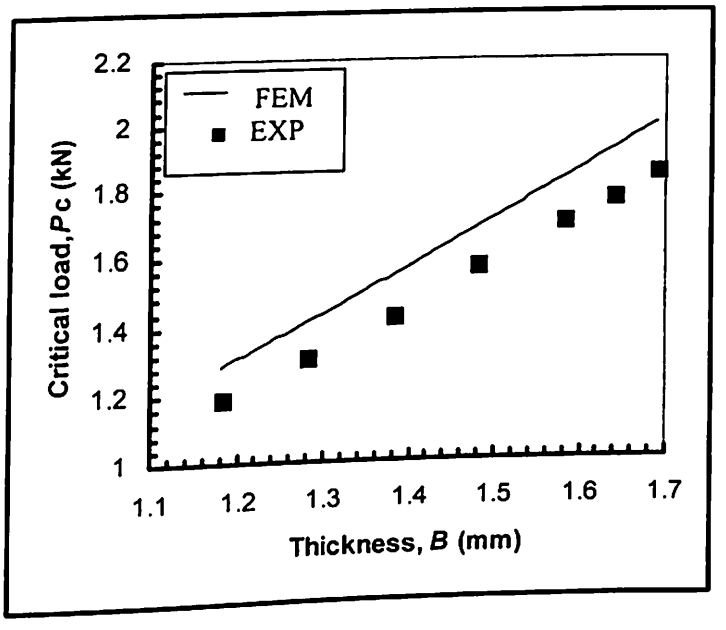

Fig. 5.16 Variation of critical load with thickness in EDD335.

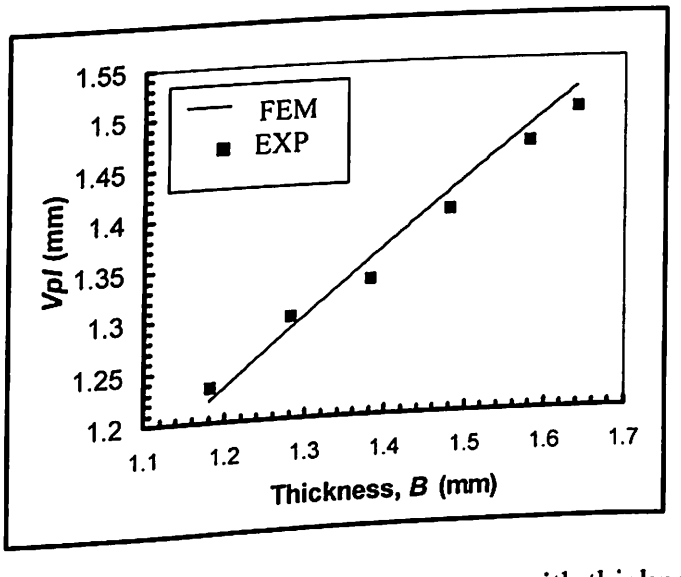

Fig. 5.17 Variation of plastic load-line displacement with thickness in EDD335.

Table 5.11 and Table 5.12 show the results on *J*-integral using ASTM E 813-87 and 3-D FE analysis, respectively. Fig. 5.18 shows an increase in *J*-integral with increase in thickness.

Table 5.11 Experimental results on *J*-Integral for EDD335 steel sheet

Sp-code	(*B*) mm	J_{el} N/mm	J_{pl} N/mm	J_c N/mm
S1	1.18	13.175	193.48	206.66
S2	1.28	13.498	197.76	211.26
S3	1.38	13.834	218.26	232.09
S4	1.48	14.515	211.97	226.49
S5	1.58	14.965	226.60	241.56
S6	1.64	15.035	229.48	244.51

Table 5.12 3-D FEA results on *J*-Integral for EDD335 steel sheet

Sp-code	(*B*) mm	J_{el} N/mm	J_{pl} N/mm	J_C N/mm
S1	1.18	16.42	196.32	212.74
S2	1.28	17.32	209.64	226.96
S3	1.38	18.02	224.42	242.44
S4	1.48	18.89	221.76	240.65
S5	1.58	19.76	234.89	254.65
S6	1.64	20.12	237.07	257.19

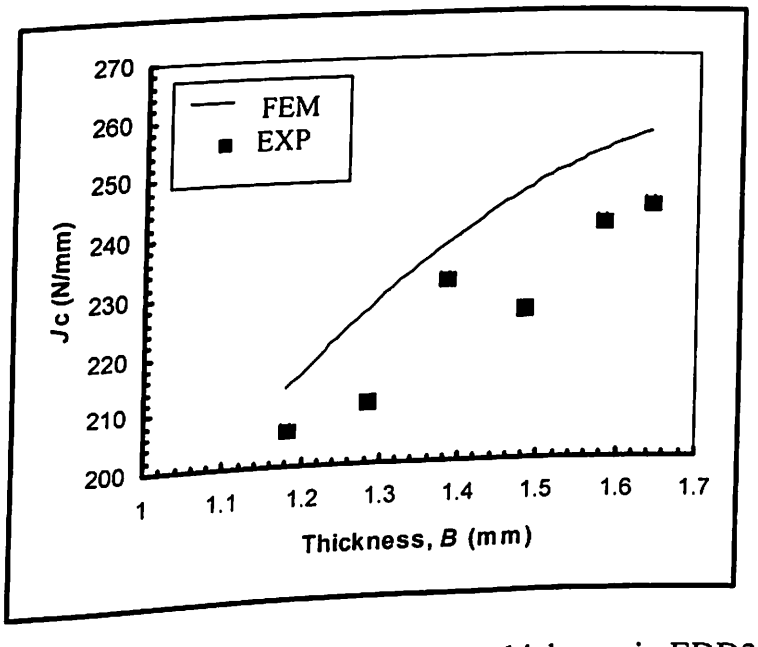

Fig. 5.18 Variation of critical *J*-integral with thickness in EDD335.

Experimental results on elastic and plastic *CTOD*, measured using various techniques, are tabulated in Table 5.13. This table also shows the CFOA values. Table 5.14 shows the results on elastic and plastic *CTOD* using 3-D FE analysis.

Table 5.13 Experimental results on various *CTOD* for EDD335 steel sheet

Sp-code	(B) mm	δ_{el} mm	$(\delta_{pl})_{PHM}$ mm	$(\delta_{pl})_{CFOA}$ mm	$(\delta_{pl})_{J}$ mm	$(\delta_c)_{PHM}$ mm	$(\delta_c)_{CFOA}$ mm	$(\delta_c)_{J}$ mm	CFOA (°)
S1	1.18	0.0393	0.5347	0.5735	0.5776	0.5740	0.6128	0.6169	3.6085
S2	1.28	0.0403	0.5727	0.6146	0.5903	0.6129	0.6549	0.6306	3.7343
S3	1.38	0.0413	0.5777	0.6429	0.6515	0.6190	0.6842	0.6928	3.7680
S4	1.48	0.0433	0.6067	0.6914	0.6327	0.6500	0.7347	0.6761	3.8717
S5	1.58	0.0447	0.6393	0.7285	0.6764	0.6840	0.7722	0.7211	4.0319
S6	1.64	0.0449	0.6491	0.7511	0.6850	0.6949	0.7960	0.7299	4.0777

Table 5.14 3-D FEA results on *CTOD* for EDD335 steel sheet

Sp-code	(B) mm	δ_{el} mm	$(\delta_{pl})_{FEM}$ mm	$(\delta_C)_{FEM}$ mm
S1	1.18	0.0420	0.6188	0.6608
S2	1.28	0.0429	0.6278	0.6707
S3	1.38	0.0443	0.6522	0.6965
S4	1.48	0.0468	0.7012	0.7480
S5	1.58	0.0473	0.7166	0.7639
S6	1.64	0.0482	0.7645	0.8127

Fig. 5.19 shows an increase in elastic *CTOD* with increase in thickness and Fig. 5.20 shows an increase in critical *CTOD* with increase in thickness.

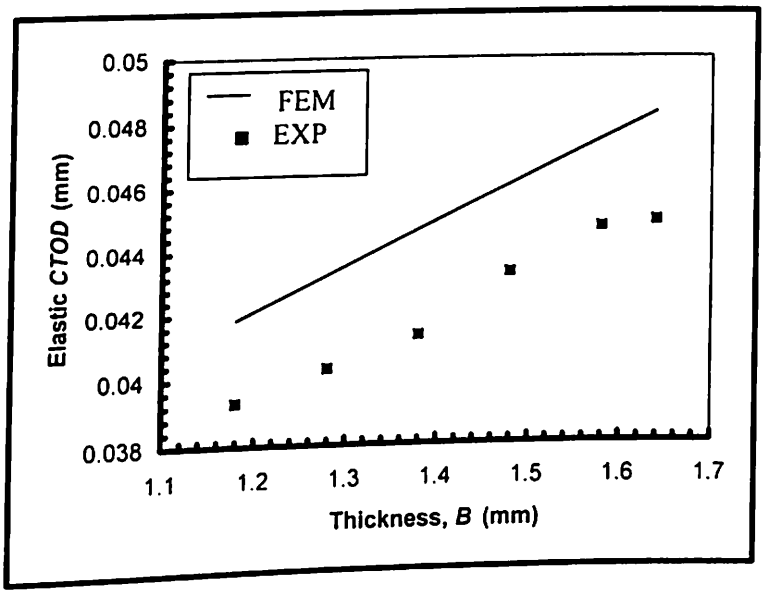

Fig. 5.19 Variation of elastic *CTOD* with thickness in EDD335.

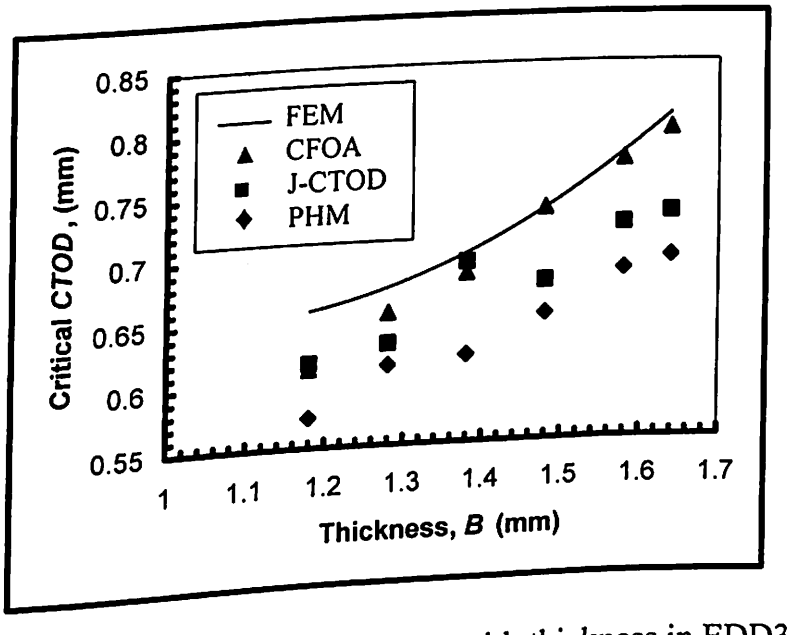

Fig. 5.20 Variation of critical *CTOD* with thickness in EDD335.

5.7.2 Thickness effect on EDD277

In case of EDD277, four specimens are tested for every category of thickness. Out of four, one of the specimens is used to verify the fracture criterion before load drop (BLD) point. Other three specimens are tested at crack initiation (CI) point and an average of three readings on crack initiation results is reported. Table 5.15 shows the fracture test results and Table 5.16 shows the results of 3-D FE analysis on critical load and load-line displacements in case of EDD277. The load – load-line displacement plots are shown in Appendix B2.

Table 5.15 Fracture test results to study the effect of thickness in EDD277 steel sheet

Sp-code	(B) mm	Critical load (P_c) kN	LLD (V_{pl}) mm	Fracture status
1.4a	1.4	0.972	3.08	CI
1.4b	1.4	0.969	3.12	CI
1.4c	1.4	0.968	3.21	CI
1.4d	1.4	0.965	2.8	BLD
1.9a	1.9	1.318	3.53	CI
1.9b	1.9	1.326	3.50	CI
1.9c	1.9	1.307	3.56	BLD
1.9d	1.9	1.349	3.38	CI
2.4a	2.4	1.762	3.60	CI
2.4b	2.4	1.780	3.70	CI
2.4c	2.4	1.733	3.80	CI
2.4d	2.4	1.721	3.05	BLD
2.9a	2.9	2.120	4.29	BLD
2.9b	2.9	2.170	4.05	CI
2.9c	2.9	2.145	4.00	CI
2.9d	2.9	2.155	4.04	CI
3.2a	3.2	2.470	4.30	CI
3.2b	3.2	2.459	4.32	CI
3.2c	3.2	2.486	4.38	CI
3.2d	3.2	2.440	4.17	BLD

Table 5.16 3-D FEA results on EDD277 steel sheet

(B) mm	Critical load (P_c) kN	LLD (V_{pl}) mm
1.4	1.0482	3.18
1.9	1.4108	3.50
2.4	1.8814	3.80
2.9	2.3400	4.10
3.2	2.7189	4.30

Results on critical load and load-line displacement are plotted with respect to thickness in Fig. 5.21 and 5.22. Similar to EDD335 material, both of these figures show increase in critical load as well as load-line displacement with increase in thickness.

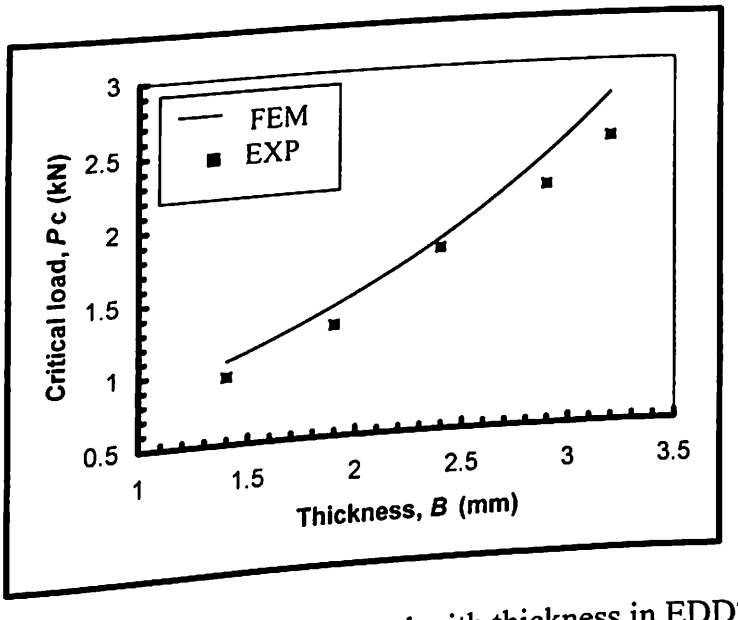

Fig. 5.21 Variation of critical load with thickness in EDD277.

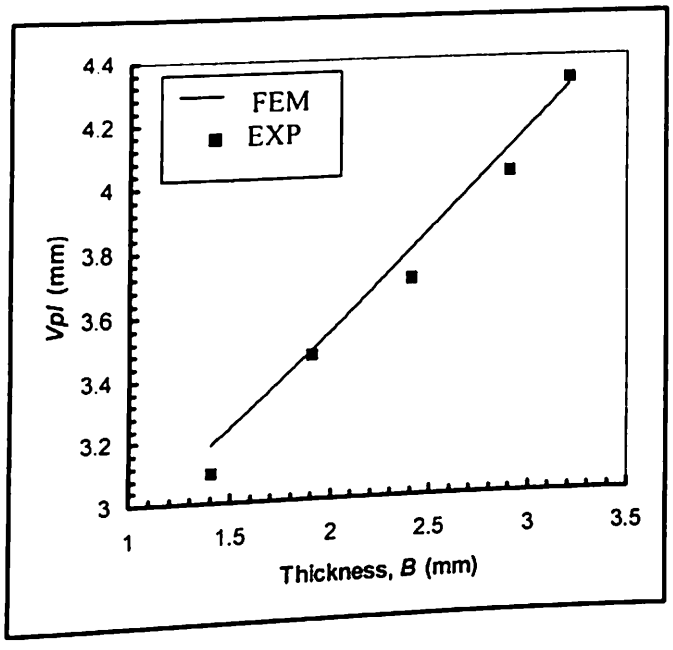

Fig. 5.22 Variation of plastic load-line displacement with thickness in EDD277.

Table 5.17 and 5.18 shows the results on *J*-integral using experimental and 3-D FE analysis, respectively. Fig. 5.23 shows an increase in *J*-integral with increase in thickness.

Table 5.17 Experimental results on *J*-Integral for EDD277 steel sheet

Sp-code	(*B*) mm	J_{el} N/mm	J_{pl} N/mm	J_c N/mm
1.4a	1.4	6.202	339.37	345.57
1.4b	1.4	6.165	346.02	352.18
1.4c	1.4	6.1577	356.94	363.10
1.9a	1.9	6.189	396.49	402.67
1.9b	1.9	6.268	385.66	391.92
1.9d	1.9	6.487	388.21	394.69
2.4a	2.4	6.934	423.21	430.14
2.4b	2.4	7.077	465.09	472.16
2.4c	2.4	6.707	480.65	487.35
2.9b	2.9	7.206	478.83	486.03
2.9c	2.9	7.040	467.36	474.40
2.9d	2.9	7.106	476.34	483.44
3.2a	3.2	7.665	510.49	518.15
3.2b	3.2	7.596	509.72	517.31
3.2c	3.2	7.765	512.92	520.68

Table 5.18 3-D FEA results on *J*-Integral for EDD277 steel sheet

(*B*) mm	J_{el} N/mm	J_{pl} N/mm	J_C N/mm
1.4	6.70	373.11	392.14
1.6	6.76	392.35	405.66
1.9	6.92	421.32	432.03
2.2	7.14	447.88	454.10
2.4	7.31	470.79	467.98
2.6	7.42	491.45	483.29
2.9	7.67	515.11	508.36
3.0	7.83	524.07	518.16
3.2	8.28	549.92	542.67

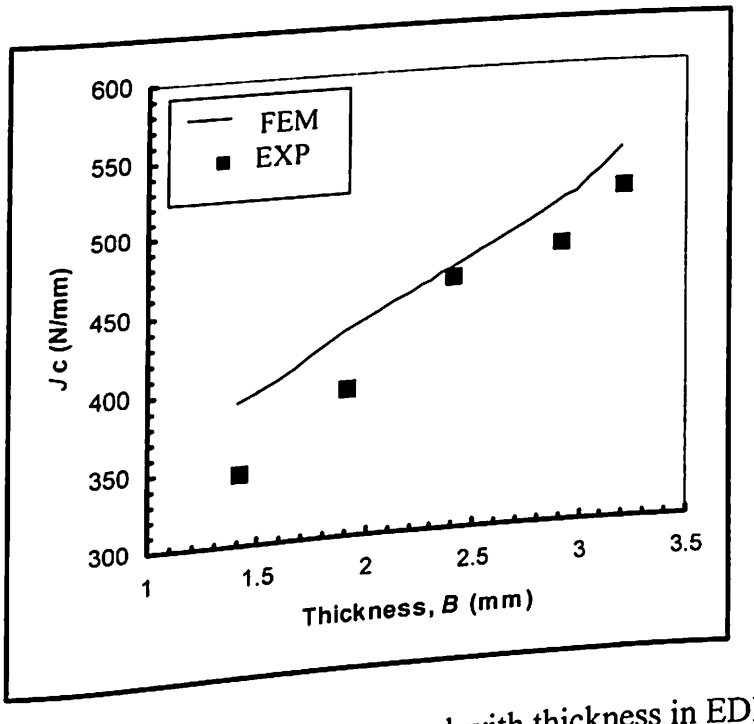

Fig. 5.23 Variation of critical *J*-integral with thickness in EDD277.

Experimental results of elastic and plastic *CTOD*, measured using various techniques, are tabulated in Table 5.19. CFOA values are also shown in this table. Table 5.20 shows the results on elastic and plastic *CTOD* using 3-D FE model.

Table 5.19 Experimental results on various *CTOD* for EDD277 steel sheet

Sp-code	(B) mm	δ_{el} mm	$(\delta_{pl})_{PHM}$ mm	$(\delta_{pl})_{CFOA}$ mm	$(\delta_{pl})_{J}$ mm	$(\delta_c)_{PHM}$ mm	$(\delta_c)_{CFOA}$ mm	$(\delta_c)_{J}$ mm	CFOA (°)
1.4a	1.4	0.0224	1.3339	1.3908	1.2251	1.3563	1.4132	1.2475	9.1934
1.4b	1.4	0.0223	1.3512	1.4189	1.2491	1.3735	1.4412	1.2714	9.2617
1.4c	1.4	0.0223	1.3903	1.4426	1.2886	1.4126	1.4649	1.3109	9.2811
1.9a	1.9	0.0224	1.5288	1.6010	1.4313	1.5512	1.6234	1.4537	10.5015
1.9b	1.9	0.0226	1.5158	1.5924	1.3922	1.5384	1.6150	1.4148	10.3765
1.9d	1.9	0.0250	1.5591	1.7242	1.5278	1.5841	1.7492	1.5528	9.6487
2.4a	2.4	0.0256	1.6024	1.7406	1.6790	1.6280	1.7662	1.7046	10.206
2.4b	2.4	0.0242	1.6457	1.8278	1.7351	1.6699	1.8520	1.7593	10.6605
2.4c	2.4	0.0260	1.7540	1.8841	1.7286	1.7800	1.9101	1.7546	10.7287
2.9b	2.9	0.0277	1.8623	1.9648	1.8429	1.8900	1.9925	1.8706	11.7728
2.9c	2.9	0.0274	1.8709	1.9536	1.8401	1.8983	1.9810	1.8675	11.7615
2.9d	2.9	0.0256	1.7497	1.8442	1.7196	1.7753	1.8698	1.7452	11.9429
3.2a	3.2	0.0277	1.8623	1.9648	1.8429	1.8900	1.9925	1.8706	12.6905
3.2b	3.2	0.0274	1.8709	1.9536	1.8401	1.8983	1.9810	1.8675	12.8602
3.2c	3.2	0.0280	1.8969	1.9760	1.8516	1.9249	2.004	1.8796	13.0639

Table 5.20 3-D FEA results on *CTOD* for EDD277 steel sheet

(B) mm	δ_{el} mm	$(\delta_{pl})_{FEM}$ mm	$(\delta_C)_{FEM}$ mm
1.4	0.0242	1.4046	1.4288
1.9	0.025	1.5617	1.5867
2.4	0.0264	1.7037	1.7301
2.9	0.0277	1.8216	1.8493
3.2	0.0299	1.9715	2.0014

Fig. 5.24 shows an increase in elastic *CTOD* with increase in thickness and Fig. 5.25 shows an increase in critical *CTOD* with increase in thickness.

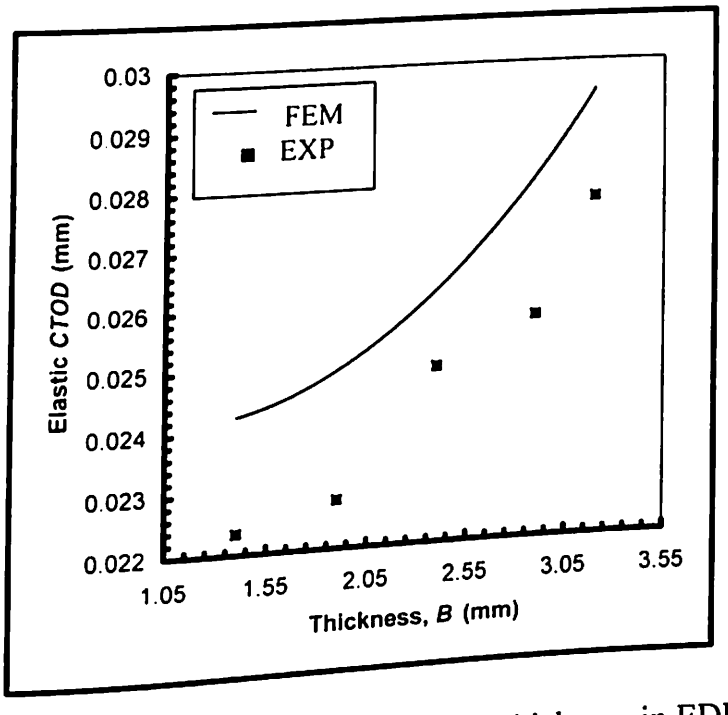

Fig. 5.24 Variation of elastic *CTOD* with thickness in EDD277.

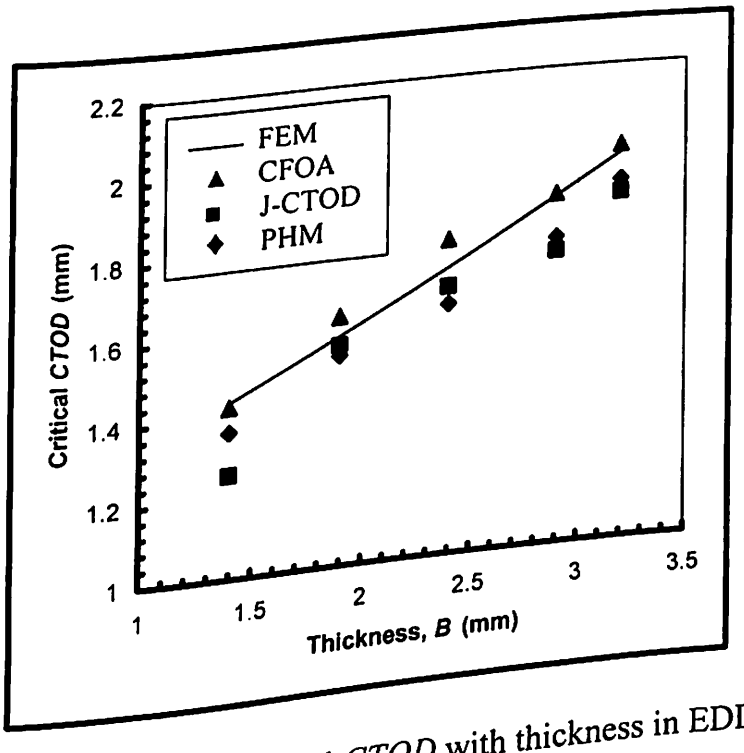

Fig. 5.25 Variation of critical *CTOD* with thickness in EDD277.

The effect of thickness on fracture parameters is studied in case of EDD335 and EDD277 steel sheets. The increase in fracture parameters with increase in thickness is based on the increase in critical load and increase in load-line displacement as shown in figures 5.16, 5.17, 5.21 and 5.22 for both the materials.

This fracture behaviour is unlike that for thick plates, wherein the fracture toughness decreases as thickness increases as reported by Srawely and Brown (1975) and Pandey *et al.* (1997). This specific fracture behaviour is also observed by Liu and Ke (1976) using critical stress intensity factor as a fracture toughness parameter. However, according to Anderson (1994), use of stress intensity factor as a fracture parameter becomes invalid concepts in materials possessing high ductility. They also tried to measure the *CTOD* by using Moire fringe technique, which is too elaborate to employ in practice. The existing method like PHM and proposed method like CFOA can be used, as degree of blunting is high enough in case of EDD steel sheets. The investigation by Liu (1976) did neither show a physical event of crack initiation nor discuss about the reason behind the increasing fracture toughness behaviour. The reason behind the increase in fracture toughness with increase in thickness is explained in section 5.7.3.

5.7.3 Physical significance of fracture behaviour

Firrao and Roberti (1983), Atkins and Mai (1987), Castrodeza *et al.* (2004) have reported that, close to the free surfaces, material deforms in plane stress condition and in the interior, plane strain condition exist. In some cases, degree of plane strain is higher than the degree of plane stress, whereas in other cases it is other way round, depending on material as well as size. In the present work for EDD steel sheets, it has

been already shown (in sub-section 5.4.1) that for the thickness range (1 – 3.2 mm), there exist a predominantly plane stress condition.

The fracture toughness depends on thickness of the specimen and plastic area under the load – load-line displacement curve. This is shown with the help of Eq. (3.7). In case of EDD steel sheet, elastic contribution towards the J or $CTOD$ values is negligible indicating that plasticity is the only source of toughness. In Eq. (3.7), B and A_{pl} are the variables. These variables are closely associated with each other.

For lower range of sheet thickness, both the free surfaces are as good as merged into each other and are absolutely traction free. The specimen cannot offer much resistance in spite of high amount of plasticity ahead of crack tip, because of a very thin cross sectional area. As thickness increases, the load carrying capacity increases and fracture occurs at relatively high critical load. It is concluded that increase in A_{pl} is associated with increase in B. However, there is a critical limit of thickness, beyond which, the A_{pl} decreases because of increase in B. The reason is, in lower range of thickness, the material is free to move in the plane of sheet because of predominantly plane stress condition. However, for a higher range of sheet/plate thickness, material is constrained and is not able to move in its plane because the stress in thickness direction has a finite value, which is not too much smaller than the stresses in the x- and y-direction. The effect of stress in thickness direction reduces the A_{pl} value. Thus beyond a critical limit of thickness, the fracture toughness decreases as thickness increases. This is supported with the help of a 3-D finite element stress analysis performed on a plate with a circular hole, for a wide range of thickness (1 – 15 mm) by Talan *et al.* (2003). In the report of Talan *et al.* (2003), the

variation of principal stresses in three directions is shown with the help of Mohr's circle diagram. The same study can be extended to crack in a sheet. In their study, the maximum shear stress is considered to be the indirect measure of fracture toughness.

As mentioned by Pandey *et al.* (1997), for the range of thickness 0.76 to 7.1 mm, the fracture toughness decreases as thickness increases in particle reinforced Al alloy composites. This is due to the low strain and reduced plasticity ahead of crack tip, which is a material behaviour. Hence the material as well as thickness is responsible for the increase of fracture toughness.

5.8 Effect of Strain Rate on Fracture Behaviour

The results on fracture parameters are generated to investigate the effect of strain rate in EDD277. Table 5.21 shows the fracture test results in case of EDD277 and Table 5.22 shows the results of 3-D FE analysis on critical load and load-line displacements at various strain rates. The load – load-line displacement plots are shown in Appendix B3.

Table 5.21 Fracture test results to study the effect of strain rate in EDD277

Sp-code	(B) mm	Strain rate (mm/min)	Critical load (P_c) kN	LLD (V_{pl}) mm	Fracture status
1.4A	1.4	0.2	0.972	3.20	CI
1.4B	1.4	0.4	0.968	3.20	CI
1.4C	1.4	0.6	0.960	3.16	CI
1.4D	1.4	1.0	0.855	2.92	CI
1.4E	1.4	1.5	0.822	2.78	CI
1.4F	1.4	2.5	0.781	2.55	CI

Table 5.22 3-D FEA results on EDD277 steel sheet

Strain rate (mm/min)	Critical load (P_C) kN	LLD (V_{pl}) mm
0.2	0.996	3.263
0.4	0.990	3.249
0.6	0.985	3.227
1.0	0.896	3.074
1.5	0.869	2.855
2.5	0.775	2.560

Results on critical load and load-line displacements are plotted in Fig. 5.26 and 5.27 with respect to strain rate. In both of these figures, the experimental as well as FEA results shows sharp decrease in critical load as well as load-line displacement beyond a strain rate level of 0.6 mm/min.

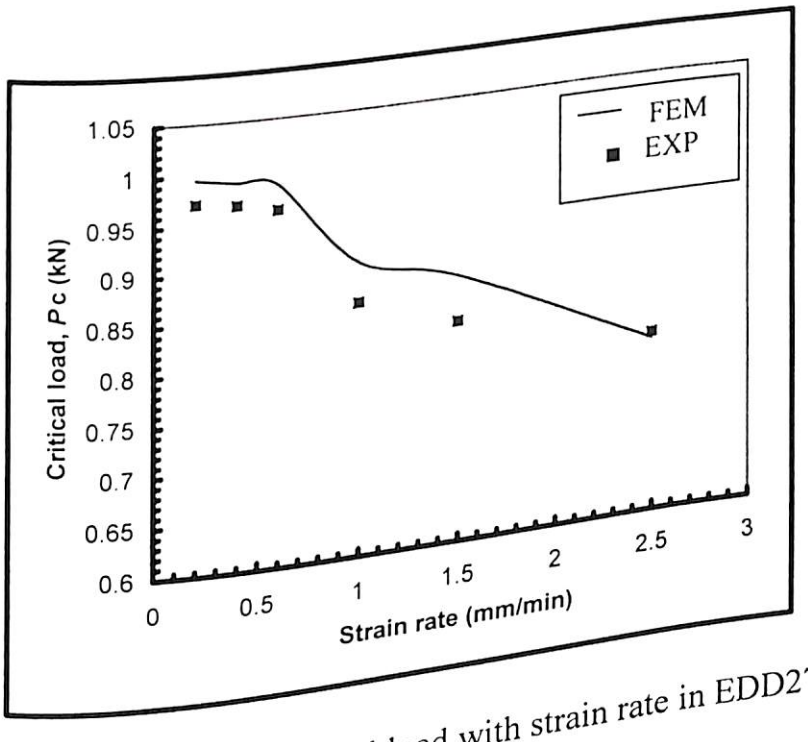

Fig. 5.26 Variation of critical load with strain rate in EDD277.

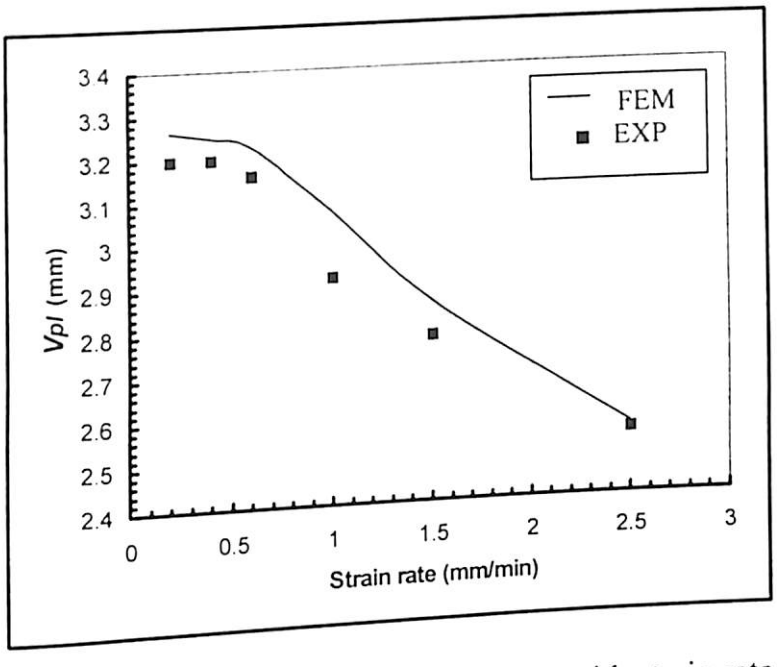

Fig. 5.27 Variation of plastic load-line displacement with strain rate in EDD277.

Table 5.23 and 5.24 shows the results on *J*-integral using ASTM E 813-87 and 3-D FE analysis, respectively at various strain rates. In Fig. 5.28, the 3-D FE analysis result shows a slow and continuous decrease in *J*-integral with increase in strain rate. The slope of decrement is steep beyond 0.6 mm/min. However, the experimental results on *J*-integral show a sharp decrease only beyond 0.6 mm/min strain rate.

Table 5.23 Experimental results on *J*-Integral for EDD277 steel sheet

Sp-code	Strain rate (mm/min)	J_{el} N/mm	J_{pl} N/mm	J_c N/mm
1.4A	0.2	6.1989	339.37	345.57
1.4B	0.4	6.1509	338.02	344.17
1.4C	0.6	6.0486	336.42	342.47
1.4D	1.0	4.8003	314.97	319.77
1.4E	1.5	4.4356	281.92	286.36
1.4F	2.5	4.0048	245.19	249.19

Table 5.24 3-D FEA results on *J*-Integral for EDD277 steel sheet

Strain rate (mm/min)	J_{el} N/mm	J_{pl} N/mm	J_C N/mm
0.2	7.1024	361.56	368.67
0.4	6.7107	358.91	365.62
0.6	6.4803	354.41	360.89
1.0	5.5404	339.11	344.65
1.5	5.3312	312.19	317.52
2.5	4.6562	272.77	277.42

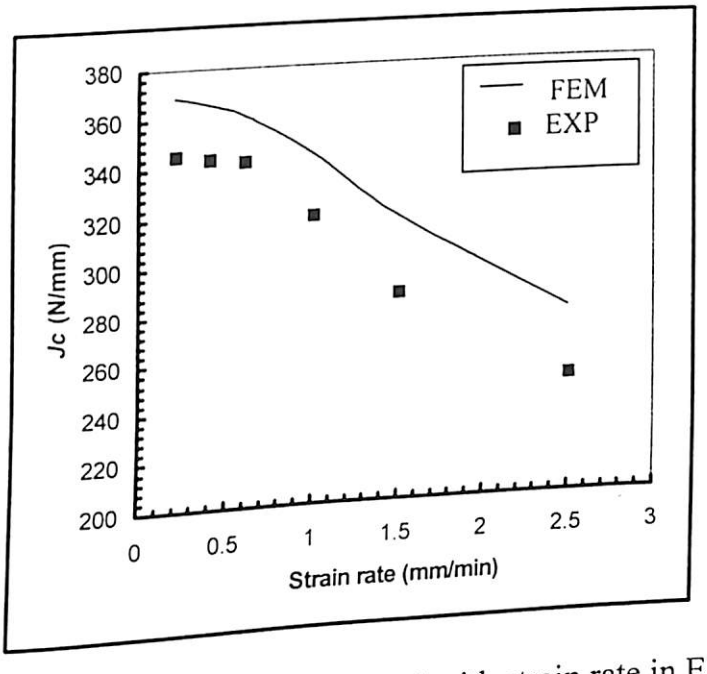

Fig. 5.28 Variation of critical *J*-integral with strain rate in EDD277.

Experimental results on elastic and plastic *CTOD*, measured using various methods are tabulated in Table 5.25. Table 5.25 also shows the values of CFOA. Table 5.26 shows the results on elastic and plastic *CTOD* using 3-D FE analysis.

Table 5.25 Experimental results on various *CTOD* for EDD277 steel sheet

Sp-code	Strain. rate mm/min	δ_{el} mm	$(\delta_{pl})_{PHM}$ mm	$(\delta_{pl})_{CFOA}$ mm	$(\delta_{pl})_J$ mm	$(\delta_c)_{PHM}$ mm	$(\delta_c)_{CFOA}$ mm	$(\delta_c)_J$ mm	CFOA (°)
1.4A	0.2	0.0224	1.3859	1.4273	1.2251	1.4083	1.4497	1.2475	9.65
1.4B	0.4	0.0222	1.3859	1.4177	1.2202	1.4081	1.4399	1.2424	9.70
1.4C	0.6	0.0218	1.3686	1.4021	1.2145	1.3903	1.4239	1.2363	9.57
1.4D	1.0	0.0170	1.2646	1.3437	1.1370	1.2816	1.3607	1.1540	8.58
1.4E	1.5	0.0160	1.2040	1.2715	1.0177	1.2200	1.2875	1.0337	8.21
1.4F	2.5	0.0145	1.1044	1.1925	0.8851	1.1189	1.207	0.8996	7.39

Table 5.26 3-D FEA results on *CTOD* for EDD277 steel sheet

Strain rate (mm/min)	δ_{el} mm	$(\delta_{pl})_{FEM}$ mm	$(\delta_C)_{FEM}$ mm
0.2	0.02565	1.4352	1.4608
0.4	0.02543	1.4208	1.4462
0.6	0.02522	1.4133	1.4385
1.0	0.02240	1.3567	1.3791
1.5	0.01933	1.2924	1.3117
2.5	0.01681	1.2178	1.2346

Fig. 5.29 shows a constant elastic *CTOD* up to 0.6 mm/min strain rate, beyond which, there is a decrease in elastic *CTOD* with increase in strain rate. Similarly Fig. 5.30 shows a constant critical *CTOD* up to 0.6 mm/min strain rate, beyond which there is a decrease in critical *CTOD* with increase in strain rate.

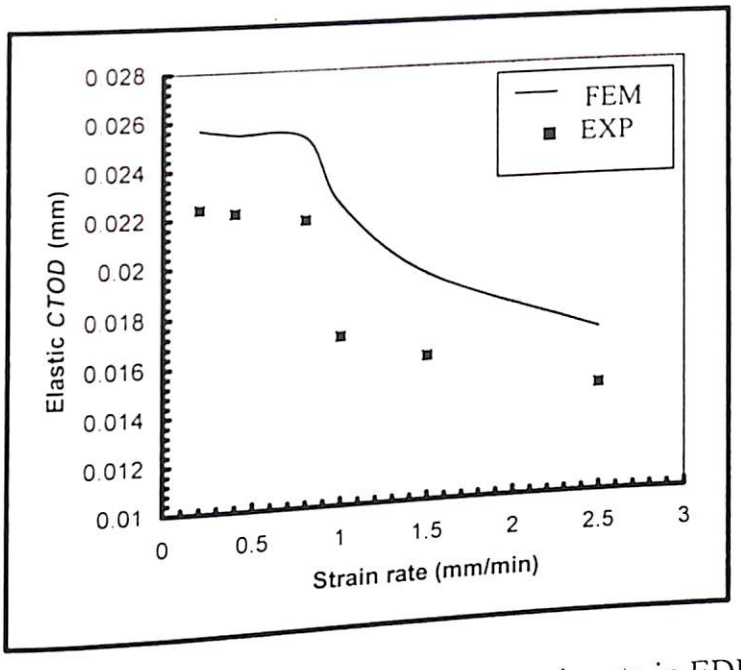

Fig. 5.29 Variation of elastic *CTOD* with strain rate in EDD277.

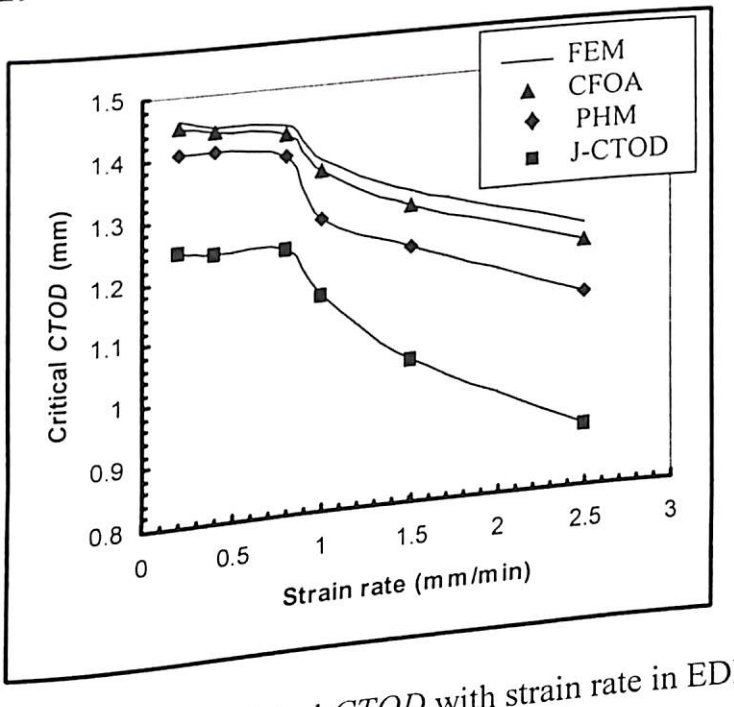

Fig. 5.30 Variation of critical *CTOD* with strain rate in EDD277.

In the present study, only the general macroscopic behaviour involving strain rate is considered. The effect of strain rate on fracture parameters shows very small difference in results up to about 0.6 mm/min. However, beyond this strain rate level,

it is found that EDD sheet has considerable sensitivity at high strain rate even at room temperature.

The reason may be same as in case of strain rate effects on strength and ductility. According to Callister (2003), as strain rate increases, the tensile strength of steel and other alloys increases, however, the ductility values tend to diminish. With high strain rate, plastic deformation becomes a difficult process, as dislocation motion is restricted. Dislocation movements through crystal lattice involve atomic diffusion and displacements under the applied stress. When the strain rate increases, the atomic diffusion vis-à-vis the dislocations motion becomes difficult because of short duration. In other words, process of deformation becomes limited resulting in reduced plasticity and toughness. Elastic contribution towards J or $CTOD$ values is negligible indicating that the plasticity is the source of toughness. Therefore, it is concluded that for higher formability, the forming of the EDD steel sheet should be done at lower strain rates. The strain rate 0.6 m/min is found to be critical strain rate in case of EDD277. Beyond the critical strain rate, the results found are not good for forming operations.

5.9 Influence of Notch Radius on Fracture Behaviour

The results on fracture parameters are generated to investigate the influence of notch radius in EDD258 using fatigue pre-cracked and notched specimens. Table 5.27 shows the fracture test results in case of EDD258 and Table 5.28 shows the results of 3-D FE analysis on critical load and load-line displacements for various notch radii. The load – load-line displacement plots are shown in Appendix B4.

Table 5.27 Fracture test results to study the effect of notch radii in EDD258 steel

Sp-code	Notch radius (ρ) mm	Critical load (P_c) kN	LLD (V_{pl}) mm	Fracture status
SP1	0.07	2.488	4.68	CI
SP2	0.085	2.420	3.10	CI (faulty)
SP3	0.10	2.500	4.62	CI
SP4	0.11	2.611	4.22	CI
SP5	0.12	2.539	4.61	CI
SP6	0.13	2.485	4.61	CI
SP7	0.14	2.490	4.60	CI
SP8	0.15	2.587	4.55	CI
SP9	0.16	2.591	4.34	CI
SP10	0.17	2.622	4.58	CI
SP11	0.18	2.618	4.61	CI
SP12	0.25	2.710	5.21	CI
SP13	0.40	2.754	5.26	CI
SP14	0.60	2.853	5.42	CI
SP15	0.75	2.912	5.74	CI
SP16	0.075	2.460	4.49	BLD

Table 5.28 3-D FEA results on EDD258 steel sheet

Notch radius (ρ) mm	Critical load (P_c) kN	LLD (V_{pl}) mm
0.07	2.6856	4.60
0.085	2.6913	4.61
0.10	2.7192	4.63
0.11	2.7208	4.64
0.12	2.7209	4.65
0.13	2.7223	4.66
0.14	2.7228	4.66
0.15	2.7300	4.69
0.16	2.7460	4.69
0.17	2.8199	4.76
0.18	2.8651	4.88
0.25	2.9447	5.17
0.40	3.0285	5.38
0.60	3.1347	5.51
0.75	3.2385	5.65

Fig. 5.31 and Fig. 5.32 shows plots of critical load and load line displacement, respectively for various notch radii. In FE analysis, the load as well as the load-line displacement is increasing continuously. This rate of increase is relatively low up to 0.16 mm notch radius and thereafter the increase is at high rate with respect to notch radius. However, experimental results show minor fluctuations in load and load-line displacement values up to 0.16 mm notch radius.

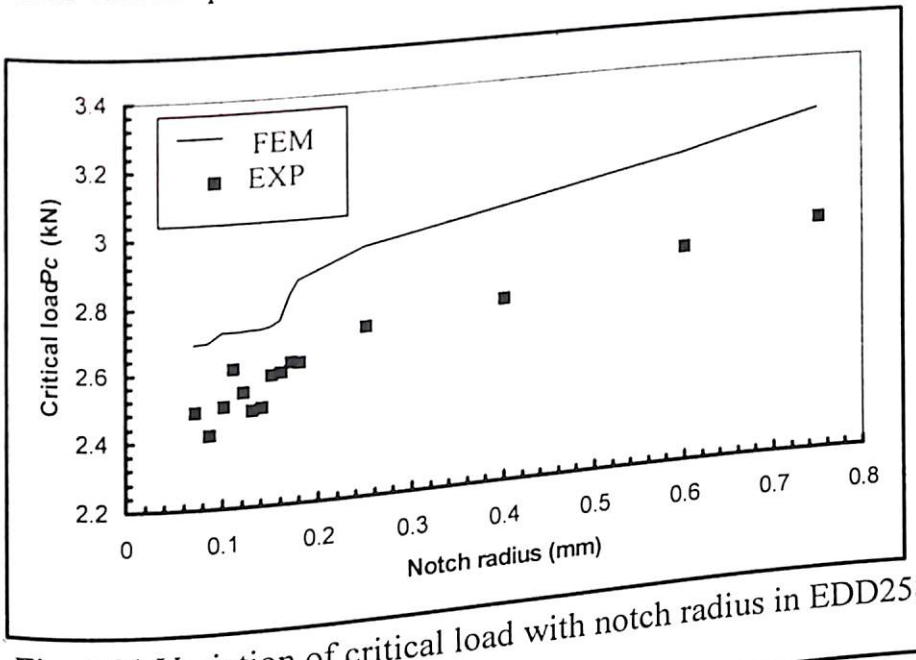

Fig. 5.31 Variation of critical load with notch radius in EDD258.

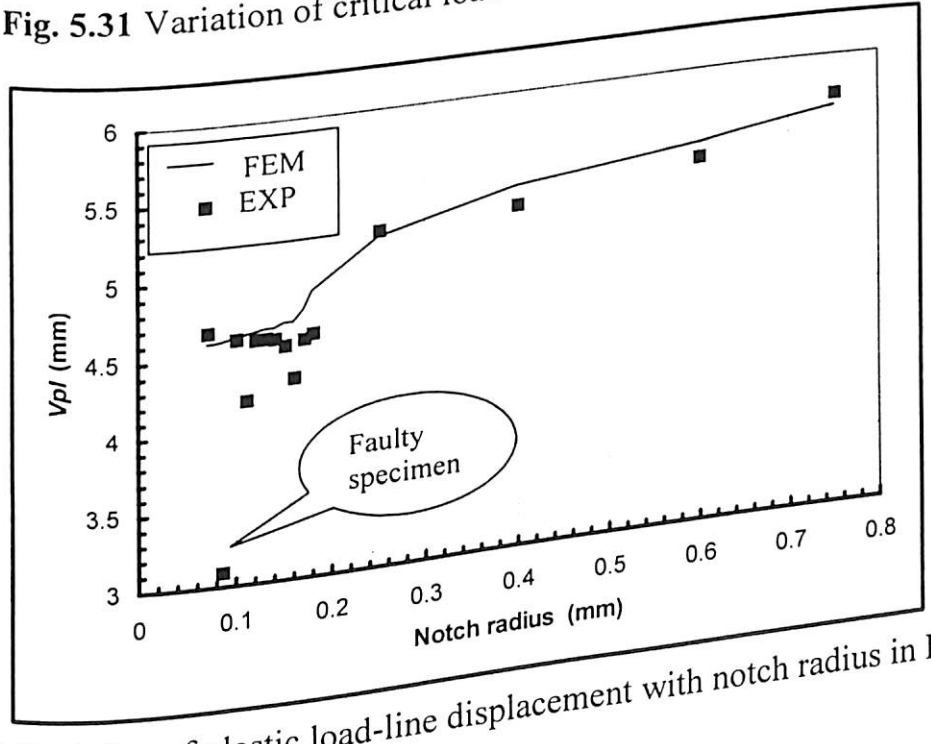

Fig. 5.32 Variation of plastic load-line displacement with notch radius in EDD258.

It is observed from the experimental results that, critical loads are fluctuating between 2.5 kN and 2.611 kN till a notch radius of 0.16 mm. This scatter in experimental data is expected. Thereafter, the critical load values as well as load-line displacement increases with increase in notch radius. According to Srinivas and Kamat (1992) and Faucher *et al.* (1990), larger load is required to open the notch, as the degree of blunting increases with increase in notch radius. The result of specimen having a notch radius of 0.085 mm is an odd result because of difficulties observed in fatigue pre-cracking as discussed in section 3.9.

Table 5.29 and 5.30 shows the results on *J*-integral using ASTM E 813-87 and 3-D FE analysis, respectively for various notch radii.

Table 5.29 Experimental results on *J*-Integral for EDD258 steel sheet

Sp-code	Notch radius (ρ) mm	J_{el} N/mm	J_{pl} N/mm	J_c N/mm
SP1	0.07	7.77	572.34	580.11
SP2	0.085	7.35	358.88	366.23
SP3	0.10	7.85	551.77	559.62
SP4	0.11	8.56	533.12	541.68
SP5	0.12	7.35	533.08	540.43
SP6	0.13	8.02	517.25	525.27
SP7	0.14	7.79	554.03	561.82
SP8	0.15	8.41	502.26	510.67
SP9	0.16	8.43	574.54	582.97
SP10	0.17	8.63	582.55	591.18
SP11	0.18	8.61	592.32	600.93
SP12	0.25	9.22	625.21	634.43
SP13	0.40	9.53	636.66	646.19
SP14	0.60	10.23	653.46	663.69
SP15	0.75	10.65	670.56	681.21

Table 5.30 3-D FEA results on *J*-Integral for EDD258 steel sheet

Notch radius (ρ) mm	J_{el} N/mm	J_{pl} N/mm	J_C N/mm
0.07	8.30	556.30	564.60
0.085	8.30	556.82	565.12
0.10	8.33	557.19	565.52
0.11	8.33	558.56	566.89
0.12	8.36	559.33	567.69
0.13	8.36	559.85	568.21
0.14	8.38	559.97	568.35
0.15	8.38	560.18	568.56
0.16	8.41	561.79	570.20
0.17	8.41	572.98	581.39
0.18	8.56	585.88	594.44
0.25	9.00	606.47	615.47
0.40	9.62	618.32	627.94
0.60	10.31	645.59	655.90
0.75	10.75	660.65	671.40

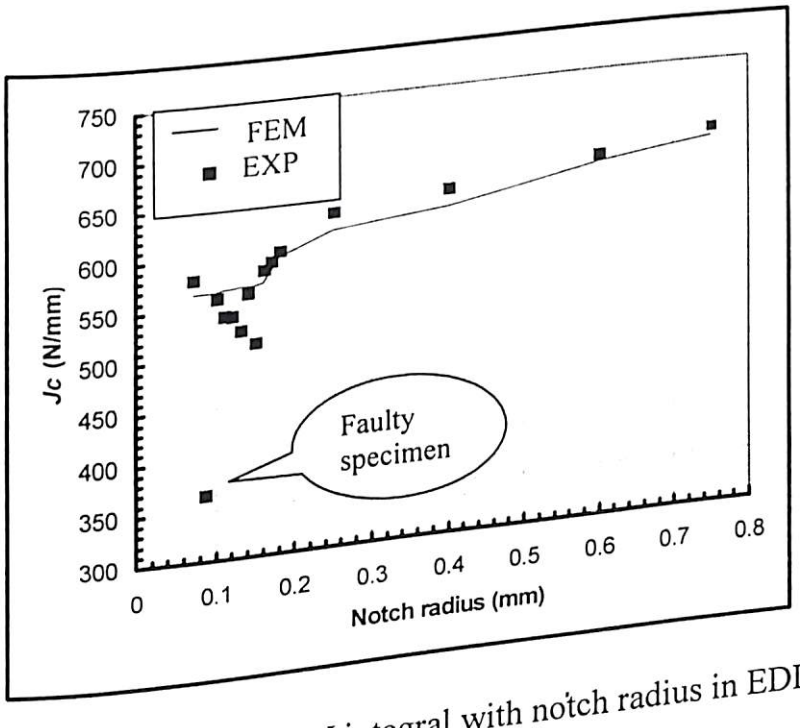

Fig. 5.33 Variation critical *J*-integral with notch radius in EDD258.

Fig. 5.33 shows the variation of J_c with respect to notch radius. As expected from load – load-line displacement results, the results on J-integral show fluctuations in J_c up to about 0.16 mm notch radius. Thereafter, there is an increase in fracture toughness with increase in notch radii. Therefore, notch radius of 0.16 mm is considered to be a critical notch radius value, below which, fracture toughness remains almost independent of notch radius. According to Srinivas and Kamat (1992) and Schindler (1991), the fracture toughness beyond the critical notch radius is referred as apparent fracture toughness ($J_{c,APP}$).

Experimental results on elastic and plastic *CTOD*, measured using various techniques, are tabulated in Table 5.31 for different notch radii. This table also shows the CFOA values for different notch radii. Table 5.32 shows the results on elastic and plastic *CTOD* using 3-D FE analysis for various notch radii.

Table 5.31 Experimental results on various *CTOD* for EDD258 steel sheet

Sp-code	Notch radius (ρ) mm	δ_{el} mm	$(\delta_{pl})_{PHM}$ mm	$(\delta_{pl})_{CFOA}$ mm	$(\delta_{pl})_J$ mm	$(\delta_c)_{PHM}$ mm	$(\delta_c)_{CFOA}$ mm	$(\delta_c)_J$ mm	CFOA (°)
SP1	0.07	0.0301	2.0269	2.0269	2.2183	2.0570	2.2170	2.2484	13.53
SP2	0.085	0.0285	1.3426	1.3426	1.3910	1.3711	1.4297	1.4195	9.25
SP3	0.10	0.0304	2.0009	2.0009	2.1386	2.0313	2.2310	2.1690	13.14
SP4	0.11	0.0332	1.8276	1.8276	2.0663	1.8608	2.0479	2.0995	11.98
SP5	0.12	0.0314	1.9965	1.9965	2.0662	2.0279	2.2519	2.0976	12.98
SP6	0.13	0.0294	1.9965	1.9965	2.0048	2.0259	2.2046	2.0342	13.22
SP7	0.14	0.0302	1.9922	1.9922	2.1474	2.0224	2.2378	2.1776	12.99
SP8	0.15	0.0326	1.9706	1.9706	1.9467	2.0032	2.1717	1.9793	13.09
SP9	0.16	0.0327	1.8796	1.8796	2.2268	1.9123	2.1727	2.2595	11.96
SP10	0.17	0.0335	1.9835	1.9835	2.2579	2.0170	2.2180	2.2914	13.01
SP11	0.18	0.0334	1.9965	1.9965	2.2958	2.0299	2.2248	2.3292	13.14
SP12	0.25	0.0358	2.2564	2.2564	2.4232	2.2922	2.4561	2.4590	15.12
SP13	0.40	0.0369	2.2781	2.2781	2.4676	2.3150	2.5081	2.5045	15.1
SP14	0.60	0.0397	2.3474	2.3474	2.5327	2.3871	2.5838	2.5724	15.5
SP15	0.75	0.0413	2.4859	2.6312	2.5990	2.5272	2.6725	2.6403	16.8

Table 5.32 3-D FEA results on *CTOD* for EDD258 steel sheet

Notch radius (ρ) mm	δ_{el} mm	$(\delta_{pl})_{FEM}$ mm	$(\delta_C)_{FEM}$ mm
0.07	0.0322	2.1584	2.1906
0.085	0.0322	2.1603	2.1925
0.10	0.0323	2.1625	2.1948
0.11	0.0323	2.1673	2.1996
0.12	0.0324	2.1704	2.2028
0.13	0.0324	2.1710	2.2034
0.14	0.0325	2.1718	2.2043
0.15	0.0325	2.1735	2.206
0.16	0.0326	2.1799	2.2125
0.17	0.0326	2.2580	2.3006
0.18	0.0332	2.2726	2.3163
0.25	0.0349	2.3532	2.3694
0.40	0.0373	2.4222	2.4595
0.60	0.0400	2.4895	2.5397
0.75	0.0417	2.5744	2.6261

The results on critical *CTOD* for different notch radii are presented in two plots. First plot i.e. Fig. 5.34 (a) shows the *CTOD* values up to critical notch radius and second plot i.e. Fig. 5.34 (b) shows the apparent *CTOD* values from 0.16 mm to 0.75 mm notch radii.

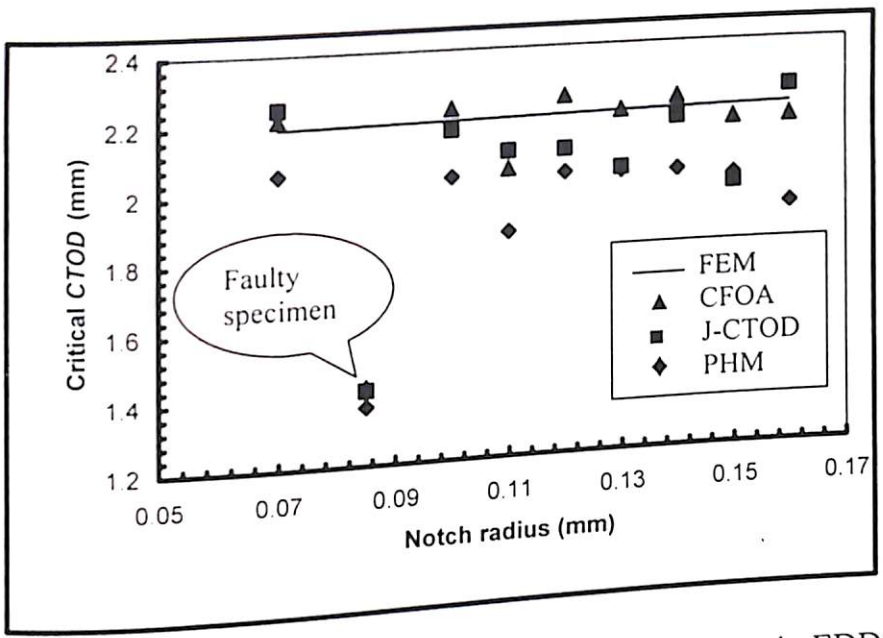

Fig. 5.34 (a) Variation of critical *CTOD* with notch radius in EDD258.

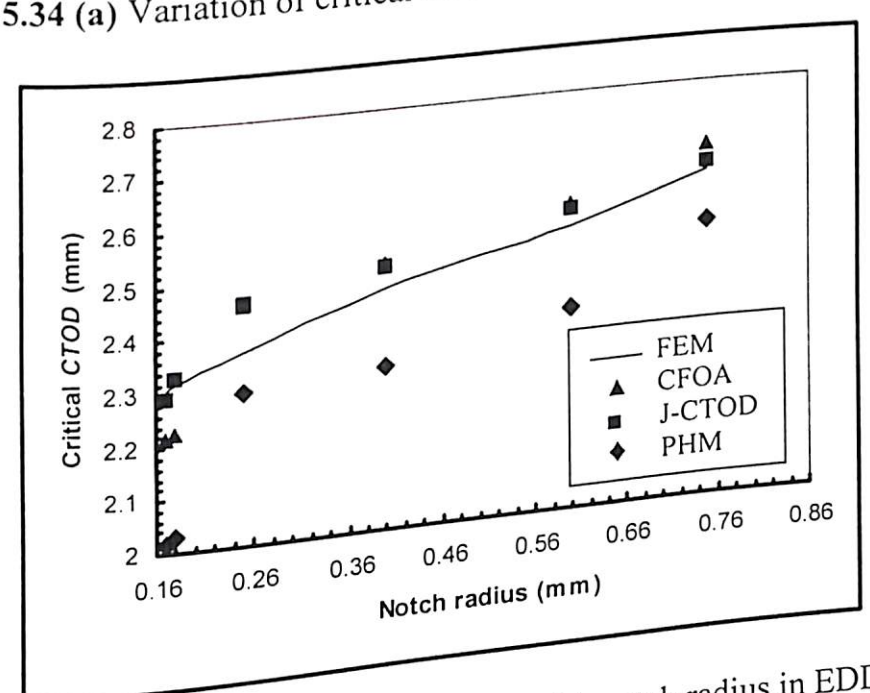

Fig. 5.34 (b) Variation of critical *CTOD* with notch radius in EDD258.

The linear increase of apparent fracture toughness can be expressed by Eq. (5.7):

$$CTOD_{c,App} = 0.74\,\rho' + CTOD_c \tag{5.7}$$

where, $\rho' = (\rho - 0.16)$, slope of the line = 0.74 and $CTOD_c$ is equal to 2.2125 mm as a constant value.

Table 5.33 shows the critical notch radii reported by various investigators. Survey shows that all six investigators showed a linear dependence of apparent fracture toughness on notch radius. The present study also agrees with linear dependence. The critical notch radii are relatively large depending on the material chosen for their study.

Table 5.33 Reported values of critical notch radius by various investigators

Investigator and year	Critical notch root radius, ρ_c (mm)	Variation of apparent fracture toughness
Landes and Begley (1979)	0.85	Linear
Firrao and Roberti (1983)	0.25	Linear
Yoda (1987)	1.8	Linear
Faucher *et al.* (1990)	0.33	Linear
Schindler (1991)	0.42	Linear
Srinivas and Kamat (1992)	0.38	Linear
Present study Kulkarni (2004d)	**0.16**	Linear

Srinivas and Kamat (1992) have given the explanation for the increase in apparent fracture toughness with increase in notch radii. According to him, the fracture toughness is proportional to the work done for fracture per unit of ligament area. It is asserted that the existence of a finite notch root radius causes an increase in the value of toughness, because an additional energy is used for plastic deformation in order to increase the stress concentration at the notch root to an equivalent level at the crack tip. There is a critical notch radius below which this effect appears negligible. In the present study, this observation is verified with the 3-D FE stress analysis. This is discussed in sub-section 5.9.1.

5.9.1 FE analysis

In order to understand the reason of increase of fracture parameters with increase in notch radius, the stress plots along the unbroken ligament at mid-thickness section are studied for a few notch radii (ρ = 0.05, 0.1, 0.12, 0.17, 0.2 and 0.3 mm). These stress plots are shown in Fig. 5.35 – 5.40.

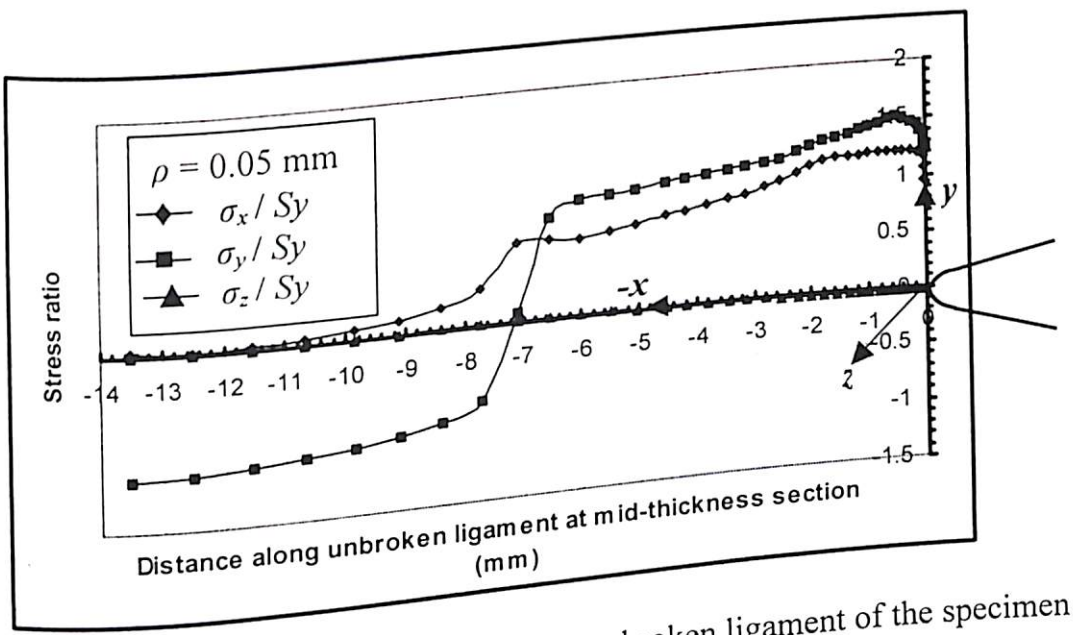

Fig. 5.35 Normalised stresses σ_x, σ_y, σ_z along the unbroken ligament of the specimen at mid-section thickness in EDD335 (ρ = 0.05 mm).

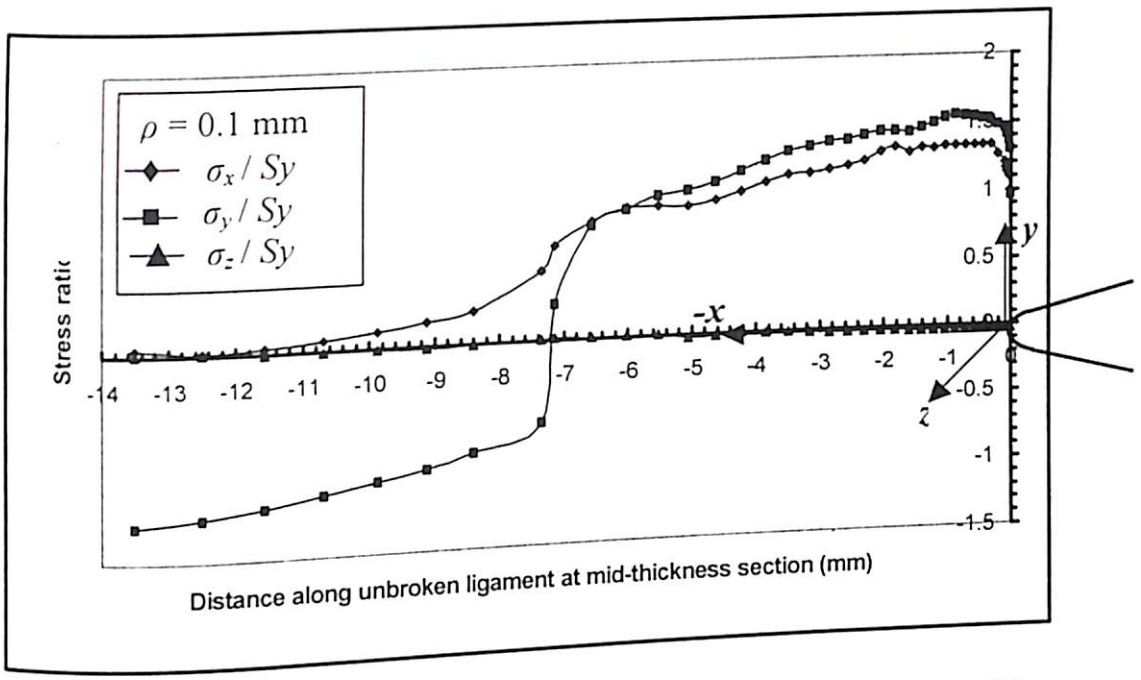

Fig. 5.36 Normalised stresses σ_x, σ_y, σ_z along the unbroken ligament of the specimen at mid-section thickness in EDD335 (ρ = 0.1 mm).

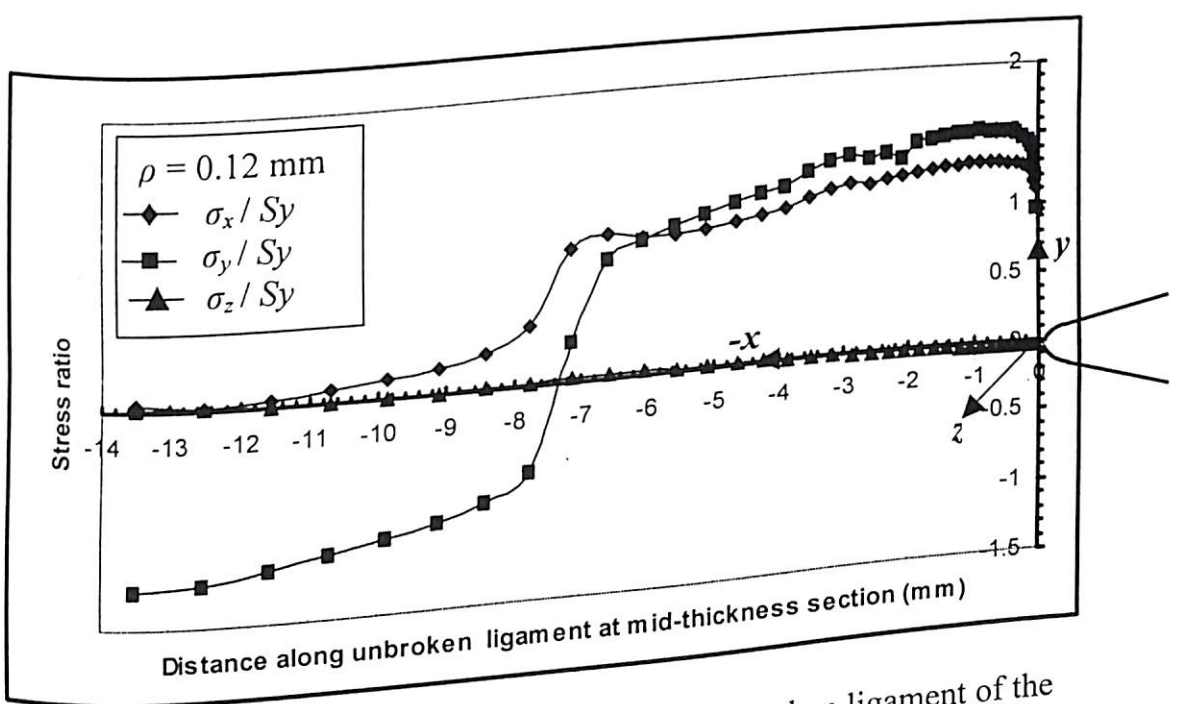

Fig. 5.37 Normalised stresses σ_x, σ_y, σ_z along the unbroken ligament of the specimen at mid-section thickness in EDD335 (ρ = 0.12 mm).

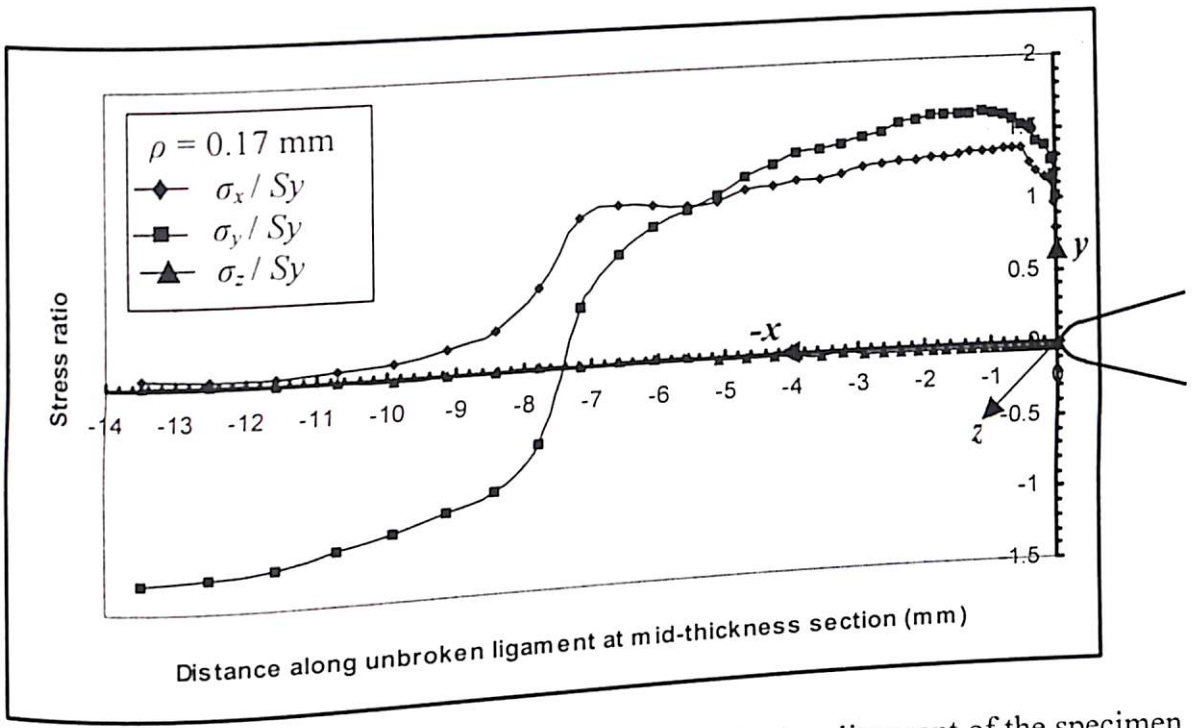

Fig. 5.38 Normalised stresses σ_x, σ_y, σ_z along the unbroken ligament of the specimen at mid-section thickness in EDD335 ($\rho = 0.17$ mm).

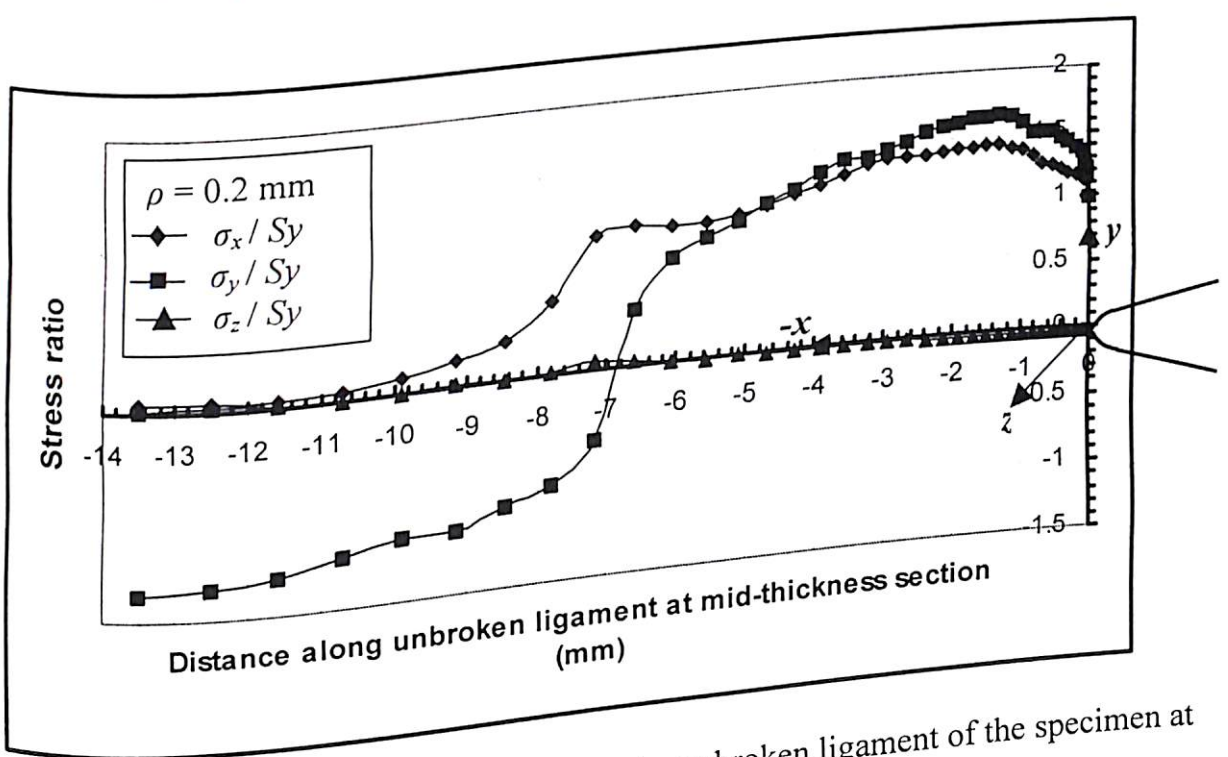

Fig. 5.39 Normalised stresses σ_x, σ_y, σ_z along the unbroken ligament of the specimen at mid-section thickness in EDD335 ($\rho = 0.2$ mm).

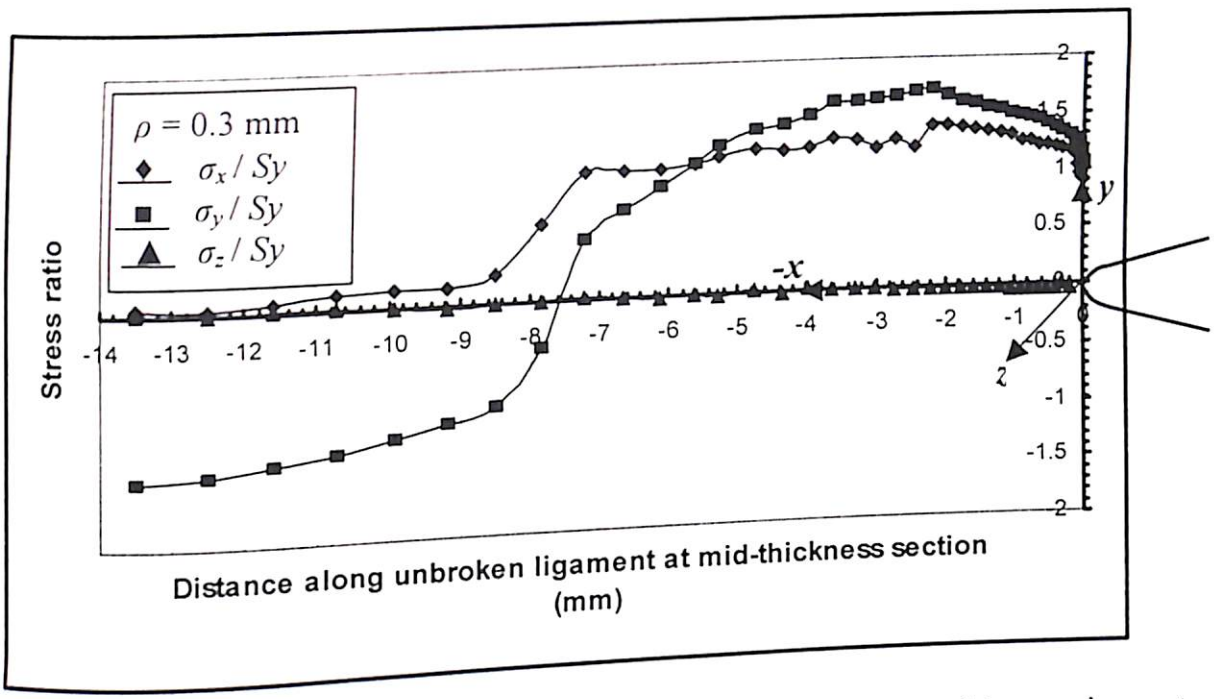

Fig. 5.40 Normalised stresses σ_x, σ_y, σ_z along the unbroken ligament of the specimen at mid-section thickness in EDD335 (ρ = 0.3 mm).

The peak stress in these curves coincides with the location of maximum stress triaxiality. From these plots, it is found that the stresses are localised in the vicinity of crack tip for lower value of notch radii (0.05, 0.1, 0.12 and 0.17mm). Consequently, crack initiation occurs at lower critical load, because of high stress concentration in the vicinity of crack tip. For 0 – 0.16 mm notch radii, the maximum stress triaxiality occurs within 0.5 mm distance from the crack tip. As mentioned by Kulkarni and Ravi Prakash (2004d), the stress triaxiality reduces at crack tip because of blunting. For higher value of notch radii (0.17 mm onwards), the maximum stress triaxiality occurs at sufficiently long distance from crack tip; rather it is reduced in the vicinity of crack tip and spread away over part of unbroken ligament length.

This is also observed from the plastic zones for increasing notch radii shown in Fig. 5.41. The plastic zone is increasing gradually with notch radii and assists the degree of blunting. This increase is very slow till 0.16 mm notch radius and thereafter, the increase and spread of plastic zone are found more. Two more notch radii, 2.0 mm and 3.0 mm are also studied in addition to the listed values of notch radii in Tables. The FE results on the plastic zones for 2.0 and 3.0 mm notch radii are shown in Appendix C. For a notch radius of 2.0 mm and 3.0 mm, it is observed that a load is almost uniformly distributed over the entire unbroken ligament length. These observations support the experimental observations.

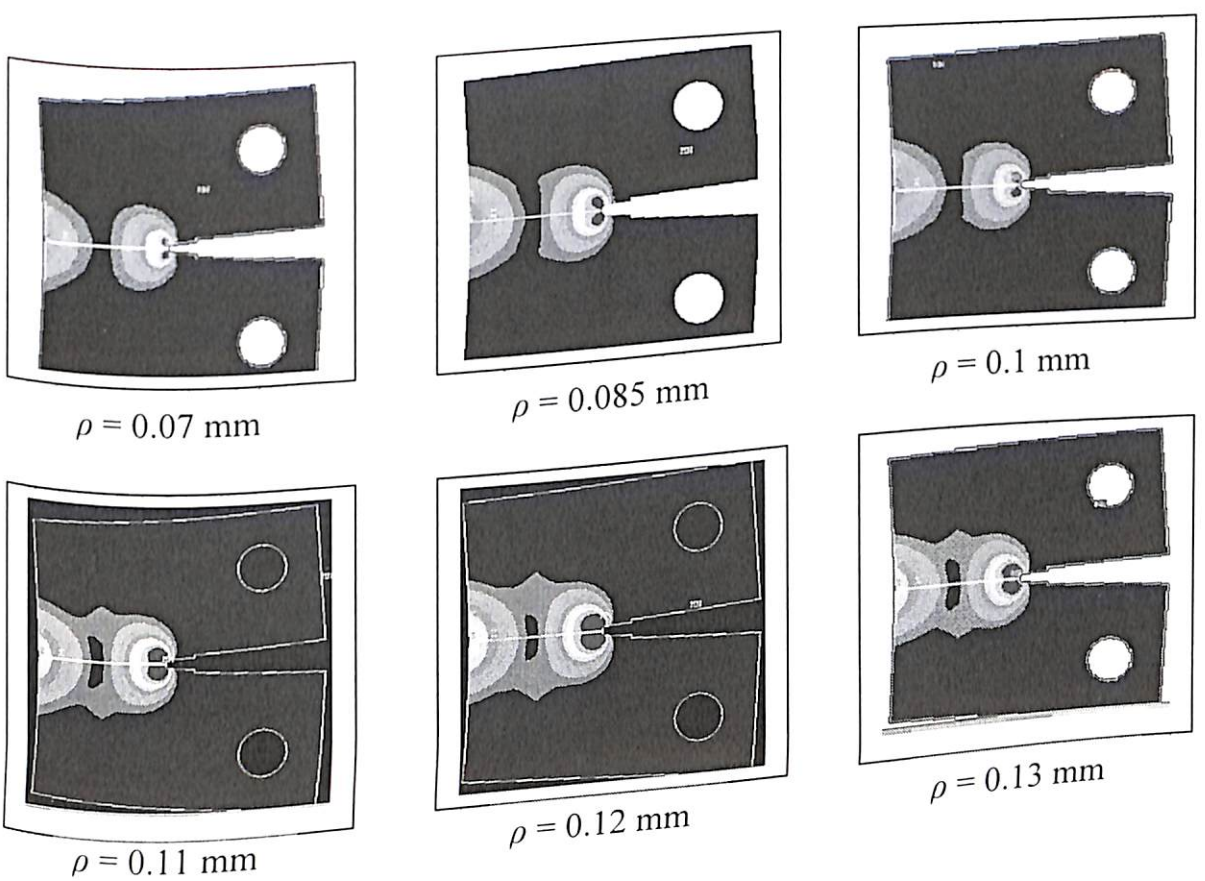

Fig. 5.41 Plastic zone ahead of crack tip for various notch radii by FE analysis.

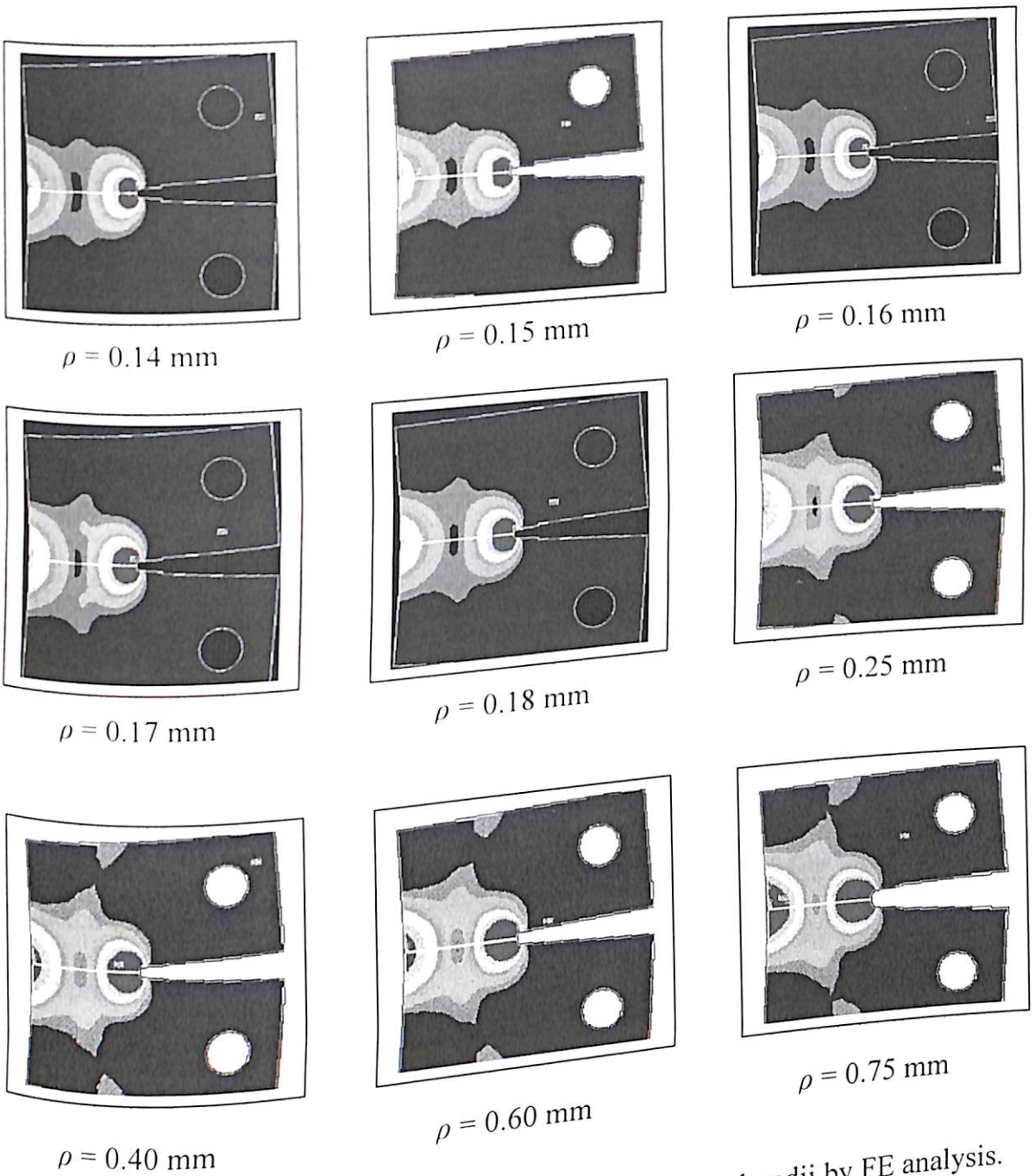

Fig. 5.41 Plastic zone ahead of crack tip for various notch radii by FE analysis.

In the present study, 0.2 mm wire diameter is used to create a notch having 0.1 mm notch radius. However, because of unavoidable heating during WEDM process, the maximum average notch radius has gone up to 0.13 mm. This value is sufficiently below the critical value (0.16 mm) for the validity of the present fracture study. Otherwise it is a time consuming and costly procedure for preparation of fatigue pre-cracked specimens. In addition to this, some specimens like SP2 are wasted after during a fatigue pre-cracking process.

5.10 Crack Tip Contraction as a Fracture Criterion

Crack tip contraction at the tip of the crack is measured with the help of a pointer micrometer as explained in Fig. 3.6. The measurement is little difficult to locate deep portion from both sides of the neck. However, to minimise the error, three readings are taken and an average value of three readings is reported for each specimen tested in the present work.

Liu's report (1981) indicated that near tip strain in thickness direction or crack tip contraction could be used as a fracture criterion. He used a replica technique, which is cumbersome in practice. From the present study, it is found that the amount of crack tip contraction at crack tip is nearly equal to the plastic *CTOD* measured by using the CFOA method. Similarly, FE analysis shows the same observations. The necking values for EDD335 and EDD277 observed to study the effect of thickness are shown in Table 5.34 and Table 5.35, respectively. The effect of thickness on crack tip contraction is plotted separately for experimental results and FE results for both

the materials. This is demonstrated in Fig. 5.42, and 5.43 for EDD335 and in Fig. 5.44 and 5.45 for EDD277.

Table 5.34 Amount of crack tip contraction and difference between plastic *CTOD* and amount of crack tip contraction in EDD335

B (mm)	$(\delta_n)_{EXP}$ (mm)	$(\delta_{pl})_{CFOA}$ (mm)	$[(\delta_{pl})_{CFOA} - (\delta_n)_{EXP}]$ (mm)	$(\delta_n)_{FEM}$ (mm)	$(\delta_{pl})_{FEA}$ (mm)	$[(\delta_{pl})_{FEA} - (\delta_n)_{FEA}]$ (mm)
1.18	0.5524	0.5735	0.0211	0.5659	0.5735	0.0164
1.28	0.5875	0.6146	0.0271	0.6132	0.6146	0.0191
1.38	0.6128	0.6429	0.0301	0.6578	0.6429	0.0283
1.48	0.6547	0.6914	0.0367	0.6844	0.6914	0.0368
1.58	0.6885	0.7275	0.0390	0.7108	0.7275	0.0402
1.64	0.7002	0.7511	0.0509	0.7214	0.7511	0.0531

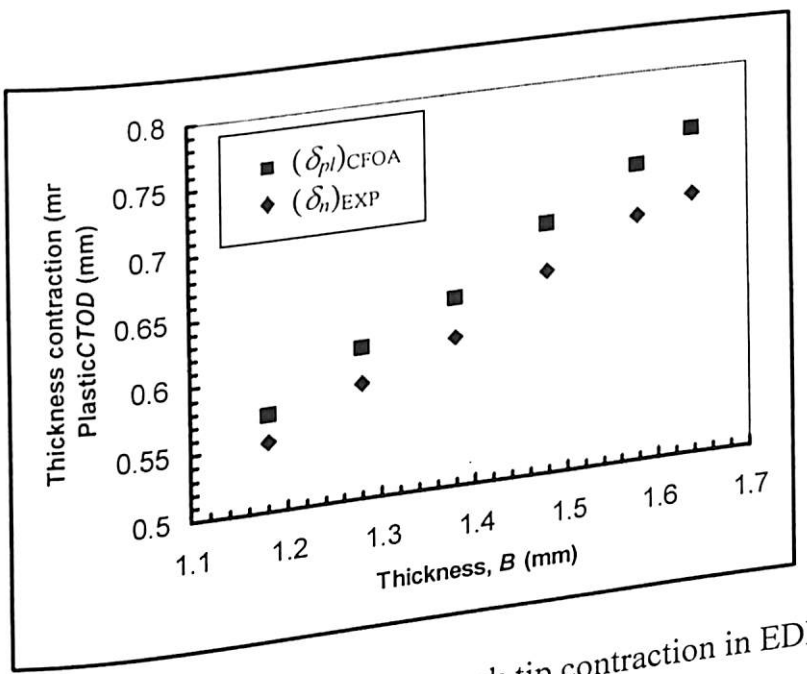

Fig. 5.42 Thickness effect on amount of crack tip contraction in EDD335 using experimental results.

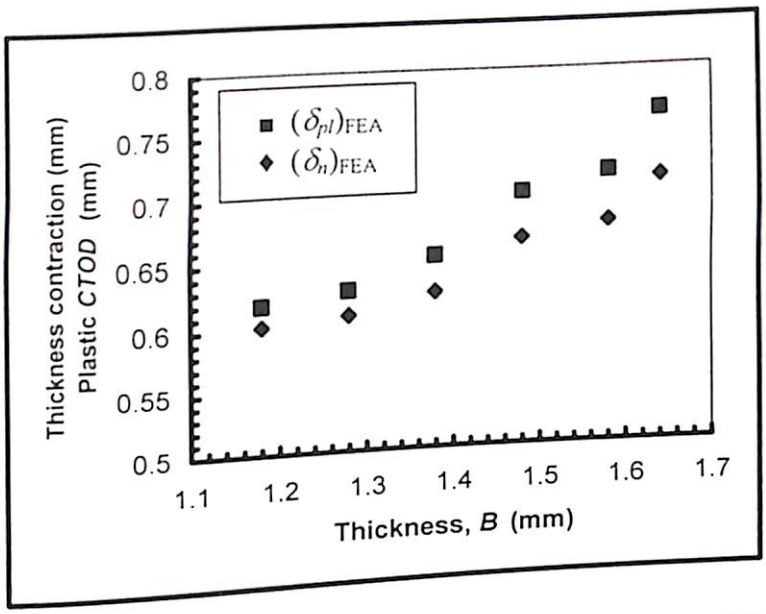

Fig. 5.43 Thickness effect on amount of crack tip contraction in EDD335 using FEA.

Table 5.35 Amount of crack tip contraction and difference between plastic *CTOD* and amount of crack tip contraction in EDD277

B (mm)	$(\delta_n)_{EXP}$ (mm)	Avg. $(\delta_n)_{EXP}$	$(\delta_{pl})_{CFOA}$ (mm)	Avg. $(\delta_{pl})_{CFOA}$	$[(\delta_{pl})_{CFOA} - (\delta_n)_{EXP}]$ (mm)	$(\delta_n)_{FEM}$ (mm)	$(\delta_{pl})_{FEA}$ (mm)	$[(\delta_{pl})_{FEA} - (\delta_n)_{FEA}]$ (mm)
1.4a	1.3566	1.3568	1.3908	1.4174	0.0606	1.3572	1.4046	0.0474
1.4b	1.3569		1.4189					
1.4c	1.3567		1.4426					
1.9a	1.5639	1.5637	1.601	1.6392	0.0755	1.5092	1.5617	0.0525
1.9b	1.5634		1.5924					
1.9d	1.5637		1.7242					
2.4a	1.723	1.7227	1.7406	1.8175	0.0948	1.6365	1.7037	0.0672
2.4b	1.7227		1.8278					
2.4c	1.7223		1.8841					
2.9b	1.815	1.8146	1.9648	1.9209	0.1063	1.7368	1.8216	0.0848
2.9c	1.8141		1.9536					
2.9d	1.8146		1.8442					
3.2a	1.8237	1.8266	1.9648	1.9648	0.1382	1.8491	1.9715	0.1224
3.2b	1.8332		1.9536					
3.2c	1.8229		1.976					

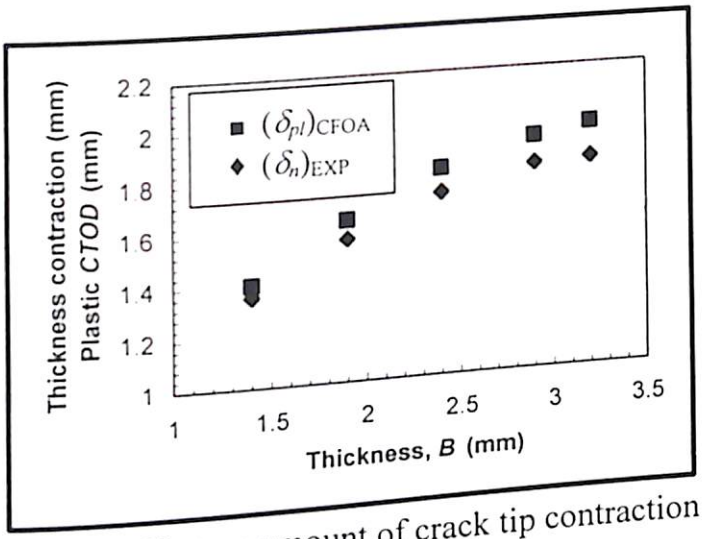

Fig. 5.44 Thickness effect on amount of crack tip contraction in EDD277 using experimental results.

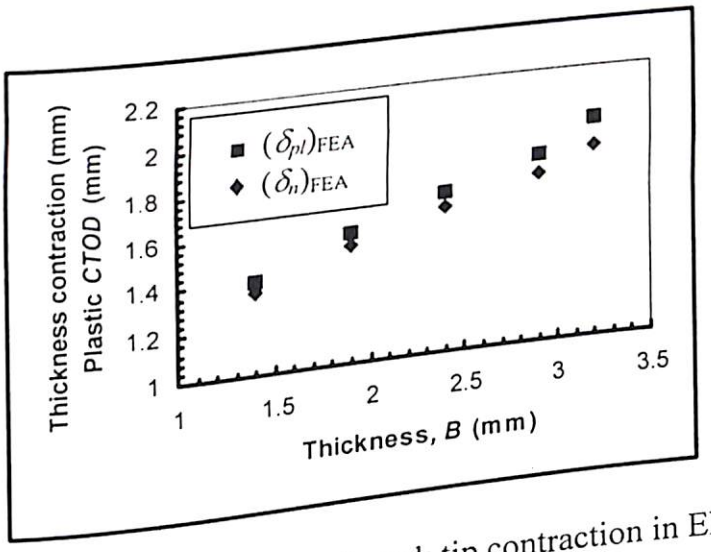

Fig. 5.45 Thickness effect on amount of crack tip contraction in EDD277 using FEA.

Increase in crack tip contraction is also observed, like increase in *CTOD* with increase in thickness of sheet as demonstrated in Fig. 5.20 and 5.25. In Fig. 5.46, one-sided crack tip contraction is encircled. Problems of the effect of necking preceding fracture are also studied by Atkins (1993, 1995 and 1997). However, Atkin's investigations are restricted to, how damage should be added in a 'plane strain neck'.

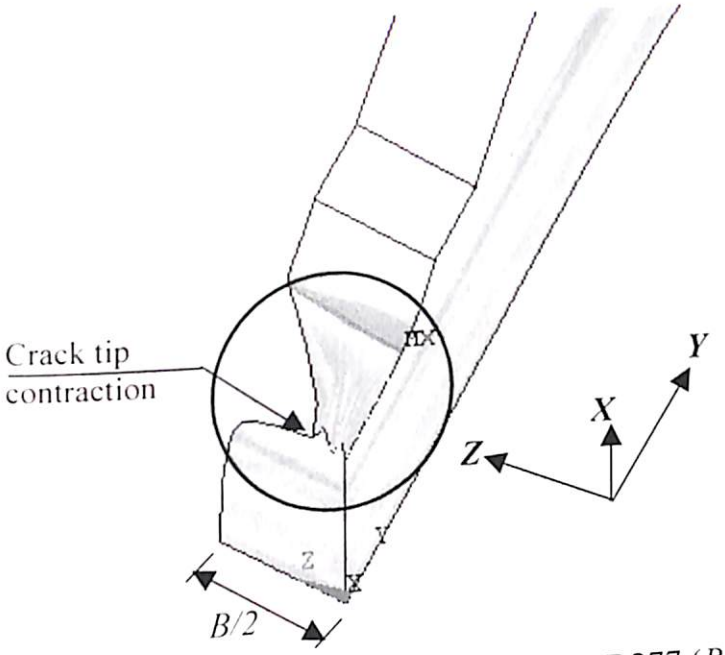

Fig. 5.46 One-sided crack tip contraction in EDD277 (B = 1.4 mm).

Fig. 5.44 and Fig. 5.45 show that the difference in plastic *CTOD* and amount of necking increases with increase in thickness. This is found by experimental as well as FE results. This is because of slow rise of stress in z-direction decreases the material flow in z-direction. Though the difference is not so distinctive, still using crack tip contraction as a fracture criterion becomes questionable.

The effect of notch radius and strain rate on crack tip contraction is plotted in Fig. 5.47 and 5.48, respectively. Both of these figures show no effect on the crack tip contraction. In these figures, the results of plastic *CTOD* based on CFOA model, is also shown. This concludes that irrespective of discontinuity at the tip and strain rate, the material ahead of crack tip experiences same amount of contraction before the crack initiation.

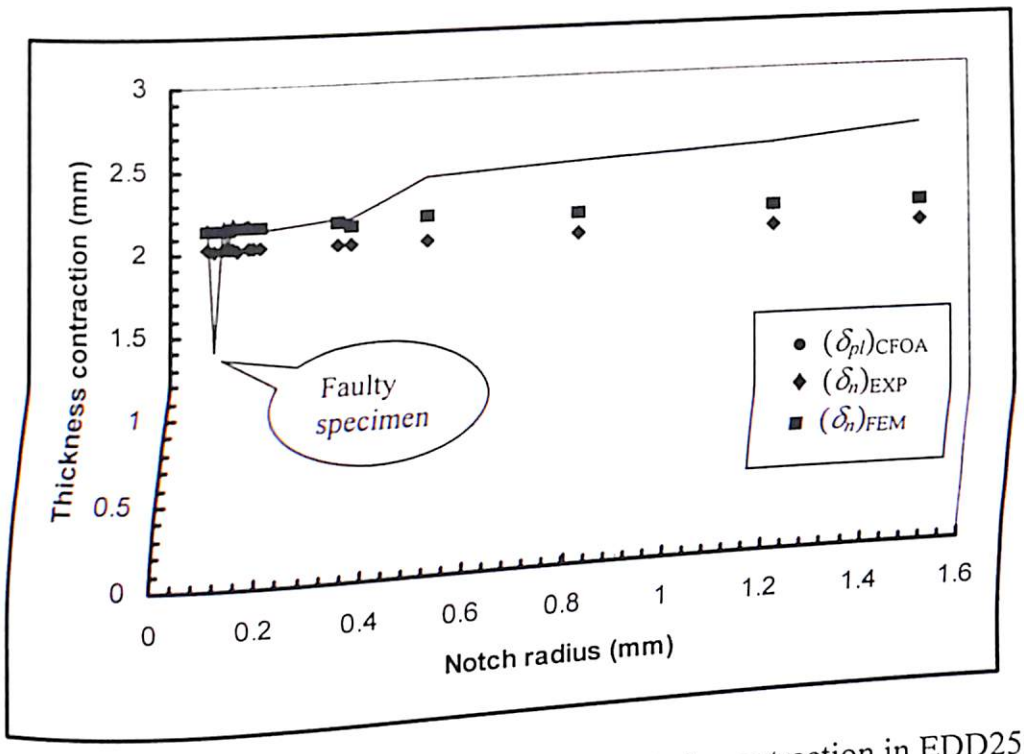

Fig. 5.47 Effect of notch radius on amount of crack tip contraction in EDD258.

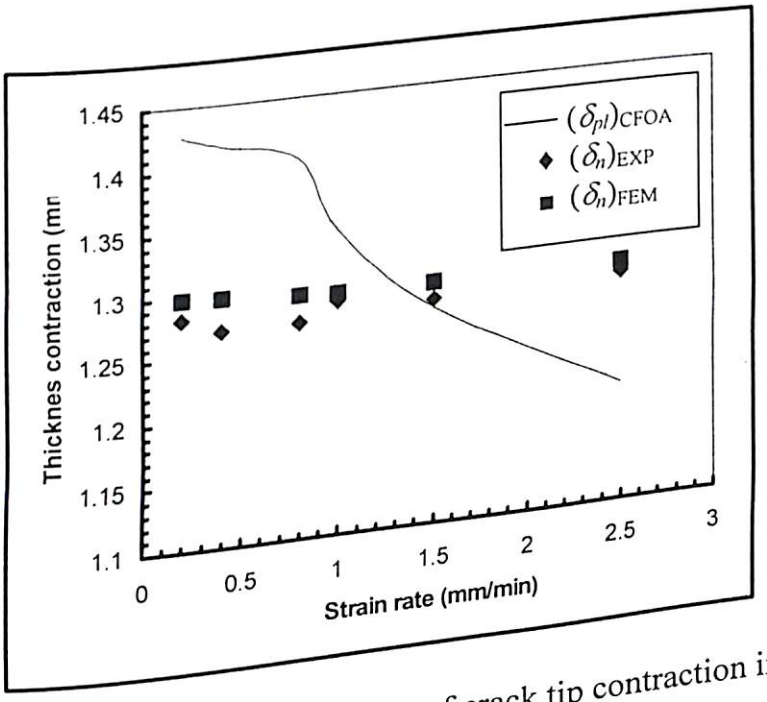

Fig. 5.48 Effect of strain rate on amount of crack tip contraction in EDD277.

5.11 Crack Growth Behaviour

Experimental results are generated on fracture parameters to study the crack growth behaviour in EDD258 steel using multiple specimens. Table 5.36 shows the fracture tests results on eight CT specimens. The data in the table shows load (P_{unl}) and load line displacement (V_{unl}) values at various unloading points for every specimen along with the area under the load – load-line displacement curve (A_{pl}). The load – load-line displacement plots are shown in Appendix B5. Fig. 5.49 shows photographs of all eight specimens. Table 5.36 shows the fracture status of every specimen.

Table 5.36 Fracture test results for crack growth study

Sp. Code	B (mm)	Status	P_{unl} (kN)	V_{unl} (mm)	A_{pl} (N-mm)
R1	3.2	Complete Rupture	0.767	34.16	---
R3	3.2	Before crack initiation	2.831	4.18	8192.50
R2	3.2	At crack initiation	2.865	4.03	13016.68
R4	3.2	Crack growth	1.761	8.5	19299.40
R5	3.2	Crack growth	0.958	12.5	24510.80
R6	3.2	Crack growth	0.847	16.5	29765.49
R7	3.2	Crack growth	0.691	20.5	32723.30
R8	3.2	Crack growth	0.674	23.84	34821.90

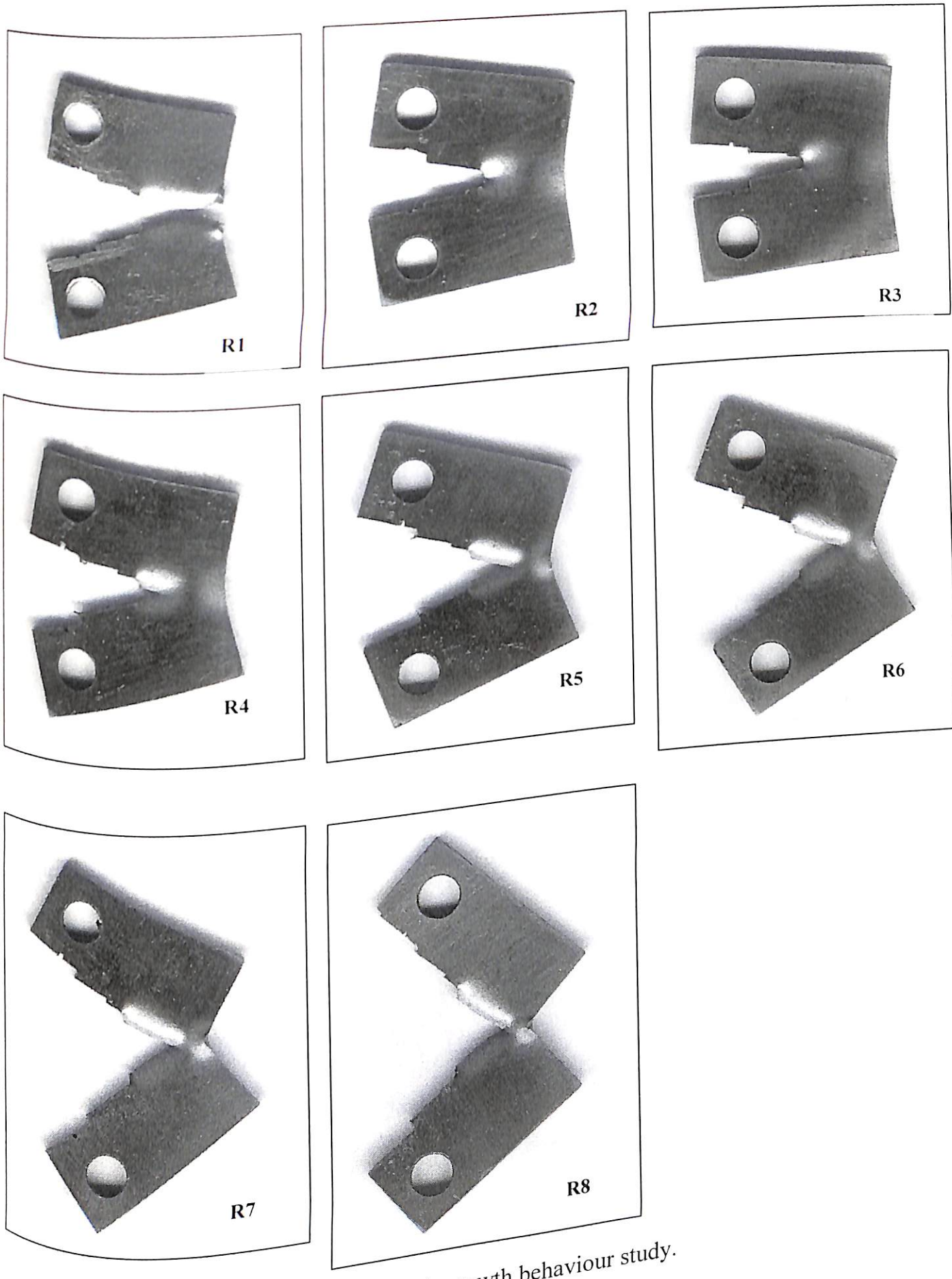

Fig.5.49 Tested specimens for crack growth behaviour study.

Fig. 5.50 shows crack extension measurement on surface of R4 specimen. This measurement is performed using a scanned image and drafting software AutoCAD2000. The scale factor is taken with reference to the undeformed boundary of the specimen. The crack extension measurement on surface is referred as $(\Delta a)_s$.

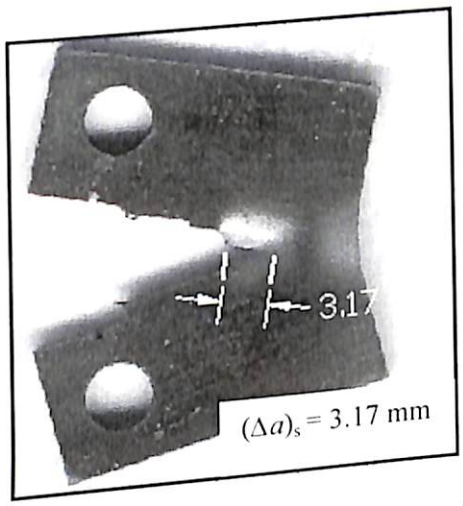

Fig. 5.50 Measurement of ductile crack extension on surface of R4 specimen.

Fig. 5.51 shows the measurement of ductile crack extension on broken ligaments of R4 specimen using digital vernier caliper. The crack extension measurement on broken ligament is referred as $(\Delta a)_b$.

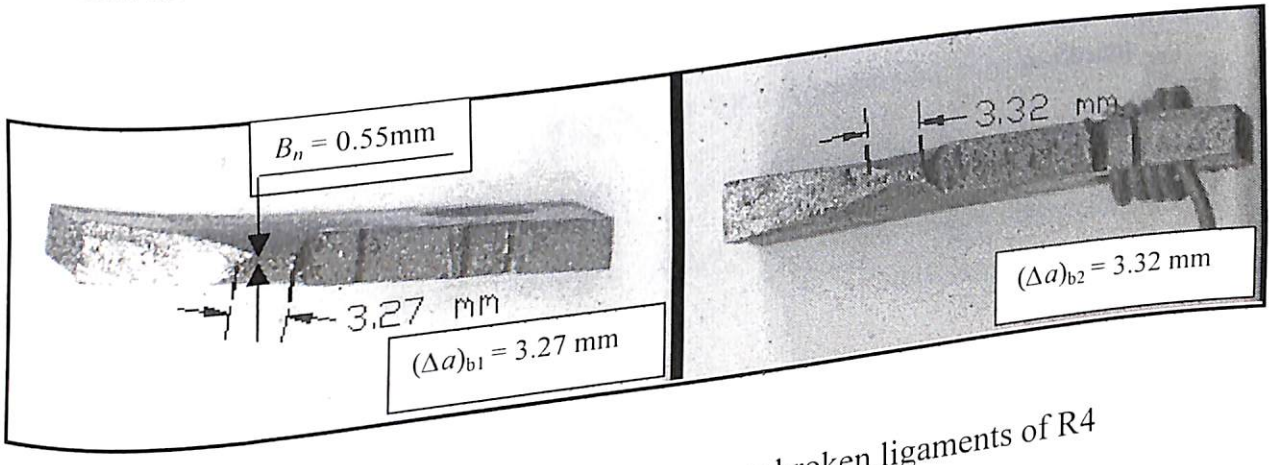

Fig. 5.51 Measurement of ductile crack extension on broken ligaments of R4 specimen.

The table 5.37 shows the measured values for crack extension on surface as well as on broken ligaments. The crack extension, measured on surface is slightly less than the average value of crack extension measured from two broken ligaments. For analysis purpose, an average value of crack extension from broken ligaments is taken. The crack extension area (dA) is measured as multiplication of net section thickness (B_n) and crack extension (Δa).

Table 5.37 Crack growth and fracture surface dimensions

Sp. code	$(\Delta a)_s$ (mm)	$(\Delta a)_{b1}$ (mm)	$(\Delta a)_{b2}$ (mm)	$^*(\Delta a)_{avg.}$ (mm)	B_n (mm)	dA $(B_n X (\Delta a)_{avg})$ (mm^2)
R1	12.00	12.00	12.00	12.00	0.55	----
R3	0.00	0.00	0.00	0.00	3.20	0.000
R2	0.10	0.11	0.13	0.12	3.20	0.384
R4	3.17	3.27	3.32	3.29	0.55	3.295
R5	6.19	6.21	6.27	6.24	0.55	6.240
R6	7.45	7.66	7.65	7.66	0.55	7.655
R7	7.89	8.02	8.05	8.04	0.55	8.035
R8	8.36	8.51	8.49	8.50	0.55	8.500

$^* (\Delta a)_{avg.} = [(\Delta a)_{b1} + (\Delta a)_{b2}]/2$

Fig. 5.52 shows crack extension results for various load-line displacement values. Fig. 5.53 shows the load corresponding to various crack extension in crack growth behaviour. After a crack initiation point, the load starts dropping continuously. Fig. 5.53 shows an average fit curve.

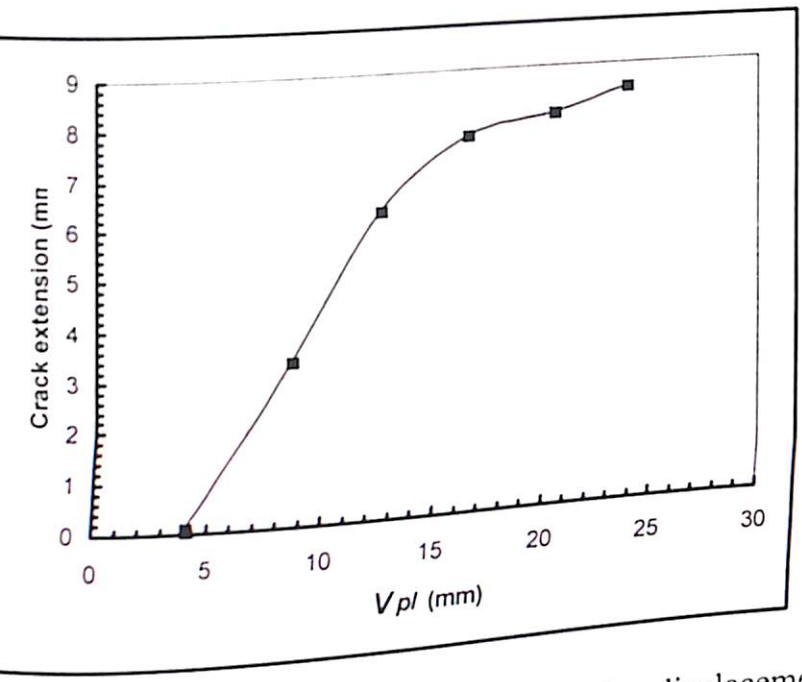

5.52 Crack extension versus plastic load-line displacement.

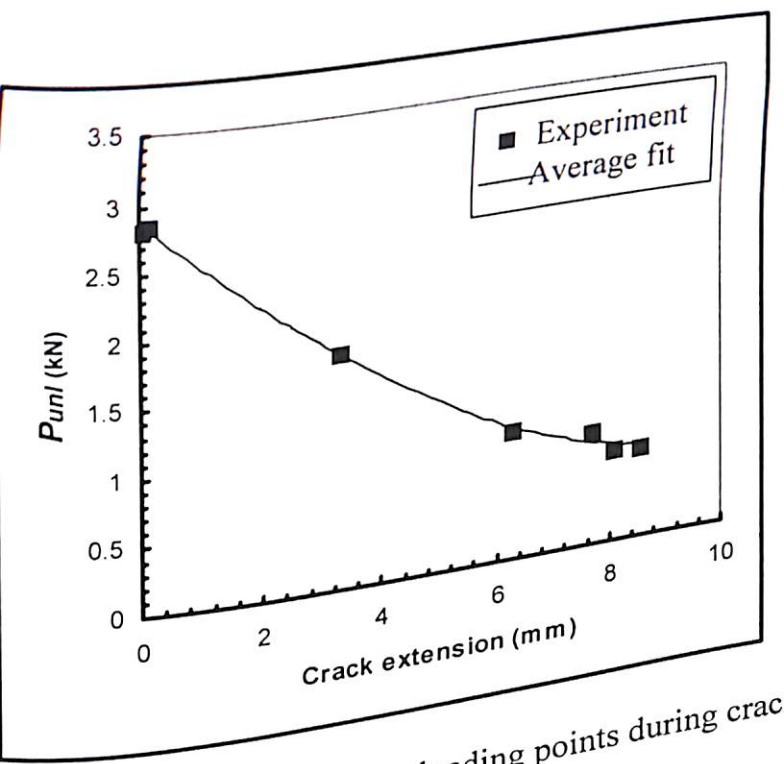

The load corresponding to unloading points during crack growth.

Sp. Code	η_i	γ_i	a_i (mm)	b_i (mm)	J_{pl} (N/mm)
R1	2.5220	1.7600	12.00	12.00	Rupture
R3	2.5220	1.7600	12.00	12.00	482.18
R2	2.2601	1.7600	12.00	12.00	723.10
R4	2.1893	1.2757	15.29	8.705	1565.40
R5	2.1253	1.1824	18.24	5.760	2052.90
R6	2.0945	1.1376	19.66	4.345	2919.80
R7	2.0862	1.1256	20.04	3.965	3564.60
R8	2.0761	1.1108	20.50	3.50	3946.70

The R curve is also plotted with the help of $CTOA$ and $CTOD$ results. The crack growth $CTOA$ and crack growth $CTOD$ are measured with the help of critical $CTOA$ model discussed in sub-section 3.10.2. The crack initiation $CTOD$ (δ_{CI}) is measured using CFOA model. Table 5.39 shows $CTOA$ and $CTOD$ values for various crack extensions. The $CTOA$ is measured at current crack tip. Fig. 5.55 shows the variation of $CTOA$ with respect to crack extension.

Table 5.39 Crack growth $CTOD$ (δ_{CG}) using $CTOA$ model (δ_{CI} = 2.7852 mm)

Sp. Code	$(\Delta a)_{avg}$ (mm)	$CTOA$, θ_{CT} (°)	$\delta_{CG} = \delta_{CI} + 2(\Delta a)_{avg} \tan\left(\frac{\theta_{CT}}{2}\right)$ (mm)
R1	12.00	Rupture	Rupture
R3	0.00	0	BLD
R2	0.12	0	2.7852
R4	3.29	29	4.4869
R5	6.24	39	7.2046
R6	7.66	50	9.9290
R7	8.04	58	11.6985
R8	8.50	70	14.6887

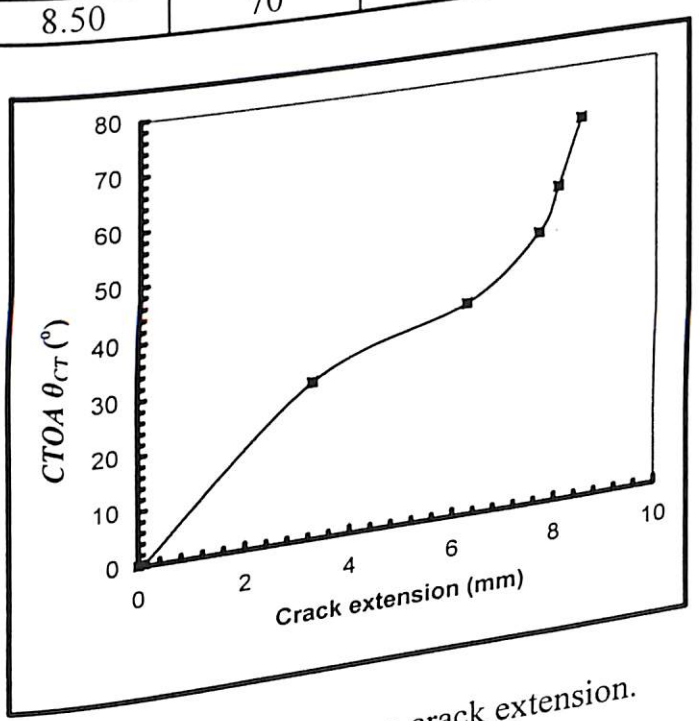

Fig. 5.55 $CTOA$ versus crack extension.

Table 5.38 shows the J_{pl} values and the parameters related to calculate J_{pl} values, following ASTM standard E 1820-01. These J_{pl} values are plotted against crack extension to predict the R (i.e. resistance) curve behaviour as shown in Fig. 5.54.

Table 5.38 Calculated value of J_{pl} values as per ASTM E 1820-01

Sp. Code	η_i	γ_i	a_i (mm)	b_i (mm)	J_{pl} (N/mm)
R1	2.5220	1.7600	12.00	12.00	Rupture
R3	2.5220	1.7600	12.00	12.00	482.18
R2	2.2601	1.7600	12.00	12.00	723.10
R4	2.1893	1.2757	15.29	8.705	1565.40
R5	2.1253	1.1824	18.24	5.760	2052.90
R6	2.0945	1.1376	19.66	4.345	2919.80
R7	2.0862	1.1256	20.04	3.965	3564.60
R8	2.0761	1.1108	20.50	3.50	3946.70

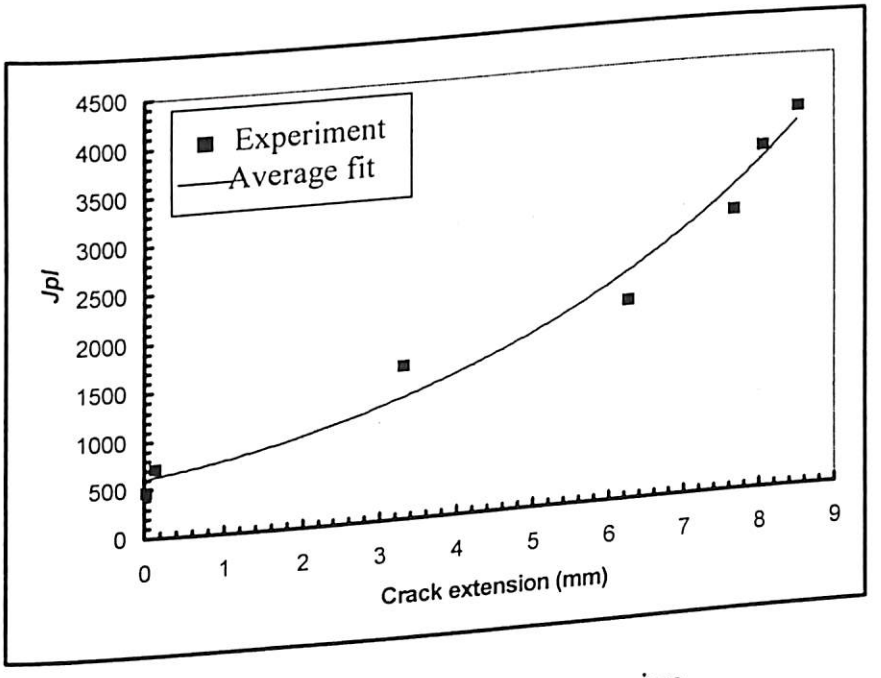

Fig. 5.54 J_{pl} versus crack extension.

The R curve is also plotted with the help of *CTOA* and *CTOD* results. The crack growth *CTOA* and crack growth *CTOD* are measured with the help of critical *CTOA* model discussed in sub-section 3.10.2. The crack initiation *CTOD* (δ_{CI}) is measured using CFOA model. Table 5.39 shows *CTOA* and *CTOD* values for various crack extensions. The *CTOA* is measured at current crack tip. Fig. 5.55 shows the variation of *CTOA* with respect to crack extension.

Table 5.39 Crack growth *CTOD* (δ_{CG}) using *CTOA* model (δ_{CI} = 2.7852 mm)

Sp. Code	$(\Delta a)_{avg.}$ (mm)	*CTOA*, θ_{CT} (°)	$\delta_{CG} = \delta_{CI} + 2(\Delta a)_{avg} \tan\left(\frac{\theta_{CT}}{2}\right)$ (mm)
R1	12.00	Rupture	Rupture
R3	0.00	0	BLD
R2	0.12	0	2.7852
R4	3.29	29	4.4869
R5	6.24	39	7.2046
R6	7.66	50	9.9290
R7	8.04	58	11.6985
R8	8.50	70	14.6887

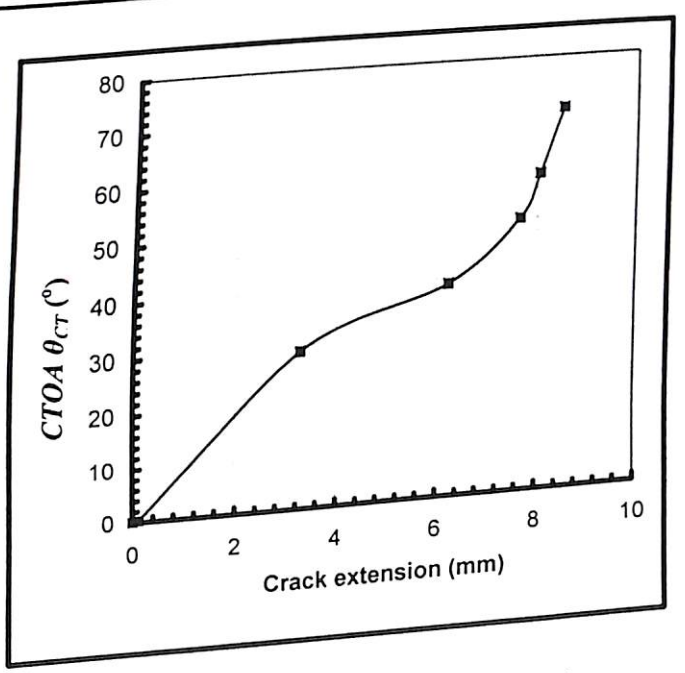

Fig. 5.55 *CTOA* versus crack extension.

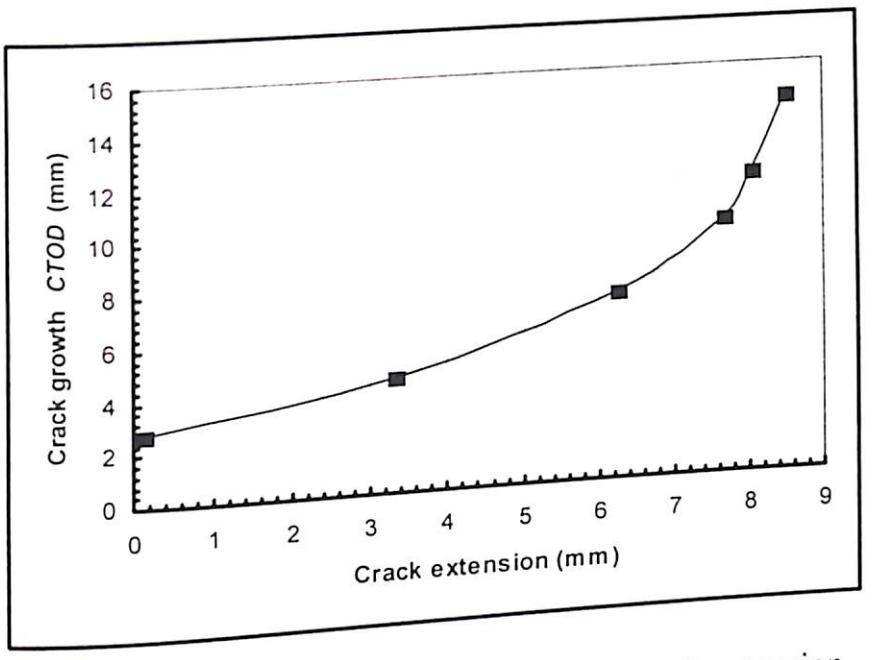

Fig. 5.56 crack growth *CTOD* (δ_{CG}) versus crack extension.

The *CTOD-R* curve, obtained using critical *CTOA* model is shown in Fig. 5.56. From the critical *CTOA* model, it is confirmed that *CTOD* is geometrically related with δ_{CG} through *CTOA*. All three, *J-R*, *CTOA-R* and *CTOD-R* are the conventional *R*-curves to characterise the crack growth behaviour. These figures describe the rising nature of *R*-curves. The rising nature of *R*- curves implies continued increase in crack growth toughness (J_{pl} and δ_{CG}) during slow and stable tearing. According to Kumar (1989) and Pardoen and Delannay (2000), the increase in tearing resistance is the governing parameter for stability rather than the critical initiation toughness value. The apparent increase in crack growth toughness may be effectively utilised in structural design by keeping tolerance for some crack extension.

The study of crack growth behaviour is tried with the help of normal FE analysis. However, crack propagation requires the re-meshing, which is not possible by normal FEM.

A number of studies by Shih *et al.* (1979), Kanninen *et al.* (1979), Brocks and Yuan (1991) and Newman *et al.* (1991) showed that *CTOA* at initiation is larger, and in some cases much larger than the value needed for stable crack growth. Recent observations by Dawicke *et al.* (1999), on 2.3 mm thick 2024-T3 aluminum alloy showed constant value of *CTOA* (= 5.25°). Newman *et al.* (2003) also showed a constant value of *CTOA* from initiation to failure. These findings suggest that the local crack tip toughness does not really contribute to the continued increase in toughness. An attempt has been made here to look into the cause of increase in *CTOA* with crack extension.

There are two kinds of stress-strain field ahead of crack tip namely, elastic and elastic-plastic. In the vicinity of crack tip, it is the plastic deformation that controls the *CTOD* during crack extension. On the other hand, elastic stress field (far field) is present beyond the plastically deformed zone. This means that the elastic contribution is not significant and hardly has any effect, whereas the plastic contribution is highly significant. In case of EDD steel sheets, the significant deformation ahead of the crack tip is large enough to offer continuous resistance. δ_{CG} being a near field displacement parameter may more reliably characterise the fibrous cracking process.

According to Sumpter (1999), the rise in R curve is due to the increased plastic energy dissipation through plastic zone size. This is explained with the help of Fig. 5.57. He defined various energies as illustrated in Fig. 5.57. These are the unit initiation energy, the unit propagation energy and the sum of these two energies gives the unit total energy. According to him, the unit propagation energy is the true energy dissipation.

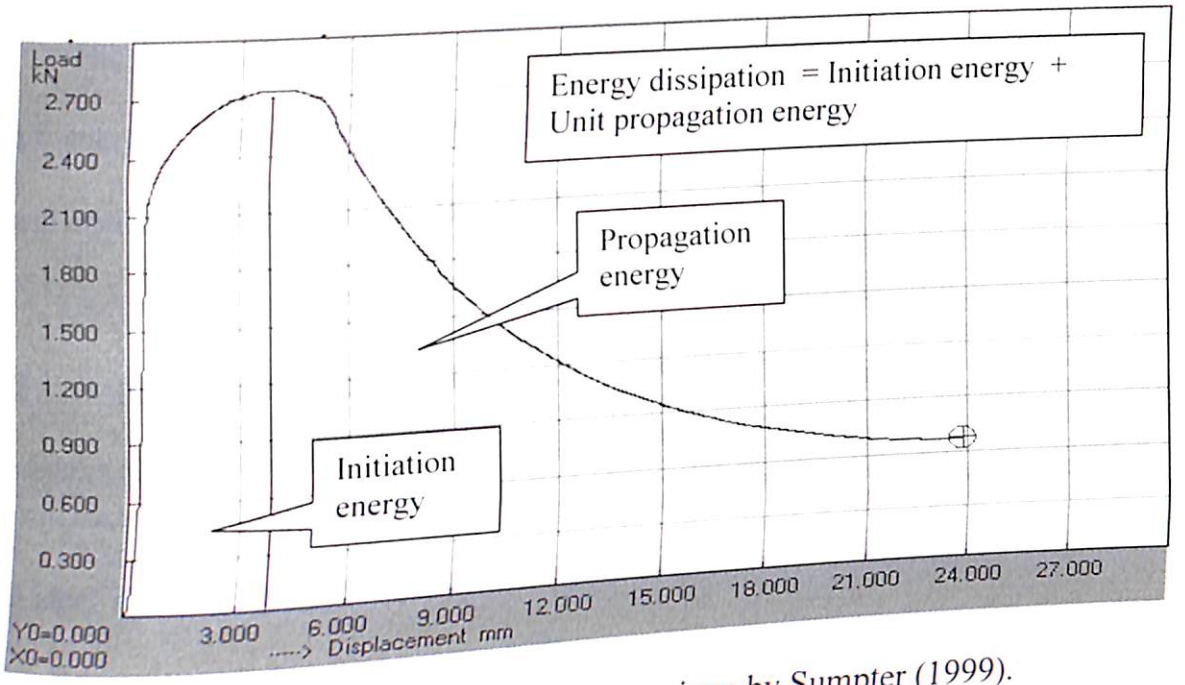

Fig. 5.57 *Definition of unit energy given by Sumpter (1999).*

However, the unit propagation energy is not the true energy dissipation because it ignores the crack initiation energy, which is reclaimed during propagation. The correct definition of energy dissipation for a completely fractured specimen is shown in Fig. 5.58.

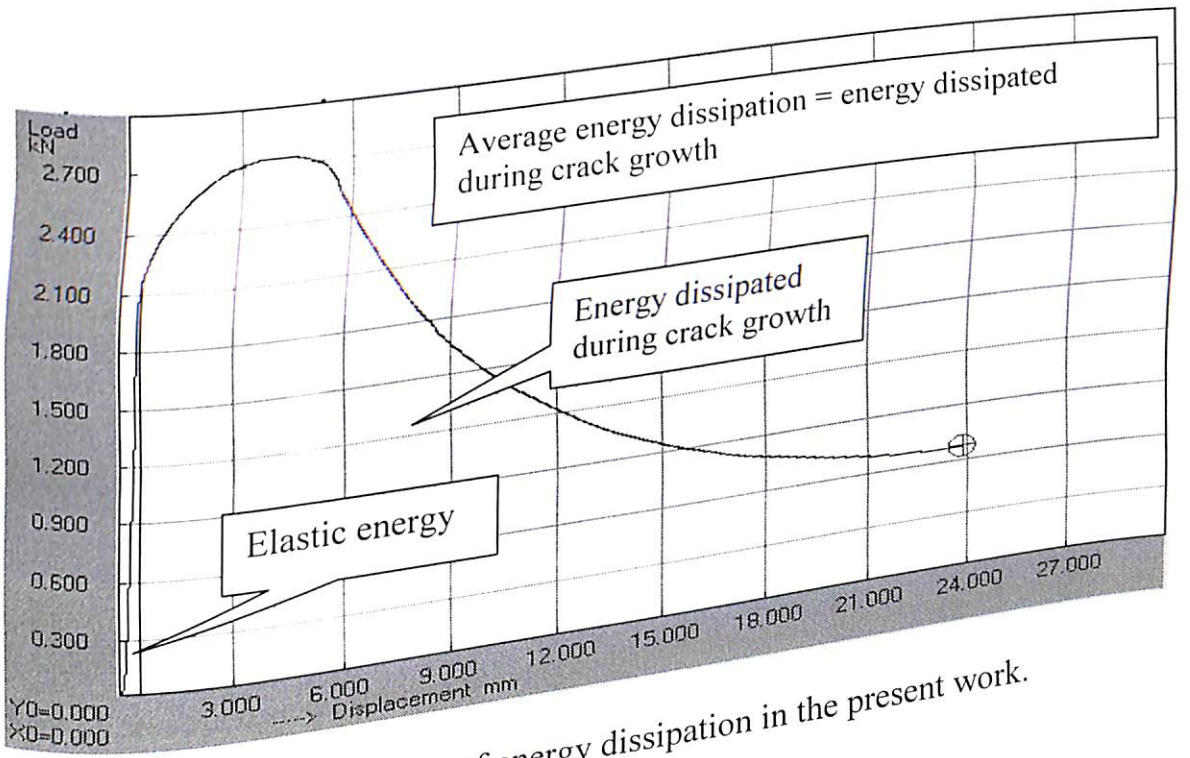

Fig. 5.58 *Definition of energy dissipation in the present work.*

The propagation energy should include crack initiation energy and exclude the elastic energy. This is also confirmed by ASTM E 1820-01 i.e. Eq. (3.15) and the present critical *CTOA* model i.e. Eq. (3.17).

5.12 Microstructure ahead of Crack Tip

The microstructure photographs are taken before and after the fracture test in all three EDD steel sheets. Fig. 5.59 (a) shows the representative microstructure of EDD335 before fracture test. Similarly Fig. 5.59 (b), (c) and (d) show a representative microstructure after the fracture test at surface level, 1/4th thickness section level and mid-thickness section level, respectively.

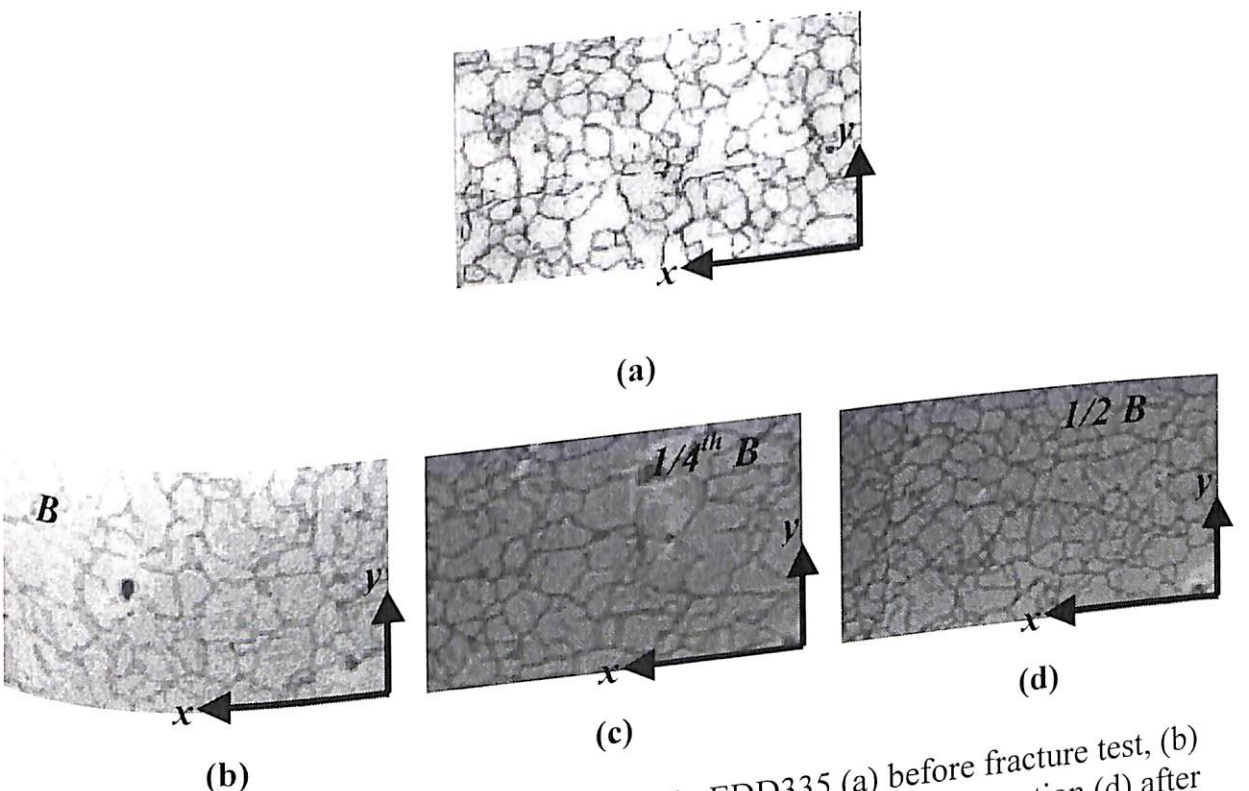

Fig. 5.59 Microstructure ahead of crack tip in EDD335 (a) before fracture test, (b) after fracture test at surface (c) after fracture test at 1/4th thickness section (d) after fracture tests at mid-thickness section. (400X).

The normal grain structure (before fracture test) in Fig. 5.59 (a) shows equi-axed grains of ferrite. After the fracture test, grains are elongated in *x*- as well as *y*-direction. This is shown in Fig. 5.59 (b), 5.59 (c) and 5.59 (d). As observed from these figures, the surface level grains are more elongated than at $1/4^{th}$. and mid-thickness section level. This is because the material at surface level is relatively free and not constrained like interior of thickness. The microstructure photographs for EDD277 and EDD258 are shown in Appendix E.

5.13 Evaluation of Fracture Surface

Fig. 5.60, 5.61 and 5.62 shows the fracture surface of EDD258, EDD277 and EDD335 steel sheet specimens, respectively at crack initiation. As discussed in section 5.10, there is a substantial amount of necking at the tip. The crack initiates at the center of necking zone and reaches the surface without any significant travel. This is also observed by removing material, layer by layer along the thickness direction as discussed in section 5.2. The shiny part shows a complete brittle fracture ahead of the small ductile tearing.

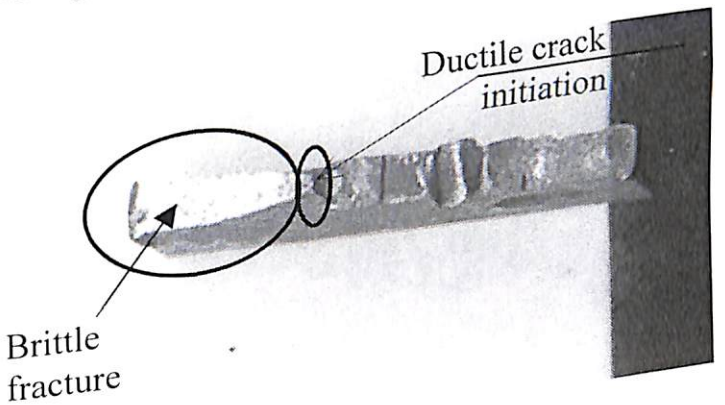

Fig. 5.60 General features of fracture surfaces produced at crack initiation in EDD258.

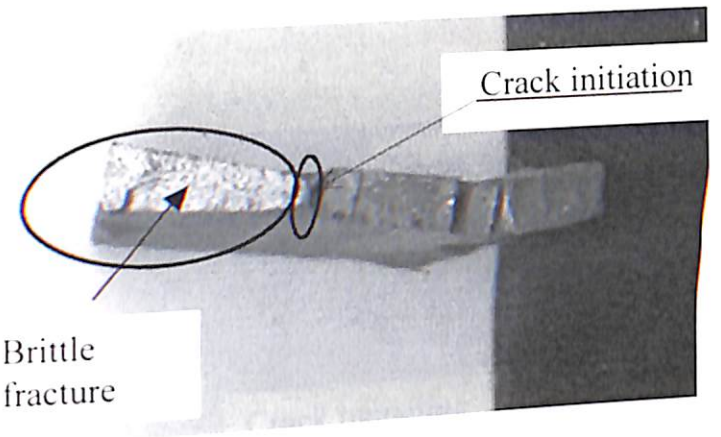

Fig. 5.61 General features of fracture surfaces produced at crack initiation in EDD277.

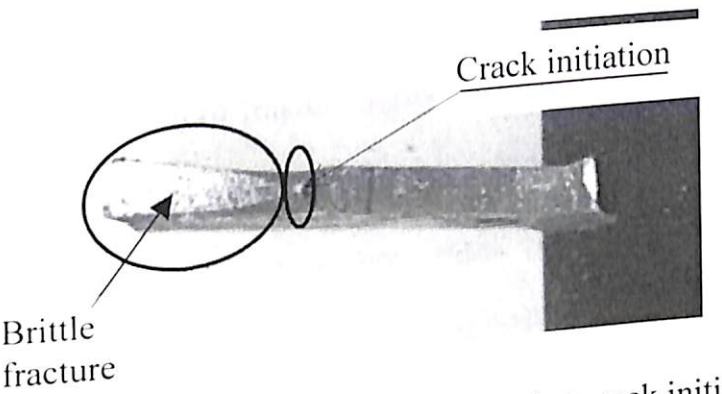

Fig. 5.62 General features of fracture surfaces produced at crack initiation in EDD335.

Figures 5.63 and 5.64 show the fracture surfaces in case of stable tearing of EDD258 sheet with 3.2 mm thickness. As illustrated in the Fig. 5.63, the overall fracture surface consists of three distinct regions: high degree of double shear-lip, crack tunneling and a shiny part of brittle fracture. Fig. 5.64 shows only crack tunneling and double shear-lips, as it is a completely torn specimen (R1).

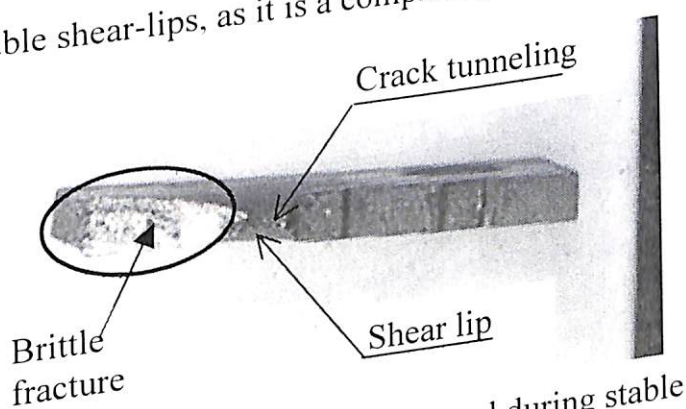

Fig. 5.63 General features of fracture surfaces produced during stable tearing in EDD258.

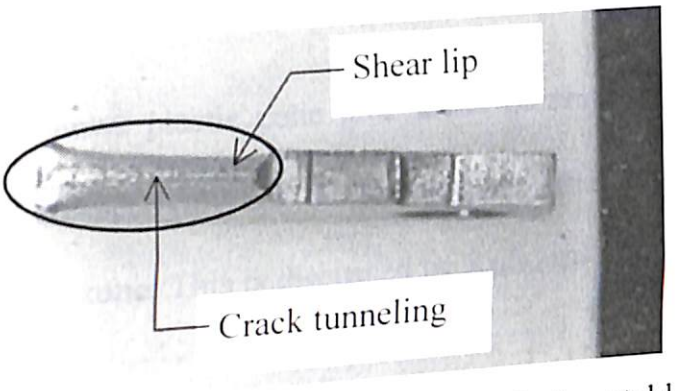

Fig. 5.64 General features of fracture surfaces produced during stable and complete tearing in EDD258.

Detailed observation of fracture surface showed that the fracture phenomenon starts with crack initiation in the necking zone and as the crack starts propagating, necking ends to form shear-lips from both sides. Shear-lips from both sides try to merge in each other, however, a crack tunneling is formed in between two shear lips. According to Anderson (1994), the high degree of shear-lips over almost entire thickness is an indication of predominantly plane stress fracture behaviour. The crack tunneling, according to Newman (2003), is an indication of the stable tearing of EDD steel sheet. These macroscopic observations are unlike that of reported by Mahmoud and Lease (2002) for 2.3 mm 2024-T351 aluminum alloy sheet. Their study shows that, the stable tearing region exhibits a clear transition from flat to slant fracture with the flat portion starting at the end of crack front. Although crack tunneling would be expected to be a significant factor in the stable tearing process, the experimental characterisation of this phenomenon is quite difficult. Comprehensive studies made by Dawicke and Sutton (1994) utilising companion specimens techniques or marker band approaches are needed to thoroughly evaluate the role of tunneling in the stable tearing process.

5.14 Plastic Zone Analysis

Fig. 5.65 and 5.66 shows plastic zone plot ahead of crack tip by FE analysis and experimental work, respectively for S1 specimen. The elastic-plastic boundary is plotted for only tensile zone. This is discussed by Kulkarni *et al.* (2004a).

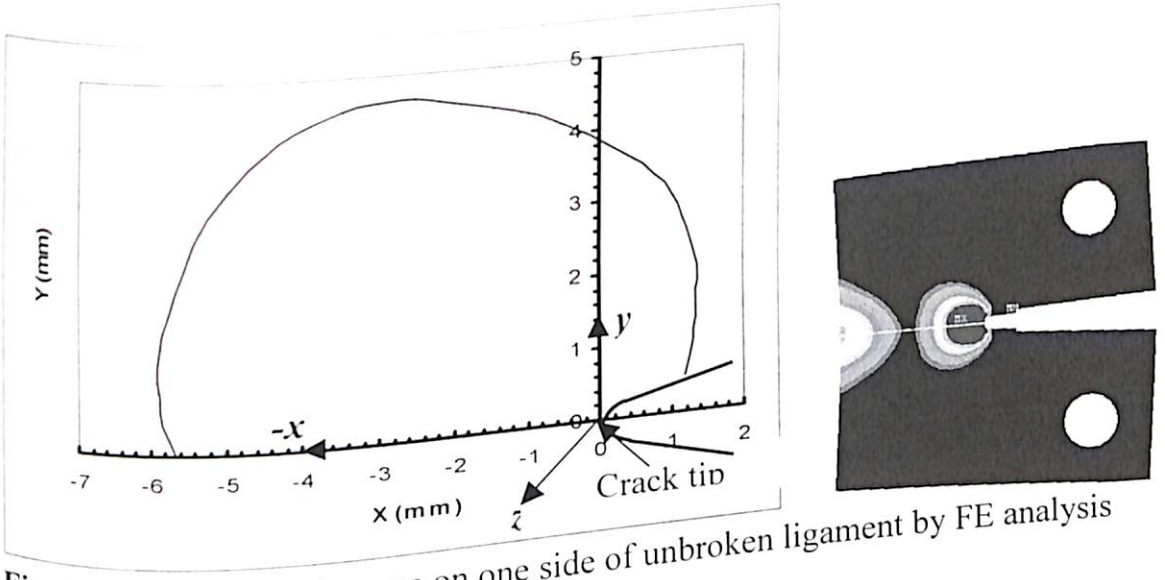

Fig. 5.65 Tensile plastic zone on one side of unbroken ligament by FE analysis in EDD335 (B=1.18).

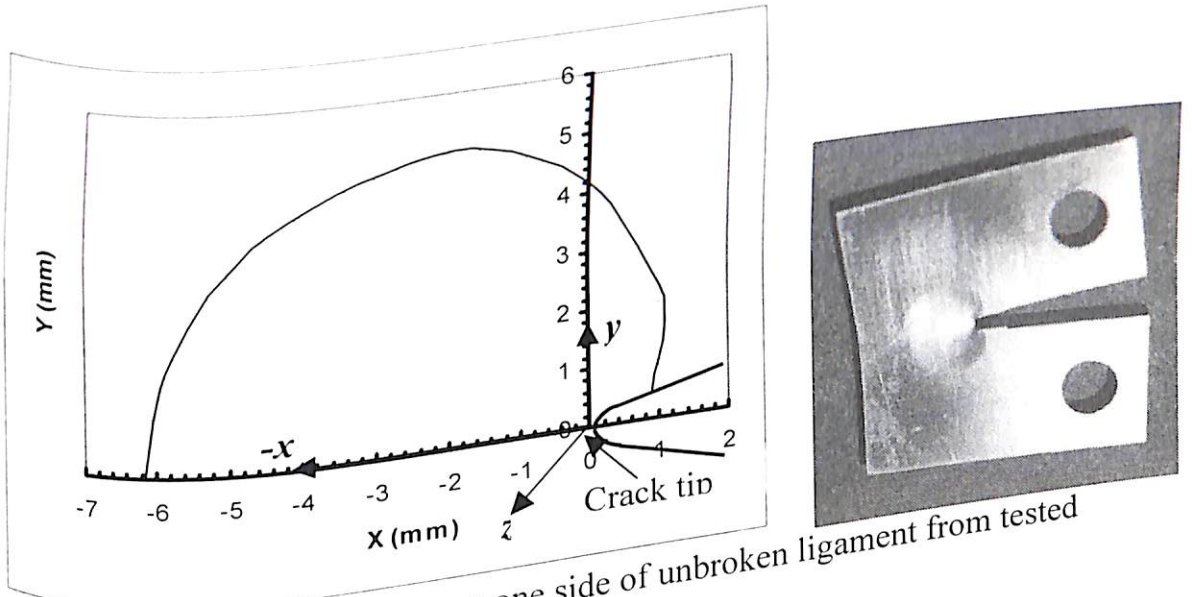

Fig. 5.66 Tensile plastic zone on one side of unbroken ligament from tested specimen in EDD335 (B=1.18).

Table 5.40 shows the hardness values measured at key locations for all three EDD steel sheets. The plastic zone size can also be measured with the help of hardness check at various points across the elastic-plastic boundary; e.g. location points 2-3 and 6-5 along line 1-7 in Fig. 5.67 – 5.69.

Table 5.40 Hardness measurement in HV across the plastic zone ahead of crack tip

Location (point)	EDD335	EDD277	EDD258
1	166	134	124
2	166	134	125
3	185	149	145
4	188	158	153
5	186	152	149
6	165	134	124
7	166	135	124
8	182	153	146
9	167	137	127

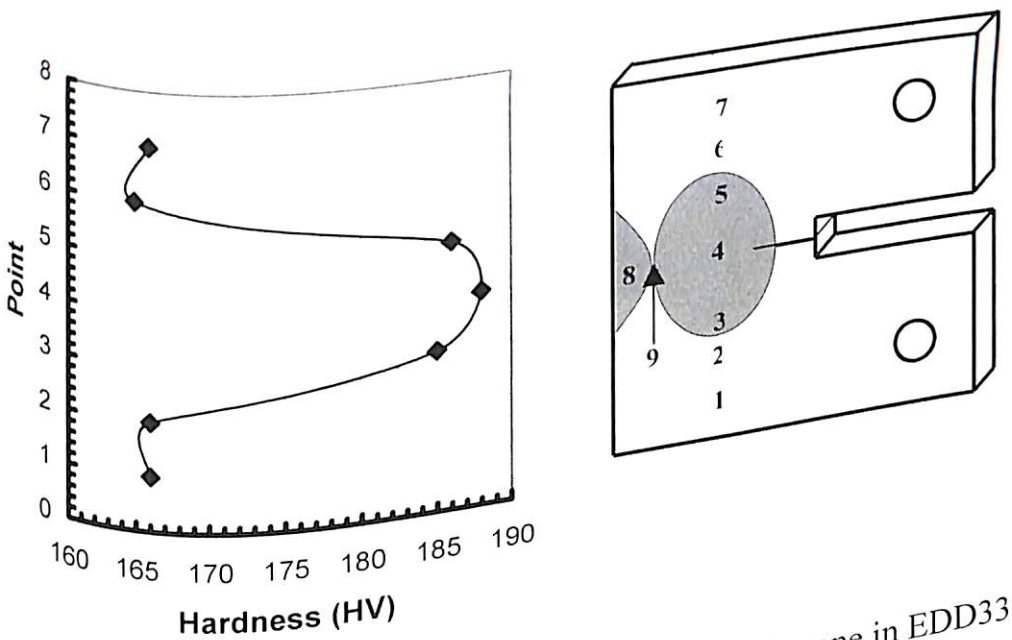

Fig. 5.67 Hardness measurement across the plastic zone in EDD335.

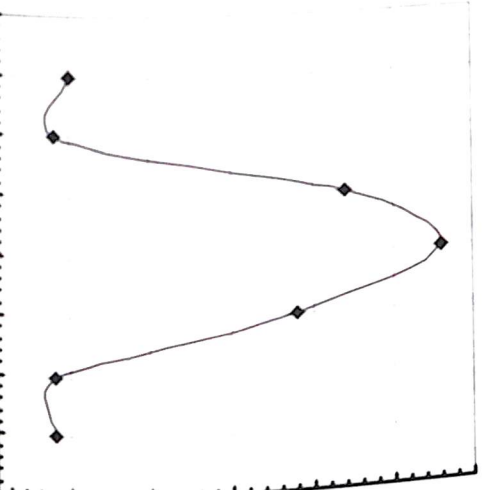

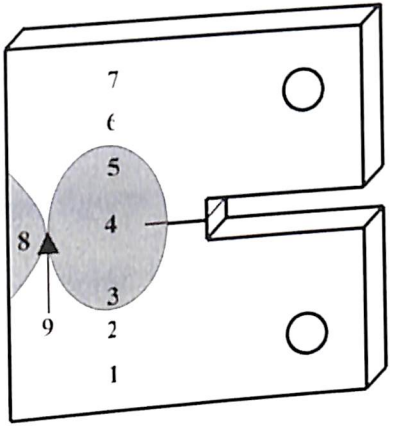
7
6
5
4
8
3
9
2
1

and EDD258, respectively. The point 4 is ahead of the crack-tip and severely deformed showing highest harness value. The trend shown by 2-3-4-5-6 is almost parabolic and symmetric to the unbroken ligament length. The point 8 is also highly deformed in the compressive plastic zone. These figures also show the apparent axis of rotation (i.e. point 9). This is a common point of tensile plastic zone and compressive plastic zone, at which the hardness value is equal to the hardness value in elastic field i.e. points 1, 2, 6 and 7. The above findings are also confirmed by Cotterell *et al.* (2002). He reported significantly higher hardness values in the region close to the crack tip, where localised deformation is occurred.

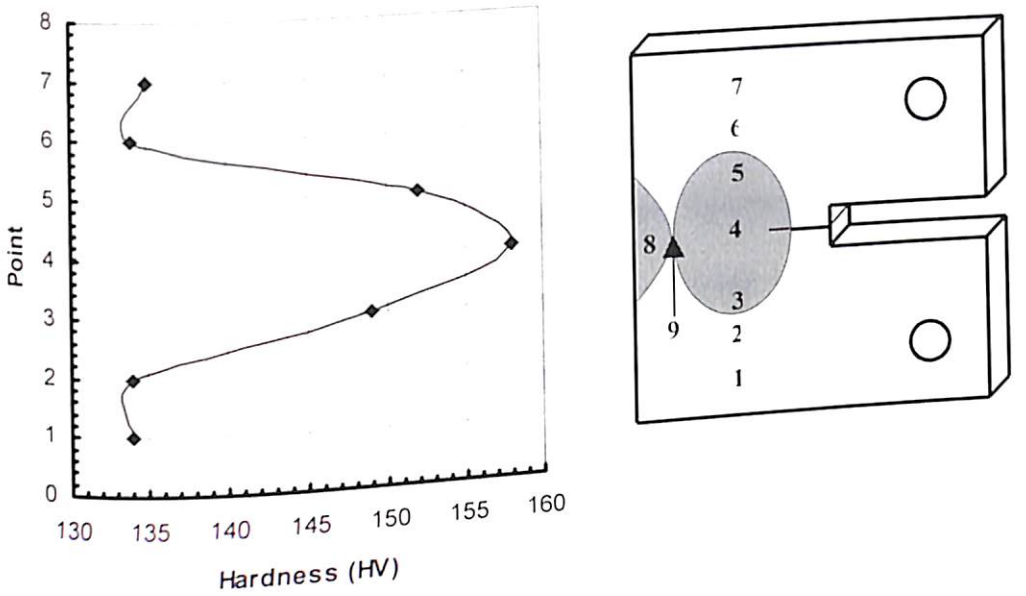

Fig. 5.68 Hardness measurement across the plastic zone in EDD277.

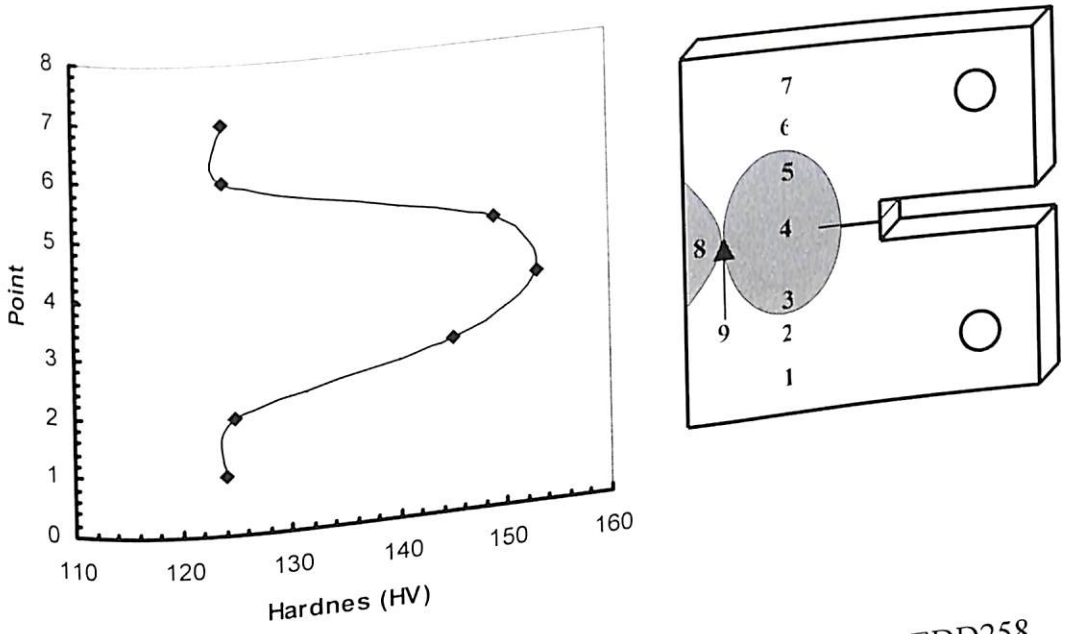

Fig. 5.69 Hardness measurement across the plastic zone in EDD258.

Figures 5.67, 5.68 and 5.69 show the hardness measurement across the plastic zone and perpendicular to unbroken ligament length for EDD335, EDD277

and EDD258, respectively. The point 4 is ahead of the crack-tip and severely deformed showing highest harness value. The trend shown by 2-3-4-5-6 is almost parabolic and symmetric to the unbroken ligament length. The point 8 is also highly deformed in the compressive plastic zone. These figures also show the apparent axis of rotation (i.e. point 9). This is a common point of tensile plastic zone and compressive plastic zone, at which the hardness value is equal to the hardness value in elastic field i.e. points 1, 2, 6 and 7. The above findings are also confirmed by Cotterell *et al.* (2002). He reported significantly higher hardness values in the region close to the crack tip, where localised deformation is occurred.

Chapter 6

CONCLUSIONS

6.1 Conclusions

EDD steel sheets are widely used among the most important sheet metals in industrialised countries. From engineering and economic viewpoint, a thorough understanding of fracture behaviour of EDD steel sheets and their products is essential to manufacturers as well as users. From this study, key findings and conclusions are summarised in subsequent paragraphs.

The formability and fracture mechanics are the two approaches to understand the fracture behaviour in EDD steel sheets. Using formability approach, intrinsic and simulative tests give relative engineering index of formability. Because of complex interactions of material and process variables, it is difficult to single out a single parameter responsible for the crack initiation phenomena. From literature, it is found that prevention of failure in stressed structural components of EDD steel materials currently requires fracture mechanics based design parameters. However, analysis of formability parameters is important to understand the forming qualities of EDD steel sheets. According to ASTM E 8M and E 517-92, the study of formability shows that EDD277 and EDD258 steel sheet has relatively high formability than EDD335 steel sheet.

In fracture mechanics, the fracture criterion is to measure the load levels at which crack initiates and propagates. In present work, similar principle is extended to predict the fracture limits using fracture based design parameters like critical load,

critical *CTOD* and critical *J*-integral. Fracture behaviour of EDD steel sheets is studied in its generation phase as well as in application phase in detail.

The precise determination of crack initiation event necessitates successive experimental attempts. A 'load drop technique' is suggested for determining fracture criterion of EDD steel sheets, which assists in detecting the physical event of crack initiation. Using load drop technique, precise determination of critical load is possible without any change in experimental set up.

The CFOA model is suggested to find the plastic *CTOD* in addition to existing PHM, *J-CTOD* relation and 3-D FE analysis. The PHM results on plastic *CTOD* are found to be conservative because the value of PRF in PHM depends only on initial crack length and unbroken ligament length and the model does not account for non-linearity between plastic load-line displacement and plastic *CTOD*. The suggested CFOA model accounts for this non-linearity. In this model, the value of PRF depends upon the crack flank opening angle, which in turn depends upon the thickness of specimen. CFOA model is found to be consistent and well agreed with FE analysis. The critical *J*-integral is obtained following ASTM E 813-87 and using the area under the load – load-line displacement curve.

Experimental results on critical load, *J*-integral and *CTOD* are well supported by 3-D FE analysis. FE analysis shows that the stress σ_z is much lower compared to the in plane stresses (σ_x and σ_y) proving a predominantly plane stress fracture behaviour. The size of the plastic zone at the mid-thickness section is found to be similar to the size of plastic zone on surface. This observation also supports a predominantly plane stress fracture behaviour. The amount of crack tip necking (δn)

and location of an apparent axis of rotation could be precisely determined with the help of FE analysis. The critical load values by FE analysis are slightly overestimated and within 5-12% of experimental results. This discrepancy is attributed towards assumed idealised conditions in FE model.

The *J-CTOD* relation is found to be valid in predominantly plane stress region with Shih factor (d_n) in the range 0.9-1.1. This factor is found to be independent of thickness and notch radius. From the strain rate effect study, it is found that there is no consistency in *J-CTOD* relation for higher strain rate. Elastic contribution towards the *J* or *CTOD* values is negligible indicating that plasticity is the only source of toughness.

The critical *CTOD* and critical *J*-integral in EDD steel sheets increases with increase in thickness, unlike that of thin plates. Liu's proposition: 'crack tip opening displacement is equal to crack tip necking' is found to be invalid. The equality holds good for lower value of thickness, however, as thickness increases, the difference between *CTOD* and thickness contraction increases. This is because the stress in *z*-direction increases slowly and restricts the deformation ahead of crack tip.

Experimental as well as FE analysis shows that the strain rate has no significant effect on fracture toughness till the strain rate is 0.6 mm/min at room temperature, however, there is a sharp decrease in fracture toughness beyond 0.6 mm/min. This is because the dislocation motion is restricted with high strain rate. Therefore, in order to have high formability, the forming of the sheet should be done at lower strain rates.

Influence of notch radius on fracture toughness has been studied with a wide range of notch radii. The critical notch radius is found to be 0.16 mm. This study is essential to verify the validity of results of notched specimens having notch radii in the range of 0.11-0.13 mm. With this study, it is recommended that fatigue pre-cracking, which is a time consuming job, is not essential. The WEDM process can be successively used for pre-cracking. The FEM study showed that as radius of notch increases, the stress triaxiallity reduces in the vicinity of crack tip increasing the fracture toughness.

In application phase, the crack growth behaviour is described with the help of *J-R*, *CTOA-R* and *CTOD-R* curves. *J*-integral is calculated incrementally using ASTM E 1820-01 (2001). Critical *CTOA* model can be used to determine crack growth *CTOD*. The increase in resistance during crack extension is because of high degree of shear lips, crack tunneling and large plastic zone ahead of crack tip. The rising nature of *R* curves implies continued increase in toughness during stable tearing, and the increase in tearing resistance is the governing parameter for stability rather than the critical initiation toughness value. From the critical *CTOA* model, it is concluded that *CTOD* is geometrically related with δ_{CG} through *CTOA*. δ_{CG} being a near field displacement parameter may more reliably characterise the fibrous cracking process. The crack growth behaviour can not be characterised using normal FE analysis, as re-meshing is not possible using normal finite element method. With the help of *CTOA* model, it is shown that the crack initiation energy is reclaimed during propagation. This is also supported by ASTM standard E 1820-01. The correct

definition of energy dissipation for a completely fractured specimen should include crack initiation energy.

Metallographic study showed that the surface level grains are more strained than at $1/4^{th}$- and mid-thickness-section level. This is because the material at the surface level is free and stretched more in x- and y-direction. Fracture surface showed high degree of shear-lips and crack tunneling. The high degree of shear-lips with crack tunneling over the entire broken ligament is an indication of predominantly plane stress fracture behaviour. The crack tunneling plays a significant role in the stable tearing process of EDD steel sheet. The plastic zone in general yielding fracture mechanics touches ligament boundary of specimen and also increases with increase in specimen thickness.

6.2 Advantages of the Present Study

The study on formability and fracture behaviour of EDD steel sheets is equally important to manufacturers as well as users in order to understand and analyse the crack initiation and crack propagation in products as well as structures. This study is also useful to determine safe load value in the design of EDD steel sheet products as well as structures.

6.3 A Few Suggestions in Design

A few suggestions in design are suggested as follows.

(a) Selection of EDD steel sheet with sufficiently high thickness will have more fracture toughness.

(b) At lower strain rates, higher formability can be achieved.

(c) Higher the crack tip radius, lower the chances for crack to grow under the designed load.

(d) The crack extension can be tolerated provided it does not affect the function of the product.

6.4 Future Scope for Work

- Generally the EDD steel sheets are used at atmospheric temperature, however, low temperature and high temperature effect on fracture toughness can be studied for specific applications.
- The crack growth characterisation can be studied in detail using meshless techniques, because re-meshing is not possible by using normal FE analysis.
- The crack tunneling can be studied in detail to understand the stable tearing of EDD steel sheet.
- This study can be extended to light metal alloy used for aerospace applications.

REFERENCES

American Society for Testing and Materials, E 1152-87, Philadelphia, PA (1987).

American Society for Testing and Materials, E 813-87, Philadelphia, PA (1987).

American Society for Testing and Materials, E 1290-89, Philadelphia, PA (1989).

American Society for Testing and Materials, E 399-91, Philadelphia, PA (1991).

American Society for Testing and Materials, E 517-92, Philadelphia, PA (1992).

American Society for Testing and Materials, E 8 M, Philadelphia, PA (1999).

American Society for Testing and Materials, E 1820-01, Philadelphia, PA (2001).

ANSYS 7.0 (2002): Procedure Manual, Swanson Analysis System, Inc., US.

Anderson (1994): Fracture Mechanics: Fundamentals & Applications, Second Edition Published by CRC Press, UK.

Annual Book of ASTM Standards (1987): *Metals Test Methods and Analytical Procedures*, ASTM Publications, Philadelphia, 03.01.

Atkins A.G. (1993): Fracture in Forming. *Proc. Int. Conf. On Advances in Materials and Processing Technologies*, (Ed. Hashmi). Dublin: City University, pp. 234-245.

Atkins A.G. (1995): Deformability versus Fracture Limit Diagrams in Material Processing Defects. (S.K. Ghosh & M. Predeleanu, Eds) Material Processing Defects. *Elsevier Studies in Applied Mechanics* vol. 43, pp. 235-250.

Atkins A.G. (1997): Strange Multiplier Crack Paths in Ductile Fracture. *Proc. 9th Int. Conf. On Fracture*, Sydney, pp. 2391–2402.

Atkins A.G. and Mai Y.W. (1987): Fracture Strains in Sheet Metal Forming and Specific Essential Work on Fracture. *Engineering Fracture Mechanics*, vol. 27, pp. 291-297.

Bhattacharya Sova and Kumar A.N. (1991): A New Approach for CTOD Evaluation in Slow Crack Growth Situations. *Engineering Fracture Mechanics*, vol. 40 (6), pp.1089-1103.

Bhattacharya Sova and Kumar A.N. (1995a): Rotational Factor using Bending Moment Approach under Elasto-Plastic Situation – I. Notch 3PB geometry. *Engineering Fracture Mechanics*, vol. 50 (4), pp. 493-505.

Bhattacharya Sova and Kumar A.N. (1995b): Modeling of Rotational Factor in Notched Bend Specimen under General and Local Yield Situation. *Theoretical and Applied Fracture Mechanics*, vol. 24, pp. 33-46.

Blackburn (1976): On the Use of Singular Finite Elements in Linear Fracture Mechanics. *International Journal for Numerical Methods in* Engineering, vol. 10, pp. 25-37.

Bray J.W., Handerhan K.J., Garrison W.M. and Thompson A.W. (1992): Fracture Toughness and the Extents of Primary Void Growth. *Metallurgical Transactions*, A 1992; 23A, pp. 485-496.

Brocks W. and Yuan H. (1991): Defect Assessment in Components – Fundamentals and applications. ESIS Publications, USA, vol. 9.

BS: 5762 (1979): Crack Opening Displacement (COD), British Standard Institution, London, pp. 1-12.

Caddell Robert M. (1980): Deformation and Fracture of Solids. Published by Prentice-Hall, INC. Englewood Cliffs, New Jersey 07632.

Callister William D. Jr. (2003): Materials Science and Engineering An Introduction. Sixth Edition. Published by John Wiley and Sons, Inc.

Castrodeza E.M., Ipina J.E.P. and Bastian F.L. (2004): Fracture Toughness Evaluation of Unidirectional Fibre Metal Laminates using Traditional CTOD (δ) and Schwalbe (δ_5) Methodologies. *Engineering Fracture Mechanics* vol. 71, pp. 1127-1138.

Cotterell B. (2002): The Past, Present, and Future of Fracture Mechanics. *Engineering Fracture Mechanics*, vol. 69, pp. 533-553.

Cotterell M. Schambergerova J., Ziegelheim J. and Janovec J. (2002): Dependence of Micro-hardness on Deformation of Deep-drawing Steel Sheets. *Journal of Materials Processing Technology*, vol. 124, pp. 293-296.

Dasarathy C. and Hudd R.C. (1974): Effect of Al Content on the Deep Drawing Properties of Continuous Annealed Al-killed Sheet Steels. Technical Report No. 632/A/1974, B.S.C., Strip Mill Division, Port Talbot Works.

Dawicke D.S., Newman J.C. Jr., and Bigelow C.A. (1999): Three Dimensional CTOA and Constraint Effects during Stable Tearing in a Thin Sheet Material. ASTM STP 1256, American Society for Testing and Materials, Philadelphia, pp. 223-242.

Dawicke D.S. and Sutton M.A. (1994): CTOA and Crack Tunneling Measurements in Thin Sheet 2024-T351 Aluminium Alloy. *Experimental mechanics*, vol. 34, pp. 357-366.

Degiorgi V.G. and Matic P. (1990): An Experimental and Computational Investigation of Crack Growth Initiation in Three-Point Bend Fracture Specimens. *Engineering Fracture Mechanics, vol. 37, pp. 1039-1058.*

Dieter G.E. (1988): Mechanical Metallurgy. Published by McGraw-Hill, London.

Dugdale D.S. (1960): Yielding in Steel Sheets Containing Slits. *Journal of Mechanics and Physics of Solids*, vol.8, pp. 100-108.

Eng T.N. and Gang, Q. (2001): Material fatigue behavior characterisation using wavelet-based AE technique – A Case Study of Acrylic Bone Cement. *Engineering Fracture Mechanics*, vol. 68, pp. 1477-1492.

Faucher B. Tyson W. R. Hong Y, Boutin J. (1990): Dependence of Ductile Fracture Toughness of a Weld Metal on Notch Root Radius and Inclusion Content. *International Journal of Fracture*, vol. 46, pp. 173-184.

Firrao D. and Roberti R. (1983): Ductile Fracture Nucleation ahead of Sharp Cracks. *Metallurgical Science and Technology*, vol.1, pp. 5-13.

GB 2358-80 (1980): Chinese Standards Association: Crack Opening Displacement (COD) Testing Method.

Goodwin G.M. (1968): Application of Strain Analysis to Sheet Metal Forming Problems in the Press Shop. Society of Automotive Engineers. SAE Technical paper No. Paper No. 680093.

Griffith A.A. (1920): The Phenomena of Rupture and Flow in Solids. *Philosophical Transactions*, Series A, vol. 221, pp. 163-198.

Haung You-Min and Leu Daw-Kwei (1998): Effect of Process Variables on V-Die Bending Process of Steel Sheet. *International Journal of Mechanical Sciences*, vol. 40, pp. 631-650.

Hecker S.S. (1972): Simple Technique for Determining Forming Limit Curves. *Sheet Metal Ind*, vol. 52, pp. 671-675.

Heerens J. and Schodel M. (2002): On the Determination of Crack Tip Opening Angle, CTOA, using Light Microscopy and δ_5 Measurement Technique. *Engineering Fracture Mechanics*, vol. 70, pp. 417-426.

Hosford W.F. and Caddell R.M. (1993): Metal Forming-Mechanics and Metallurgy. Published by Prentice Hall, USA.

Hutchinson J.W. (1968): Singular Behaviour at the End of a Tensile Crack Tip in a Hardening Material. *Journal of Mechanics and Physics of Solids*, vol. 16, pp. 13-31.

Irwin G.R. (1948): Fracture Dynamics. *Fracturing of Metals*, American Society for Metals, Cleveland, pp. 147-166.

Kanninen M.F., Rybicki E.F., Stonesfier R.B., Broek D., Rosenfield A.R. and Nalin G.T. (1979): Elastic-Plastic Fracture Mechanics for Two-Dimensional Stable Crack Growth and Instability Problems. ASTM STP 668, American Society for Testing and Materials, Philadelphia, pp. 121-150.

Keeler S.P. and Backofen W.A. (1963): Plastic Instability and Fracture in Sheets Stretched Over Rigid Punches. *Transactions of the ASM*, vol. 56, pp. 25-48.

Keeler, S.P. (1965): Determination of Forming Limits in Automotive Stampings. *Society of Automitive Engineers*, Technical paper No. 650535.

Kulkarni D.M. and Ravi Prakash (2001): Experimental and Finite Element Analysis of Fracture Criterion of Extra Deep Drawn Steel Sheets. *Proceedings of 10th ICF (International Congress on Fracture)*, Hawaii (US), 2-6 December 2001, pp. 432-438.

Kulkarni D.M., Ravi Prakash and Kumar A.N. (2002): Experimental and Finite Element Analysis of Fracture Criterion in General Yielding Fracture Mechanics. *Sadhana*, Indian Academy of Sciences, vol. 27, Part 6, pp. 631-642.

Kulkarni D.M., Ravi Prakash (2003a): Experimental Analysis of Fracture Criterion in General Yielding Fracture Mechanics. *Journal of Institute of Engineers (India)*, vol. 84, pp. 18-21.

Kulkarni D.M., Talan P.S, Ravi Prakash. and Kumar A.N. (2003b): Verification of *J* –CTOD Relation in General Yielding Fracture Mechanics. *Proceedings of 48th Congress of the Indian Society of Theoretical and Applied Mechanics*, pp. 82 – 90.

Kulkarni D.M., Ravi Prakash, Talan P.S. and Kumar A.N. (2004a): The Effect of Specimen Thickness on the Experimental and Finite Element Characterisation of CTOD in Extra Deep Drawn Steel Sheets. *Sadhana*, Indian Academy of Sciences, vol. 29, Part 4, pp. 365-380.

Kulkarni D.M. and Ravi Prakash (2004b): 'Failure Analysis and Prevention' a Course for Undergraduates. Special issue on 1st ICEFA (*International Conference on Engineering Failure Analysis*, Lisbon, (in press).

Kulkarni D.M. and Ravi Prakash (2004c): *R*-curve Characterisation of the Fracture Toughness of EDD Steel Sheets. *Proceedings of ICASI, International Conference on Advances in Structural Integrity*, Indian Institute of Science, Bangalore, India, pp. 241-248.

Kulkarni D.M. and Ravi Prakash (2004d): Effect of Notch Radius on Fracture Parameters in EDD Steel Sheets. *Proceedings of ICASI, International Conference on Advances in Structural Integrity*, Indian Institute of Science, Bangalore, India, pp. 89-95.

Kumar A.N. and Bhattacharya Sova (1995): Rotational Factor using Bending Moment Approach under Elasto-Plastic Situation – II. Notch 3PB geometry. *Engineering Fracture Mechanics*, vol. 50 (4), pp. 507-517.

Kumar A.N. (1988a): On the Accuracy of Crack Size Measurement. *International Journal of Fracture*, vol. 38, pp. R27-R30.

Kumar A.N. (1988b): Thickness Effect on Slow Crack Growth Measurement. *International Journal of Fracture*, vol. 36, pp. R29-R32.

Kumar A.N. (1989): On the Source of Increased CTOD during Ductile Tearing. *International Journal of Fracture*, vol. 39, pp. R35-R38.

Kumar A.N. (1991): A Comparative Study on Crack Size Measurement. *International Journal of Fracture*, vol. 47, pp. R11-R16.

Kumar A.N. (1996): Modeling of Fracture Process in Annealed Sheet of AISI 202 Stainless Steel. *Scripta Materialia*, vol. 34, pp. 369-373.

Landes J.D. and Begley J.A. (1979): Experimental Methods for Elastic-Plastic and Post-Yield Fracture Toughness Measurements. Barking: Post-yield Fracture Mechanics, Applied Science, Publications.

Liu H.W. and Ke, J.S. (1976): Thickness Effect on Crack Tip Deformation of Fracture. *Engineering Fracture Mechanics*, vol. 8, pp. 425-436.

Liu H.W. and Kuo, A.S. (1978): Fracture Toughness of Thin and Tough Plates. *International Journal of Fracture*, vol. 14, pp. R109-R112.

Liu H.W. (1981): Fracture Mechanics of Ductile and Tough Materials and its Applications to Energy Related Structures. Published by Martinus Nijhoff Publishers, the Hague.

Mahmoud S. and Lease K. (2002): The effect of Specimen Thickness on the Experimental Characterisation of Critical Crack-Tip-Opening Angle in 2024-T351 Aluminum Alloy. *Engineering Fracture Mechanics*, vol. 8, pp. 425-436.

Majerus J.N. and Santhanam S. (1997): Anisotropy in Fracture Behavior of Thin Al-7075-T651 Plates. *Engineering Fracture Mechanics*, vol.56, pp. 437-442.

McClintock F.A. (1971): Plasticity Aspects of Fracture. *Fracture: An Advanced Treatise*, Academic Press, New York, vol.1.

Mellor P.B. (1981): "Deep-Drawing and Stretch Forming," Developments in the Drawing of Metals, *Proceedings of the International Conference, the Metals Society*, London, pp. 76-86.

Merkle J.G. and Corten H.T. (1990): Elastic-Plastic Fracture Toughness Testing with Compact Tension Specimens. *Journal of Pressure Vessel Technology*, vol. 96, pp. 286-292.

Mizui N. and Okamoto A. (1990): The Effect of Carbon Content on the Mechanical Properties of Continuous Annealed Al-killed Sheet Steels. Sumitomo Search, vol. 44, pp. 113-119.

Mizui N. and Okamoto A. (1991): Effects of Mn content and Hot Band Coiling Temperature on Deep Drawability of Continuous Annealed Al-killed Sheet Steels. *Proceedings of International Symposium on Developments in the Annealing of Sheet Steels*, TMS Ferrour Metallurgy Committee, Cincinnati, OH, pp. 247-259.

Murakami Y. (1987): Stress Intensity Factors Handbook. Published by Pergamon Press, New York.

Nakazima K., Kikuma T., and Hasuka T (1968): Study on the formability of steel sheets. *Yawata Technical Report*, No. 284, pp. 140-141

Newman J.C. Jr. (1984): An Elastic-Plastic Finite Element Analysis of Crack Initiation, Stable Crack Growth and Instability. ASTM STP 833, American Society for Testing and Materials, Philadelphia, pp. 93-117.

Newman J.C. Jr., Shivakumar K.N. and McCabe D.E. (1991): Finite Element Fracture Simulation of A533B Steel Sheet Specimens. Defect Assessment in Components: Fundamentals and Applications, ESIS Pub. 9, pp. 117-126.

Newman J.C. Jr., James M.A. and Zerbst U. (2003): A review of the CTOD/CTOA Fracture Criterion. *Engineering Fracture Mechanics*, vol. 70, pp. 371-386.

Pandey A.B. Majumdar B.S. and Miracle D.B. (1997): Effects of Thickness and Precracking on the Fracture Toughness of Particle-Reinforced Al-Alloy Composites. *Metallurgical and Material Transactions*, vol. 29A, pp. 1237-1243.

Panontin T.L., Makino A., and Williams J.F. (2000): Crack Tip Opening Displacement Estimation Formulae for C(T) Specimens. *Engineering Fracture Mechanics*, vol. 67 (3) pp. 293-301.

Pardoen T. and Delannay F. (2000): A Method for the Metallographical Measurement of the CTOD at Cracking initiation and the Role of Reverse Plasticity on Unloading. *Engineering Fracture Mechanics*, vol.65, pp. 455-466.

Paulino G.H., Carpenter R.D., Liang W.W., Munir Z.A. and Gibeling J.C. (2001): Fracture Testing and Finite Element Modelling of Pure Titanium. *Engineering Fracture Mechanics*, vol.68, pp. 1417-1432.

Pluvinage G. and Lanvin A. (1993): Stretch Zone Geometrical Measurement, a Particular Way to measure Fracture Toughness. *Fatigue and Fracture of Engineering Materials and Structures*, 16, pp. 955-972.

Rao B.N. and Rahman S. (2003): Mesh-free Analysis of Cracks in Isotropic Functionally Graded Materials. *Engineering Fracture Mechanics*, vol.70, pp. 1-27.

Rao K.P. and Mohan E.V.R. (2000): Direct Evaluation of Sheet Metal Forming Properties under Various Deformation Conditions. *Fracture and Strength of Solids*, Trans Tech Publications, Switzerland, Key Engineering Materials, pp. 509-516.

Raulea L.V., Goijaerts A.M., Govaert L.E. and Baaijens F.P.T. (2001): Size Effects in the Processing of Thin Metal Sheets. *Journal of Material Processing Technology*, vol. 115, pp. 44-48.

Ray S.K. (2000-2004): Technical Reports on EDD Steel Sheets. Scientific Services Division, TISCO, Jamshedpur.

Ravi Kumar D. (2002): Formability analysis of Extra-Deep Drawing Steel. *Journal of Materials Processing Technology*, vol. 130, pp. 31-41.

Rice J.R. (1968): A Path Independent Integral and the Approximate Analysis of Stress Concentration by Notches and Cracks. *Journal of Applied Mechanics*, vol. 35, pp. 379-386.

Rice J.R. and Rosengren G.F. (1968): Plane Strain Deformation near a Crack Tip in a Power-Law Hardening Material. *Journal of the Mechanics and Physics of Solids*, vol. 16, pp. 1-12.

Rice J.R., Paris P.C. and Merkle J.G. (1973): Some Further Results of J-Integral Analysis and Estimates. ASTM STP 536, American Society of Testing and Materials, Philadelphia, pp. 231-245.

Schedin E. and Melander A. (1987): On the Strain Distribution During Punch Stretching of Low and High Grades of Sheet Steel. *Journal of Materials Processing Technology*, vol. 15, pp. 181-186.

Schindler H.J. (1991): Determination of Fracture Mechanics Material Properties utilising Notched Test Specimens. *Mechanical Behaviour of Materials*, ICM; vol. 6, pp.153-158.

Seshadri B.R. Newman J.C. Jr., Dawicke D.S. and Young R.D. (1998): Fracture Analysis of FAA/NASA Wide Stiffened Panels. Second Joint Conference on Aging Aircraft. Williamsburg, pp. 513-524.

Shih C.F. (1981): Relationship between the J-Integral and the Crack Opening Displacement for Stationary and extending Cracks. *Journal of the Mechanics and Physics of Solids*, vol. 29, pp. 305-326.

Shih C.F., de Lorenzi, H.G. and Andrews W.R (1979): Studies on Crack Initiation and Stable Crack Growth. ASTM STP 668, American Society for Testing and Materials, Philadelphia, pp. 65-120.

Srawley J.E. and Brown W.F. (1975). Fracture Toughness Testing and its Applications. ASTM STP No. 381, Philadelphia, PA, pp. 133-198.

Srinivas M. and Kamat S.V. (1992): Effect of notch root radius on ductile fracture toughness of Armco Iron. *International Journal of Fracture*, vol.58, pp. R15-R21.

Sumpter J.D.G. (1999): An Alternative View of R Curve Testing. *Engineering Fracture Mechanics*, vol. 64, pp. 161-176.

Sun X., Cao W. and Lu X. (1994): The Experimental Investigation of Deformation and Opening Displacement at a Crack Tip. *International Journal of Pressure Vessels and Piping*, vol. 60, pp. 22-31.

Swaminathan K., Padmanabhan K.A. (1991): Some Investigations on the Fracture Behaviour of an Indigenous Extra-Deep Drawing low Carbon Steel - Part I. *Transactions of Indian Institute of Metals*, vol. 44, pp. 231-247.

Takuda H., Kikuchi S., Tsukada T., Kubota K. and Hatta N. (1999): Effect of Strain rate on Deformation of a Mg-8.5Li-1Zn Alloy Sheet at Room Temperature. *Materials Science & Engineering*, vol. A271, pp. 251-256.

Talan P.S, Kulkarni D.M., Ravi Prakash. and Kumar A.N. (2003): Physical Significance of Fracture Criterion in Plane Stress, Plane Stress – Plane Strain and Plane Strain Zone.. *Proceedings of 48 th Congress of the Indian Society of Theoretical and Applied Mechanics*, pp. 72-81.

Tang C.Y. (1998): Prediction of Fracture Limits of Sheet Metals by Using a Damage Mechanics Criterion. Key Engineering Materials Vols. 145-149, pp. 453-458.

Wells A.A. (1961): Unstable Crack Propagation in Metals: Cleavage and Fast Fracture. *Proceedings of the Crack Propagation Symposium*, Cranfield, UK vol.1, Paper 84, pp. 210-230.

Wilson D.V. and Acselrad O. (1984): Strain Localisation in Biaxially Stretched Sheets Containing Compact Defetcs – I. *International Journal of Mechanical Sciences*, vol. 26, pp. 573-585.

Wilson C.D. and Landes J.D. (1994): Inconsistencies between CTOD and J Calculations. *Journal of Testing and Evaluation*, vol. 22, pp. 505-511.

Wu P.D., Graf A., Jain M. and MacEwen S.R. (2000): On Alternative Representation of Forming Limits. *Fracture and Strength of Solids,* Trans Tech Publications, Switzerland, Key Engineering Materials vol. 177, pp. 304-309.

Yoda M. (1987): The effect of the notch root radius on the J-integral fracture toughness under modes I, II and III loading. *Engineering Fracture Mechanics*, vol. 26 (3), pp.425-431.

Zhang K.S. (1996): Analysis of Deformation and Fracture for Cracked Specimen of Ductile Steel. *Engineering Fracture Mechanics*, vol. 53, pp. 625-632.

Appendices

LIST OF PUBLICATIONS

1. Kulkarni D.M., Ravi Prakash & Kumar A.N. (2002). Experimental and Finite Element Analysis of Fracture Criterion in General Yielding Fracture Mechanics. *Sadhana*, vol. 27, Part 6, pp. 631-642.

2. Kulkarni D.M., Ravi Prakash (2003). Experimental Analysis of Fracture Criterion in General Yielding Fracture Mechanics. *Journal of Institute of Engineers (India)*, vol. 84, pp. 18-21.

3. Kulkarni D.M., Ravi Prakash, Talan P.S. and Kumar A.N. (2004). The Effect of Specimen Thickness on the Experimental and Finite Element Characterisation of *CTOD* in Extra Deep Drawn Steel Sheets, *Sadhana*, vol. 29, Part 4, pp. 365-380.

CONFERENCE PAPERS

1. Kulkarni D.M. and Ravi Prakash (2001): Experimental and Finite Element Analysis of Fracture Criterion of Extra Deep Drawn Steel Sheets. *Proceedings of 10th ICF (International Congress on Fracture)*, Hawaii (US), 2-6 December 2001, pp. 432-438.

2. Kulkarni D.M., Talan P.S, Ravi Prakash and Kumar A.N. (2003): Verification of *J –CTOD* Relation in General Yielding Fracture Mechanics. *Proceedings of 48 th Congress of the Indian Society of Theoretical and Applied Mechanics*, pp. 82–90.

3. Kulkarni D.M. and Ravi Prakash (2004): 'Failure Analysis and Prevention' a Course for Undergraduates. Special issue on 1st ICEFA (*International Conference on Engineering Failure Analysis*, Lisbon, (in press).

4. Kulkarni D.M. and Ravi Prakash (2004): *R*-curve Characterisation of the Fracture Toughness of EDD Steel Sheets. *Proceedings of ICASI, International Conference on Advances in Structural Integrity*, Indian Institute of Science, Bangalore, India, pp. 241-248.

5. Kulkarni D.M. and Ravi Prakash (2004): Effect of Notch Radius on Fracture Parameters in EDD Steel Sheets. *Proceedings of ICASI, International Conference on Advances in Structural Integrity*, Indian Institute of Science, Bangalore, India, pp. 89-95.

Appendices

A1

Tensile test data on EDD335 steel

Cross sectional area : 41.976 sq. mm
Gauge length : 25 mm
Cross head velocity : 0.01875 mm/min

A 1.1 Recorded Load – Elongation data from tensile test EDD335 Steel

Sr. No.	Displacement (mm)	Load (kN)	Sr. No.	Displacement (mm)	Load (kN)
1	0.000	0.0000	16	3.1500	15.8799
2	0.0283	9.9681	17	3.6000	16.0998
3	0.0317	11.1570	18	3.9000	16.2501
4	0.0332	11.6889	19	4.6499	16.2474
5	0.0350	12.3236	20	4.9499	16.1696
6	0.5999	14.0657	21	5.0999	16.1362
7	0.7499	14.5001	22	5.2499	16.1030
8	0.8999	14.7499	23	5.4000	16.0012
9	1.3500	14.7998	24	5.5500	15.9690
10	1.4999	14.9501	25	5.7000	15.9030
11	1.6499	15.1499	26	6.1499	15.7578
12	1.8800	15.2498	27	6.4650	15.6531
13	2.1700	15.5000	28	6.7812	15.6109
14	2.4000	15.7502	29	7.1006	15.5239
15	2.8499	15.8300	30	7.4232	15.4099

A 1.2 Engineering Stress-strain data EDD335 Steel

Sr. No.	Strain (mm/mm)	Stress (N/mm^2)	Sr. No.	Strain (mm/mm)	Stress (N/mm^2)
1	0.0000	0.0000	16	0.1260	378.30
2	0.0011	0.0010	17	0.1440	383.54
3	0.0012	0.0011	18	0.1560	387.12
4	0.0013	0.0012	19	0.1859	387.06
5	0.0014	0.0013	20	0.1979	385.21
6	0.0239	335.08	21	0.2039	384.41
7	0.0299	345.43	22	0.2099	383.62
8	0.0359	351.38	23	0.2160	381.19
9	0.0540	352.57	24	0.2220	380.43
10	0.0599	356.16	25	0.2280	378.86
11	0.0659	360.92	26	0.2459	375.40
12	0.0752	363.29	27	0.2586	372.90
13	0.0868	369.26	28	0.2712	371.90
14	0.0960	375.21	29	0.2840	369.82
15	0.1139	377.12	30	0.29693	367.11

A 1.3 True stress-strain data EDD335 Steel

Sr. No.	Strain (mm/mm)	Stress (N/mm^2)	Sr. No.	Strain (mm/mm)	Stress (N/mm^2)
1	0.0000	0.000	16	0.1186	425.97
2	0.0011	0.0011	17	0.1345	438.78
3	0.0012	0.0012	18	0.1449	447.52
4	0.0013	0.0013	19	0.1705	459.058
5	0.0014	0.0014	20	0.1806	461.48
6	0.0237	343.13	21	0.1856	462.83
7	0.0295	355.80	22	0.1906	464.18
8	0.0353	364.04	23	0.1955	463.53
9	0.0525	371.61	24	0.2004	464.89
10	0.0582	377.53	25	0.2053	465.24
11	0.0639	384.74	26	0.2199	467.75
12	0.0725	390.62	27	0.2311	469.34
13	0.0832	401.31	28	0.2423	472.78
14	0.0916	411.24	29	0.2546	474.87
15	0.1079	420.11	30	0.2600	476.12

A2

Tensile test data on EDD277 steel

Cross sectional area : 41.976 sq. mm
Gauge length : 25 mm
Cross head velocity : 0.01875 mm/min

A 2.1 Recorded Load – Elongation data from tensile test EDD277 Steel

Sr. No.	Displacement (mm)	Load (kN)	Sr. No.	Displacement (mm)	Load (kN)
1	0.0000	0.0000	26	5.0985	13.8582
2	0.0275	9.7088	27	5.2493	13.8997
3	0.0287	10.1255	28	5.4010	14.0077
4	0.0305	10.7428	29	5.5503	14.0752
5	0.0317	11.1807	30	5.7004	14.1545
6	0.0325	11.4399	31	5.9006	14.2337
7	0.0330	11.6262	32	5.9996	14.3374
8	0.0375	11.6949	33	6.6005	14.3576
9	0.0400	11.7314	34	7.0493	14.2830
10	0.4489	11.9338	35	7.5011	14.1936
11	0.5995	12.1711	36	7.9494	14.1217
12	0.7510	12.1910	37	8.4006	14.0683
13	0.9008	12.3149	38	8.8512	13.9695
14	1.3501	12.4071	39	9.3010	13.8142
15	1.5008	12.5151	40	9.7498	13.7455
16	1.6496	12.6735	41	10.2010	13.7009
17	1.8798	12.8153	42	10.6509	13.6485
18	2.1689	12.8925	43	11.0993	13.6063
19	2.4008	12.9756	44	11.5498	13.5683
20	3.1508	13.1855	45	11.9984	13.5542
21	3.3513	13.2939	46	12.4488	13.5343
22	3.5991	13.3622	47	12.9009	13.5050
23	3.9009	13.4826	48	13.0985	13.4794
24	4.6504	13.6881	49	13.2512	13.4511
25	4.8407	13.8332			

A 2.2 Engineering Stress-strain data for EDD277 Steel

Sr. No.	Strain (mm/mm)	Stress (N/mm^2)	Sr. No.	Strain (mm/mm)	Stress (N/mm^2)
1	0.0000	000.00	26	0.2039	330.14
2	0.0011	231.29	27	0.2099	331.13
3	0.0011	241.22	28	0.2160	333.70
4	0.0012	255.92	29	0.2220	335.31
5	0.0012	266.36	30	0.2280	337.20
6	0.0013	272.53	31	0.2360	339.09
7	0.0013	276.97	32	0.2399	341.56
8	0.0015	278.60	33	0.2640	342.04
9	0.0016	279.47	34	0.2819	340.26
10	0.0179	284.30	35	0.3000	338.13
11	0.0239	289.95	36	0.3179	336.42
12	0.0300	290.42	37	0.3360	335.15
13	0.0360	293.38	38	0.3540	332.79
14	0.0540	295.57	39	0.3720	329.09
15	0.0600	298.15	40	0.3899	327.46
16	0.0659	301.92	41	0.4080	326.40
17	0.0751	305.30	42	0.4260	325.15
18	0.0867	307.14	43	0.4439	324.14
19	0.0960	309.11	44	0.4619	323.24
20	0.1260	314.12	45	0.4799	322.90
21	0.1340	316.70	46	0.4979	322.42
22	0.1439	318.32	47	0.5160	321.73
23	0.1560	321.19	48	0.5239	321.12
24	0.1860	326.09	49	0.5300	320.44
25	0.1936	329.55			

Sr. No.	Strain (mm/mm)	Stress (N/mm^2)	Sr. No.	Strain (mm/mm)	Stress (N/mm^2)
1	0.0000	000.00	26	0.1856	397.47
2	0.0011	231.55	27	0.1906	400.66
3	0.00115	241.50	28	0.1956	405.80
4	0.00122	256.240	29	0.2005	409.76
5	0.00127	266.700	30	0.2054	414.09
6	0.0013	272.890	31	0.2119	419.12
7	0.00132	277.340	32	0.2151	423.53
8	0.0015	279.027	33	0.2343	432.35
9	0.0016	279.927	34	0.2484	436.21
10	0.0178	289.407	35	0.2624	439.59
11	0.0237	296.908	36	0.2761	443.40
12	0.0296	299.153	37	0.2897	447.77
13	0.0354	303.952	38	0.3031	450.62
14	0.0526	311.541	39	0.3163	451.53
15	0.0583	316.049	40	0.3293	455.16
16	0.0639	321.846	41	0.3422	459.58
17	0.0725	328.258	42	0.3549	463.67
18	0.0832	333.788	43	0.3674	468.05
19	0.0917	338.806	44	0.3798	472.57
20	0.1187	353.710	45	0.392	477.87
21	0.1258	359.160	46	0.4041	482.98
22	0.1345	364.158	47	0.4161	487.75
23	0.145	371.318	48	0.4213	489.37
24	0.1706	386.754	49	0.4253	490.30
25	0.177	393.362			

A 3

Tensile test data on EDD258 steel

Cross sectional area : 41.976 sq. mm
Gauge length : 25 mm
Cross head velocity : 0.01875 mm/min

A 3.1 Recorded Load – Elongation data from tensile test EDD258 Steel

Sr. No.	Displacement (mm)	Load (kN)	Sr. No.	Displacement (mm)	Load (kN)
1	0.0000	0.0000	25	5.0985	12.9766
2	0.0200	7.0463	26	5.2493	13.1861
3	0.0225	7.9263	27	5.4010	13.2941
4	0.0250	8.8061	28	5.5503	13.3616
5	0.0292	10.3014	29	5.7004	13.4829
6	0.0330	10.8797	30	6.1488	13.6888
7	0.0375	10.9813	31	6.4996	13.8337
8	0.0400	11.0598	32	6.6005	13.8539
9	0.4489	11.0942	33	7.0493	13.7793
10	0.5995	11.2056	34	7.5011	13.7319
11	0.7510	11.3515	35	7.9494	13.7020
12	0.9008	11.4754	36	8.4006	13.6486
13	1.3501	11.5676	37	8.8512	13.6337
14	1.5008	11.6756	38	9.3010	13.5624
15	1.6496	11.9179	39	9.7498	13.5356
16	1.8798	11.9338	40	10.2010	13.4911
17	2.1689	12.1004	41	10.6509	13.4386
18	2.4008	12.1398	42	11.0993	13.3964
19	3.1508	12.2197	43	11.5498	13.3585
20	3.3513	12.3533	44	11.9984	13.3132
21	3.5991	12.4483	45	12.4488	13.2824
22	3.9009	12.5558	46	12.9009	13.2321
23	4.6504	12.6820	47	13.3508	13.1847
24	4.8407	12.8917	48	13.7982	13.1373

A 3.2 Engineering Stress-strain data EDD258 Steel

Sr. No.	Strain (mm/mm)	Stress (N/mm^2)	Sr. No.	Strain (mm/mm)	Stress (N/mm^2)
1	0.0000	000.00	25	0.2039	309.14
2	0.0008	167.865	26	0.2099	314.13
3	0.0009	188.829	27	0.2160	316.70
4	0.0010	209.790	28	0.2220	318.31
5	0.0012	245.412	29	0.2280	321.20
6	0.0013	259.190	30	0.2459	326.11
7	0.0015	261.609	31	0.2599	329.56
8	0.0016	263.479	32	0.2640	330.04
9	0.0179	264.300	33	0.2819	328.26
10	0.0239	266.954	34	0.3000	327.13
11	0.0300	270.428	35	0.3179	326.42
12	0.0360	273.380	36	0.3360	325.15
13	0.0540	275.577	37	0.3540	324.79
14	0.0600	278.151	38	0.3720	323.10
15	0.0659	283.923	39	0.3899	322.46
16	0.0751	284.301	40	0.4080	321.40
17	0.0867	288.270	41	0.4260	320.15
18	0.0960	289.210	42	0.4439	319.14
19	0.1260	291.111	43	0.4619	318.24
20	0.1340	294.295	44	0.4799	317.16
21	0.1439	296.559	45	0.4979	316.42
22	0.1560	299.119	46	0.5160	315.23
23	0.1860	302.125	47	0.5340	314.10
24	0.1936	307.122	48	0.5519	312.97

A 3.3 True stress-strain data EDD258 Steel

Sr. No.	Strain (mm/mm)	Stress (N/mm^2)	Sr. No.	Strain (mm/mm)	Stress (N/mm^2)
1	0.0000	000.00	25	0.1856	372.19
2	0.0008	168.00	26	0.1906	380.09
3	0.0009	189.03	27	0.1956	385.13
4	0.0010	210.10	28	0.2005	388.98
5	0.0012	245.70	39	0.2054	394.44
6	0.0013	259.19	30	0.2199	406.32
7	0.0015	262.00	31	0.2311	415.24
8	0.0016	263.90	32	0.2343	417.18
9	0.0178	269.04	33	0.2484	420.82
10	0.0237	273.35	34	0.2624	425.29
11	0.0296	278.55	35	0.2761	430.22
12	0.0354	283.23	36	0.2897	434.41
13	0.0526	290.46	37	0.3031	439.79
14	0.0583	294.84	38	0.3163	443.30
15	0.0639	302.65	39	0.3293	448.21
16	0.0725	305.67	40	0.3422	452.54
17	0.0832	313.28	41	0.3549	456.54
18	0.0917	316.98	42	0.3674	460.83
19	0.1187	327.80	43	0.3798	465.26
20	0.1258	333.74	44	0.392	469.38
21	0.1345	339.25	45	0.4041	473.99
22	0.1450	345.79	46	0.4161	477.90
23	0.1706	358.32	47	0.4279	481.84
24	0.1770	366.59	48	0.4395	485.71

B1

Fracture Test on EDD335 (Thickness effect study)

B1.1 Fracture test S1

1. Material

Material	Yield strength (MPa)	Modulus of Elasticity (GPa)	Poisson's ratio (ν)
EDD335 steel sheet	335	210	0.33

2. (Compact Tension (CT) specimen as per ASTM standard (E399-91).

Specimen code	Thickness B (mm)	Crack length a_0 (mm)	Width W (mm)	Notch radius (mm)
S1	1.18	10.5	24	0.124

3. Test Conditions

Test Type	Load range (kN)	Strain rate (mm/min)	Temperature (°C)
Crack initiation	0 - 5	0.2	28

4. Load – load-line displacement plot

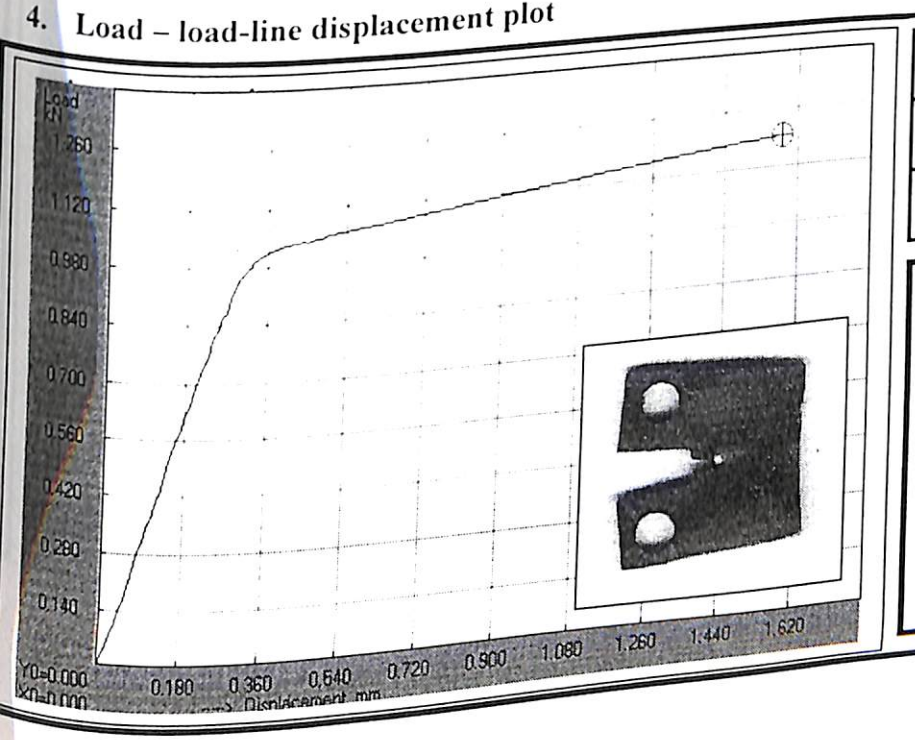

P_c (kN)	1.194
V_{pl} (mm)	1.235
A_{pl} kN-mm	1.344

Centre of Materials Science & Testing.
Birla Institutes of Technology and Science, Pilani, Rajasthan INDIA (333 031)

B1.2 Fracture test S2

1. Material

Material	Yield strength (MPa)	Modulus of Elasticity (GPa)	Poisson's ratio (ν)
EDD335 steel sheet	335	210	0.33

2. (Compact Tension (CT) specimen as per ASTM standard (E399-91).

Specimen code	Thickness B (mm)	Crack length a_0 (mm)	Width W (mm)	Notch radius (mm)
S2	1.28	10.5	24	0.117

3. Test Conditions

Test Type	Load range (kN)	Strain rate (mm/min)	Temperature (°C)
Crack initiation	0 - 5	0.2	28

4. Load – load-line displacement plot

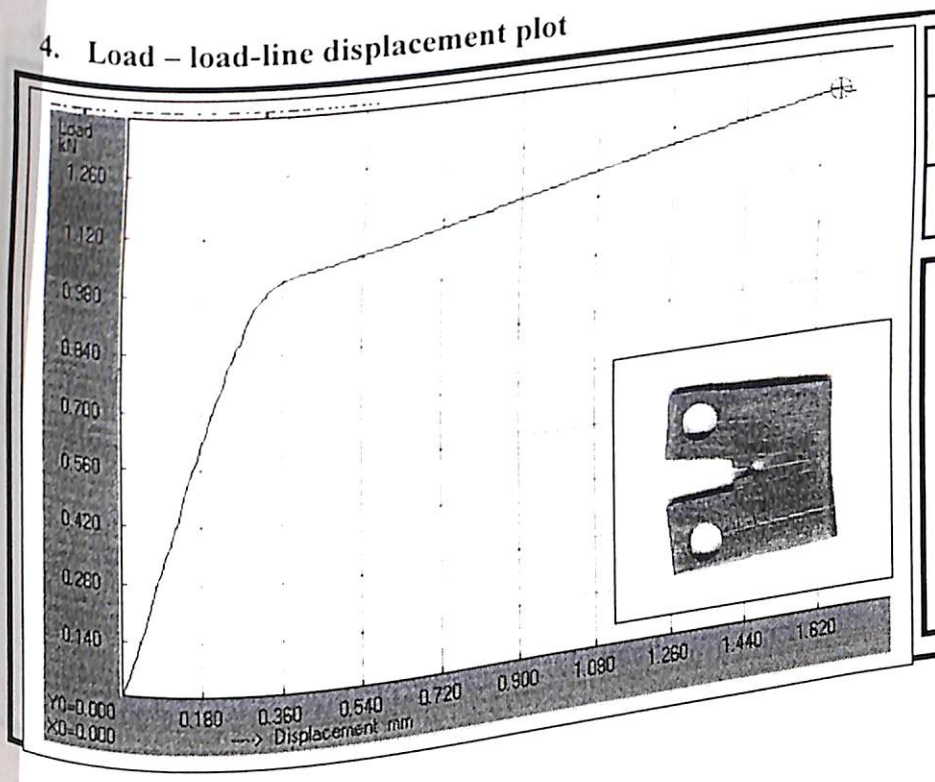

P_c (kN)	1.311
V_{pl} (mm)	1.322
A_{pl} kN-mm	1.489

Centre of Materials Science & Testing. Birla Institutes of Technology and Science, Pilani, Rajasthan INDIA (333 031)

B1.3 Fracture test S3

1. Material

Material	Yield strength (MPa)	Modulus of Elasticity (GPa)	Poisson's ratio (v)
EDD335 steel sheet	335	210	0.33

2. (Compact Tension (CT) specimen as per ASTM standard (E399-91).

Specimen code	Thickness B (mm)	Crack length a_0 (mm)	Width W (mm)	Notch radius (mm)
S3	1.38	10.5	24	0.122

3. Test Conditions

Test Type	Load range (kN)	Strain rate (mm/min)	Temperature (°C)
Crack initiation	0 - 5	0.2	28

4. Load – load-line displacement plot

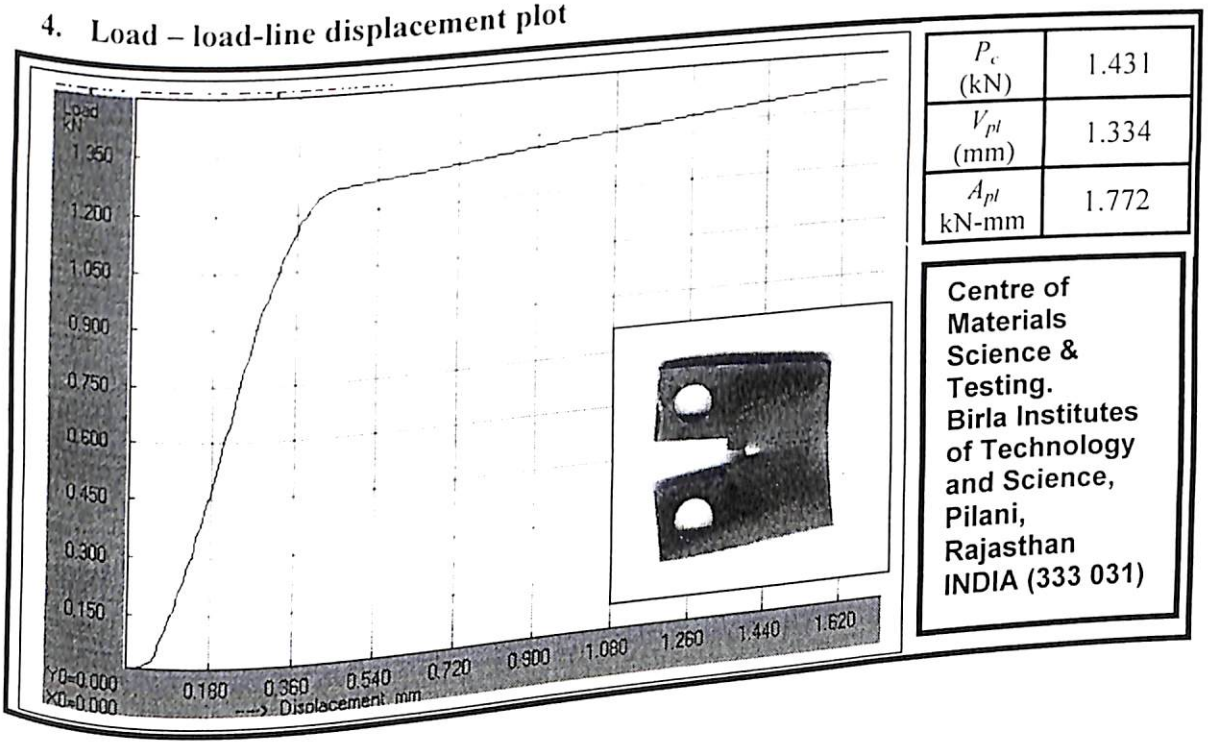

P_c (kN)	1.431
V_{pl} (mm)	1.334
A_{pl} kN-mm	1.772

Centre of Materials Science & Testing. Birla Institutes of Technology and Science, Pilani, Rajasthan INDIA (333 031)

B1.4 Fracture test S4

1. **Material**

Material	Yield strength (MPa)	Modulus of Elasticity (GPa)	Poisson's ratio (v)
EDD335 steel sheet	335	210	0.33

2. **(Compact Tension (CT) specimen as per ASTM standard (E399-91).**

Specimen code	Thickness B (mm)	Crack length a_0 (mm)	Width W (mm)	Notch radius (mm)
S4	1.48	10.5	24	0.115

3. **Test Conditions**

Test Type	Load range (kN)	Strain rate (mm/min)	Temperature (°C)
Crack initiation	0 - 5	0.2	28

4. **Load – load-line displacement plot**

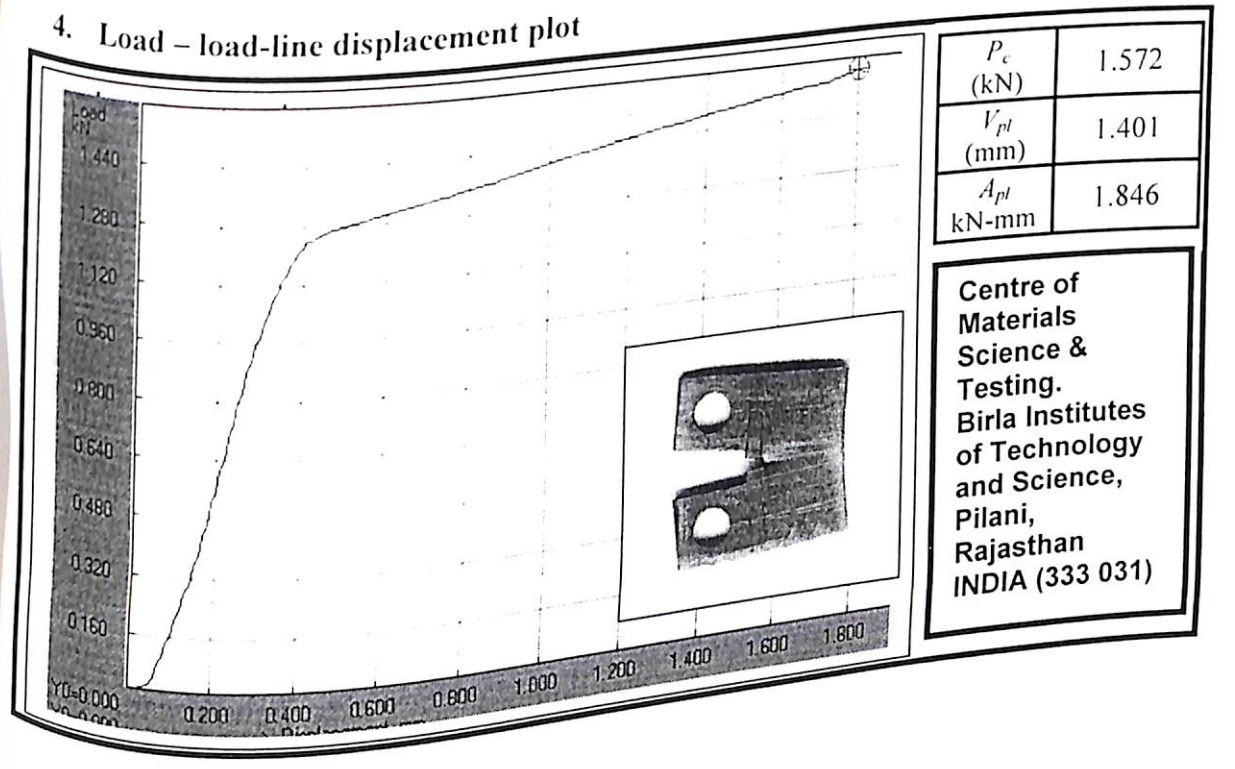

P_c (kN)	1.572
V_{pl} (mm)	1.401
A_{pl} kN-mm	1.846

Centre of Materials Science & Testing. Birla Institutes of Technology and Science, Pilani, Rajasthan INDIA (333 031)

B1.5 Fracture test S5

1. Material

Material	Yield strength (MPa)	Modulus of Elasticity (GPa)	Poisson's ratio (ν)
EDD335 steel sheet	335	210	0.33

2. (Compact Tension (CT) specimen as per ASTM standard (E399-91).

Specimen code	Thickness B (mm)	Crack length a_0 (mm)	Width W (mm)	Notch radius (mm)
S5	1.58	10.5	24	0.117

3. Test Conditions

Test Type	Load range (kN)	Strain rate (mm/min)	Temperature (°C)
Crack initiation	0 - 5	0.2	28

4. Load – load-line displacement plot

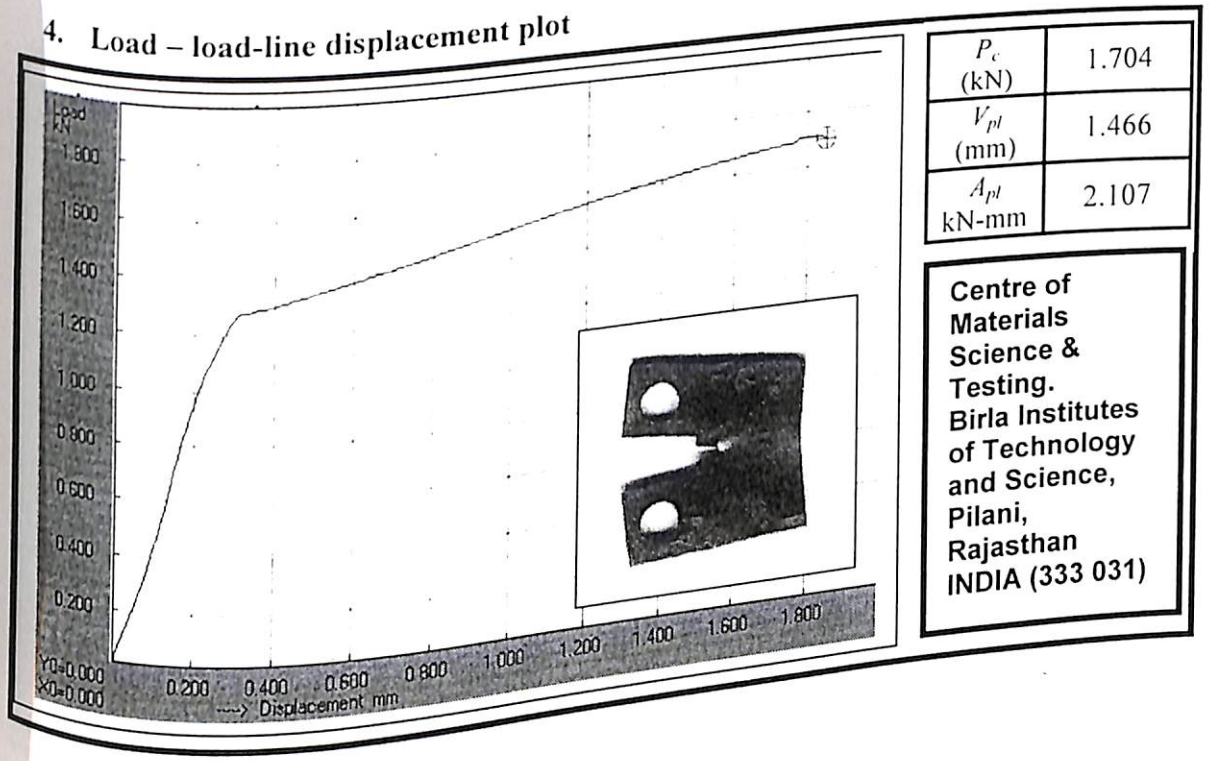

P_c (kN)	1.704
V_{pl} (mm)	1.466
A_{pl} kN-mm	2.107

Centre of Materials Science & Testing.
Birla Institutes of Technology and Science, Pilani, Rajasthan INDIA (333 031)

B1.6 Fracture test S6

1. Material

Material	Yield strength (MPa)	Modulus of Elasticity (GPa)	Poisson`s ratio (ν)
EDD335 steel sheet	335	210	0.33

2. (Compact Tension (CT) specimen as per ASTM standard (E399-91).

Specimen code	Thickness B (mm)	Crack length a_0 (mm)	Width W (mm)	Notch radius (mm)
S6	1.64	10.5	24	0.121

3. Test Conditions

Test Type	Load range (kN)	Strain rate (mm/min)	Temperature (°C)
Crack initiation	0 - 5	0.2	28

4. Load – load-line displacement plot

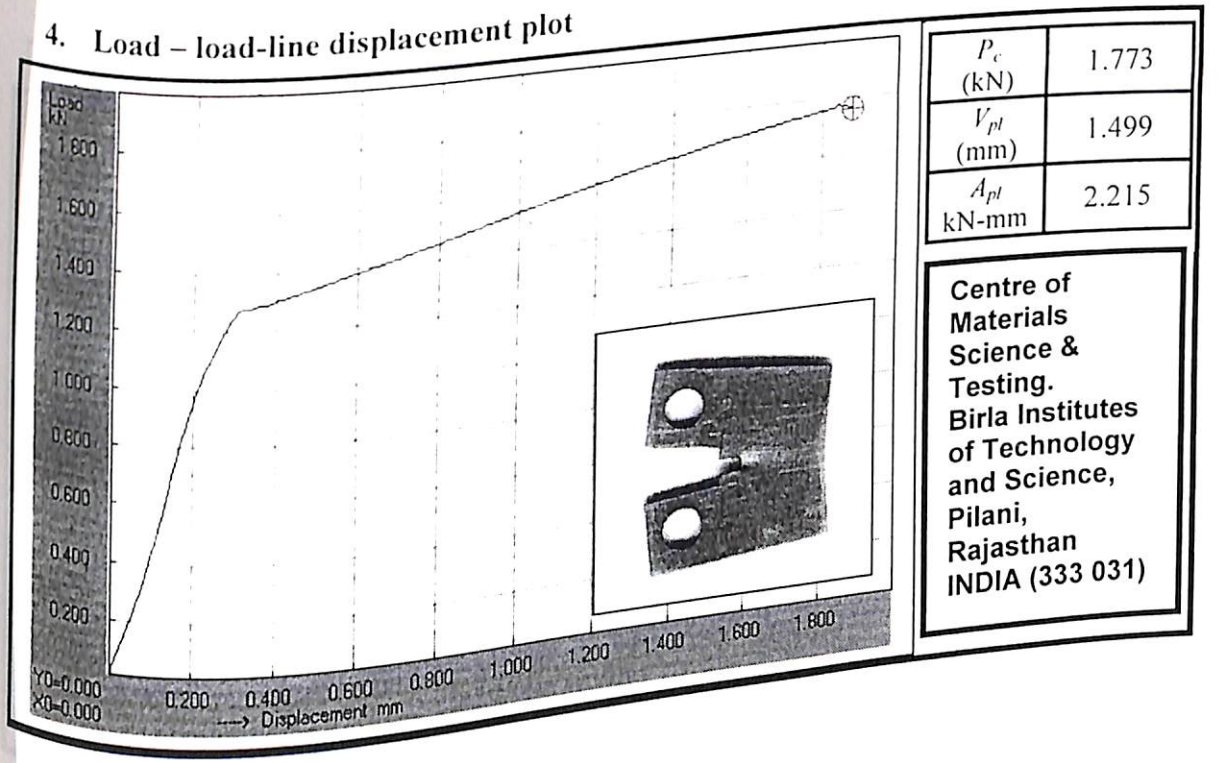

P_c (kN)	1.773
V_{pl} (mm)	1.499
A_{pl} kN-mm	2.215

Centre of Materials Science & Testing. Birla Institutes of Technology and Science, Pilani, Rajasthan INDIA (333 031)

B1.7 Fracture test S7

1. Material

Material	Yield strength (MPa)	Modulus of Elasticity (GPa)	Poisson's ratio (ν)
EDD335 steel sheet	335	210	0.33

2. (Compact Tension (CT) specimen as per ASTM standard (E399-91).

Specimen code	Thickness B (mm)	Crack length a_0 (mm)	Width W (mm)	Notch radius (mm)
S7	1.75	10.5	24	0.116

3. Test Conditions

Test Type	Load range (kN)	Strain rate (mm/min)	Temperature (°C)
BLD	0 - 5	0.2	28

4. Load – load-line displacement plot

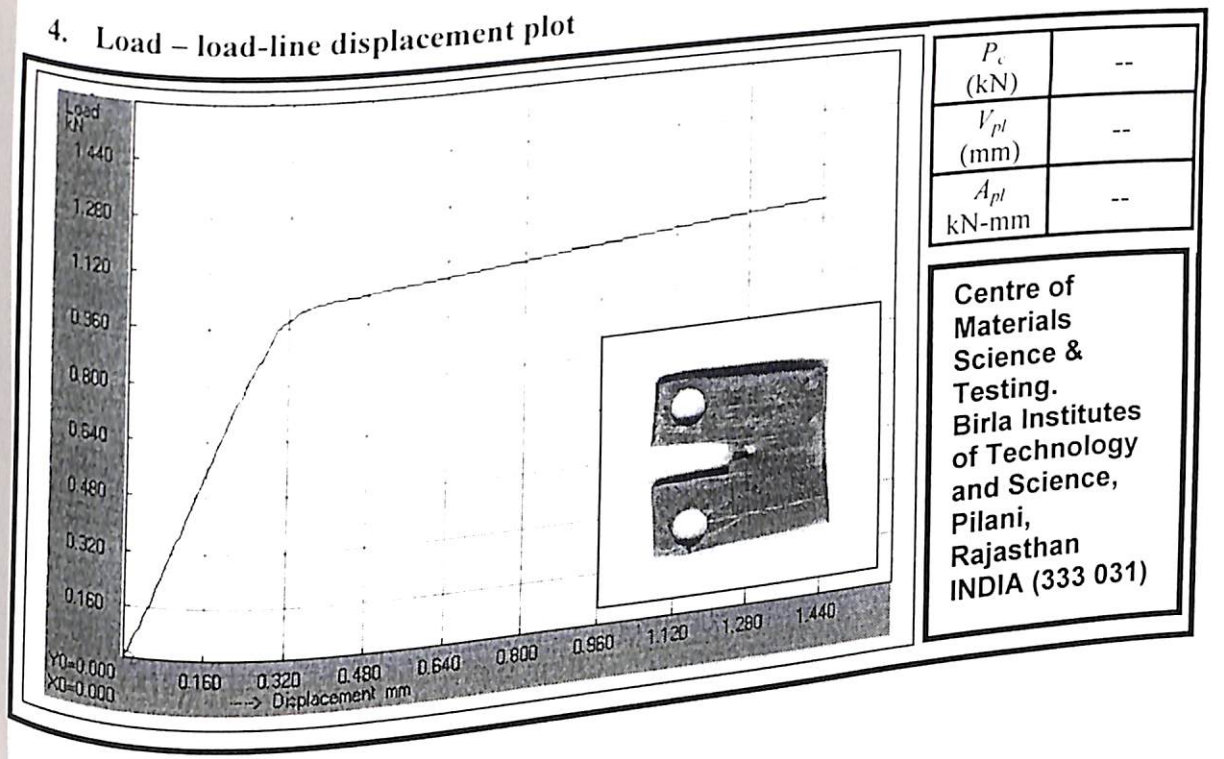

P_c (kN)	--
V_{pl} (mm)	--
A_{pl} kN-mm	--

Centre of Materials Science & Testing.
Birla Institutes of Technology and Science, Pilani, Rajasthan INDIA (333 031)

B2

Fracture Test on EDD277 (Thickness effect study)

B2.1 Fracture test 1.4a

1. Material

Material	Yield strength (MPa)	Modulus of Elasticity (GPa)	Poisson's ratio (ν)
EDD277 steel sheet	277	210	0.33

2. (Compact Tension (CT) specimen as per ASTM standard (E399-91).

Specimen code	Thickness B (mm)	Crack length a_0 (mm)	Width W (mm)	Notch radius (mm)
1.4a	1.4	10.5	24	0.125

3. Test Conditions

Test Type	Load range (kN)	Strain rate (mm/min)	Temperature (°C)
Crack initiation	0 - 5	0.2	28

4. Load – load-line displacement plot

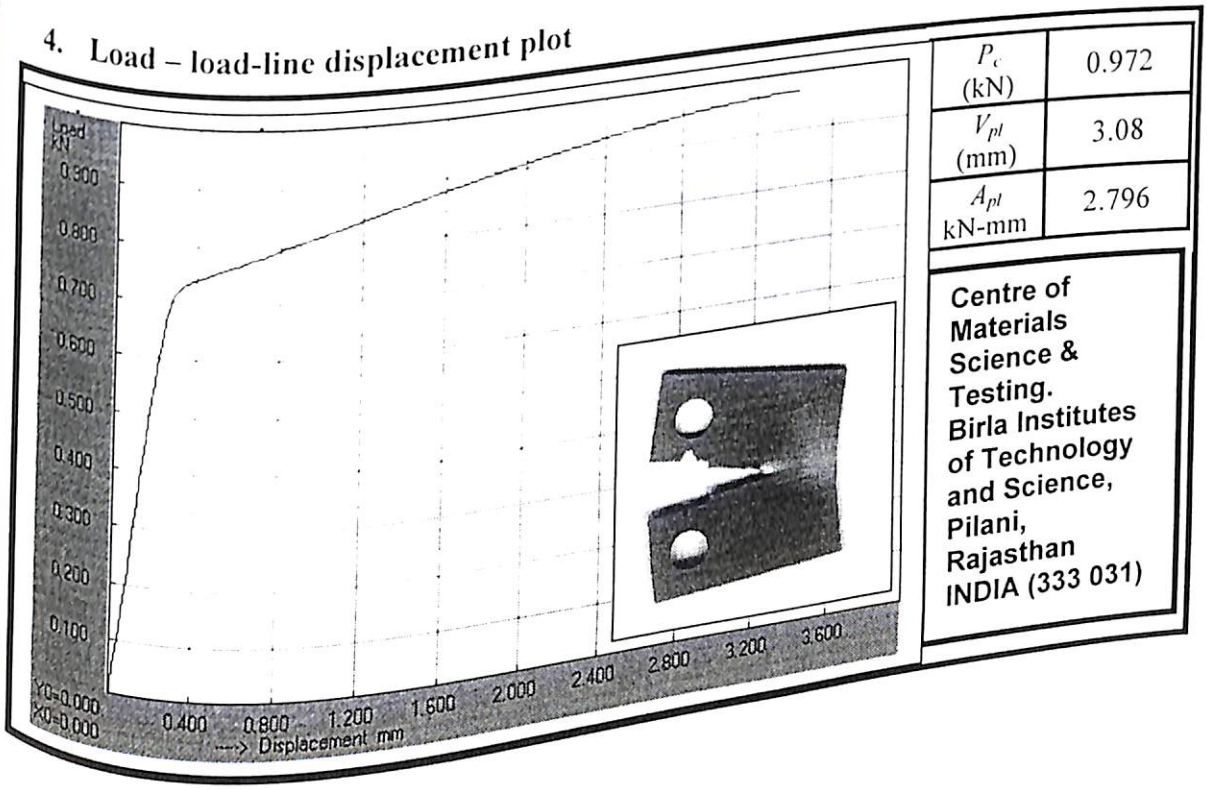

P_c (kN)	0.972
V_{pl} (mm)	3.08
A_{pl} kN-mm	2.796

Centre of Materials Science & Testing. Birla Institutes of Technology and Science, Pilani, Rajasthan INDIA (333 031)

B2.2 Fracture test 1.4b

1. Material

Material	Yield strength (MPa)	Modulus of Elasticity (GPa)	Poisson's ratio (ν)
EDD277 steel sheet	277	210	0.33

2. (Compact Tension (CT) specimen as per ASTM standard (E399-91).

Specimen code	Thickness B (mm)	Crack length a_0 (mm)	Width W (mm)	Notch radius (mm)
1.4b	1.4	10.5	24	0.123

3. Test Conditions

Test Type	Load range (kN)	Strain rate (mm/min)	Temperature (°C)
Crack initiation	0 - 5	0.2	28

4. Load – load-line displacement plot

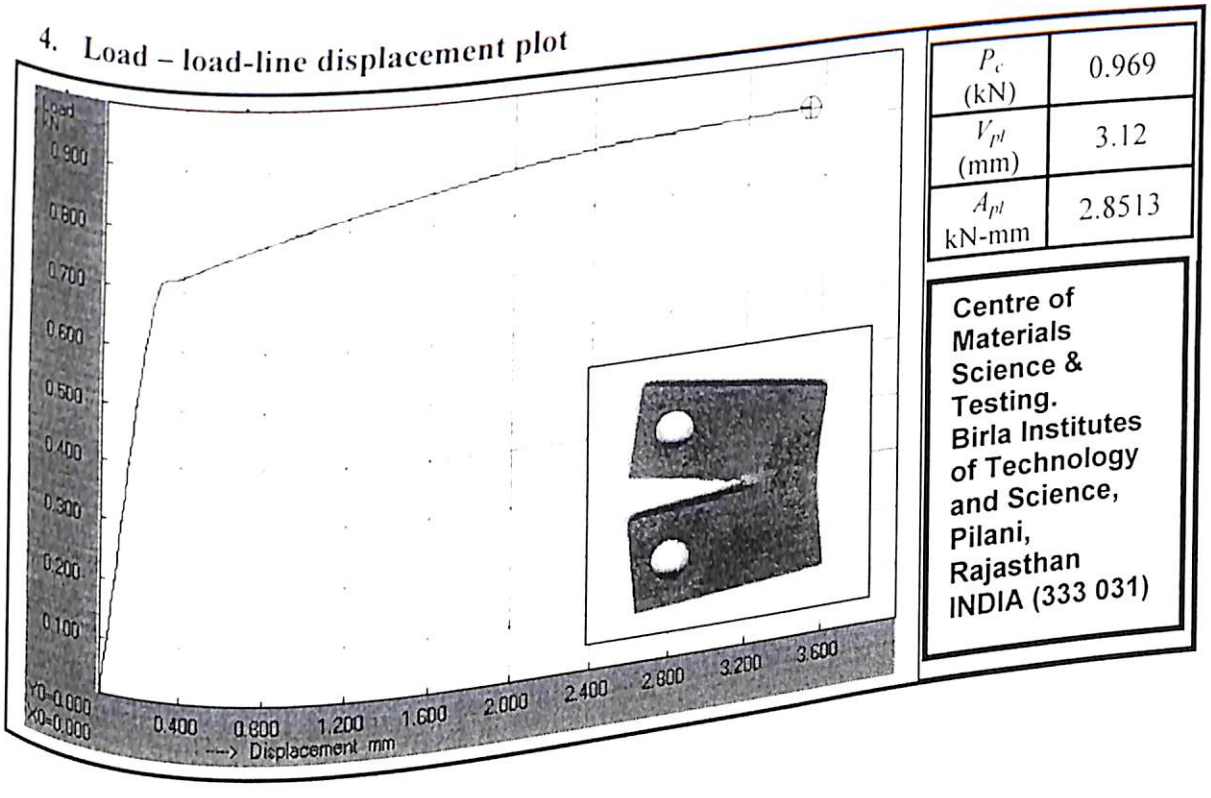

P_c (kN)	0.969
V_{pl} (mm)	3.12
A_{pl} kN-mm	2.8513

Centre of Materials Science & Testing.
Birla Institutes of Technology and Science, Pilani, Rajasthan INDIA (333 031)

B2.3 Fracture test 1.4c

1. **Material**

Material	Yield strength (MPa)	Modulus of Elasticity (GPa)	Poisson's ratio (ν)
EDD277 steel sheet	277	210	0.33

2. **(Compact Tension (CT) specimen as per ASTM standard (E399-91).**

Specimen code	Thickness B (mm)	Crack length a_0 (mm)	Width W (mm)	Notch radius (mm)
1.4c	1.4	10.5	24	0.117

3. **Test Conditions**

Test Type	Load range (kN)	Strain rate (mm/min)	Temperature (°C)
Crack initiation	0 - 5	0.2	28

4. **Load – load-line displacement plot**

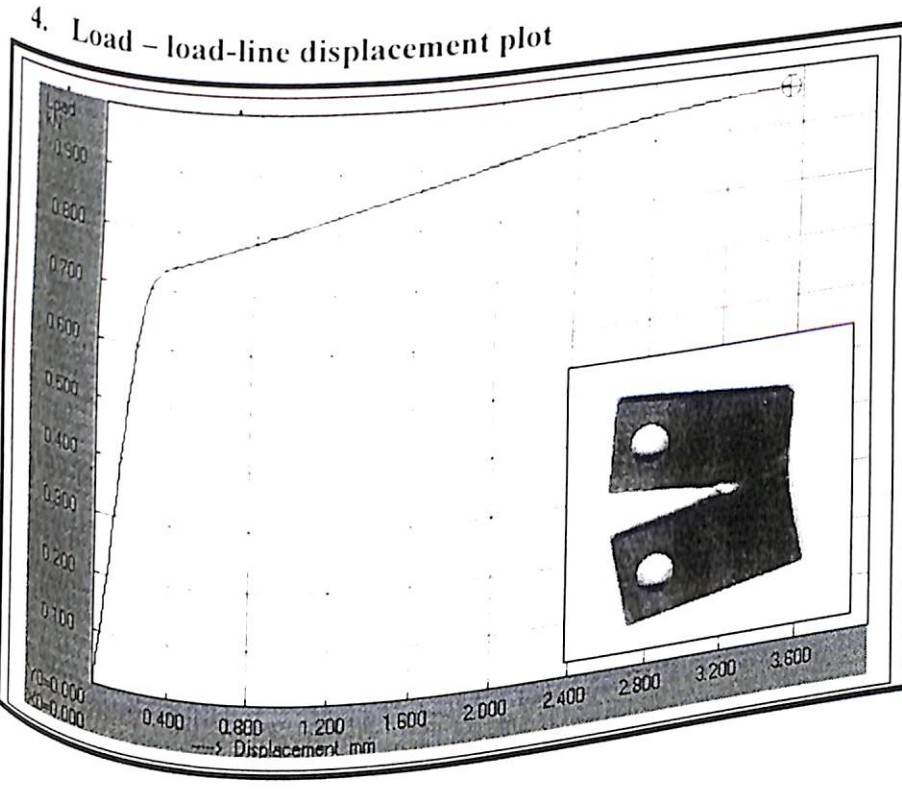

P_c (kN)	0.968
V_{pl} (mm)	3.21
A_{pl} kN-mm	2.9413

Centre of Materials Science & Testing.
Birla Institutes of Technology and Science, Pilani, Rajasthan INDIA (333 031)

B2.4 Fracture test 1.4d

1. Material

Material	Yield strength (MPa)	Modulus of Elasticity (GPa)	Poisson's ratio (ν)
EDD277 steel sheet	277	210	0.33

2. (Compact Tension (CT) specimen as per ASTM standard (E399-91).

Specimen code	Thickness B (mm)	Crack length a_0 (mm)	Width W (mm)	Notch radius (mm)
1.4d	1.4	10.5	24	0.118

3. Test Conditions

Test Type	Load range (kN)	Strain rate (mm/min)	Temperature (°C)
BLD	0 - 5	0.2	28

4. Load – load-line displacement plot

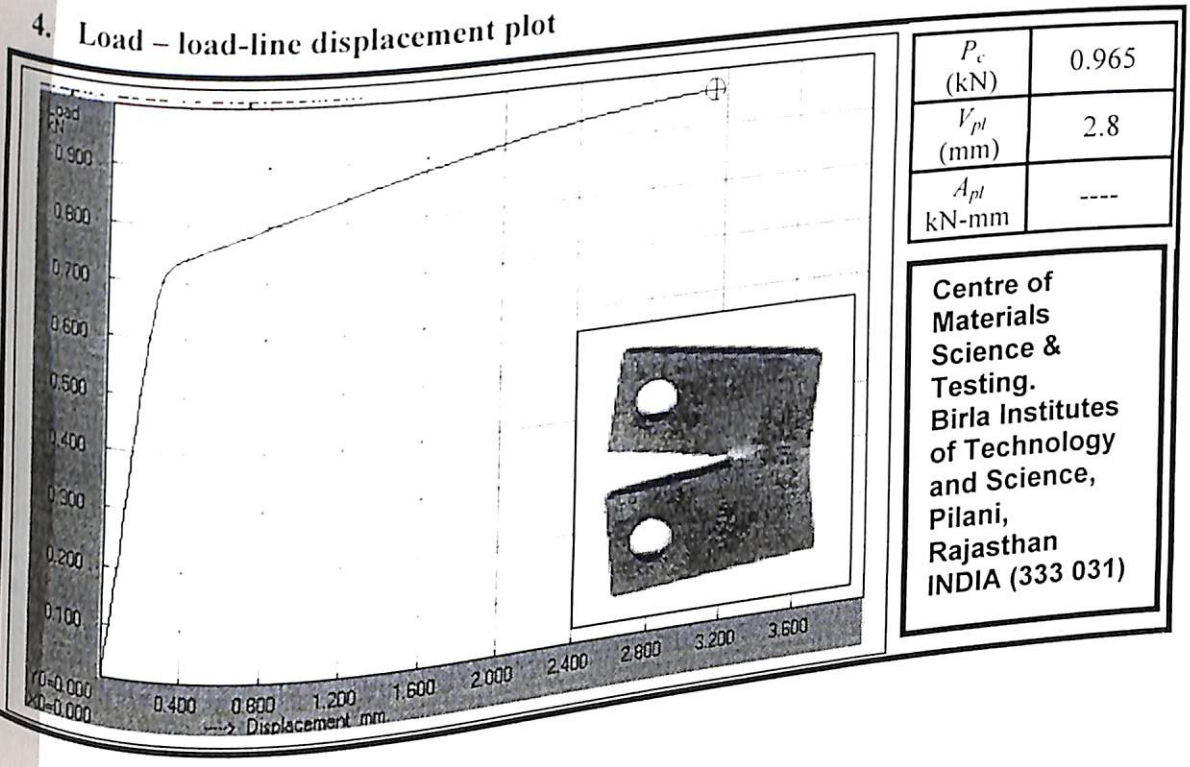

P_c (kN)	0.965
V_{pl} (mm)	2.8
A_{pl} kN-mm	----

Centre of Materials Science & Testing.
Birla Institutes of Technology and Science, Pilani, Rajasthan INDIA (333 031)

B2.5 Fracture test 1.9a

1. Material

Material	Yield strength (MPa)	Modulus of Elasticity (GPa)	Poisson's ratio (ν)
EDD277 steel sheet	277	210	0.33

2. (Compact Tension (CT) specimen as per ASTM standard (E399-91).

Specimen code	Thickness B (mm)	Crack length a_0 (mm)	Width W (mm)	Notch radius (mm)
1.9a	1.9	10.5	24	0.116

3. Test Conditions

Test Type	Load range (kN)	Strain rate (mm/min)	Temperature (°C)
Crack initiation	0 - 5	0.2	28

4. Load – load-line displacement plot

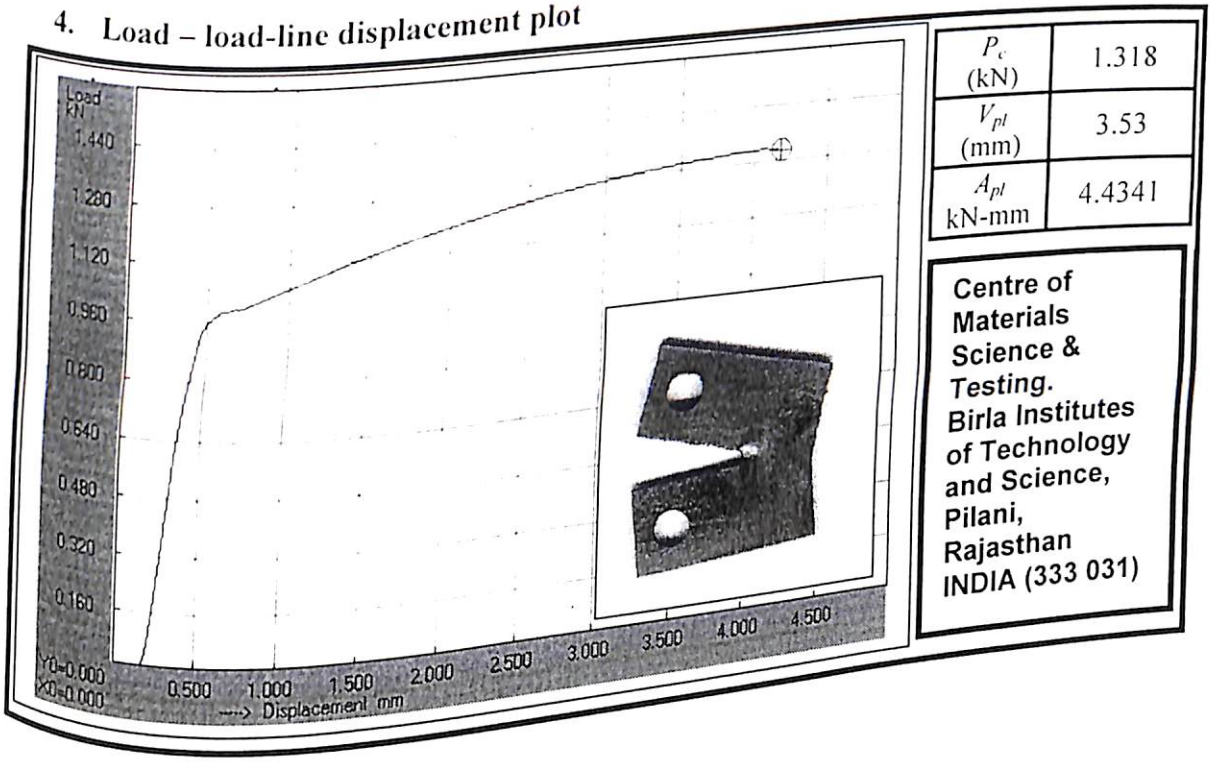

P_c (kN)	1.318
V_{pl} (mm)	3.53
A_{pl} kN-mm	4.4341

Centre of Materials Science & Testing.
Birla Institutes of Technology and Science, Pilani, Rajasthan INDIA (333 031)

B2.6 Fracture test 1.9b

1. Material

Material	Yield strength (MPa)	Modulus of Elasticity (GPa)	Poisson's ratio (ν)
EDD277 steel sheet	277	210	0.33

2. (Compact Tension (CT) specimen as per ASTM standard (E399-91).

Specimen code	Thickness B (mm)	Crack length a_0 (mm)	Width W (mm)	Notch radius (mm)
1.9b	1.9	10.5	24	0.122

3. Test Conditions

Test Type	Load range (kN)	Strain rate (mm/min)	Temperature (°C)
Crack initiation	0 - 5	0.2	28

4. Load – load-line displacement plot

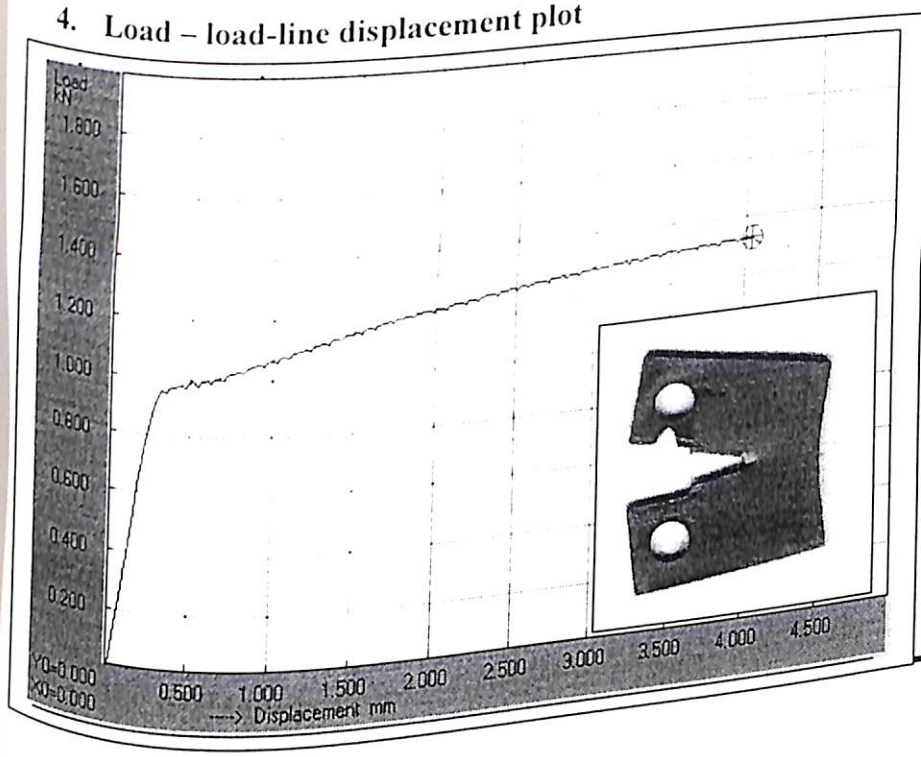

P_c (kN)	1.326
V_{pl} (mm)	3.5
A_{pl} kN-mm	4.312

Centre of Materials Science & Testing. Birla Institutes of Technology and Science, Pilani, Rajasthan INDIA (333 031)

B2.7 Fracture test 1.9c

1. Material

Material	Yield strength (MPa)	Modulus of Elasticity (GPa)	Poisson's ratio (ν)
EDD277 steel sheet	277	210	0.33

2. (Compact Tension (CT) specimen as per ASTM standard (E399-91).

Specimen code	Thickness B (mm)	Crack length a_0 (mm)	Width W (mm)	Notch radius (mm)
1.9c	1.9	10.5	24	0.125

3. Test Conditions

Test Type	Load range (kN)	Strain rate (mm/min)	Temperature (°C)
BLD	0 - 5	0.2	28

4. Load – load-line displacement plot

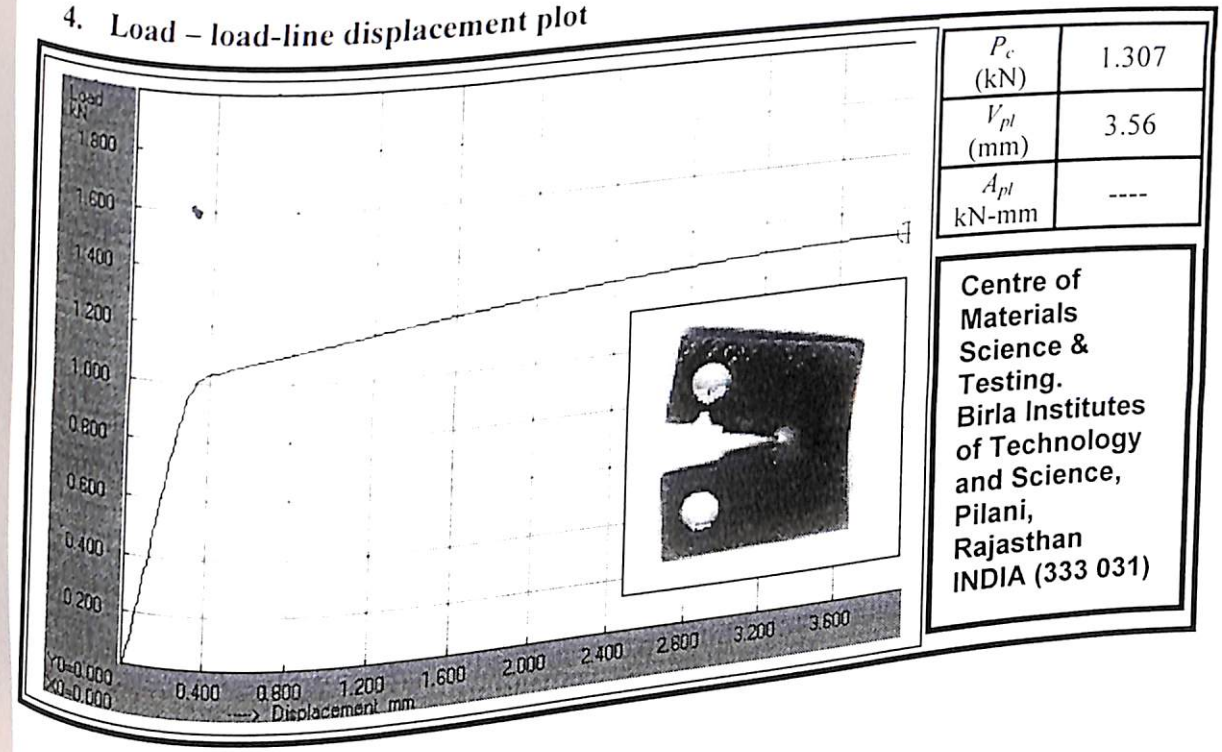

P_c (kN)	1.307
V_{pl} (mm)	3.56
A_{pl} kN-mm	----

Centre of Materials Science & Testing.
Birla Institutes of Technology and Science, Pilani, Rajasthan INDIA (333 031)

B2.8 Fracture test 1.9d

1. Material

Material	Yield strength (MPa)	Modulus of Elasticity (GPa)	Poisson's ratio (ν)
EDD277 steel sheet	277	210	0.33

2. (Compact Tension (CT) specimen as per ASTM standard (E399-91).

Specimen code	Thickness B (mm)	Crack length a_0 (mm)	Width W (mm)	Notch radius (mm)
1.9d	1.9	10.5	24	0.126

3. Test Conditions

Test Type	Load range (kN)	Strain rate (mm/min)	Temperature (°C)
Crack initiation	0 - 5	0.2	28

4. Load – load-line displacement plot

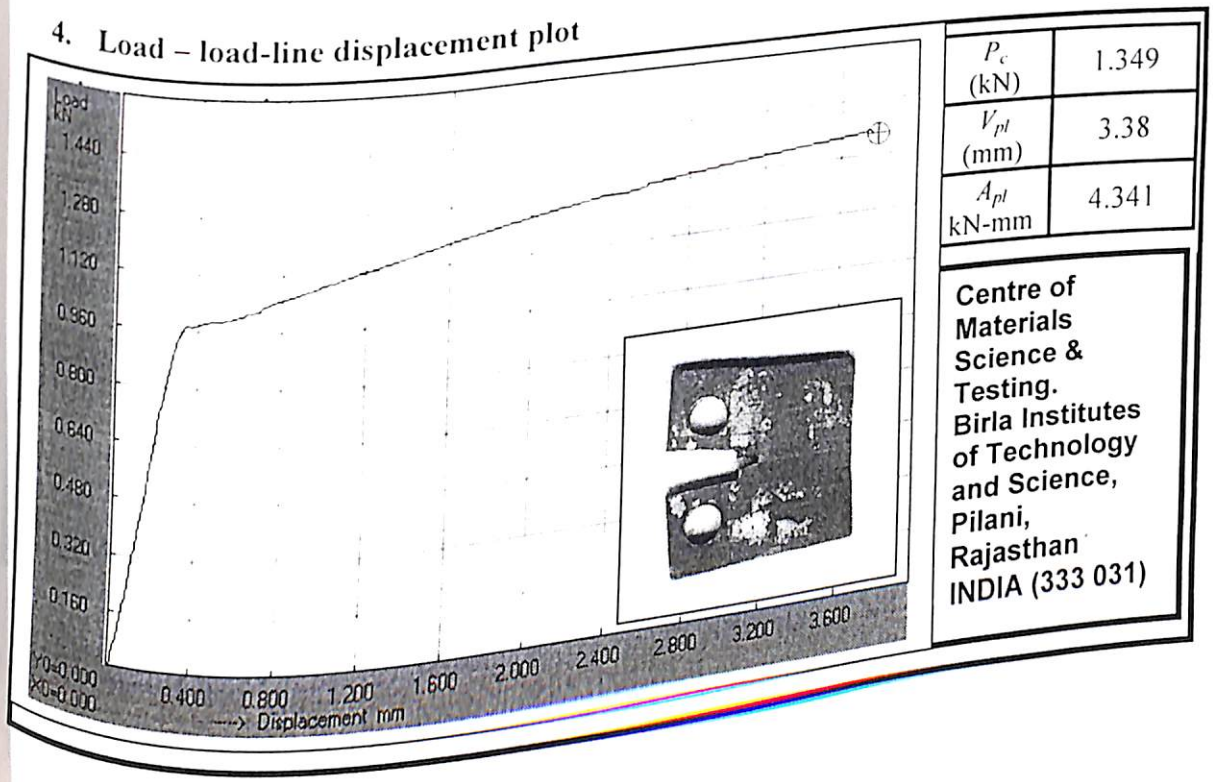

P_c (kN)	1.349
V_{pl} (mm)	3.38
A_{pl} kN-mm	4.341

Centre of Materials Science & Testing.
Birla Institutes of Technology and Science, Pilani, Rajasthan INDIA (333 031)

B2.9 Fracture test 2.4a

1. Material

Material	Yield strength (MPa)	Modulus of Elasticity (GPa)	Poisson`s ratio (v)
EDD277 steel sheet	277	210	0.33

2. (Compact Tension (CT) specimen as per ASTM standard (E399-91).

Specimen code	Thickness B (mm)	Crack length a_0 (mm)	Width W (mm)	Notch radius (mm)
2.4a	2.4	10.5	24	0.119

3. Test Conditions

Test Type	Load range (kN)	Strain rate (mm/min)	Temperature (°C)
Crack initiation	0 - 5	0.2	28

4. Load – load-line displacement plot

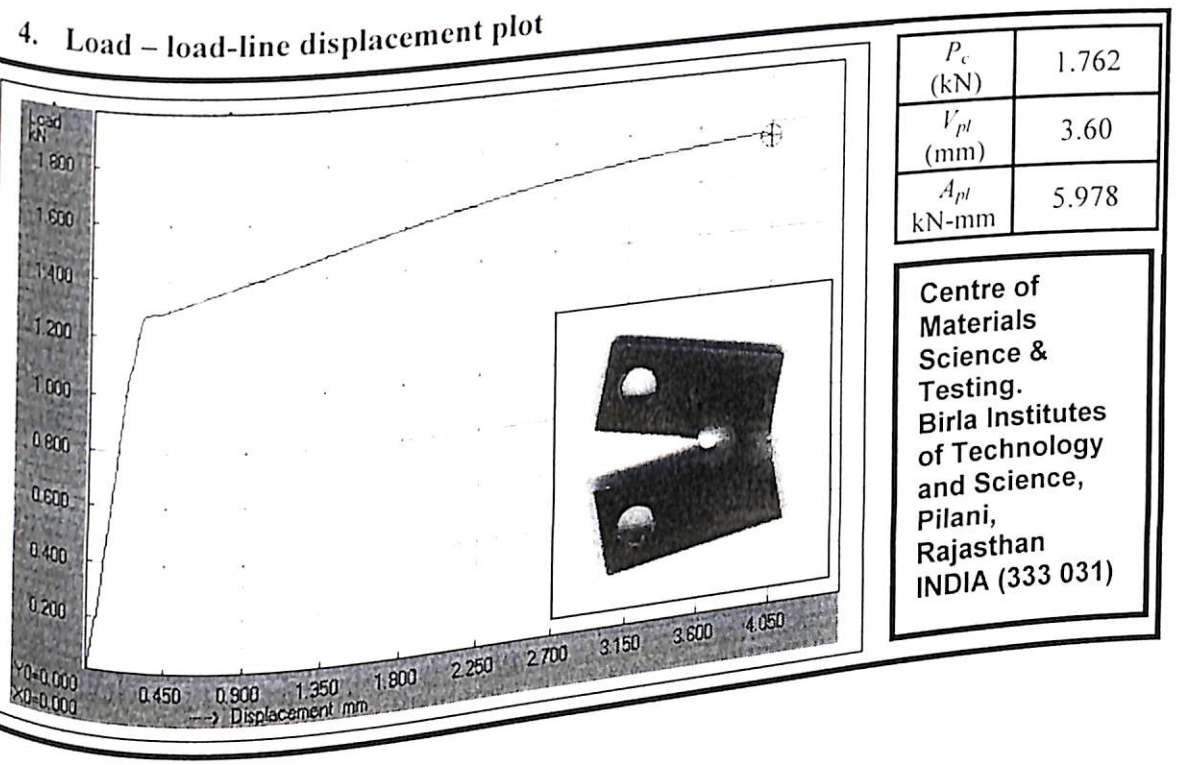

P_c (kN)	1.762
V_{pl} (mm)	3.60
A_{pl} kN-mm	5.978

Centre of Materials Science & Testing.
Birla Institutes of Technology and Science, Pilani, Rajasthan INDIA (333 031)

B2.10 Fracture test 2.4b

1. Material

Material	Yield strength (MPa)	Modulus of Elasticity (GPa)	Poisson's ratio (ν)
EDD 277 steel sheet	277	210	0.33

2. (Compact Tension (CT) specimen as per ASTM standard (E399-91).

Specimen code	Thickness B (mm)	Crack length a_0 (mm)	Width W (mm)	Notch radius (mm)
2.4b	2.4	10.5	24	0.114

3. Test Conditions

Test Type	Load range (kN)	Strain rate (mm/min)	Temperature (°C)
Crack initiation	0 - 5	0.2	28

4. Load – load-line displacement plot

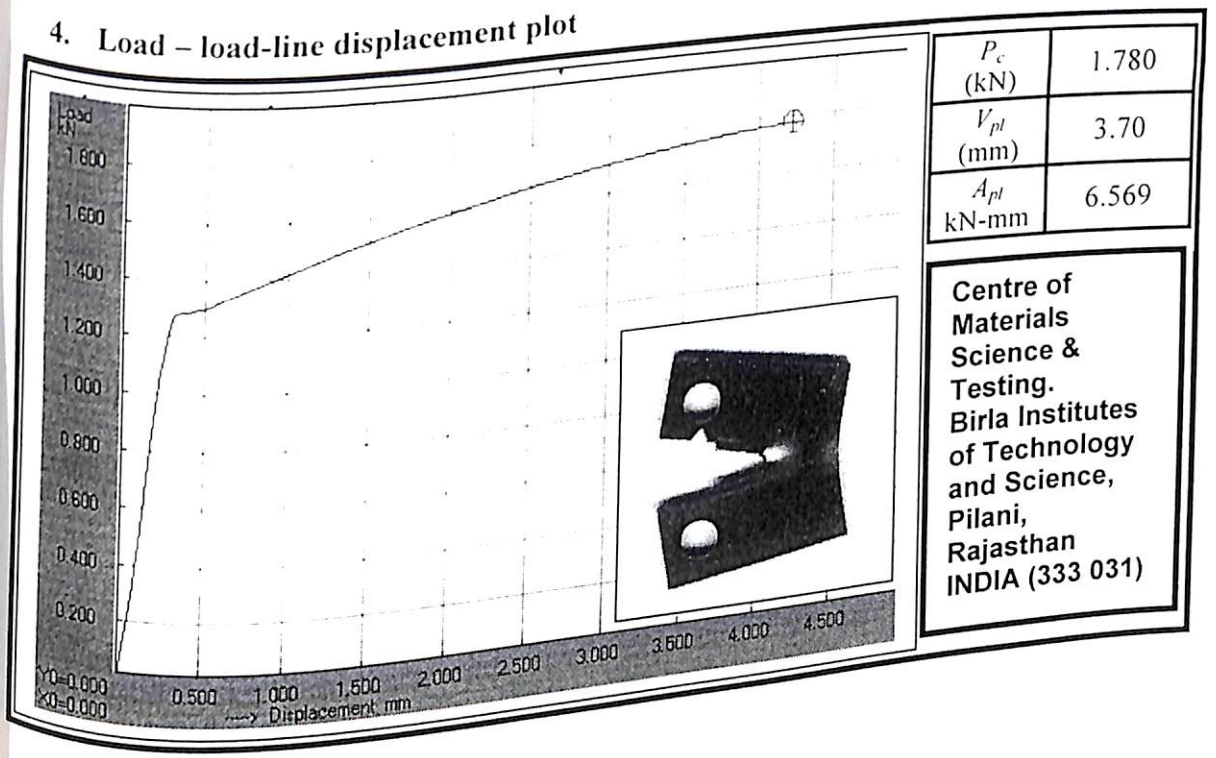

P_c (kN)	1.780
V_{pl} (mm)	3.70
A_{pl} kN-mm	6.569

Centre of Materials Science & Testing.
Birla Institutes of Technology and Science, Pilani, Rajasthan INDIA (333 031)

B2.11 Fracture test 2.4c

1. Material

Material	Yield strength (MPa)	Modulus of Elasticity (GPa)	Poisson's ratio (ν)
EDD277 steel sheet	277	210	0.33

2. (Compact Tension (CT) specimen as per ASTM standard (E399-91).

Specimen code	Thickness B (mm)	Crack length a_0 (mm)	Width W (mm)	Notch radius (mm)
2.4c	2.4	10.5	24	0.121

3. Test Conditions

Test Type	Load range (kN)	Strain rate (mm/min)	Temperature (°C)
Crack initiation	0 - 5	0.2	28

4. Load – load-line displacement plot

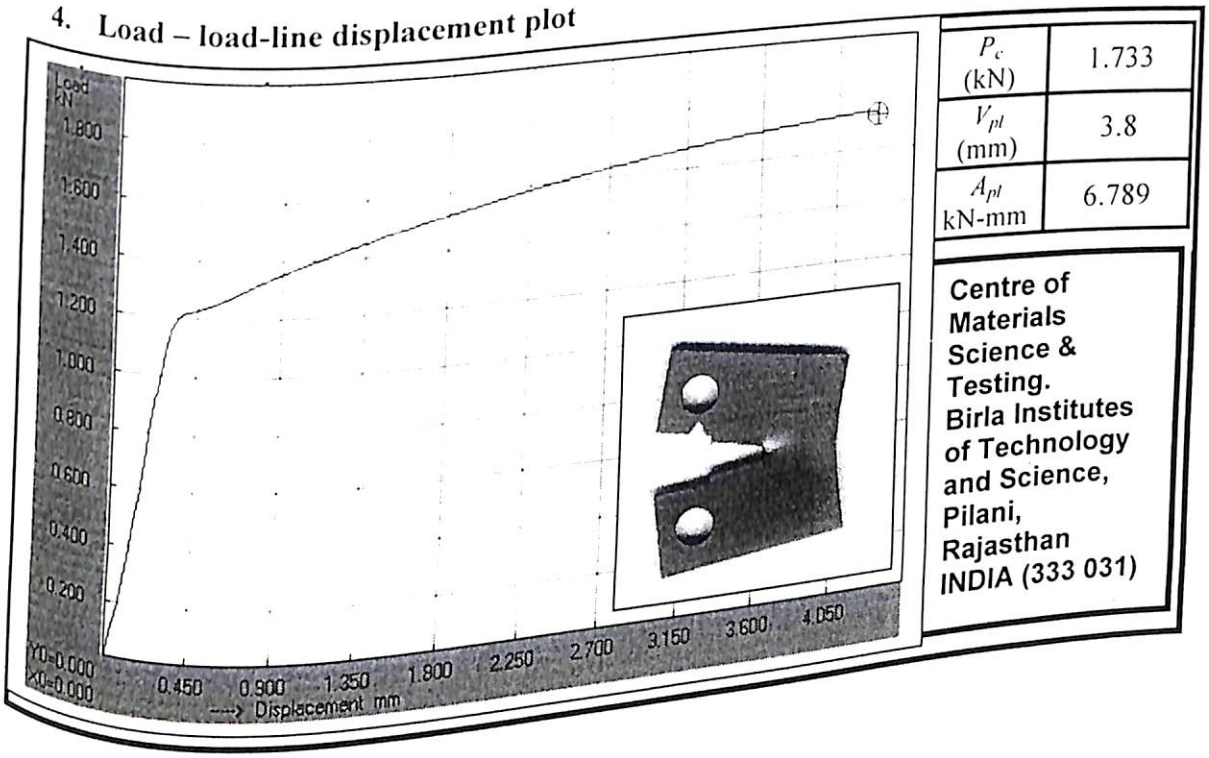

P_c (kN)	1.733
V_{pl} (mm)	3.8
A_{pl} kN-mm	6.789

Centre of Materials Science & Testing.
Birla Institutes of Technology and Science, Pilani, Rajasthan INDIA (333 031)

B2.12 Fracture test 2.4d

1. Material

Material	Yield strength (MPa)	Modulus of Elasticity (GPa)	Poisson's ratio (ν)
EDD277 steel sheet	277	210	0.33

2. (Compact Tension (CT) specimen as per ASTM standard (E399-91).

Specimen code	Thickness B (mm)	Crack length a_0 (mm)	Width W (mm)	Notch radius (mm)
2.4d	2.4	10.5	24	0.115

3. Test Conditions

Test Type	Load range (kN)	Strain rate (mm/min)	Temperature (°C)
BLD	0 - 5	0.2	28

4. Load – load-line displacement plot

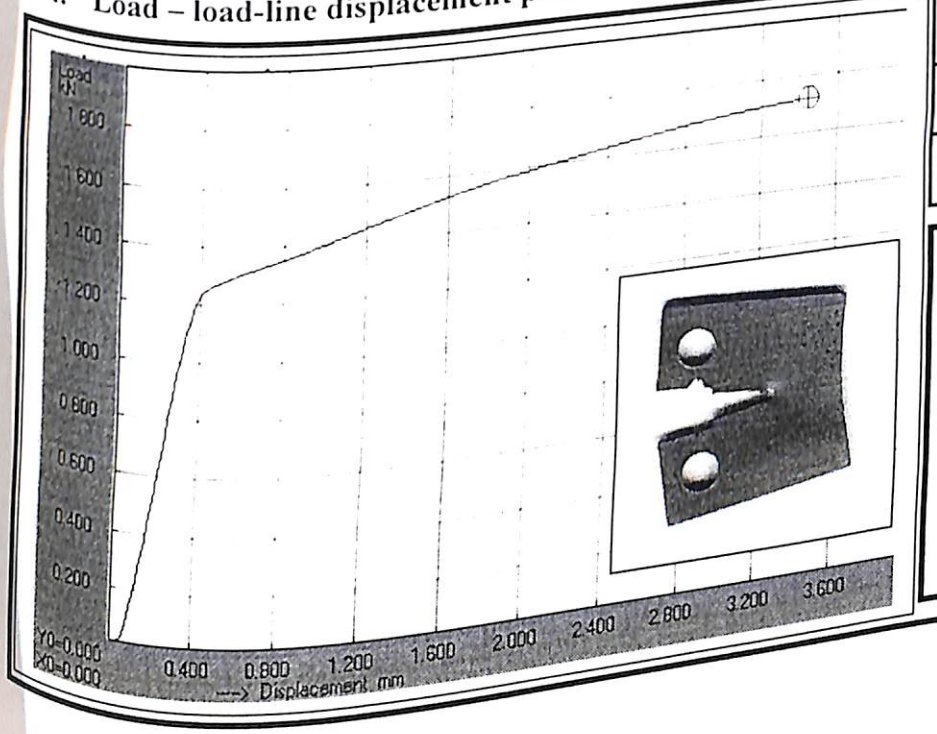

P_c (kN)	1.721
V_{pl} (mm)	3.05
A_{pl} kN-mm	----

Centre of Materials Science & Testing.
Birla Institutes of Technology and Science, Pilani, Rajasthan INDIA (333 031)

B2.13 Fracture test 2.9a

1. Material

Material	Yield strength (MPa)	Modulus of Elasticity (GPa)	Poisson's ratio (ν)
EDD277 steel sheet	277	210	0.33

2. (Compact Tension (CT) specimen as per ASTM standard (E399-91).

Specimen code	Thickness B (mm)	Crack length a_0 (mm)	Width W (mm)	Notch radius (mm)
2.9a	2.9	10.5	24	0.119

3. Test Conditions

Test Type	Load range (kN)	Strain rate (mm/min)	Temperature (°C)
BLD	0 - 5	0.2	28

4. Load – load-line displacement plot

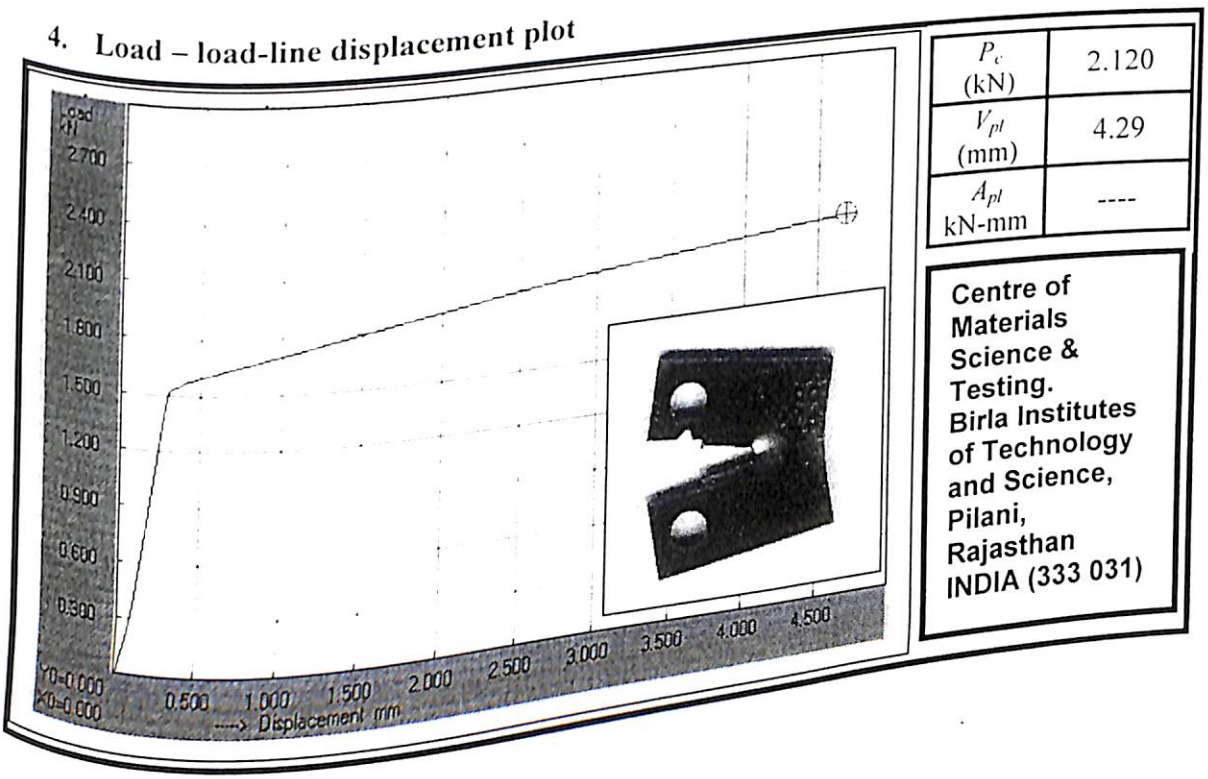

P_c (kN)	2.120
V_{pl} (mm)	4.29
A_{pl} kN-mm	----

Centre of Materials Science & Testing.
Birla Institutes of Technology and Science, Pilani, Rajasthan INDIA (333 031)

B2.14 Fracture test 2.9b

1. Material

Material	Yield strength (MPa)	Modulus of Elasticity (GPa)	Poisson's ratio (ν)
EDD277 steel sheet	277	210	0.33

2. (Compact Tension (CT) specimen as per ASTM standard (E399-91).

Specimen code	Thickness B (mm)	Crack length a_0 (mm)	Width W (mm)	Notch radius (mm)
2.9b	2.9	10.5	24	0.123

3. Test Conditions

Test Type	Load range (kN)	Strain rate (mm/min)	Temperature (°C)
Crack initiation	0 - 5	0.2	28

4. Load – load-line displacement plot

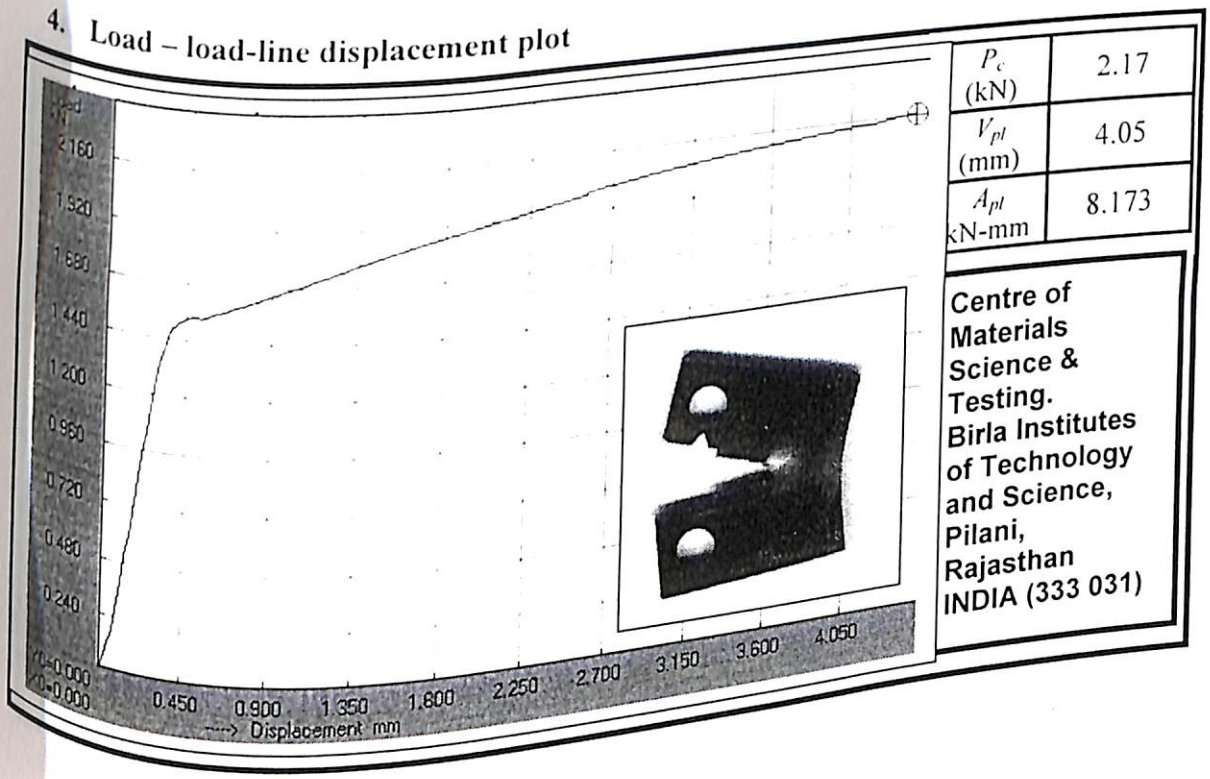

P_c (kN)	2.17
V_{pl} (mm)	4.05
A_{pl} kN-mm	8.173

Centre of Materials Science & Testing. Birla Institutes of Technology and Science, Pilani, Rajasthan INDIA (333 031)

B2.15 Fracture test 2.9c

1. Material

Material	Yield strength (MPa)	Modulus of Elasticity (GPa)	Poisson's ratio (ν)
EDD277 steel sheet	277	210	0.33

2. (Compact Tension (CT) specimen as per ASTM standard (E399-91).

Specimen code	Thickness B (mm)	Crack length a_0 (mm)	Width W (mm)	Notch radius (mm)
2.9c	2.9	10.5	24	0.118

3. Test Conditions

Test Type	Load range (kN)	Strain rate (mm/min)	Temperature (°C)
Crack initiation	0 - 5	0.2	28

4. Load – load-line displacement plot

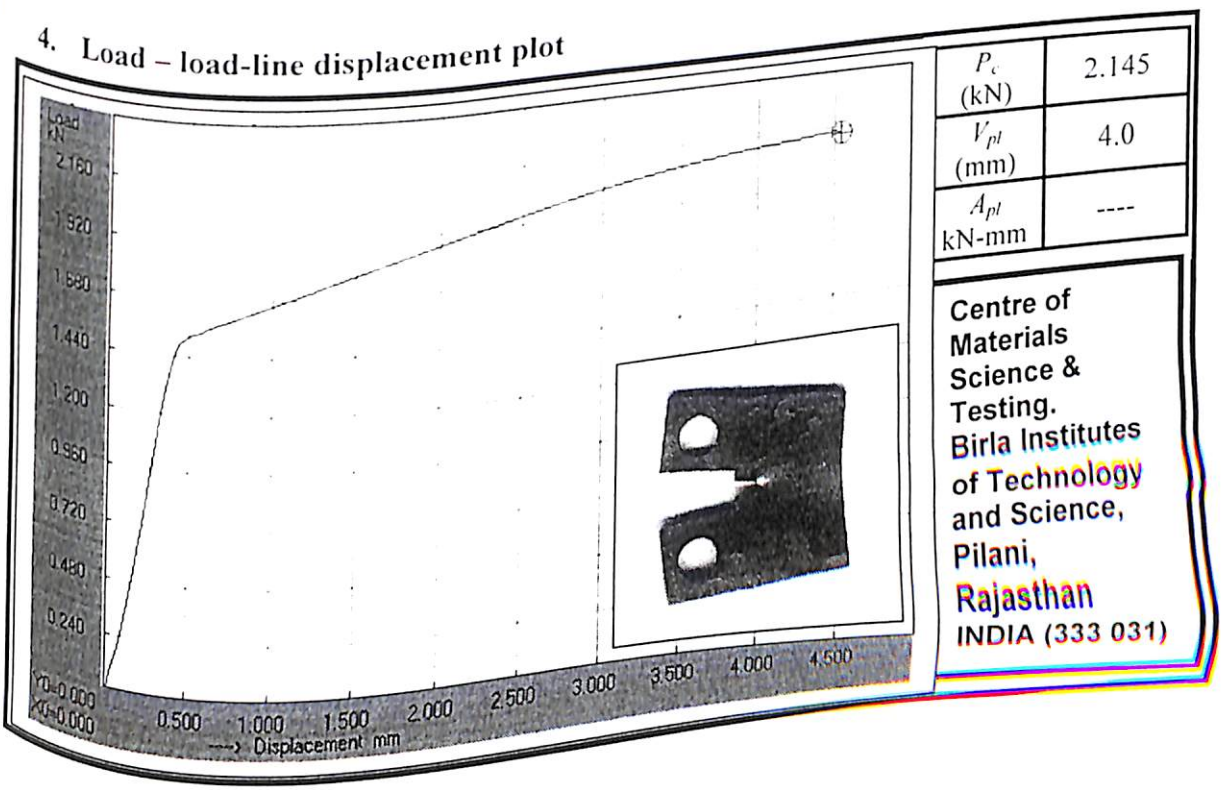

P_c (kN)	2.145
V_{pl} (mm)	4.0
A_{pl} kN-mm	----

Centre of Materials Science & Testing.
Birla Institutes of Technology and Science, Pilani, Rajasthan
INDIA (333 031)

B2.16 Fracture test 2.9d

1. Material

Material	Yield strength (MPa)	Modulus of Elasticity (GPa)	Poisson's ratio (ν)
EDD 277 steel sheet	277	210	0.33

2. (Compact Tension (CT) specimen as per ASTM standard (E399-91).

Specimen code	Thickness B (mm)	Crack length a_0 (mm)	Width W (mm)	Notch radius (mm)
2.9d	2.9	10.5	24	

3. Test Conditions

Test Type	Load range (kN)	Strain rate (mm/min)	Temperature (°C)
Crack initiation	0 - 5	0.2	28

4. Load – load-line displacement plot

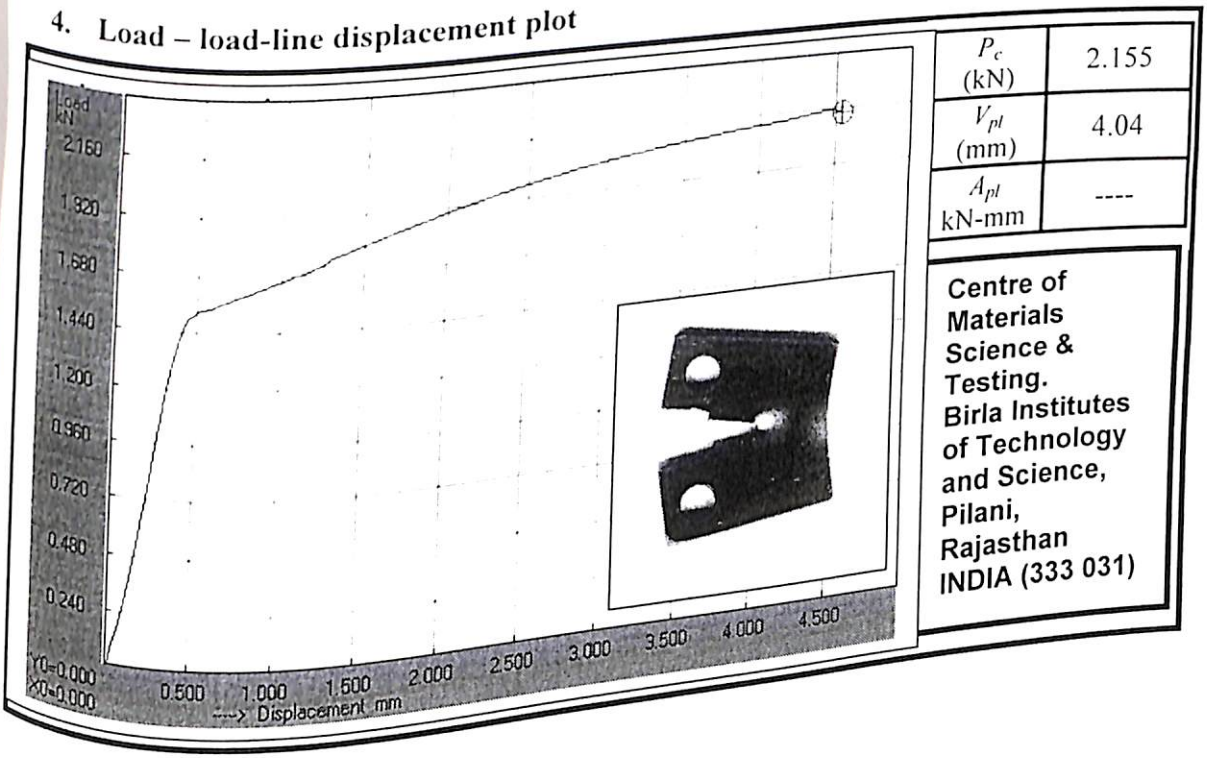

P_c (kN)	2.155
V_{pl} (mm)	4.04
A_{pl} kN-mm	----

Centre of Materials Science & Testing. Birla Institutes of Technology and Science, Pilani, Rajasthan INDIA (333 031)

B2.17 Fracture test 3.2a

1. Material

Material	Yield strength (MPa)	Modulus of Elasticity (GPa)	Poisson's ratio (ν)
EDD (0.025% C) steel sheet	277	210	0.33

2. (Compact Tension (CT) specimen as per ASTM standard (E399-91).

Specimen code	Thickness B (mm)	Crack length a_0 (mm)	Width W (mm)	Notch radius (mm)
3.2a	3.2	10.5	24	0.118

3. Test Conditions

Test Type	Load range (kN)	Strain rate (mm/min)	Temperature (°C)
Crack initiation	0 - 5	0.2	28

4. Load – load-line displacement plot

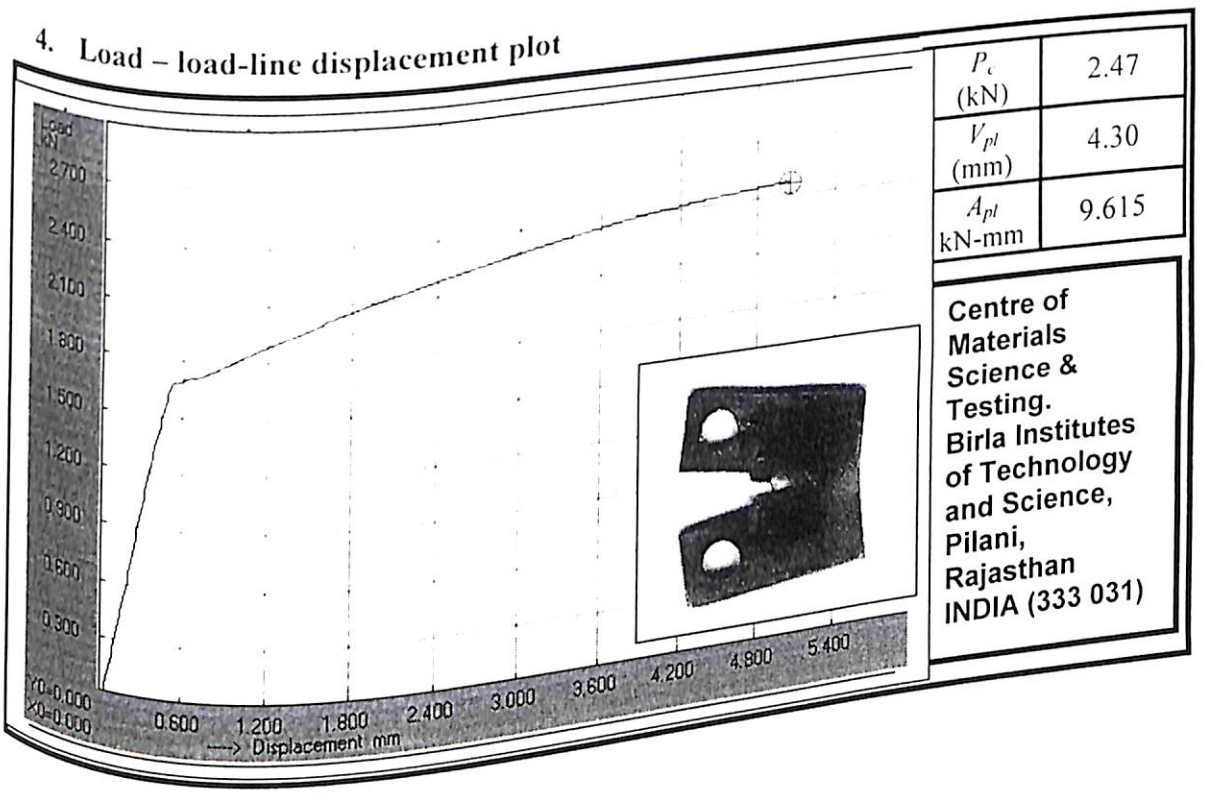

P_c (kN)	2.47
V_{pl} (mm)	4.30
A_{pl} kN-mm	9.615

Centre of Materials Science & Testing.
Birla Institutes of Technology and Science, Pilani, Rajasthan INDIA (333 031)

B2.19 Fracture test 3.2c

1. **Material**

Material	Yield strength (MPa)	Modulus of Elasticity (GPa)	Poisson's ratio (ν)
EDD277 steel sheet	277	210	0.33

2. **(Compact Tension (CT) specimen as per ASTM standard (E399-91).**

Specimen code	Thickness B (mm)	Crack length a_0 (mm)	Width W (mm)	Notch radius (mm)
3.2c	3.2	10.5	24	0.115

3. **Test Conditions**

Test Type	Load range (kN)	Strain rate (mm/min)	Temperature (°C)
Crack initiation	0 - 5	0.2	28

4. **Load – load-line displacement plot**

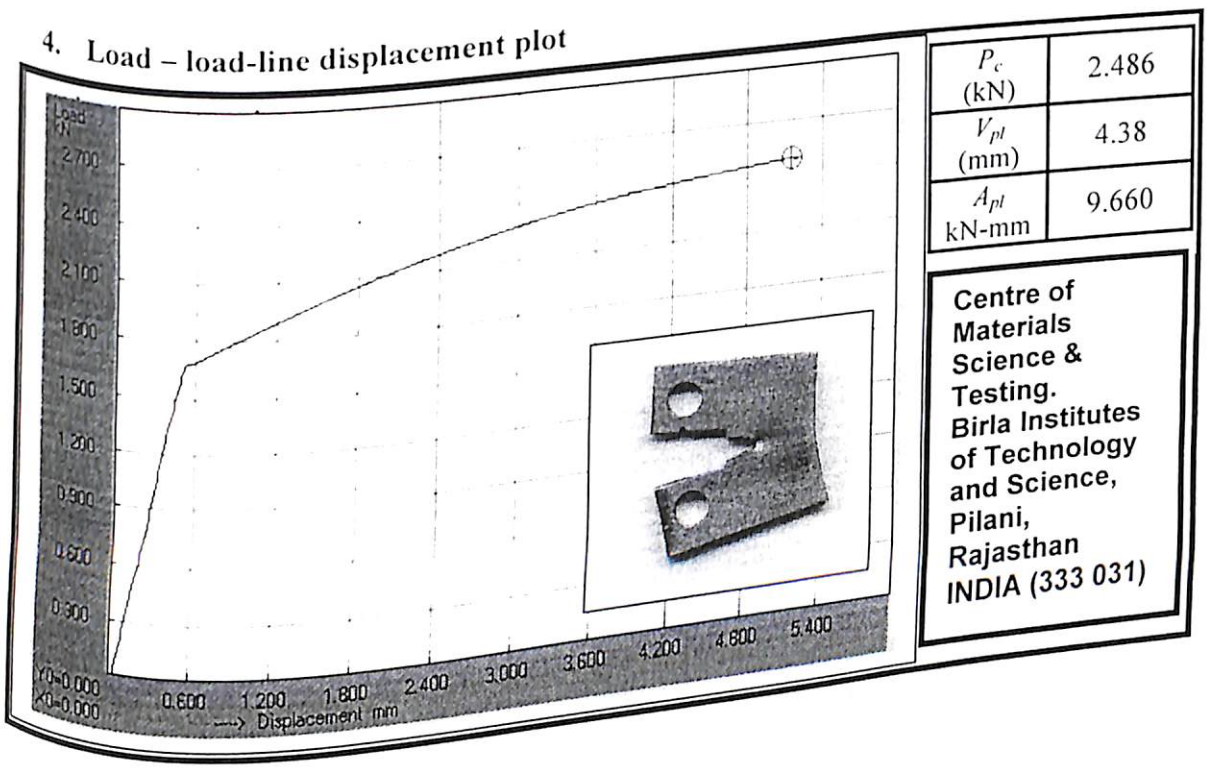

P_c (kN)	2.486
V_{pl} (mm)	4.38
A_{pl} kN-mm	9.660

Centre of Materials Science & Testing. Birla Institutes of Technology and Science, Pilani, Rajasthan INDIA (333 031)

Test Conditions			
Test Type	Load range (kN)	Strain rate (mm/min)	28
BLD	0 - 5	0.2	

4. Load – load-line displacement plot

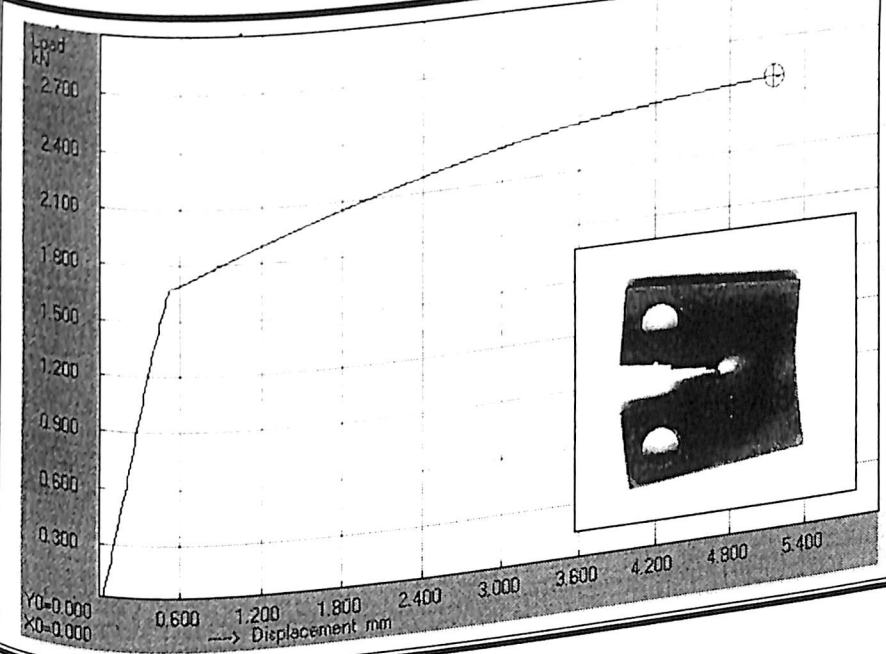

P_c (kN)	2.44
V_{pl} (mm)	4.17
A_{pl} kN-mm	----

Centre of Materials Science & Testing.
Birla Institutes of Technology and Science, Pilani, Rajasthan INDIA (333 031)

B2.20 Fracture test 3.2d

1. Material

Material	Yield strength (MPa)	Modulus of Elasticity (GPa)	Poisson's ratio (ν)
EDD277 steel sheet	277	210	0.33

2. (Compact Tension (CT) specimen as per ASTM standard (E399-91).

Specimen code	Thickness B (mm)	Crack length a_0 (mm)	Width W (mm)	Notch radius (mm)
3.2d	3.2	10.5	24	

3. Test Conditions

Test Type	Load range (kN)	Strain rate (mm/min)	Temperature (°C)
BLD	0 - 5	0.2	28

4. Load – load-line displacement plot

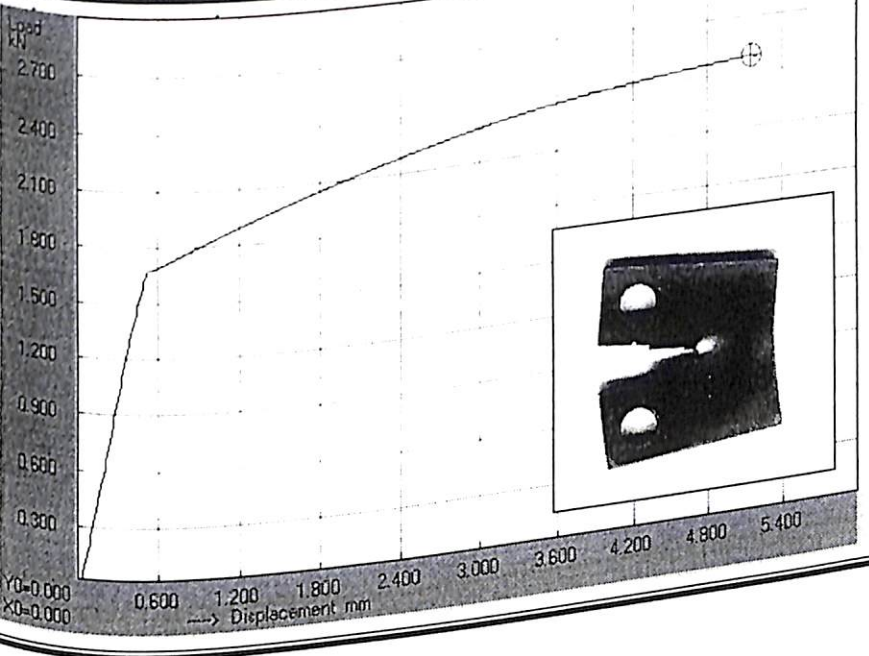

P_c (kN)	2.44
V_{pl} (mm)	4.17
A_{pl} kN-mm	----

Centre of Materials Science & Testing. Birla Institutes of Technology and Science, Pilani, Rajasthan INDIA (333 031)

B3

Fracture Test on EDD277 (Strain rate effect study)

B3.1 Fracture test 1.4A

1. Material

Material	Yield strength (MPa)	Modulus of Elasticity (GPa)	Poisson's ratio (ν)
EDD277 steel sheet	277	210	0.33

2. (Compact Tension (CT) specimen as per ASTM standard (E399-91).

Specimen code	Thickness B (mm)	Crack length a_0 (mm)	Width W (mm)	Notch radius (mm)
1.4A	1.4	10.5	24	0.125

3. Test Conditions

Test Type	Load range (kN)	Strain rate (mm/min)	Temperature (°C)
Crack initiation	0 - 5	0.2	28

4. Load – load-line displacement plot

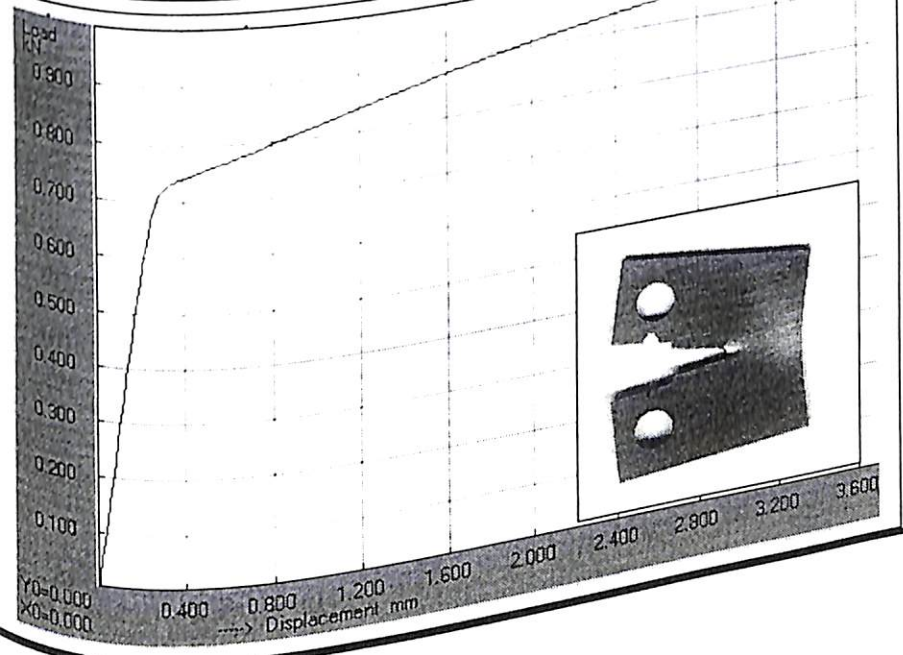

P_c (kN)	0.972
V_{pl} (mm)	3.20
A_{pl} kN-mm	2.796

Centre of Materials Science & Testing. Birla Institutes of Technology and Science, Pilani, Rajasthan INDIA (333 031)

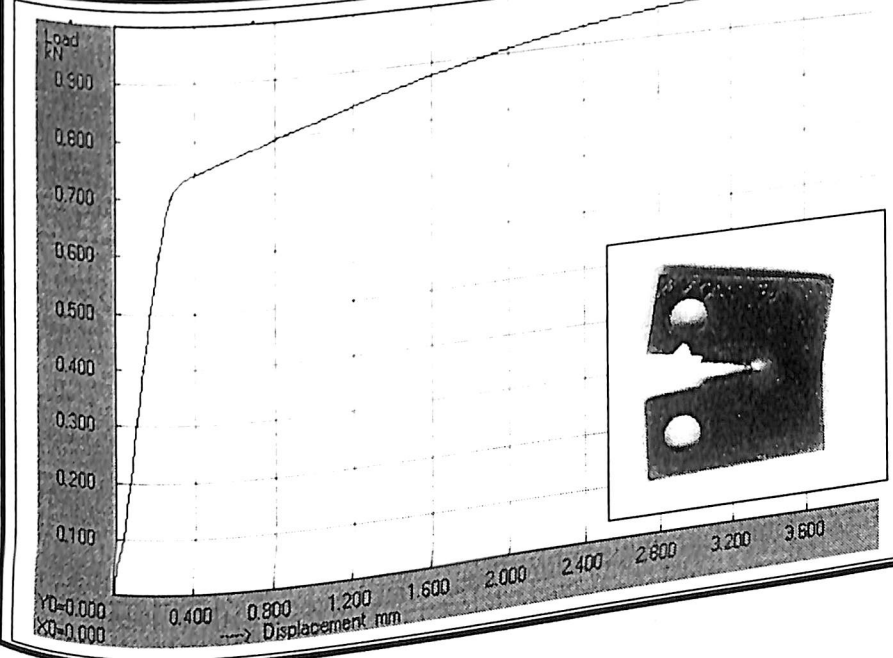

V_{pl} (mm)	3.2
A_{pl} kN-mm	2.785

Centre of Materials Science & Testing.
Birla Institutes of Technology and Science, Pilani, Rajasthan INDIA (333 031)

B3.2 Fracture test 1.4B

1. Material

Material	Yield strength (MPa)	Modulus of Elasticity (GPa)	Poisson's ratio (ν)
EDD277 steel sheet	277	210	0.33

2. (Compact Tension (CT) specimen as per ASTM standard (E399-91).

Specimen code	Thickness B (mm)	Crack length a_0 (mm)	Width W (mm)	Notch radius (mm)
1.4B	1.4	10.5	24	0.116

3. Test Conditions

Test Type	Load range (kN)	Strain rate (mm/min)	Temperature (°C)
Crack initiation	0 - 5	0.4	28

4. Load – load-line displacement plot

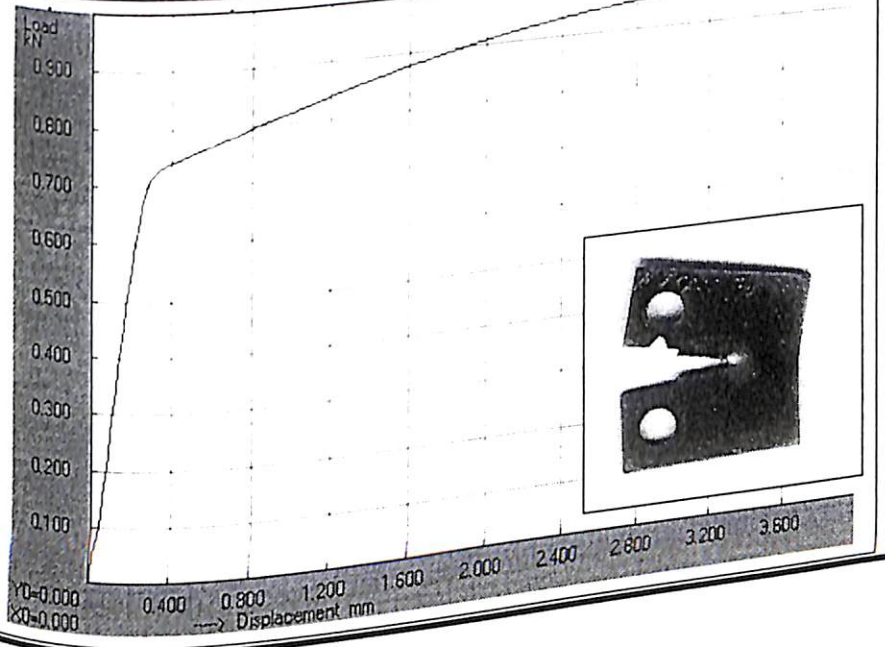

P_c (kN)	0.968
V_{pl} (mm)	3.2
A_{pl} kN-mm	2.785

Centre of Materials Science & Testing.
Birla Institutes of Technology and Science, Pilani, Rajasthan INDIA (333 031)

B3.3 Fracture test 1.4C

1. Material

Material	Yield strength (MPa)	Modulus of Elasticity (GPa)	Poisson's ratio (v)
EDD277 steel sheet	277	210	0.33

2. (Compact Tension (CT) specimen as per ASTM standard (E399-91).

Specimen code	Thickness B (mm)	Crack length a_0 (mm)	Width W (mm)	Notch radius (mm)
1.4C	1.4	10.5	24	0.1

3. Test Conditions

Test Type	Load range (kN)	Strain rate (mm/min)	Temperature (°C)
Crack initiation	0 - 5	0.6	28

4. Load – load-line displacement plot

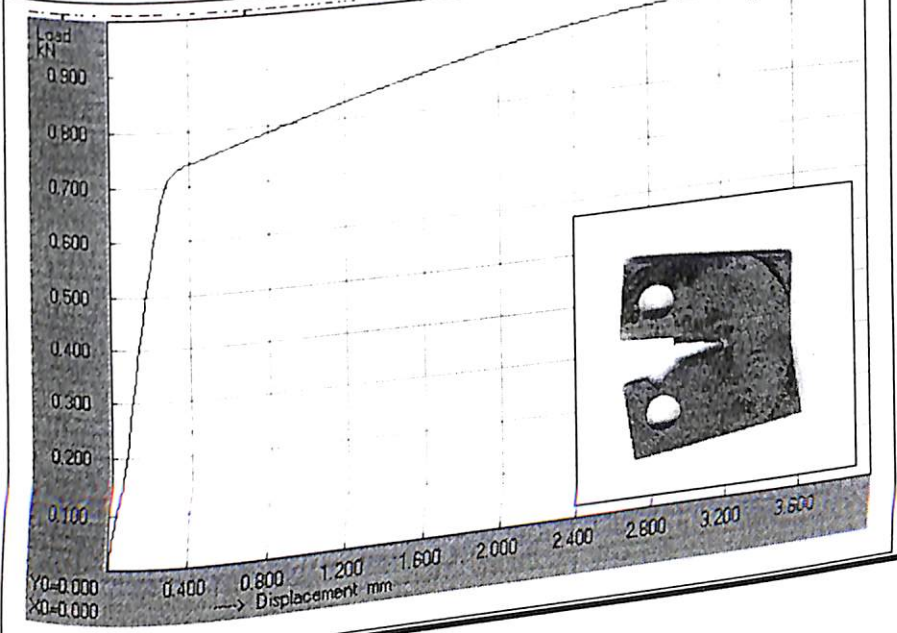

P_c (kN)	0.960
V_{pl} (mm)	3.16
A_{pl} kN-mm	2.772

Centre of Materials Science & Testing.
Birla Institutes of Technology and Science, Pilani, Rajasthan INDIA (333 031)

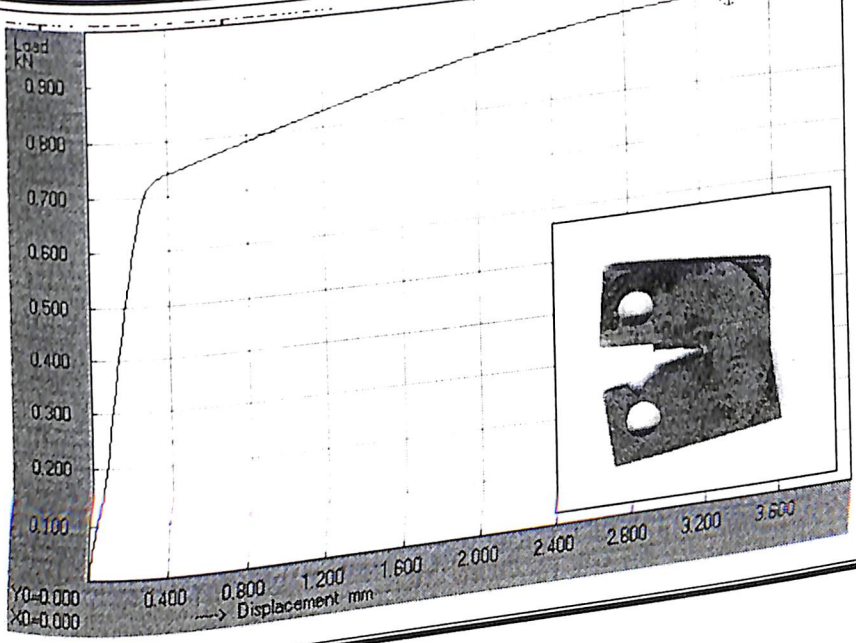

V_{pl} (mm)	3.16
A_{pl} kN-mm	2.772

Centre of Materials Science & Testing.
Birla Institutes of Technology and Science, Pilani, Rajasthan INDIA (333 031)

B3.4 Fracture test 1.4D

1. Material

Material	Yield strength (MPa)	Modulus of Elasticity (GPa)	Poisson's ratio (ν)
EDD277 steel sheet	277	210	0.33

2. (Compact Tension (CT) specimen as per ASTM standard (E399-91).

Specimen code	Thickness B (mm)	Crack length a_0 (mm)	Width W (mm)	Notch radius (mm)
1.4D	1.4	10.5	24	0.124

3. Test Conditions

Test Type	Load range (kN)	Strain rate (mm/min)	Temperature (°C)
Crack initiation	0 - 5	1.0	28

4. Load – load-line displacement plot

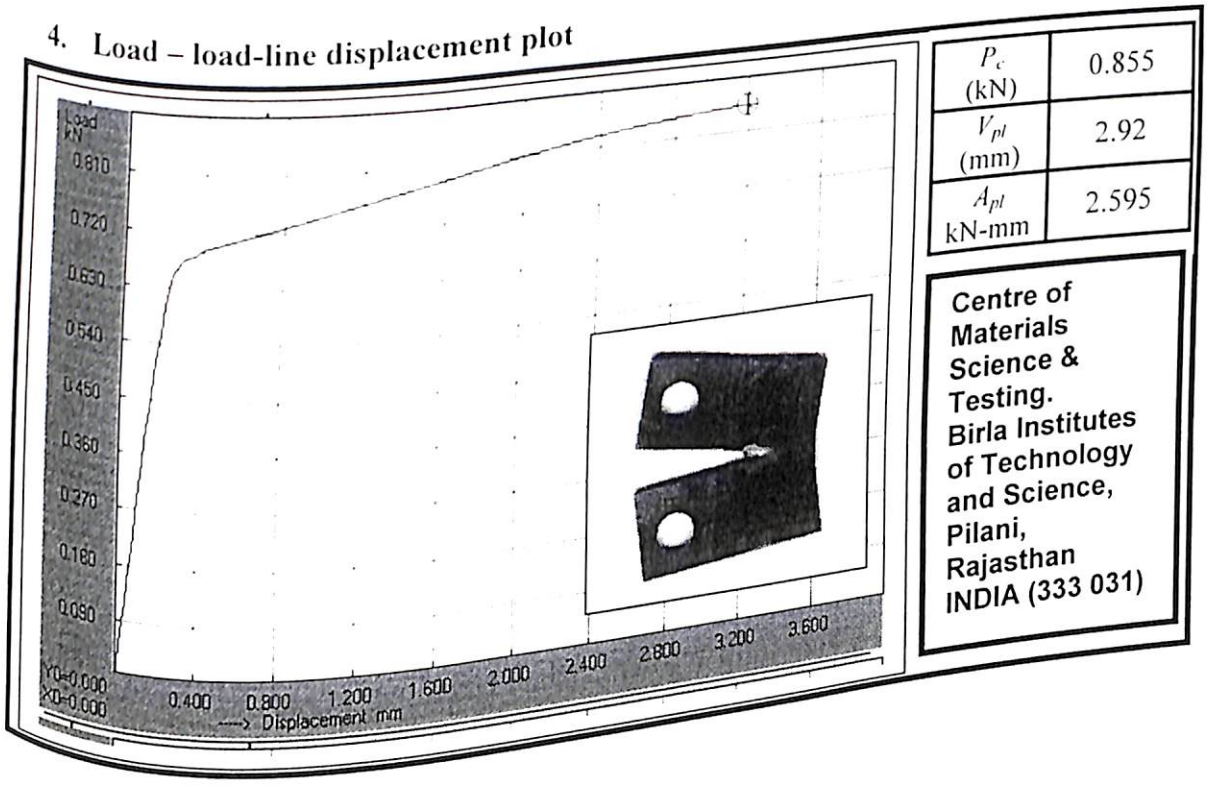

P_c (kN)	0.855
V_{pl} (mm)	2.92
A_{pl} kN-mm	2.595

Centre of Materials Science & Testing.
Birla Institutes of Technology and Science, Pilani, Rajasthan INDIA (333 031)

B3.5 Fracture test 1.4E

1. Material

Material	Yield strength (MPa)	Modulus of Elasticity (GPa)	Poisson's ratio (ν)
EDD277 steel sheet	277	210	0.33

2. (Compact Tension (CT) specimen as per ASTM standard (E399-91).

Specimen code	Thickness B (mm)	Crack length a_0 (mm)	Width W (mm)	Notch radius (mm)
1.4E	1.4	10.5	24	0.118

3. Test Conditions

Test Type	Load range (kN)	Strain rate (mm/min)	Temperature (°C)
Crack initiation	0 - 5	1.5	28

4. Load – load-line displacement plot

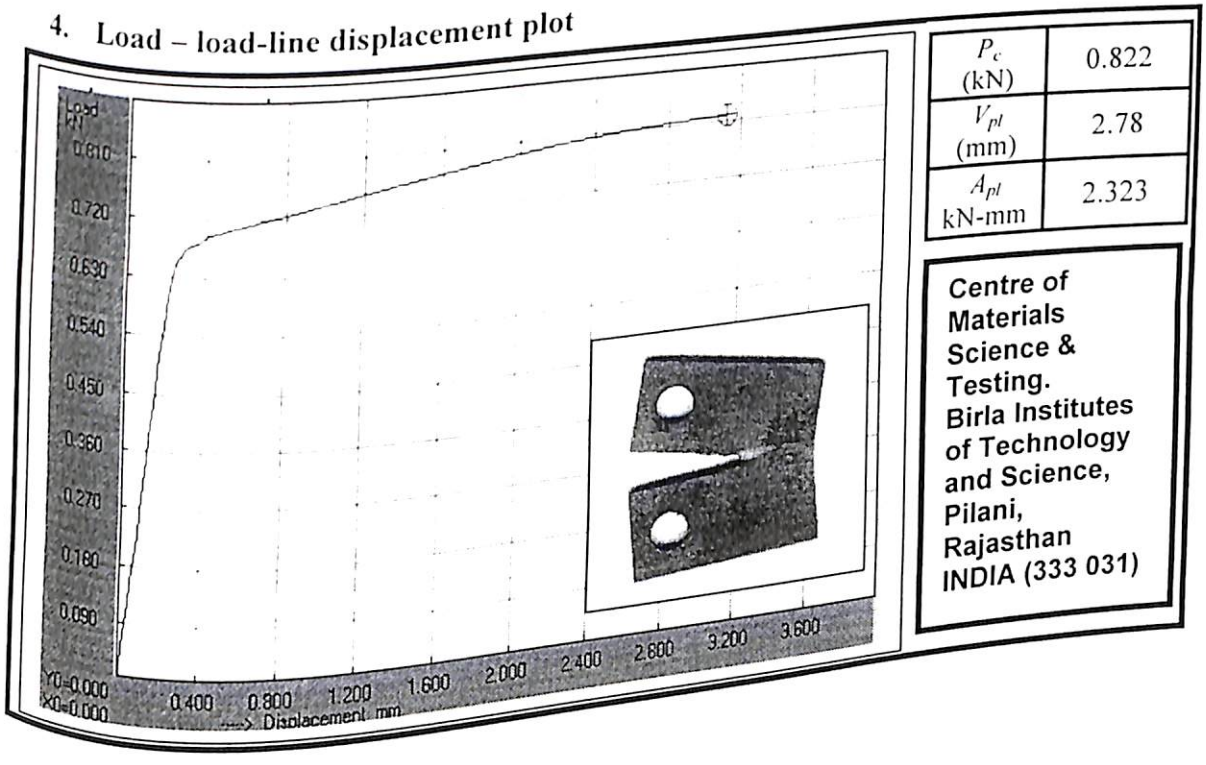

P_c (kN)	0.822
V_{pl} (mm)	2.78
A_{pl} kN-mm	2.323

Centre of Materials Science & Testing.
Birla Institutes of Technology and Science, Pilani, Rajasthan INDIA (333 031)

B3.6 Fracture test 1.4F

1. Material

Material	Yield strength (MPa)	Modulus of Elasticity (GPa)	Poisson's ratio (v)
EDD277 steel sheet	277	210	0.33

2. (Compact Tension (CT) specimen as per ASTM standard (E399-91).

Specimen code	Thickness B (mm)	Crack length a_0 (mm)	Width W (mm)	Notch radius (mm)
1.4F	1.4	10.5	24	0.122

3. Test Conditions

Test Type	Load range (kN)	Strain rate (mm/min)	Temperature (°C)
Crack initiation	0 - 5	2.5	28

4. Load – load-line displacement plot

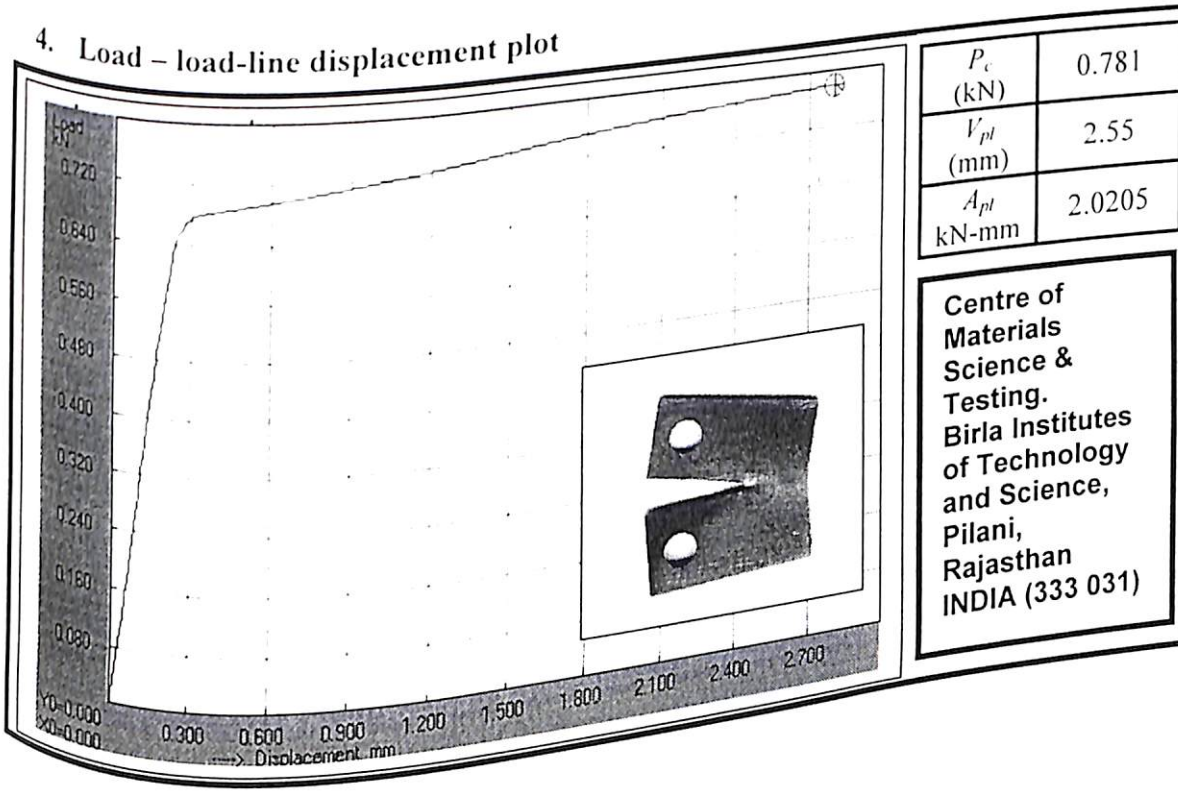

P_c (kN)	0.781
V_{pl} (mm)	2.55
A_{pl} kN-mm	2.0205

Centre of Materials Science & Testing.
Birla Institutes of Technology and Science, Pilani, Rajasthan INDIA (333 031)

B4

Fracture Test on EDD258 (Influence of notch radius)

B4.1 Fracture test SP1

1. Material

Material	Yield strength (MPa)	Modulus of Elasticity (GPa)	Poisson's ratio (ν)
EDD258 steel sheet	258	210	0.33

2. (Compact Tension (CT) specimen as per ASTM standard (E399-91).

Specimen code	Thickness, B (mm)	Crack length a_0 (mm)	Width W (mm)	Notch radius, ρ (mm)
SP1	3.2	10.5	24	0.07

3. Test Conditions

Test Type	Load range (kN)	Strain rate (mm/min)	Temperature (°C)
Crack initiation	0 - 5	0.2	28

4. Load – load-line displacement plot

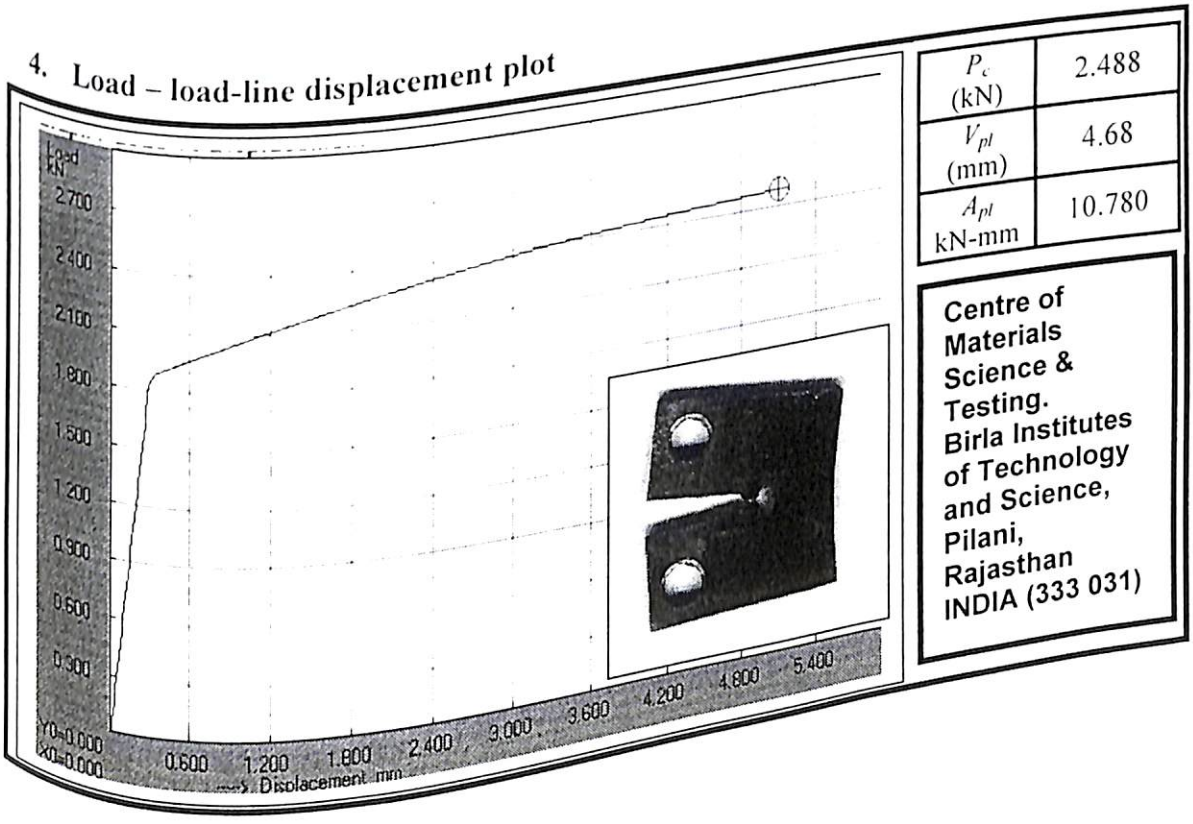

P_c (kN)	2.488
V_{pl} (mm)	4.68
A_{pl} kN-mm	10.780

Centre of Materials Science & Testing. Birla Institutes of Technology and Science, Pilani, Rajasthan INDIA (333 031)

B4.2 Fracture test SP2

1. Material

Material	Yield strength (MPa)	Modulus of Elasticity (GPa)	Poisson's ratio (ν)
EDD258 steel sheet	258	210	0.33

2. (Compact Tension (CT) specimen as per ASTM standard (E399-91).

Specimen code	Thickness, B (mm)	Crack length a_0 (mm)	Width W (mm)	Notch radius, ρ (mm)
SP2	3.2	10.5	24	0.085

3. Test Conditions

Test Type	Load range (kN)	Strain rate (mm/min)	Temperature (°C)
Crack initiation	0 - 5	0.2	28

4. Load – load-line displacement plot

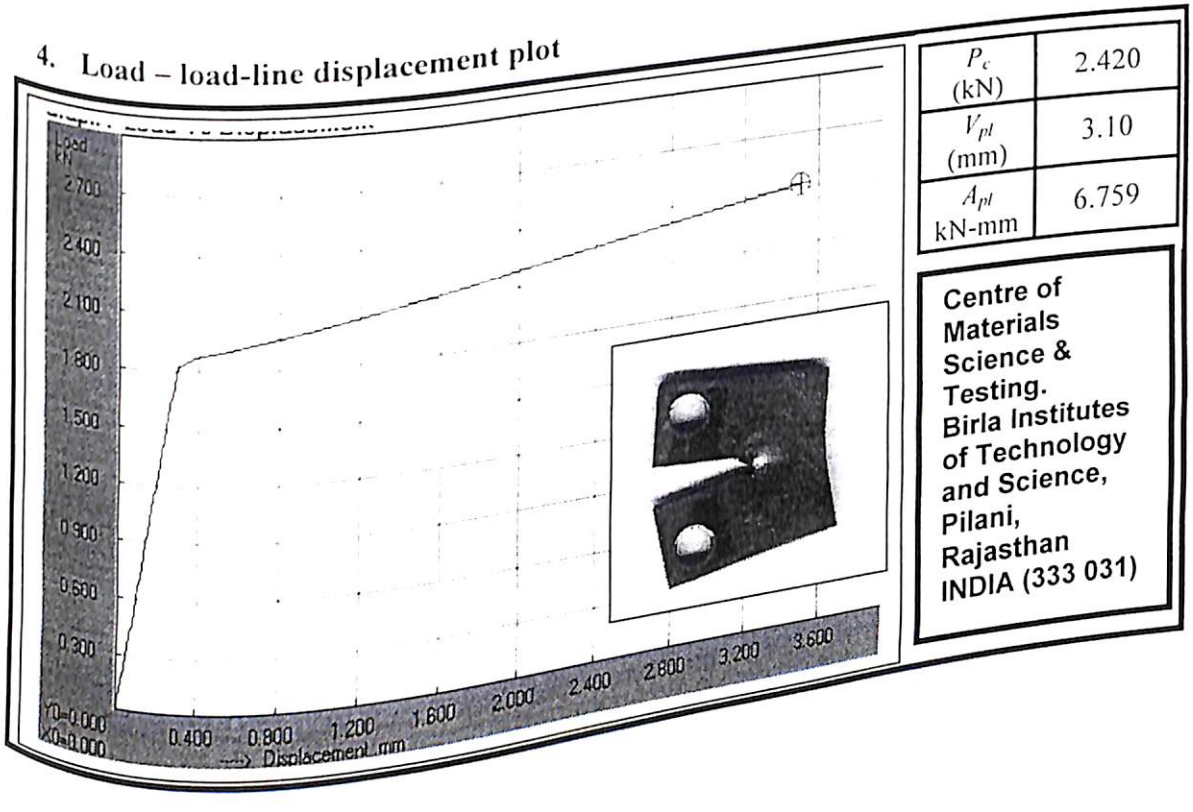

P_c (kN)	2.420
V_{pl} (mm)	3.10
A_{pl} kN-mm	6.759

Centre of Materials Science & Testing.
Birla Institutes of Technology and Science, Pilani, Rajasthan INDIA (333 031)

B4.3 Fracture test SP3

1. Material

Material	Yield strength (MPa)	Modulus of Elasticity (GPa)	Poisson's ratio (ν)
EDD258 steel sheet	258	210	0.33

2. (Compact Tension (CT) specimen as per ASTM standard (E399-91).

Specimen code	Thickness, B (mm)	Crack length a_0 (mm)	Width W (mm)	Notch radius, ρ (mm)
SP3	3.2	10.5	24	0.10

3. Test Conditions

Test Type	Load range (kN)	Strain rate (mm/min)	Temperature (°C)
Crack initiation	0 - 5	0.2	28

4. Load – load-line displacement plot

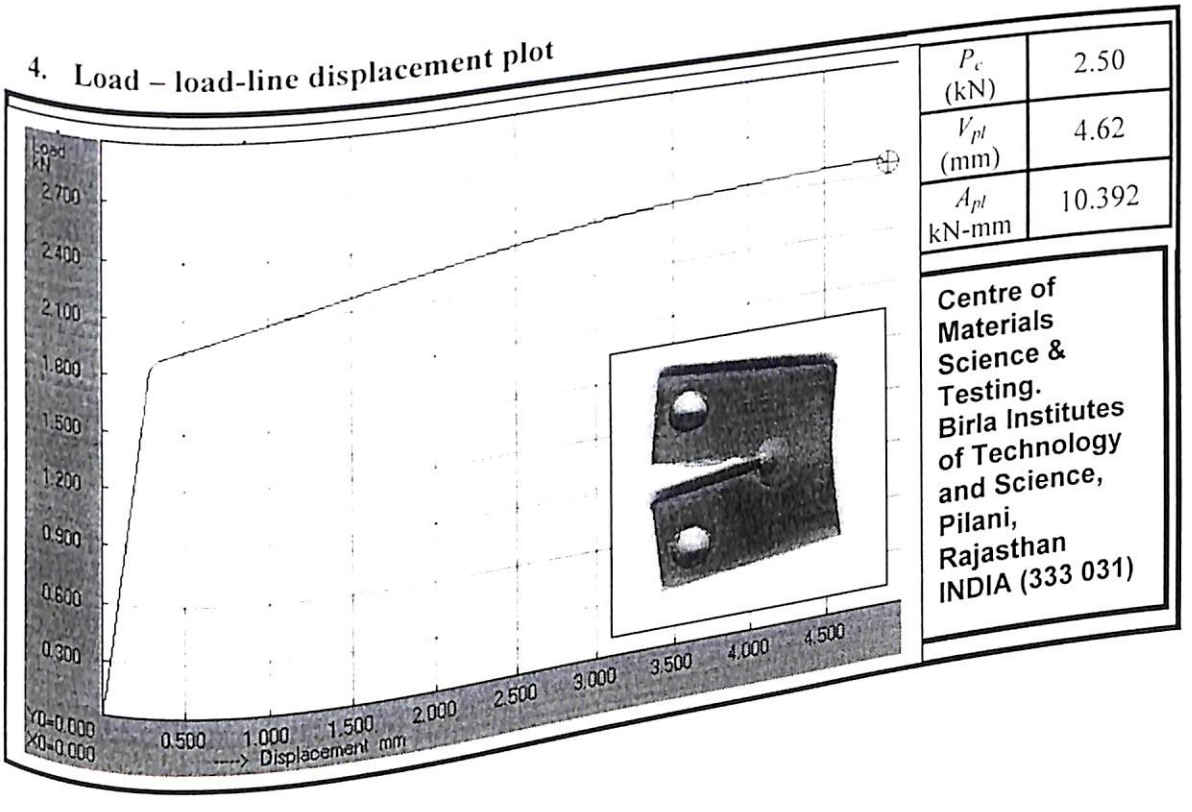

P_c (kN)	2.50
V_{pl} (mm)	4.62
A_{pl} kN-mm	10.392

Centre of Materials Science & Testing.
Birla Institutes of Technology and Science, Pilani, Rajasthan INDIA (333 031)

B4.4 Fracture test SP4

1. **Material**

Material	Yield strength (MPa)	Modulus of Elasticity (GPa)	Poisson's ratio (ν)
EDD258 steel sheet	258	210	0.33

2. **(Compact Tension (CT) specimen as per ASTM standard (E399-91).**

Specimen code	Thickness, B (mm)	Crack length a_0 (mm)	Width W (mm)	Notch radius, ρ (mm)
SP4	3.2	10.5	24	0.11

3. **Test Conditions**

Test Type	Load range (kN)	Strain rate (mm/min)	Temperature (°C)
Crack initiation	0 - 5	0.2	28

4. **Load – load-line displacement plot**

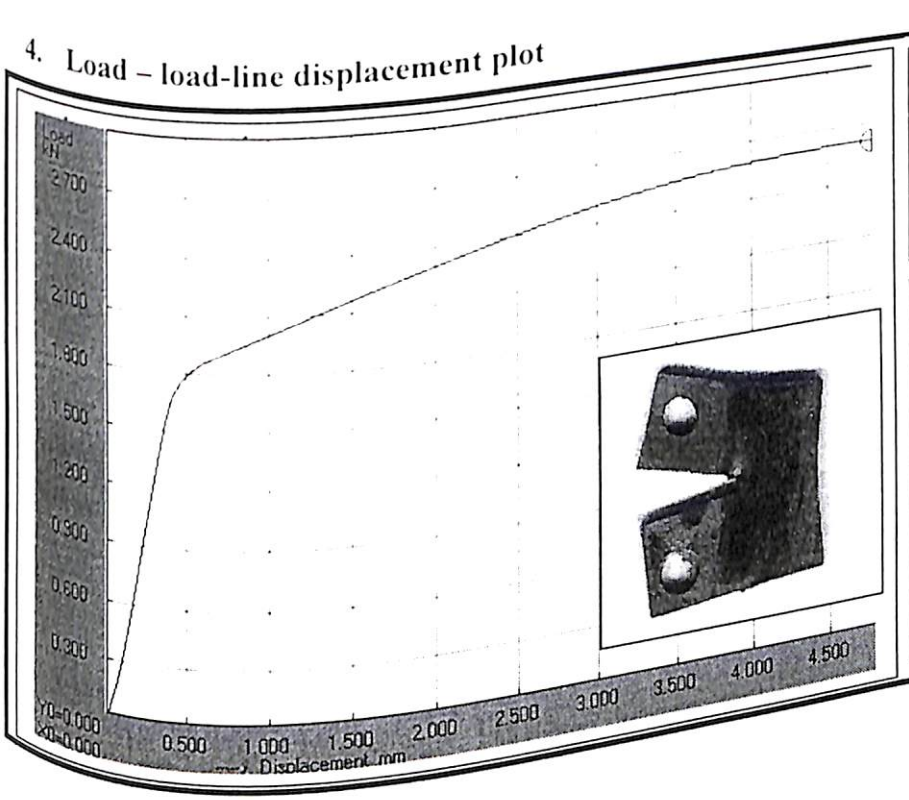

P_c (kN)	2.611
V_{pl} (mm)	4.22
A_{pl} kN-mm	10.041

Centre of Materials Science & Testing. Birla Institutes of Technology and Science, Pilani, Rajasthan INDIA (333 031)

B4.5 Fracture test SP5

1. Material

Material	Yield strength (MPa)	Modulus of Elasticity (GPa)	Poisson's ratio (ν)
EDD258 steel sheet	258	210	0.33

2. (Compact Tension (CT) specimen as per ASTM standard (E399-91).

Specimen code	Thickness, B (mm)	Crack length a_0 (mm)	Width W (mm)	Notch radius, ρ (mm)
SP5	3.2	10.5	24	0.12

3. Test Conditions

Test Type	Load range (kN)	Strain rate (mm/min)	Temperature (°C)
Crack initiation	0 - 5	0.2	28

4. Load – load-line displacement plot

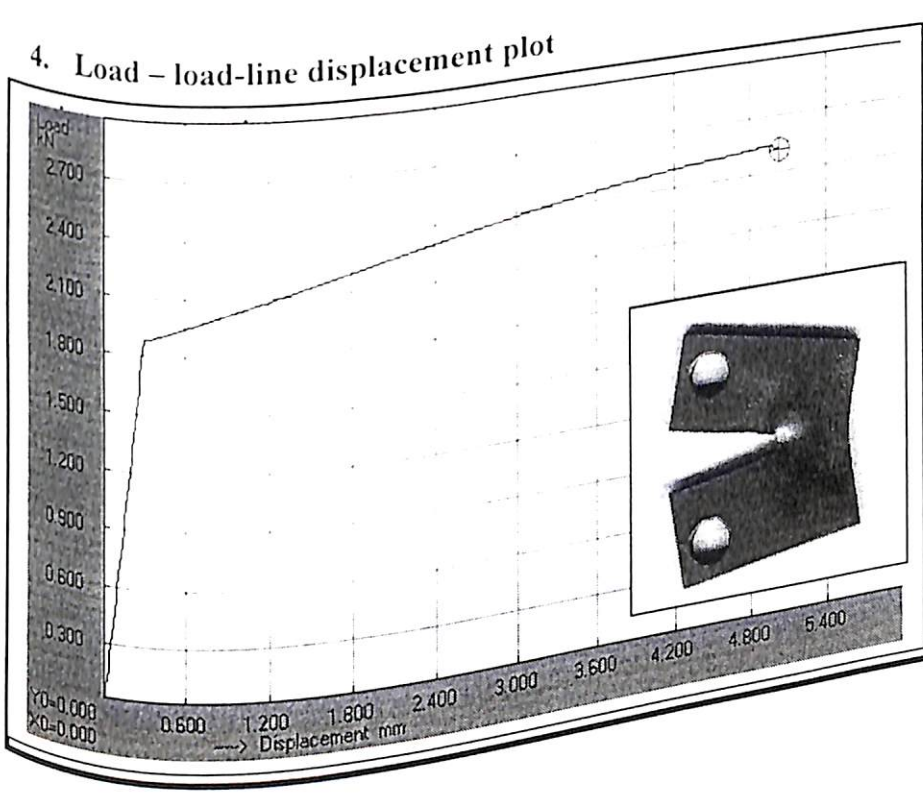

P_c (kN)	2.539
V_{pl} (mm)	4.61
A_{pl} kN-mm	10.040

Centre of Materials Science & Testing. Birla Institutes of Technology and Science, Pilani, Rajasthan INDIA (333 031)

B4.6 Fracture test SP6

1. Material

Material	Yield strength (MPa)	Modulus of Elasticity (GPa)	Poisson's ratio (ν)
EDD258 steel sheet	258	210	0.33

2. (Compact Tension (CT) specimen as per ASTM standard (E399-91).

Specimen code	Thickness, B (mm)	Crack length a_0 (mm)	Width W (mm)	Notch radius, ρ (mm)
SP6	3.2	10.5	24	0.13

3. Test Conditions

Test Type	Load range (kN)	Strain rate (mm/min)	Temperature (°C)
Crack initiation	0 - 5	0.2	28

4. Load – load-line displacement plot

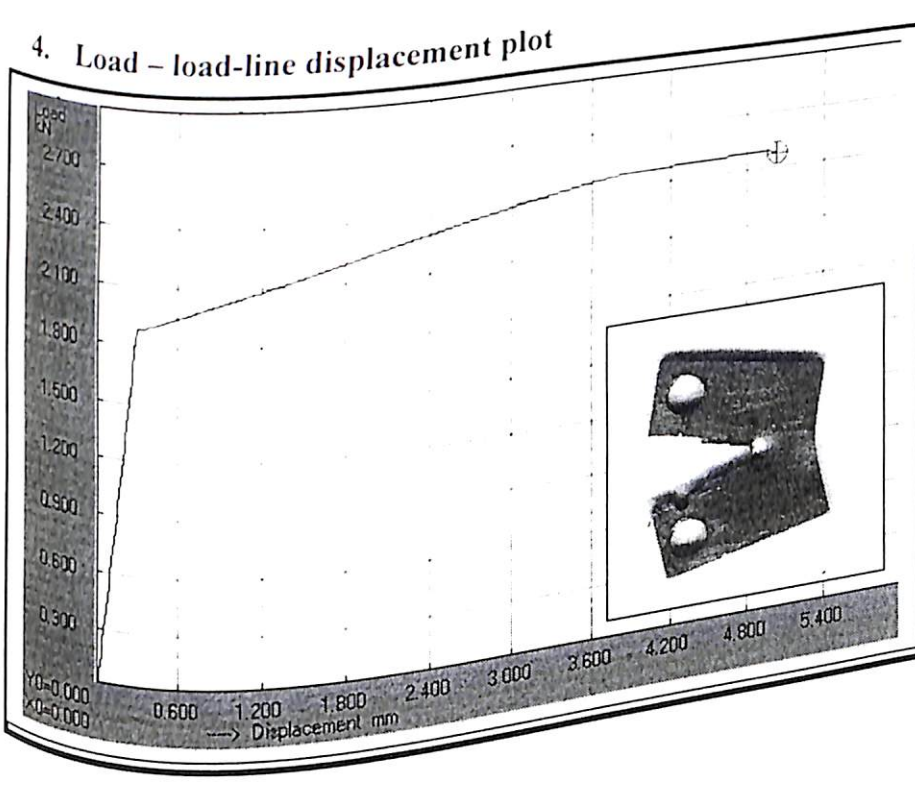

P_c (kN)	2.485
V_{pl} (mm)	4.61
A_{pl} kN-mm	9.742

Centre of Materials Science & Testing.
Birla Institutes of Technology and Science, Pilani, Rajasthan INDIA (333 031)

B4.7 Fracture test SP7

1. Material

Material	Yield strength (MPa)	Modulus of Elasticity (GPa)	Poisson's ratio (ν)
EDD258 steel sheet	258	210	0.33

2. (Compact Tension (CT) specimen as per ASTM standard (E399-91).

Specimen code	Thickness, B (mm)	Crack length a_0 (mm)	Width W (mm)	Notch radius, ρ (mm)
SP7	3.2	10.5	24	0.14

3. Test Conditions

Test Type	Load range (kN)	Strain rate (mm/min)	Temperature (°C)
Crack initiation	0 - 5	0.2	28

4. Load – load-line displacement plot

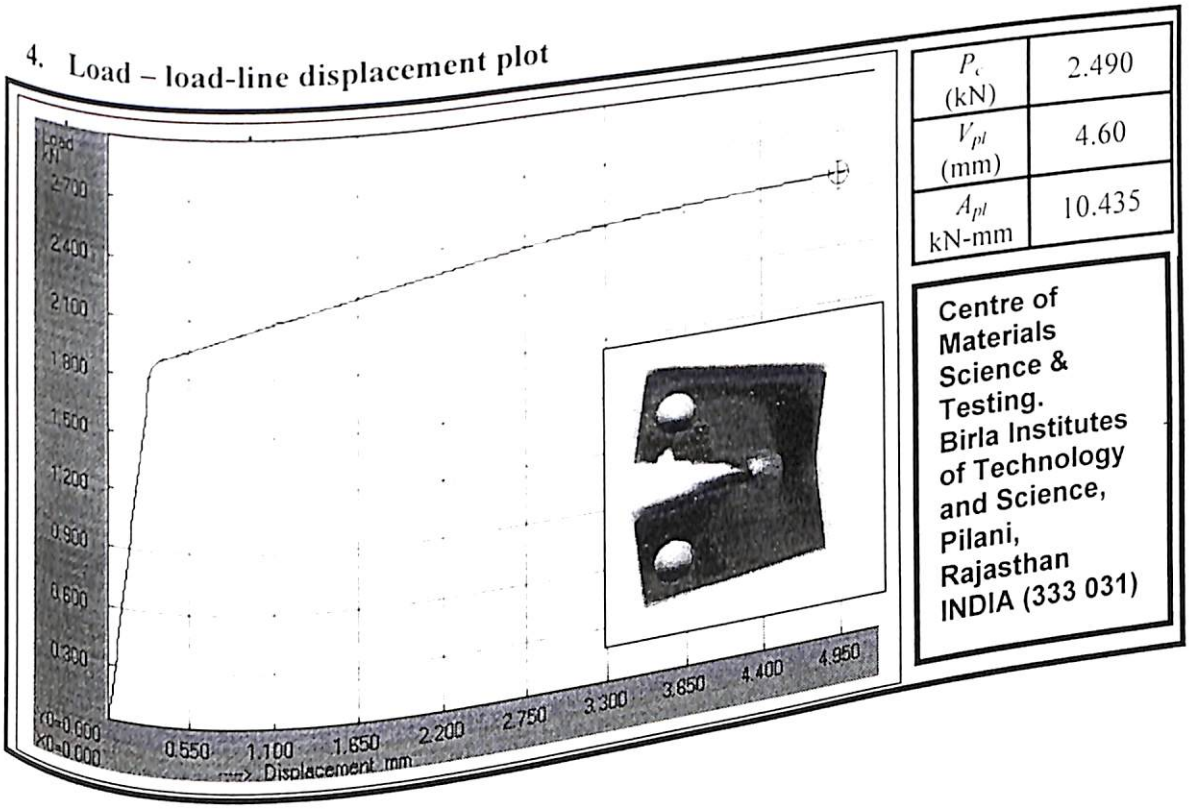

P_c (kN)	2.490
V_{pl} (mm)	4.60
A_{pl} kN-mm	10.435

Centre of Materials Science & Testing.
Birla Institutes of Technology and Science, Pilani, Rajasthan INDIA (333 031)

B4.8 Fracture test SP8

1. Material

Material	Yield strength (MPa)	Modulus of Elasticity (GPa)	Poisson's ratio (ν)
EDD258 steel sheet	258	210	0.33

2. (Compact Tension (CT) specimen as per ASTM standard (E399-91).

Specimen code	Thickness, B (mm)	Crack length a_0 (mm)	Width W (mm)	Notch radius, ρ (mm)
SP8	3.2	10.5	24	0.15

3. Test Conditions

Test Type	Load range (kN)	Strain rate (mm/min)	Temperature (°C)
Crack initiation	0 - 5	0.2	28

4. Load – load-line displacement plot

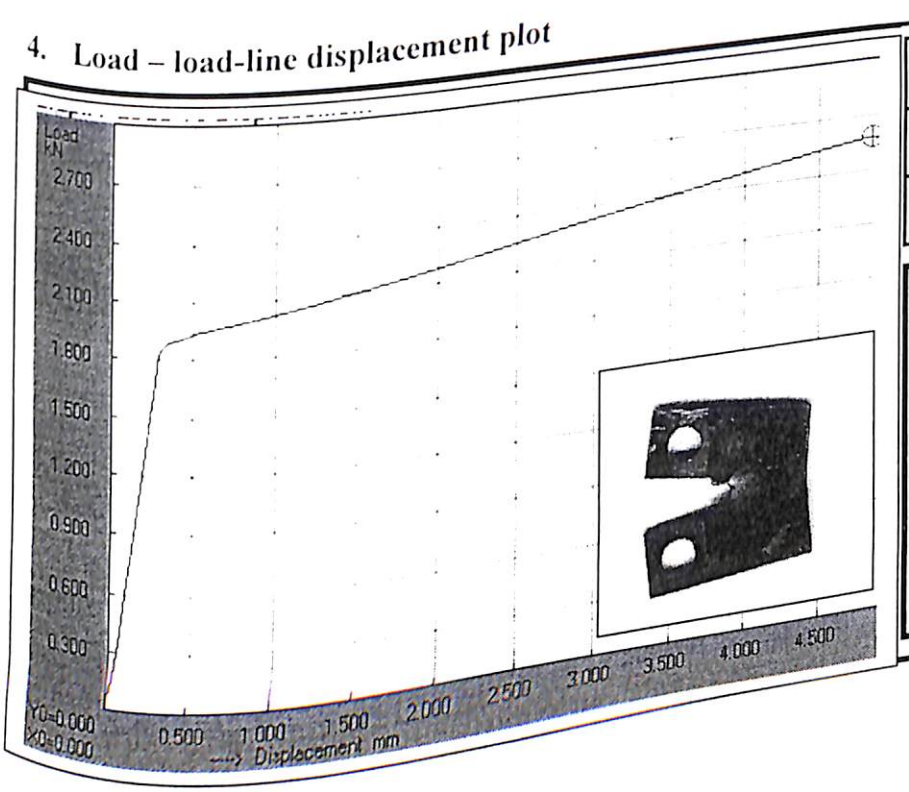

P_c (kN)	2.587
V_{pl} (mm)	4.55
A_{pl} kN-mm	9.460

Centre of Materials Science & Testing. Birla Institutes of Technology and Science, Pilani, Rajasthan INDIA (333 031)

B4.9 Fracture test SP9

1. Material

Material	Yield strength (MPa)	Modulus of Elasticity (GPa)	Poisson's ratio (ν)
EDD258 steel sheet	258	210	0.33

2. (Compact Tension (CT) specimen as per ASTM standard (E399-91).

Specimen code	Thickness, B (mm)	Crack length a_0 (mm)	Width W (mm)	Notch radius, ρ (mm)
SP9	3.2	10.5	24	0.16

3. Test Conditions

Test Type	Load range (kN)	Strain rate (mm/min)	Temperature (°C)
Crack initiation	0 - 5	0.2	28

4. Load – load-line displacement plot

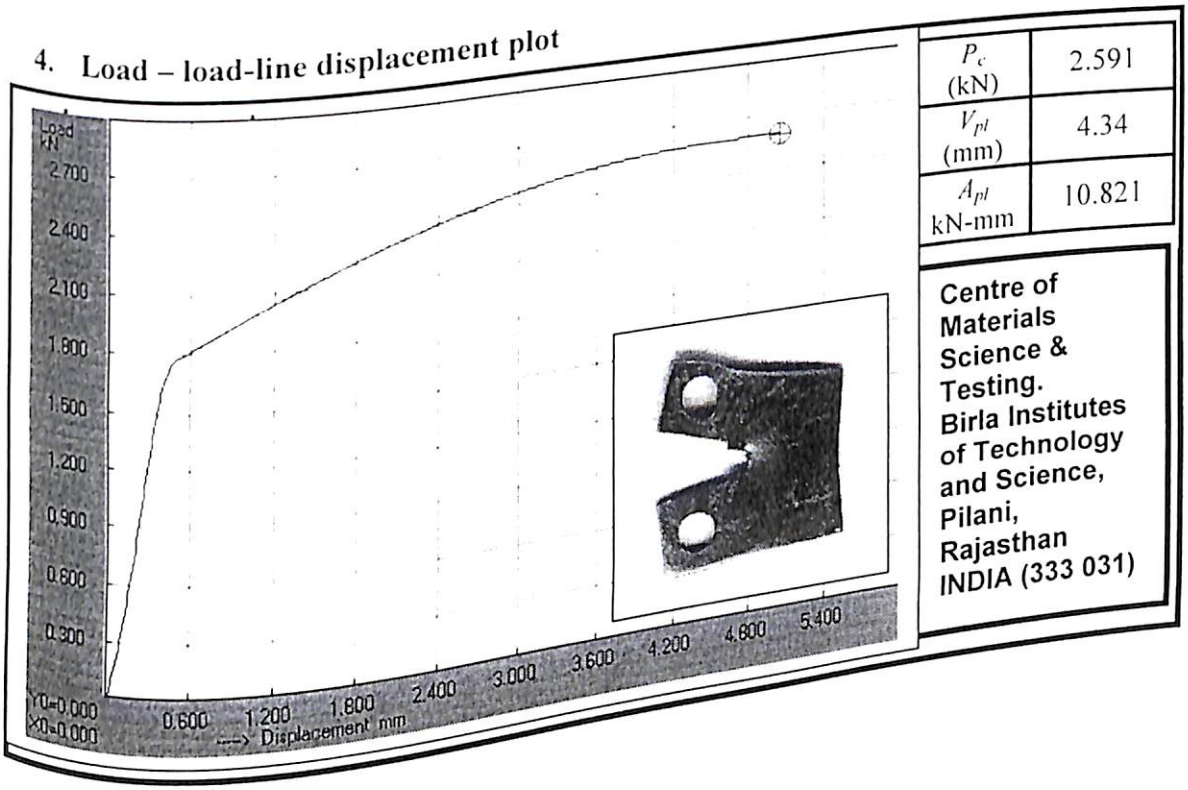

P_c (kN)	2.591
V_{pl} (mm)	4.34
A_{pl} kN-mm	10.821

Centre of Materials Science & Testing. Birla Institutes of Technology and Science, Pilani, Rajasthan INDIA (333 031)

B4.10 Fracture test SP10

1. Material

Material	Yield strength (MPa)	Modulus of Elasticity (GPa)	Poisson's ratio (ν)
EDD258 steel sheet	258	210	0.33

2. (Compact Tension (CT) specimen as per ASTM standard (E399-91).

Specimen code	Thickness, B (mm)	Crack length a_0 (mm)	Width W (mm)	Notch radius, ρ (mm)
SP10	3.2	10.5	24	0.17

3. Test Conditions

Test Type	Load range (kN)	Strain rate (mm/min)	Temperature (°C)
Crack initiation	0 - 5	0.2	28

4. Load – load-line displacement plot

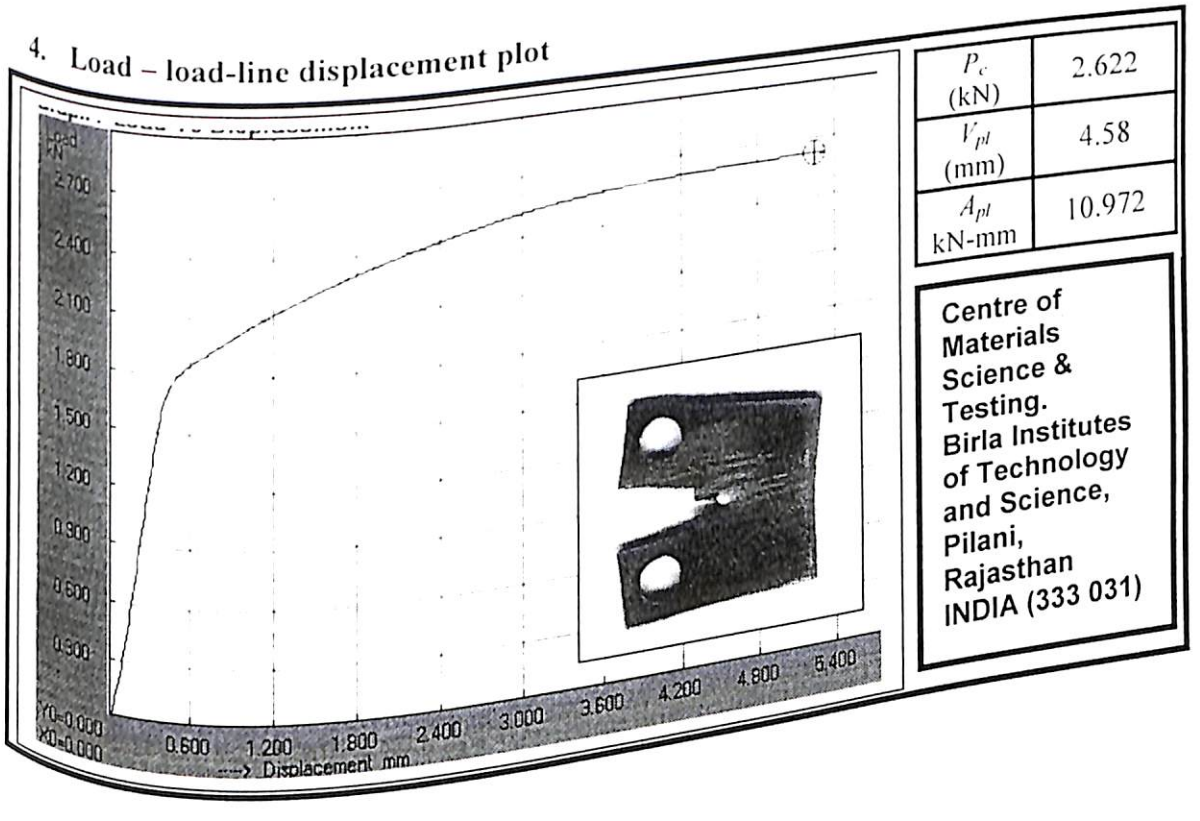

P_c (kN)	2.622
V_{pl} (mm)	4.58
A_{pl} kN-mm	10.972

Centre of Materials Science & Testing. Birla Institutes of Technology and Science, Pilani, Rajasthan INDIA (333 031)

B4.11 Fracture test SP11

1. Material

Material	Yield strength (MPa)	Modulus of Elasticity (GPa)	Poisson's ratio (ν)
EDD258 steel sheet	258	210	0.33

2. (Compact Tension (CT) specimen as per ASTM standard (E399-91).

Specimen code	Thickness, B (mm)	Crack length a_0 (mm)	Width W (mm)	Notch radius, ρ (mm)
SP11	3.2	10.5	24	0.18

3. Test Conditions

Test Type	Load range (kN)	Strain rate (mm/min)	Temperature (°C)
Crack initiation	0 - 5	0.2	28

4. Load – load-line displacement plot

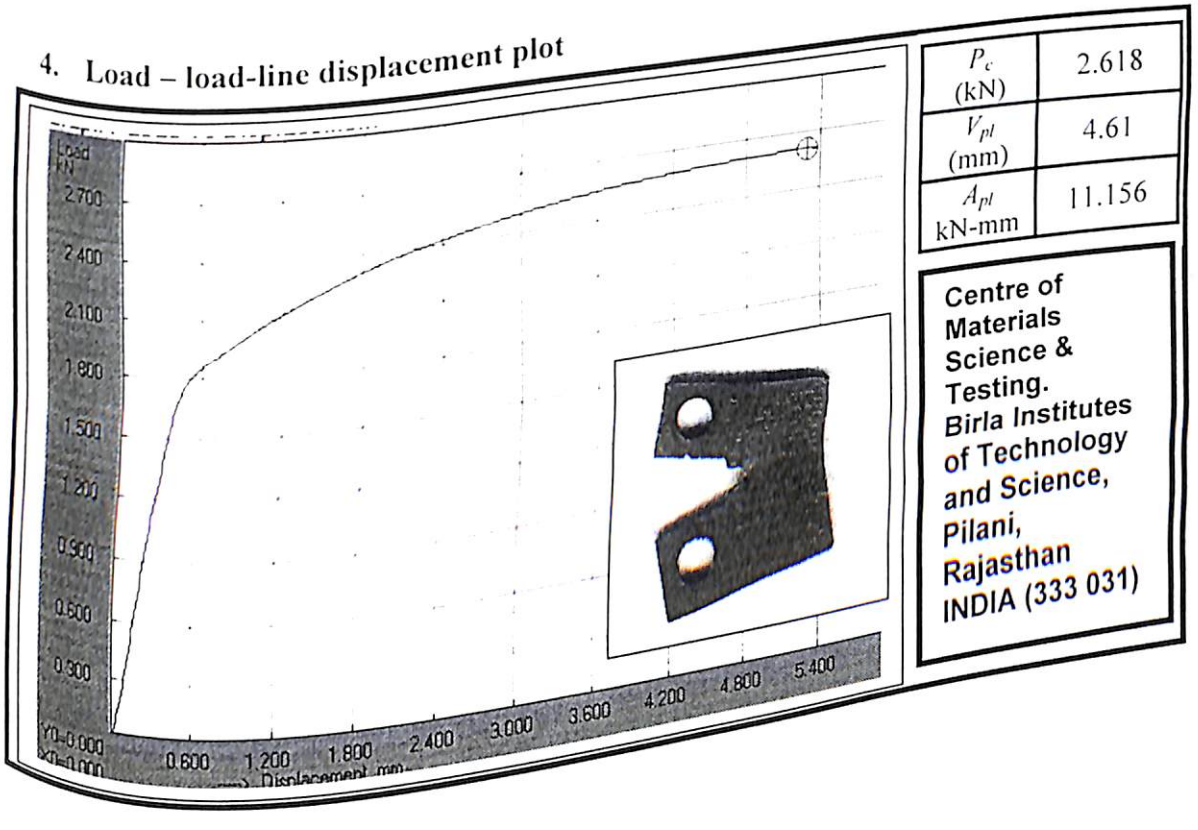

P_c (kN)	2.618
V_{pl} (mm)	4.61
A_{pl} kN-mm	11.156

Centre of Materials Science & Testing.
Birla Institutes of Technology and Science, Pilani, Rajasthan INDIA (333 031)

B4.12 Fracture test SP12

1. Material

Material	Yield strength (MPa)	Modulus of Elasticity (GPa)	Poisson's ratio (ν)
EDD258 steel sheet	258	210	0.33

2. (Compact Tension (CT) specimen as per ASTM standard (E399-91).

Specimen code	Thickness, B (mm)	Crack length a_0 (mm)	Width W (mm)	Notch radius, ρ (mm)
SP12	3.2	10.5	24	0.25

3. Test Conditions

Test Type	Load range (kN)	Strain rate (mm/min)	Temperature (°C)
Crack initiation	0 - 5	0.2	28

4. Load – load-line displacement plot

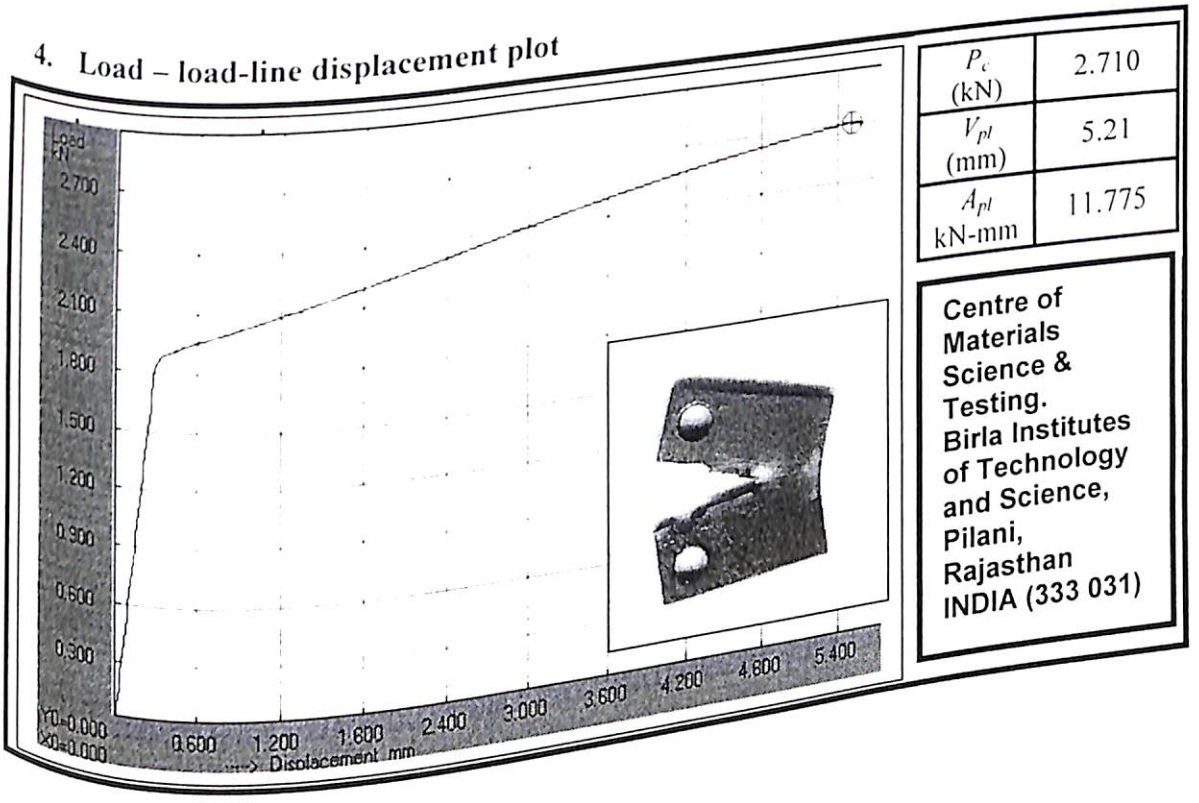

P_c (kN)	2.710
V_{pl} (mm)	5.21
A_{pl} kN-mm	11.775

Centre of Materials Science & Testing. Birla Institutes of Technology and Science, Pilani, Rajasthan INDIA (333 031)

B4.13 Fracture test SP13

1. Material

Material	Yield strength (MPa)	Modulus of Elasticity (GPa)	Poisson's ratio (v)
EDD258 steel sheet	258	210	0.33

2. (Compact Tension (CT) specimen as per ASTM standard (E399-91).

Specimen code	Thickness, B (mm)	Crack length a_0 (mm)	Width W (mm)	Notch radius, ρ (mm)
SP13	3.2	10.5	24	0.40

3. Test Conditions

Test Type	Load range (kN)	Strain rate (mm/min)	Temperature (°C)
Crack initiation	0 - 5	0.2	28

4. Load – load-line displacement plot

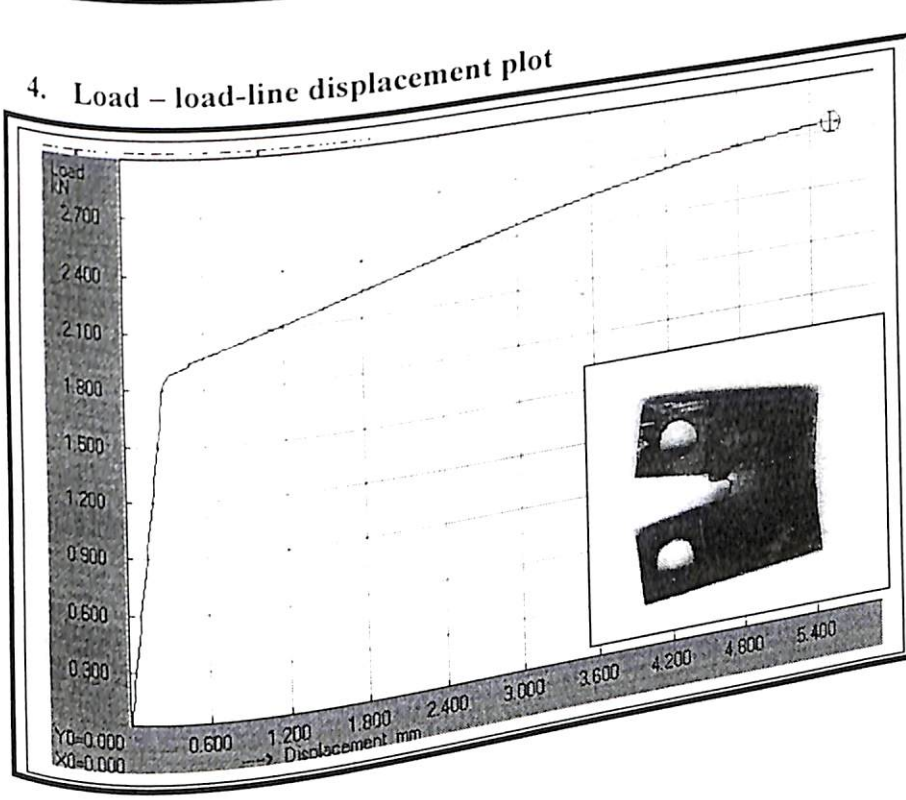

P_c (kN)	2.754
V_{pl} (mm)	5.26
A_{pl} kN-mm	11.991

Centre of Materials Science & Testing.
Birla Institutes of Technology and Science, Pilani, Rajasthan INDIA (333 031)

B4.14 Fracture test SP14

1. Material

Material	Yield strength (MPa)	Modulus of Elasticity (GPa)	Poisson's ratio (v)
EDD258 steel sheet	258	210	0.33

2. (Compact Tension (CT) specimen as per ASTM standard (E399-91).

Specimen code	Thickness, B (mm)	Crack length a_0 (mm)	Width W (mm)	Notch radius, ρ (mm)
SP14	3.2	10.5	24	0.60

3. Test Conditions

Test Type	Load range (kN)	Strain rate (mm/min)	Temperature (°C)
Crack initiation	0 - 5	0.2	28

4. Load – load-line displacement plot

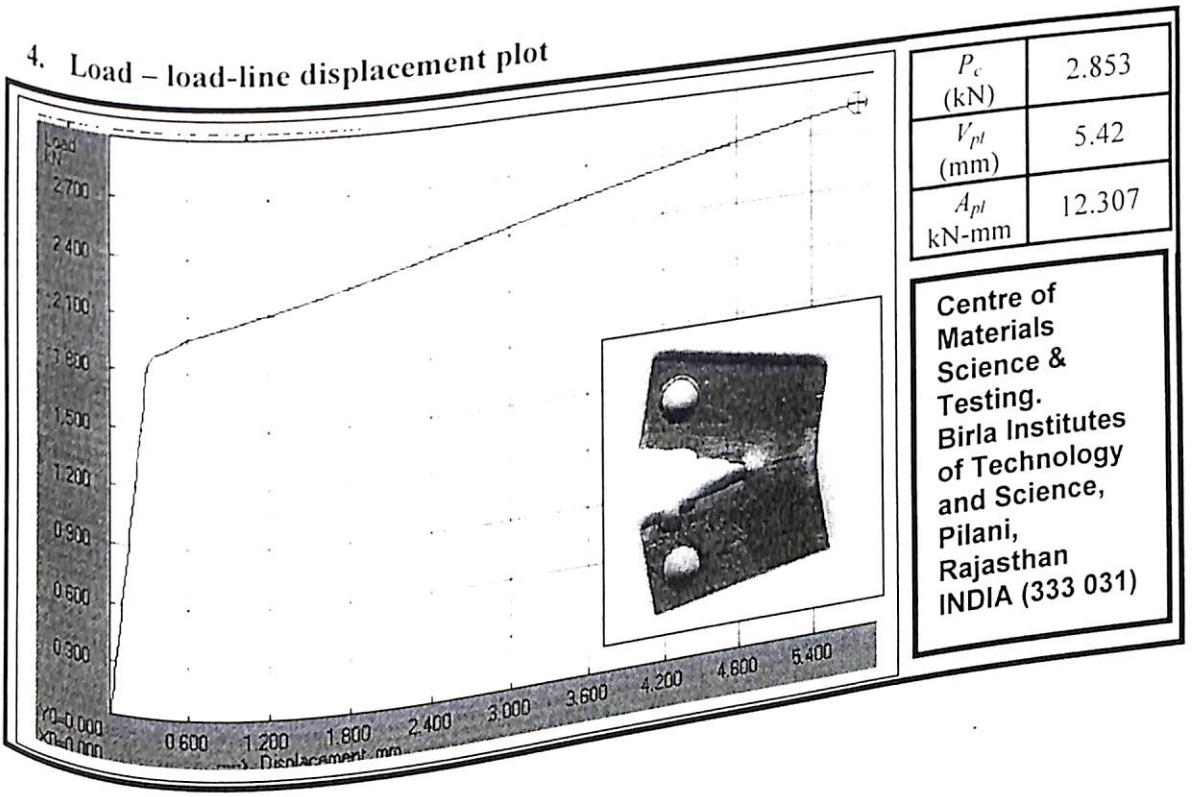

P_c (kN)	2.853
V_{pl} (mm)	5.42
A_{pl} kN-mm	12.307

Centre of Materials Science & Testing. Birla Institutes of Technology and Science, Pilani, Rajasthan INDIA (333 031)

B4.15 Fracture test SP15

1. Material

Material	Yield strength (MPa)	Modulus of Elasticity (GPa)	Poisson's ratio (ν)
EDD258 steel sheet	258	210	0.33

2. (Compact Tension (CT) specimen as per ASTM standard (E399-91).

Specimen code	Thickness, B (mm)	Crack length a_0 (mm)	Width W (mm)	Notch radius, ρ (mm)
SP15	3.2	10.5	24	0.75

3. Test Conditions

Test Type	Load range (kN)	Strain rate (mm/min)	Temperature (°C)
Crack initiation	0 - 5	0.2	28

4. Load – load-line displacement plot

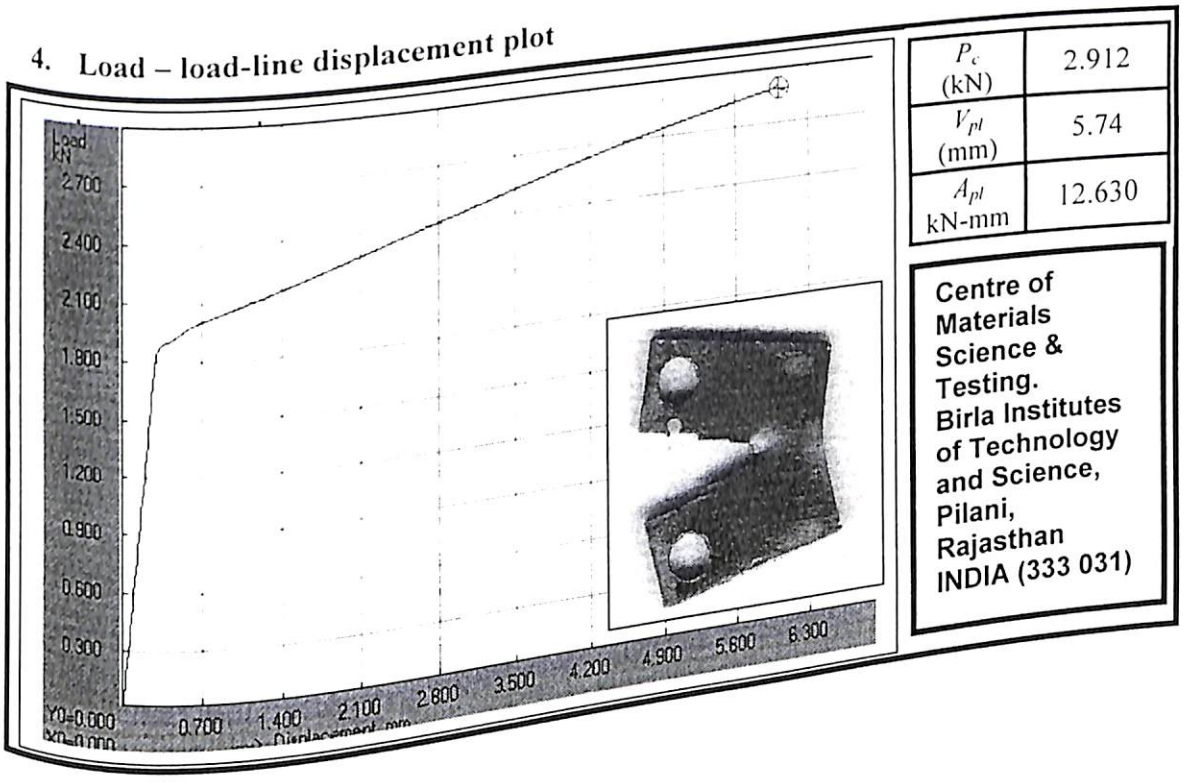

P_c (kN)	2.912
V_{pl} (mm)	5.74
A_{pl} kN-mm	12.630

Centre of Materials Science & Testing. Birla Institutes of Technology and Science, Pilani, Rajasthan INDIA (333 031)

B4.16 Fracture test SP16

1. Material

Material	Yield strength (MPa)	Modulus of Elasticity (GPa)	Poisson's ratio (ν)
EDD258 steel sheet	258	210	0.33

2. (Compact Tension (CT) specimen as per ASTM standard (E399-91).

Specimen code	Thickness, B (mm)	Crack length a_0 (mm)	Width W (mm)	Notch radius, ρ (mm)
SP16	3.2	10.5	24	0.077

3. Test Conditions

Test Type	Load range (kN)	Strain rate (mm/min)	Temperature (°C)
BLD	0 - 5	0.2	28

4. Load – load-line displacement plot

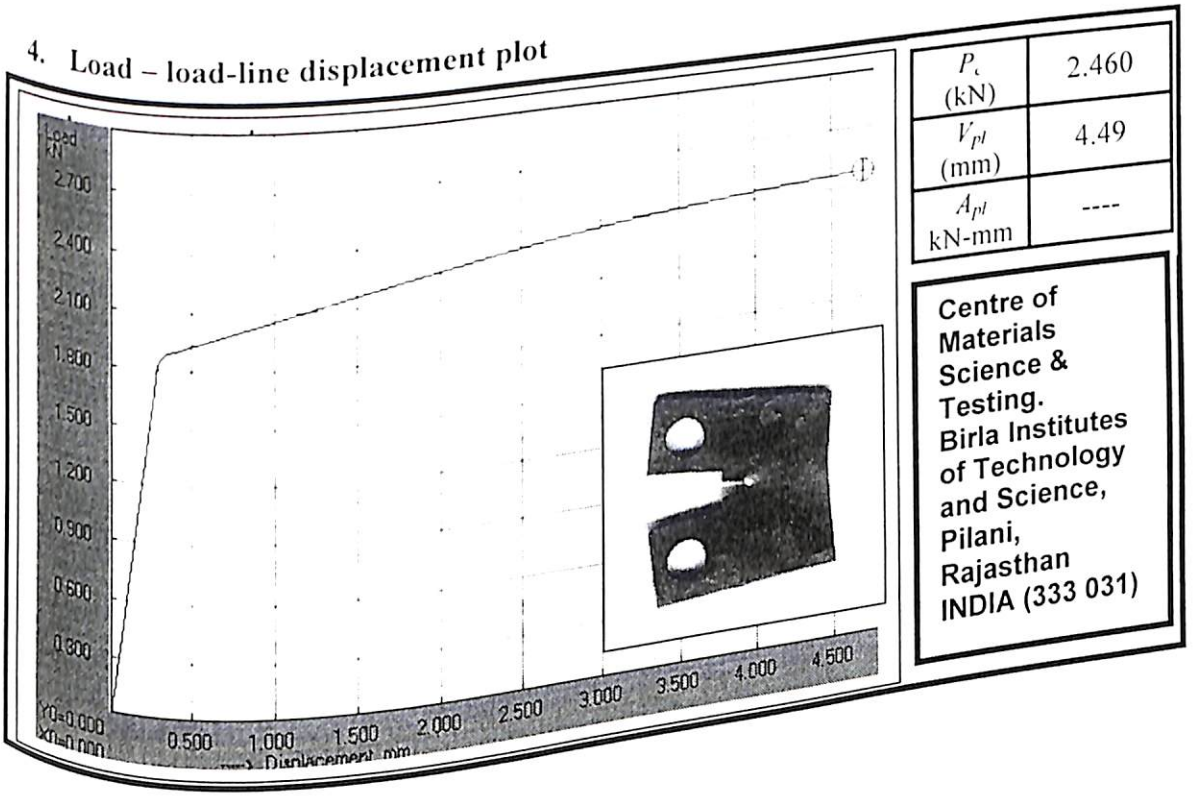

P_c (kN)	2.460
V_{pl} (mm)	4.49
A_{pl} kN-mm	----

Centre of Materials Science & Testing.
Birla Institutes of Technology and Science, Pilani, Rajasthan INDIA (333 031)

B5

Fracture Test on EDD258 (Crack growth behaviour)

B5.1 Fracture test R1

1. Material

Material	Yield strength (MPa)	Modulus of Elasticity (GPa)	Poisson's ratio (ν)
EDD258 steel sheet	258	210	0.33

2. (Compact Tension (CT) specimen as per ASTM standard (E399-91).

Specimen code	Thickness, B (mm)	Crack length a_0 (mm)	Width W (mm)	Notch radius, ρ (mm)
R1	*3.2*	*10.5*	*24*	*0.115*

3. Test Conditions

Test Type	Load range (kN)	Strain rate (mm/min)	Temperature (°C)
Rupture	0 - 5	0.2	28

4. Load – load-line displacement plot

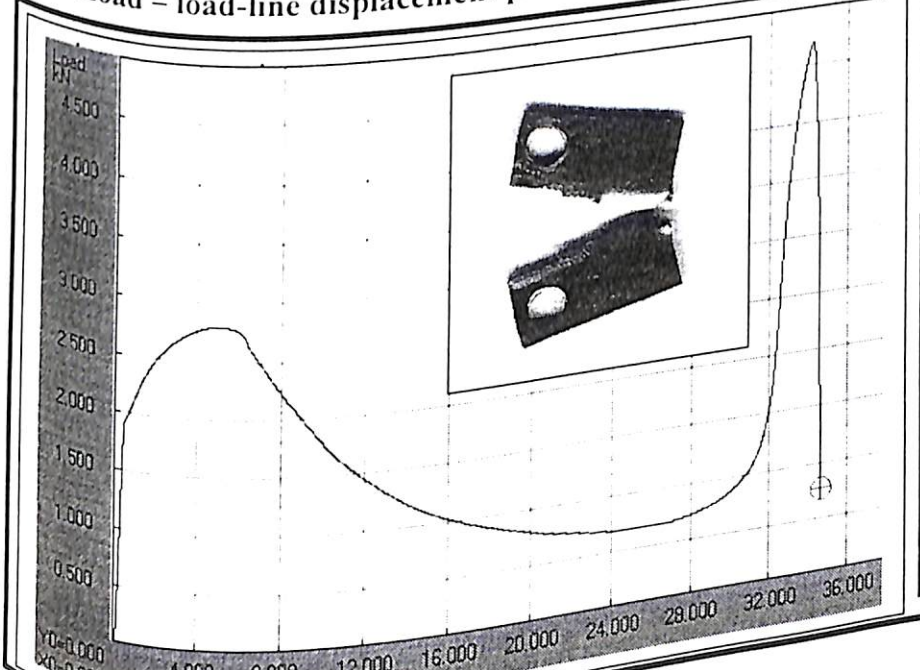

P_{unl} (kN)	0.767
V_{unl} (mm)	34.16
A_{pl} kN-mm	----

Centre of Materials Science & Testing.
Birla Institutes of Technology and Science, Pilani, Rajasthan INDIA (333 031)

B5.2 Fracture test R2

1. Material

Material	Yield strength (MPa)	Modulus of Elasticity (GPa)	Poisson's ratio (ν)
EDD258 steel sheet	258	210	0.33

2. (Compact Tension (CT) specimen as per ASTM standard (E399-91).

Specimen code	Thickness, B (mm)	Crack length a_0 (mm)	Width W (mm)	Notch radius, ρ (mm)
R2	3.2	10.5	24	0.116

3. Test Conditions

Test Type	Load range (kN)	Strain rate (mm/min)	Temperature (°C)
Crack initiation	0 - 5	0.2	28

4. Load – load-line displacement plot

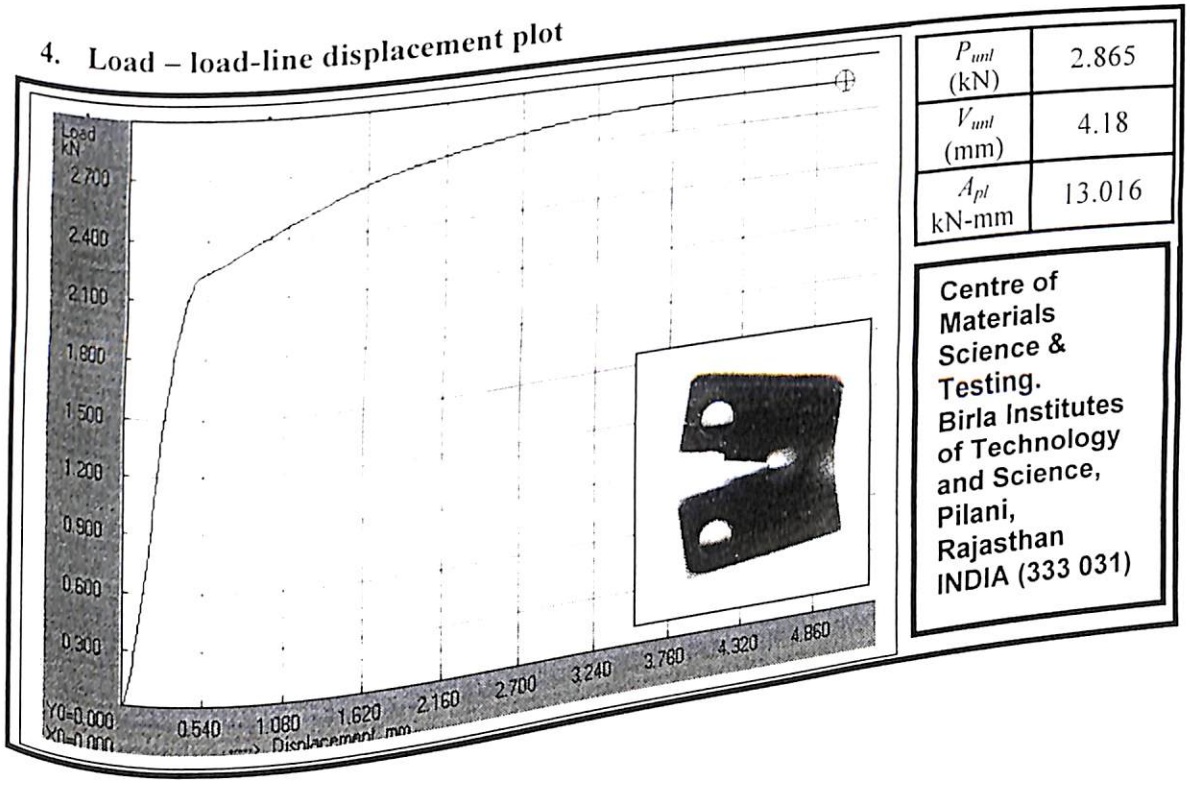

P_{unl} (kN)	2.865
V_{unl} (mm)	4.18
A_{pl} kN-mm	13.016

Centre of Materials Science & Testing.
Birla Institutes of Technology and Science, Pilani, Rajasthan INDIA (333 031)

B5.3 Fracture test R3

1. Material

Material	Yield strength (MPa)	Modulus of Elasticity (GPa)	Poisson's ratio (ν)
EDD258 steel sheet	258	210	0.33

2. (Compact Tension (CT) specimen as per ASTM standard (E399-91).

Specimen code	Thickness, B (mm)	Crack length a_0 (mm)	Width W (mm)	Notch radius, ρ (mm)
R3	3.2	10.5	24	0.121

3. Test Conditions

Test Type	Load range (kN)	Strain rate (mm/min)	Temperature (°C)
BLD	0 - 5	0.2	28

4. Load – load-line displacement plot

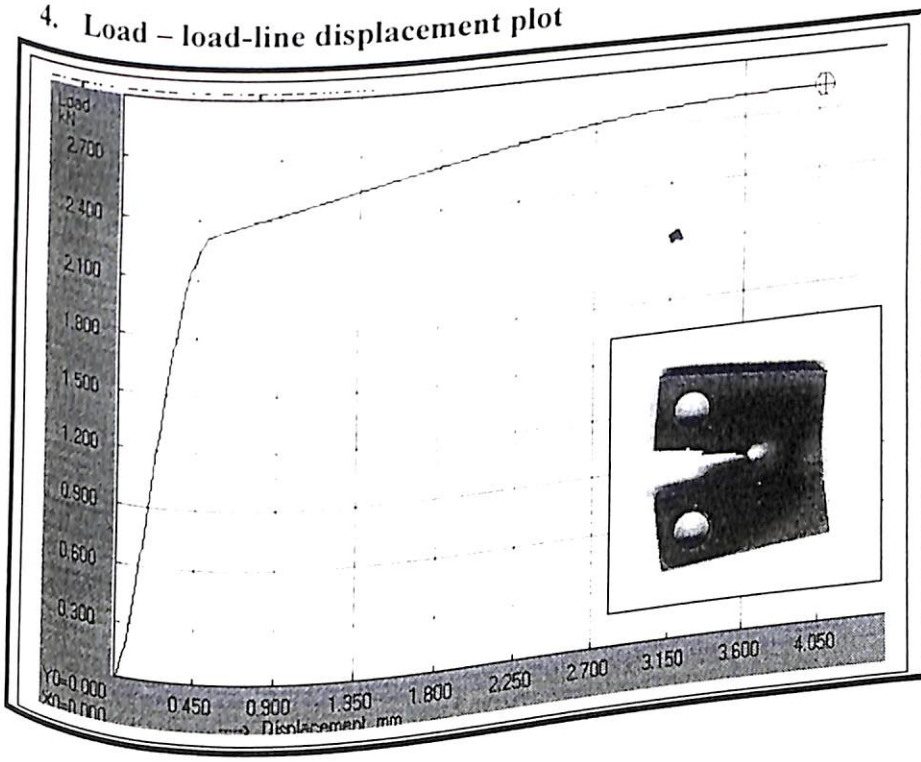

P_{unl} (kN)	2.831
V_{unl} (mm)	4.08
A_{pl} kN-mm	8.192

Centre of Materials Science & Testing.
Birla Institutes of Technology and Science, Pilani, Rajasthan INDIA (333 031)

B5.4 Fracture test R4

1. Material

Material	Yield strength (MPa)	Modulus of Elasticity (GPa)	Poisson's ratio (ν)
EDD258 steel sheet	258	210	0.33

2. (Compact Tension (CT) specimen as per ASTM standard (E399-91).

Specimen code	Thickness, B (mm)	Crack length a_0 (mm)	Width W (mm)	Notch radius, ρ (mm)
R4	3.2	10.5	24	0.116

3. Test Conditions

Test Type	Load range (kN)	Strain rate (mm/min)	Temperature (°C)
Crack growth	0 - 5	0.2	28

4. Load – load-line displacement plot

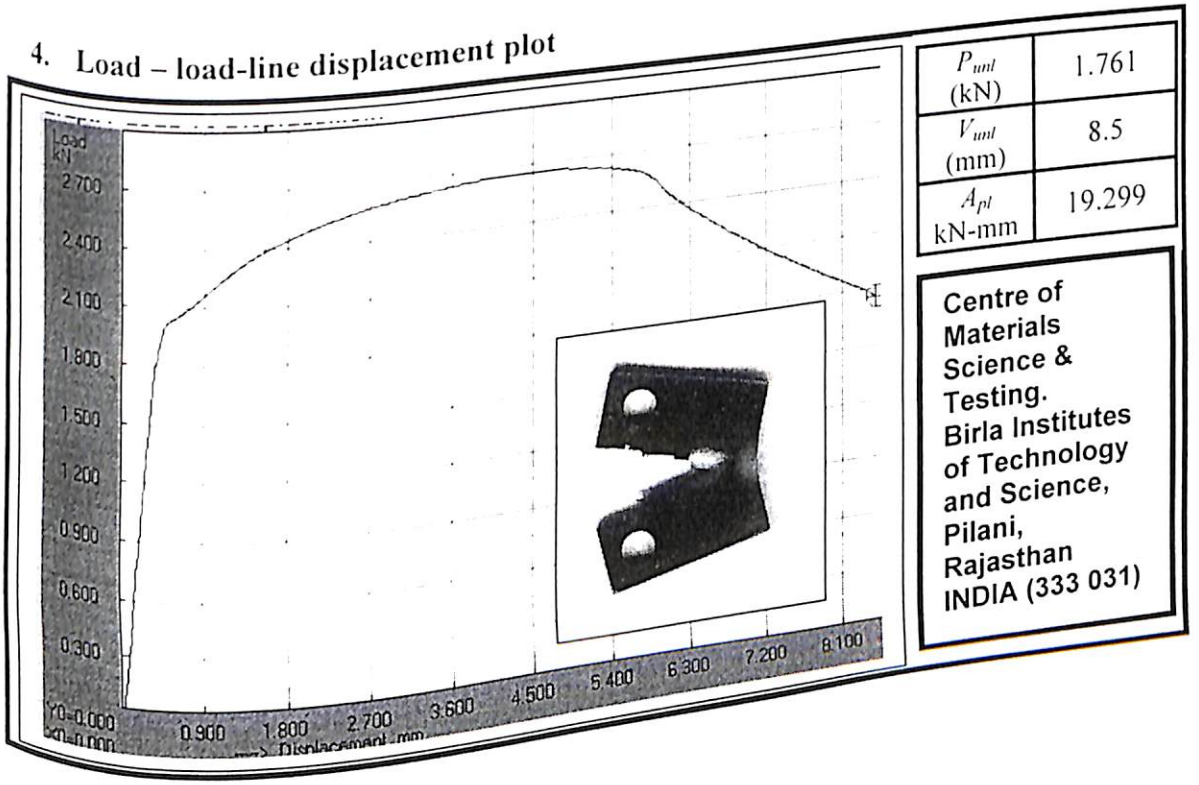

P_{uml} (kN)	1.761
V_{uml} (mm)	8.5
A_{pl} kN-mm	19.299

Centre of Materials Science & Testing.
Birla Institutes of Technology and Science, Pilani, Rajasthan INDIA (333 031)

B5.5 Fracture test R5

1. Material

Material	Yield strength (MPa)	Modulus of Elasticity (GPa)	Poisson's ratio (ν)
EDD258 steel sheet	258	210	0.33

2. (Compact Tension (CT) specimen as per ASTM standard (E399-91).

Specimen code	Thickness, B (mm)	Crack length a_0 (mm)	Width W (mm)	Notch radius, ρ (mm)
R5	3.2	10.5	24	0.122

3. Test Conditions

Test Type	Load range (kN)	Strain rate (mm/min)	Temperature (°C)
Crack growth	0 - 5	0.2	28

4. Load – load-line displacement plot

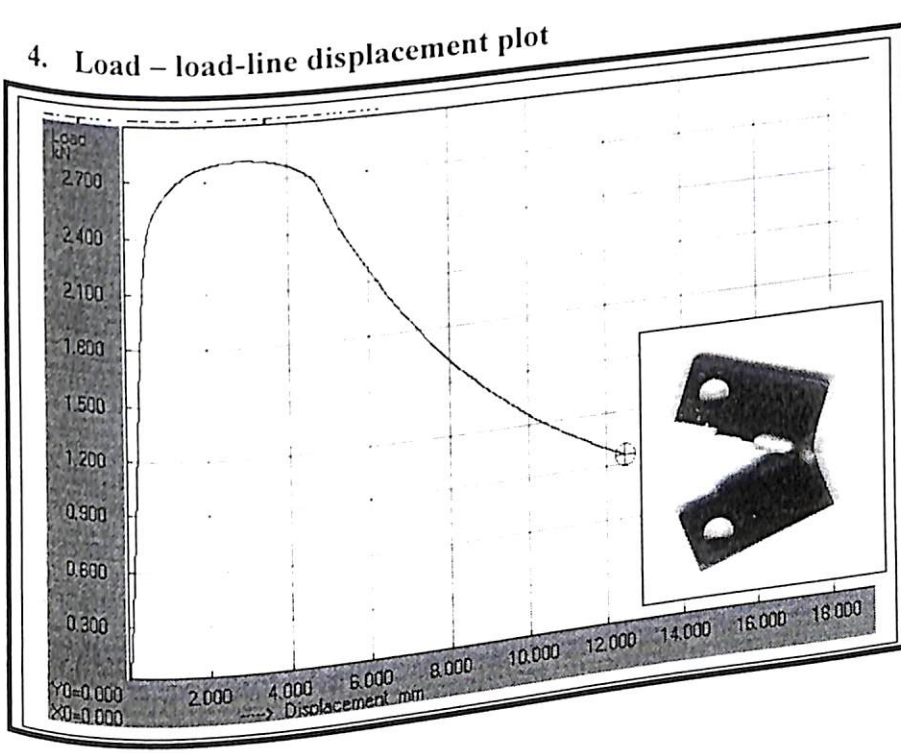

P_{unl} (kN)	0.958
V_{unl} (mm)	12.5
A_{pl} kN-mm	24.510

Centre of Materials Science & Testing.
Birla Institutes of Technology and Science, Pilani, Rajasthan INDIA (333 031)

B5.6 Fracture test R6

1. Material

Material	Yield strength (MPa)	Modulus of Elasticity (GPa)	Poisson's ratio (ν)
EDD258 steel sheet	258	210	0.33

2. (Compact Tension (CT) specimen as per ASTM standard (E399-91).

Specimen code	Thickness, B (mm)	Crack length a_0 (mm)	Width W (mm)	Notch radius, ρ (mm)
R6	3.2	10.5	24	0.118

3. Test Conditions

Test Type	Load range (kN)	Strain rate (mm/min)	Temperature (°C)
Crack growth	0 - 5	0.2	28

4. Load – load-line displacement plot

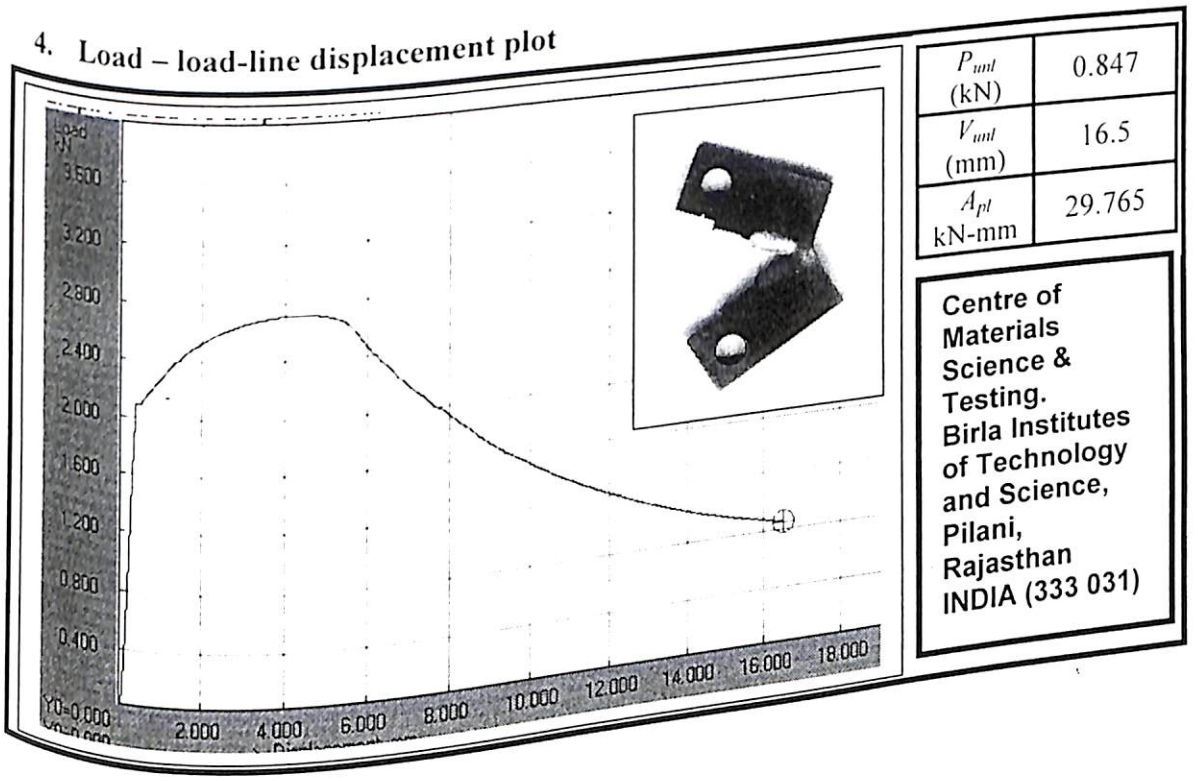

P_{unl} (kN)	0.847
V_{unl} (mm)	16.5
A_{pl} kN-mm	29.765

Centre of Materials Science & Testing.
Birla Institutes of Technology and Science, Pilani, Rajasthan INDIA (333 031)

B5.7 Fracture test R7

1. Material

Material	Yield strength (MPa)	Modulus of Elasticity (GPa)	Poisson's ratio (ν)
EDD258 steel sheet	258	210	0.33

2. (Compact Tension (CT) specimen as per ASTM standard (E399-91).

Specimen code	Thickness, B (mm)	Crack length a_0 (mm)	Width W (mm)	Notch radius, ρ (mm)
R7	3.2	10.5	24	0.116

3. Test Conditions

Test Type	Load range (kN)	Strain rate (mm/min)	Temperature (°C)
Crack growth	0 - 5	0.2	28

4. Load – load-line displacement plot

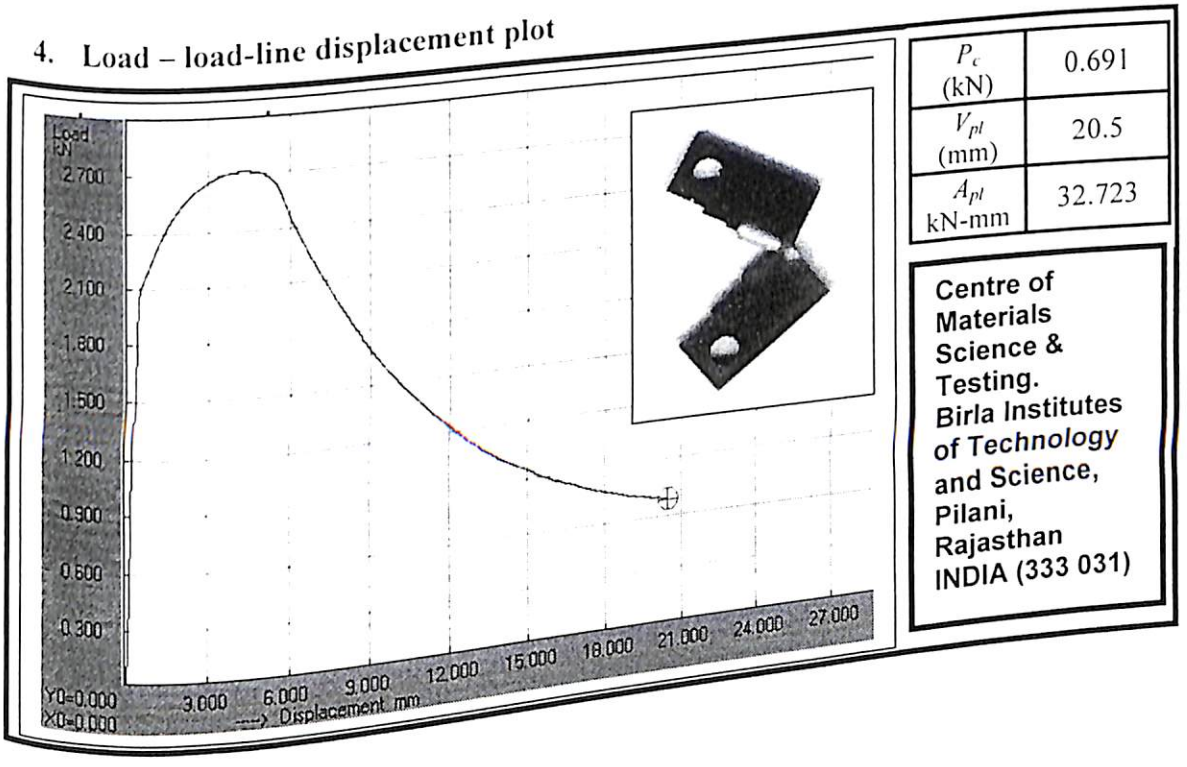

P_c (kN)	0.691
V_{pl} (mm)	20.5
A_{pl} kN-mm	32.723

Centre of Materials Science & Testing.
Birla Institutes of Technology and Science, Pilani, Rajasthan INDIA (333 031)

B5.8 Fracture test R8

1. Material

Material	Yield strength (MPa)	Modulus of Elasticity (GPa)	Poisson's ratio (ν)
EDD258 steel sheet	258	210	0.33

2. (Compact Tension (CT) specimen as per ASTM standard (E399-91).

Specimen code	Thickness, B (mm)	Crack length a_0 (mm)	Width W (mm)	Notch radius, ρ (mm)
R8	3.2	10.5	24	0.113

3. Test Conditions

Test Type	Load range (kN)	Strain rate (mm/min)	Temperature (°C)
Crack growth	0 - 5	0.2	28

4. Load – load-line displacement plot

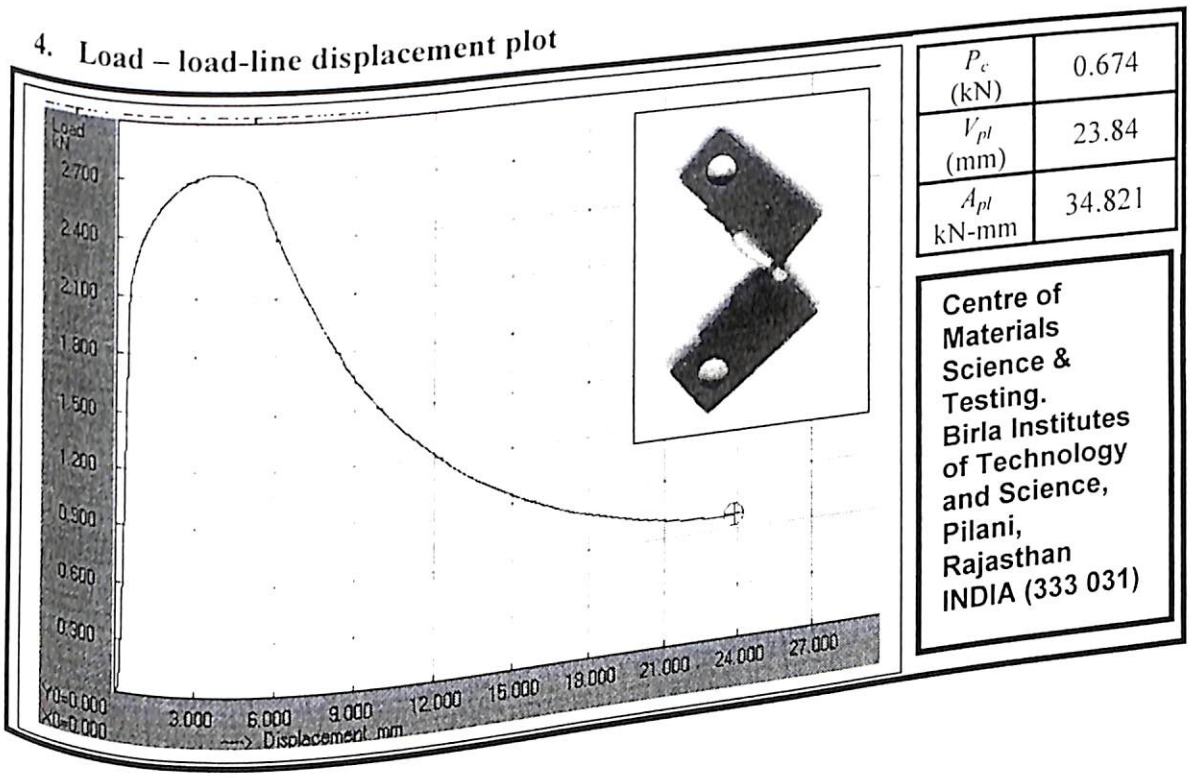

P_c (kN)	0.674
V_{pl} (mm)	23.84
A_{pl} kN-mm	34.821

Centre of Materials Science & Testing. Birla Institutes of Technology and Science, Pilani, Rajasthan INDIA (333 031)

B6

Fracture Test on other Engineering materials (Crack initiation study)

B6.1 Fracture test Al

1. Material

Material	Yield strength (MPa)	Modulus of Elasticity (GPa)	Poisson's ratio (ν)
Aluminium	34	70	0.33

2. (Compact Tension (CT) specimen as per ASTM standard (E399-91).

Specimen code	Thickness, B (mm)	Crack length a_0 (mm)	Width W (mm)	Notch radius, ρ (mm)
Al	2.0	10.5	24	0.1

3. Test Conditions

Test Type	Load range (kN)	Strain rate (mm/min)	Temperature (°C)
Crack initiation	0 - 5	0.2	28

4. Load – load-line displacement plot

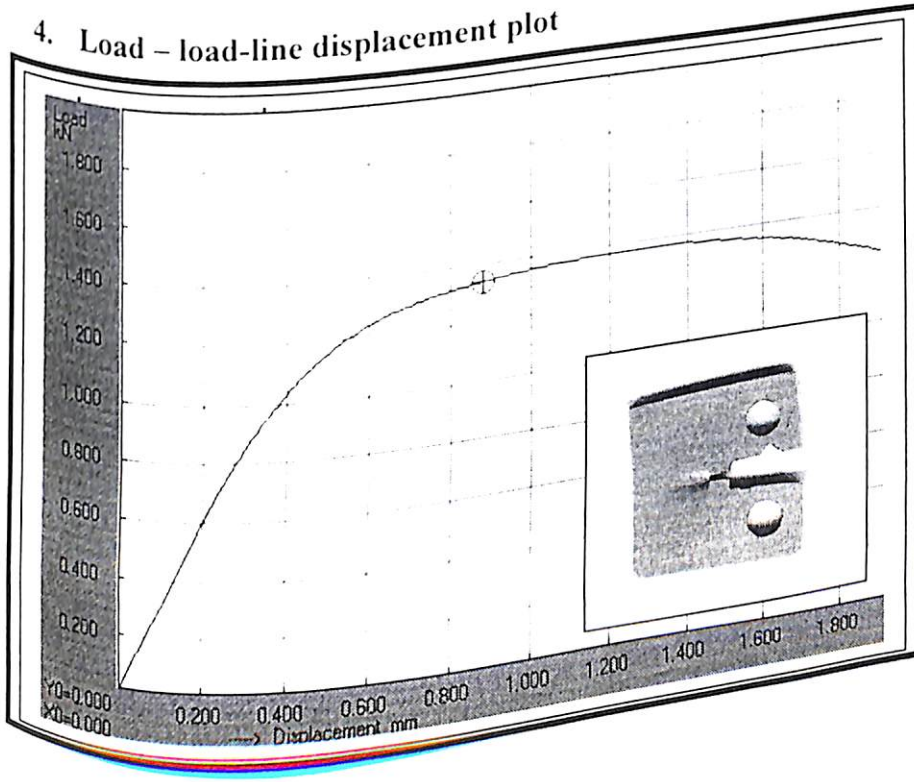

P_c (kN)	1.338
V_{pl} (mm)	----
A_{pl} kN-mm	----

Centre of Materials Science & Testing.
Birla Institutes of Technology and Science, Pilani, Rajasthan INDIA (333 031)

B6.2 Fracture test Cu

1. Material

Material	Yield strength (MPa)	Modulus of Elasticity (GPa)	Poisson's ratio (ν)
Copper	380	90	0.26

2. (Compact Tension (CT) specimen as per ASTM standard (E399-91).

Specimen code	Thickness, B (mm)	Crack length a_0 (mm)	Width W (mm)	Notch radius, ρ (mm)
Cu	2.0	10.5	24	0.1

3. Test Conditions

Test Type	Load range (kN)	Strain rate (mm/min)	Temperature (°C)
Crack initiation	0 - 5	0.2	28

4. Load – load-line displacement plot

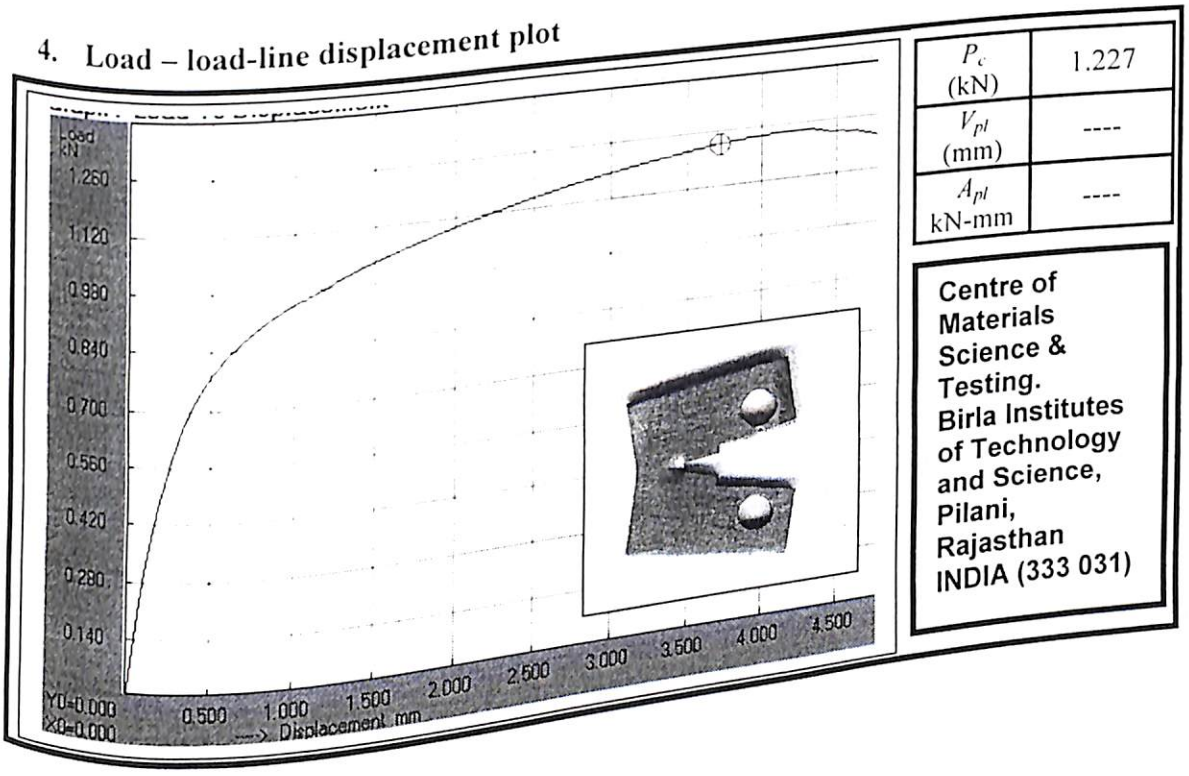

P_c (kN)	1.227
V_{pl} (mm)	----
A_{pl} kN-mm	----

Centre of Materials Science & Testing.
Birla Institutes of Technology and Science, Pilani, Rajasthan INDIA (333 031)

B6.3 Fracture test Br

1. Material

Material	Yield strength (MPa)	Modulus of Elasticity (GPa)	Poisson's ratio (ν)
Brass	225	80	0.33

2. (Compact Tension (CT) specimen as per ASTM standard (E399-91).

Specimen code	Thickness, B (mm)	Crack length a_0 (mm)	Width W (mm)	Notch radius, ρ (mm)
Br	2.0	10.5	24	0.1

3. Test Conditions

Test Type	Load range (kN)	Strain rate (mm/min)	Temperature (°C)
Crack initiation	0 - 5	0.2	28

4. Load – load-line displacement plot

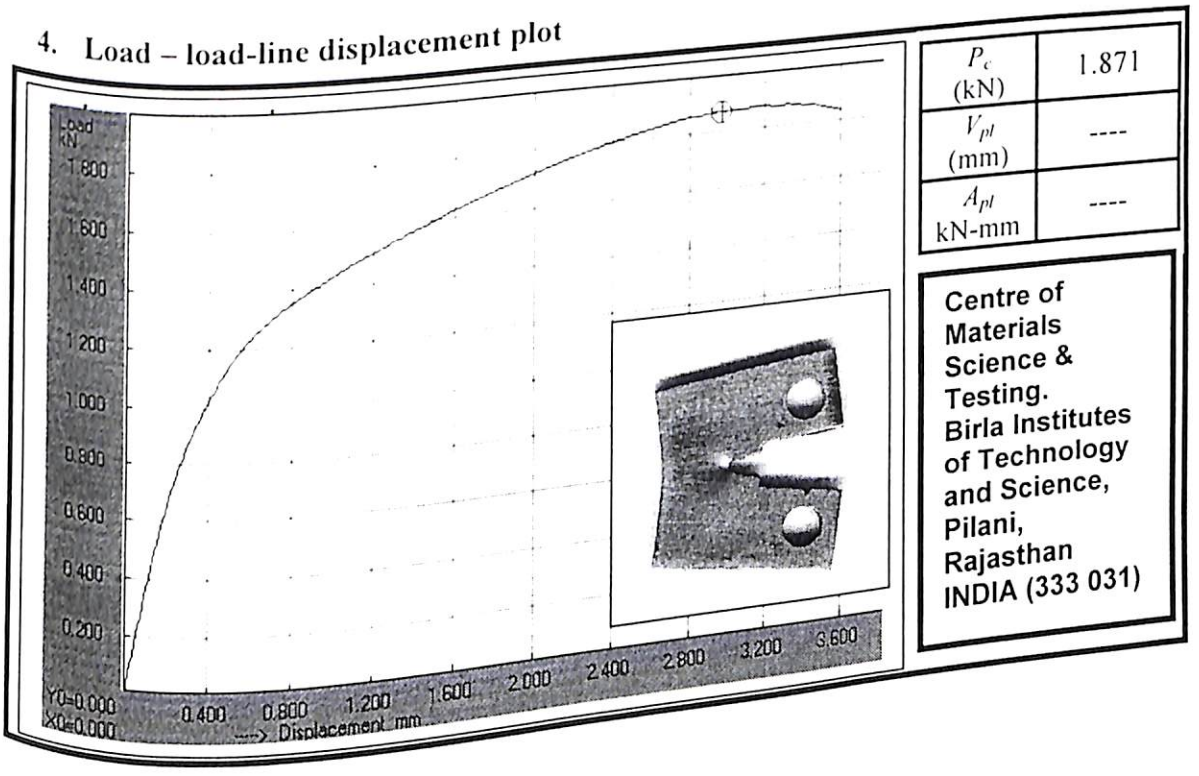

P_c (kN)	1.871
V_{pl} (mm)	----
A_{pl} kN-mm	----

Centre of Materials Science & Testing. Birla Institutes of Technology and Science, Pilani, Rajasthan INDIA (333 031)

B6.4 Fracture test MS

1. Material

Material	Yield strength (MPa)	Modulus of Elasticity (GPa)	Poisson's ratio (v)
Mild Steel	330	208	0.33

2. (Compact Tension (CT) specimen as per ASTM standard (E399-91).

Specimen code	Thickness, B (mm)	Crack length a_0 (mm)	Width W (mm)	Notch radius, ρ (mm)
MS	2.0	10.5	24	0.1

3. Test Conditions

Test Type	Load range (kN)	Strain rate (mm/min)	Temperature (°C)
Crack initiation	0 - 5	0.2	28

4. Load – load-line displacement plot

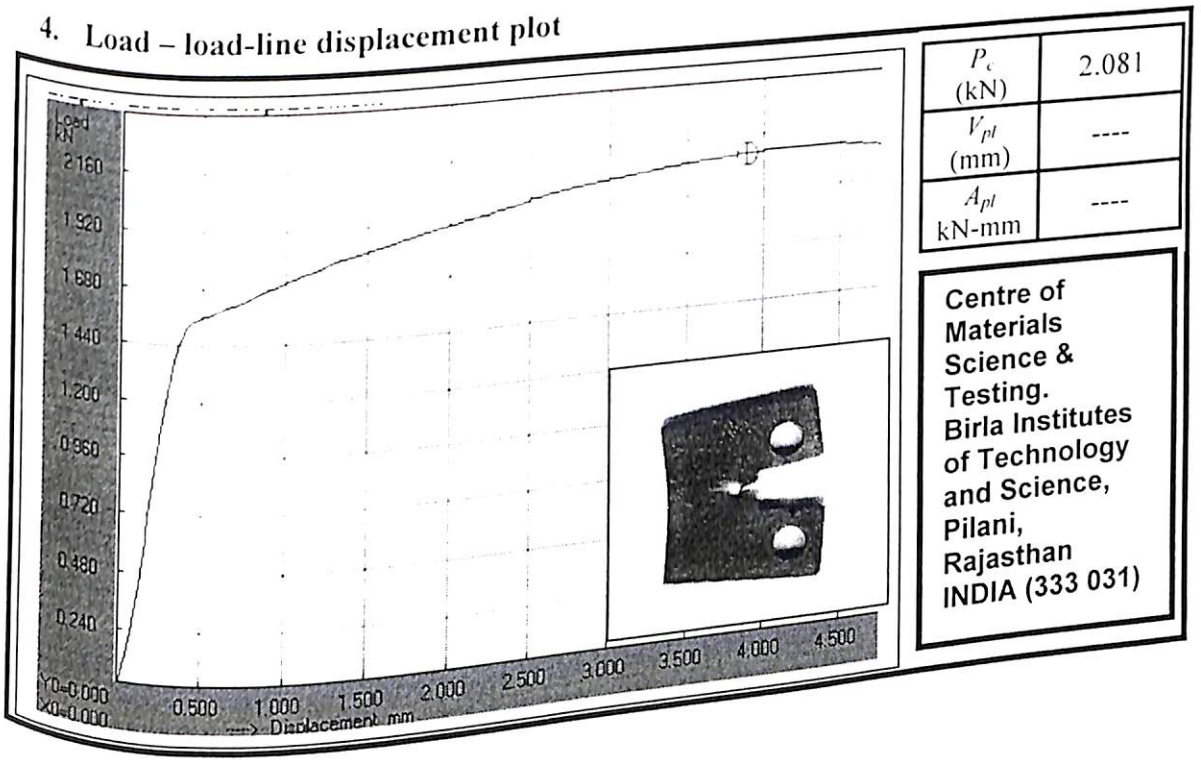

P_c (kN)	2.081
V_{pl} (mm)	----
A_{pl} kN-mm	----

Centre of Materials Science & Testing.
Birla Institutes of Technology and Science, Pilani, Rajasthan INDIA (333 031)

C

Influence of notch radius on fracture toughness

Plastic zone in front of crack tip for by FE analysis

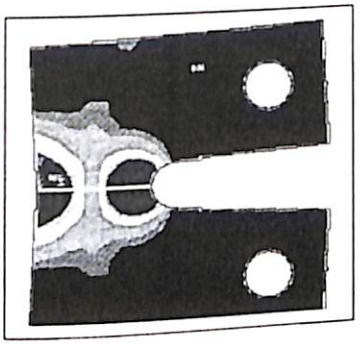

ρ = 0.20 mm

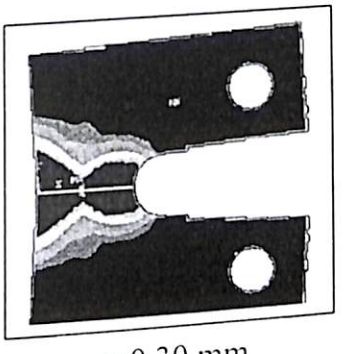

ρ = 0.30 mm

D

Measurement of notch radius using a micrograph (100X)

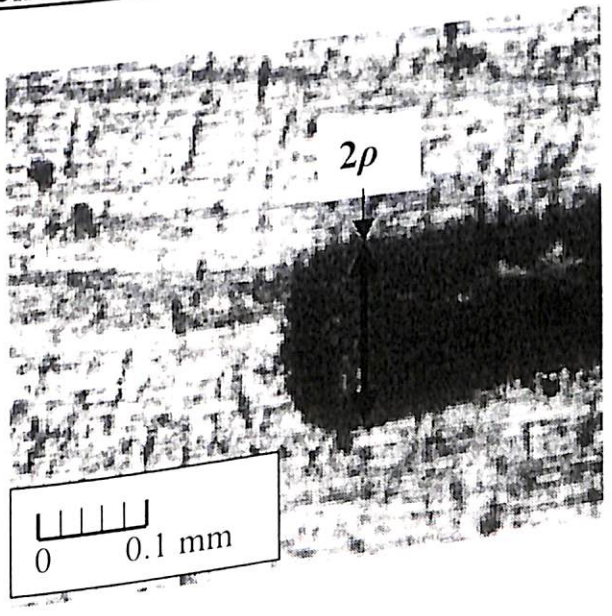

E

Microstructure ahead of crack tip

E1 Microstructure in ahead of crack tip EDD277

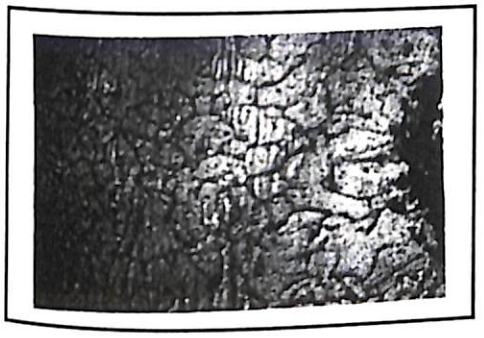

(a) before fracture test (400X)

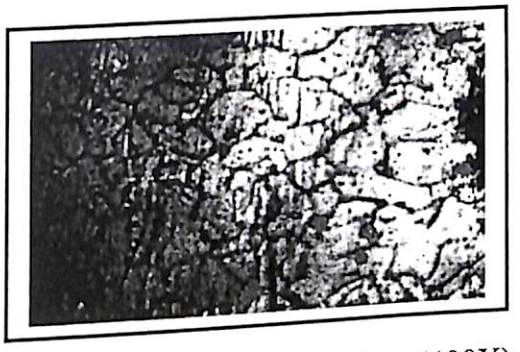

(b) after fracture test at surface (400X)

E2 Microstructure ahead of crack tip in EDD258

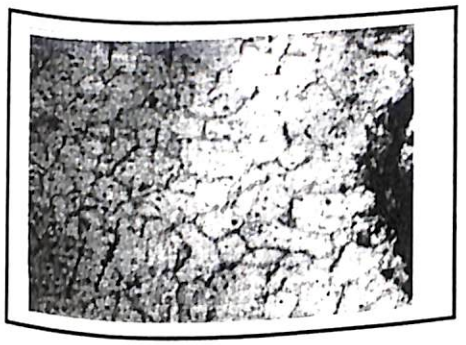

(a) before fracture test (400X)

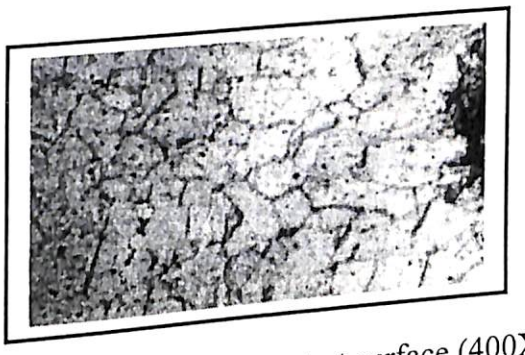

(b) after fracture test at surface (400X)

F

Specifications of machines and equipments used for the thesis work

1. **Computerised Universal Testing Machine**

Make	FIE, Kolhapur (INDIA)
Model	UNITEK 100
Specifications	Load unit cells 0 – 5 kN, 0 – 100 kN Displacement rate 0.2 – 250 mm/min

2. **CMOD Gauge**

Make	WAZAU, Germany
Model	WAC 07.02.01 (for CT type specimens)
Specifications	Measuring range 3-13 mm

3. **Micro Hardness Tester**

Make	SHIMADZU, Canada
Model	HMV
Specifications	Load duration: 5 to 999 seconds, Load 9 types: 98.07, 245.2, 490.3, 980.7mN, 1.96, 2.942, 4.903, 9.807, 19.61 N Measurement mode: Vickers hardness HV

4. **Flat bed scanner**

Make	HP
Model	Scan Jet 3970 Digital Flat bed scanner

5. **Chemical Analyser**

Make	Worldwide Analytical System WAS, USA
Model	Model Foundry Master

6. **Gas Analyser**

Make	LECO Corporation, USA
Model	CS-244

BRIEF BIOGRAPHY OF THE SUPERVISOR

Prof Ravi Prakash has 30 years of teaching and research experience. He is currently, Dean, Research and Consultancy Division at BITS, Pilani. Earlier he was the Dean for Faculty Division II. He has been Science Counsellor, Embassy of India, Washington D.C., USA. He has also been the Coordinator, School of Biomedical Engineering, Institute of Technology, Banaras Hindu University. Presently, besides being Dean, he is Coordinator for Centre for Materials Science and Technology, Centre for Robotics and Intelligent Systems and Center for Desert Development Technology. He has published over 100 research papers in various international journals / conferences of repute. He is Fellow of the Institution of Engineers (India) (FIE), Fellow of Ultrasonic Society of India, Fellow of Indian Society for Nondestructive Testing, Member of American Society of Mechanical Engineers (ASME), USA, Member of Indian Society of Mechanical Engineers (ISME) etc.

BRIEF BIOGRAPHY OF THE CANDIDATE

Kulkarni Dhananjay Madhukar did his B.E. Mechanical Engineering from University of Pune (Maharashtra) in 1993. He did his Master of Technology in Mechanical System Design from Indian Institute of Technology, Kharagpur in 1998. He started his research in Fracture Mechanics since 2000 at Birla Institute of Technology and Science, Pilani (Rajasthan). His areas of research are Fracture Mechanics, Finite Element Analysis and Computer Aided Design.

He has an industrial experience of two years. He has developed a single bearing alternator in Crompton Greaves Limited, Ahmednagar (Maharashtra). He has published a book on D.G. set, which is widely used by Indian D.G. set manufacturers for selection, installation and troubleshooting operations. Being an academician, he has taught various courses in Mechanical Engineering in University of Poona and BITS, Pilani since 1994. He has also taught various courses for distance learning programmes of BITS, Pilani in the area of Mechanical Engineering. He has published the EDD notes on Engineering Graphics, which will be soon published in book form by Tata Mc Graw Hill publishing Ltd, New Delhi. He has also published papers in various Indian journals of repute and presented papers in various national/international conferences. Presently he is working as a Lecturer in Mechanical Engineering in BITS-Pilani, Goa Campus. Besides being Lecturer, he is a Coordinator for computer center and community welfare unit.